UNIVERSITY OF CALIFORNIA
SANTA CRUZ

MODULATION OF CIRCADIAN CYCLING BY THE C-TERMINAL TRANSACTIVATION DOMAIN OF BMAL1

A dissertation dubmitted in partial satisfaction
of the requirements for the degree of

DOCTOR OF PHILOSOPHY

in

CHEMISTRY

by

Chelsea LeBrun Gustafson

June 2016

The Dissertation of Chelsea Lebrun Gustafson is approved:

_____
Professor Michael Stone, Chair

_____
Professor Seth Rubin

_____
Professor Carrie Partch

_____
Tyrus Miller
Vice Provost and Dean of Graduate Studies

TABLE OF CONTENTS

ABSTRACT x

ACKNOWLEDGEMENTS xi

CHAPTER 1—EMERGING MODELS FOR THE MOLECULAR BASIS OF MAMMALIAN CIRCADIAN TIMING 1
- Abstract 1
- The Molecular Oscillator *A*s A Key Mechanism In Human Health 1
- Transcription Feedback Loops Drive Molecular Oscillations 3
- Protein Architecture Of Core Circadian Transcriptional Regulators 6
- PAS Domains 8
- PERIOD: A PAS Dimer At The Heart Of The Clock 11
- CRY1: The Circadian Repressor 15
- CLOCK:BMAL1—The Principal Circadian Transcription Factor 19
- Modeling Circadian Oscillators 22
- Conclusion 23
- Thesis Summary 24
- References 25

CHAPTER 2—CRYPTOCHROME 1 REGULATES THE CIRCADIAN CLOCK THROUGH DYNAMIC INTERACTIONS WITH THE BMAL1 C-TERMINUS 35
- Abstract 35
- Introduction 35
- Only BMAL1 Can Generate Cell-Autonomous Circadian Rhythms 36
- BMAL Paralogs Have Similar Steady-State Activities 38
- The C-Terminus Of BMAL1 Is Needed For Circadian Cycling 38
- BMAL1 C-Terminal TAD Determines Circadian Period 39
- The BMAL1 TAD Is Intrinsically Unstructured 42
- CRY1 And CBP(p300) Compete For BMAL1 TAD Binding 42
- Dynamic Interactions Of TAD With CRY1 And CBP(p300) 43
- TAD Mutations Alter Affinity For CRY1 And CBP(p300) 45
- TAD Mutations Perturb Circadian Timekeeping 47
- CRY1 Binds To Multiple Sites On CLOCK–BMAL1 47
- Discussion 49
- Methods 52
  - Lentiviral DNA Constructs, Preparation And Transduction 52
  - Luminescence Recording And Data Analysis 52
  - Transient Transfection And Reporter Assays 53
  - qPCR Analysis 55
  - Expression And Purification Of Recombinant Proteins 55
  - Peptide Synthesis And Purification 56
  - NMR Spectroscopy 56
  - Isothermal Titration Calorimetry (ITC) 57
  - Fluorescence Polarization (FP) 58
  - Accession Codes 58

References 58
Supplemental Figures For Chapter 2 62

CHAPTER 3—A SLOW CONFORMATIONAL SWITCH IN THE BMAL1 TRANSACTIVATION DOMAIN MODULATES CIRCADIAN CYCLING 71
Summary 71
Introduction 71
Results 73
A Proline Isomerization Actis As A Molecular Switch In The C-terminus Of BMAL1 73
Conservation Of TAD Switch In BMAL1 And iBMAL 74
Trp And Pro Are The Key Residues Comprising The TAD Switch 75
The *Trans* Locked Tad Switch Drives A Short Circadian Phenotype In Cycling Mef Cells 76
Both Isomers Of The Tad Switch Interact With Transcriptional Activators And Repressors 77
Isomerization Of The Switch Is Much Slower Than The Lifetimes Of The Complexes 79
Peptidyl-Prolyl Isomerases Can Modulate The TAD Switch 80
Discussion 81
Experimental Procedures 84
Lentiviral DNA Constructs, Preparation And Transduction 84
Bioluminescence Recording And Data Analysis 85
Expression And Purification Of Recombinant Proteins 85
Peptide Synthesis And Purification 88
NMR Spectroscopy 88
Fluorescence Anisotropy Experiments 90
References 91
Supplemental Figures For Chapter 3 97

CHAPTER 4—TRANSCRIPTIONAL ACTIVATION AT E-BOX ELEMENTS: INTERACTIONS OF THE BMAL1 TAD WITH TRANSCRIPTIONAL ACTIVATORS 106
Introduction 106
The Generic Process Of Transcriptional Activation 106
CBP/p300 Are Promiscuous Co-Activators 106
CBP/p300 In Circadian Rythyms 108
The KIX Domain Structure And Function 109
TAZ1 Structure And Function 111
Multivalent And Coopoerative Interactions Of TAD To CBP/p300 Domains 112
Results And Discussion 113
Dynamic Interactions Of CBP KIX Bound To BMAL1 TAD Exhibit Multiple Chemical Exchange Regimes 113
Determination Of Appropriate Switch Peptide Construct Length 116
Mapping BMAL1 TAD Binding Onto CBP KIX 116
Mutations On The C-MYB Binding Face Of CBP Decrease Interaction With BMAL1 TAD 117
Binding Of Mutant Switch Peptides To CBP KIX 120

W624 *trans*-locked Mutants Can Be Inhibited By CRY1 In Fibroblasts....124
Multivalent Interactions With CBP As A Potential Cooperative Mechanism....126
Temperature Variations May Allow For Dynamics To Be Captured....129
Future Directions....130
Methods....132
Expression And Purification Of Recombinant Proteins....132
Peptide Synthesis And Purification....134
NMR Spectroscopy....134
Fluorescence Anisotropy Experiments....135
Circular Dichroism Spectroscopy....135
Isothermal Titration Calorimetry (ITC)....135
Steady-State Mammalian Two-Hybrid Assays....136
References....136

CHAPTER 5—CONCLUSIONS AND FUTURE DIRECTIONS....141
Evolutionally Tuned Circadian Oscillations Regulate Physiology....141
Motions Of Disordered Regions Define Timescale Of Biological Processes....142
Molecular Motions Of The BMAL1 TAD....144
Differential Interaction Of *Cis* And *Trans* Isomers....148
Dynamic Transitions At The Heart Of The Molecular Oscillator....149
Future Directions....149
References....150

LIST OF FIGURES

Figure 1.1: Transcription/translation feedback loops control mammalian circadian timing 3

Figure 1.2: Multiple transcriptional regulatory complexes within the circadian feedback loop. 5

Figure 1.3: Domain architecture of core circadian transcriptional regulators.....7

Figure 1.4: The PAS domain 9

Figure 1.5: The PER2 PAS-AB dimer structure 12

Figure 1.6:Conservation and disorder in PER2.....14

Figure 1.7 Competition for the CC helix controls CRY function in the feedback loop.....17

Figure 1.8: The CLOCK:BMAL1 bHLH-PAS dimer structure 20

Figure 1.9: Organization of ring oscillators..... 22

Figure 2.1: Only BMAL1 can restore circadian rhythms in *Bmal1*$^{-/-}$ *Per2*^{Luc} fibroblasts 37

Figure 2.2: The BMAL1 C-terminus is needed for circadian function 40

Figure 2.3: A helical motif within the BMAL1 H domain controls circadian period length 41

Figure 2.4: CBP(p300) and CRY1 interact with BMAL1 TAD 44

Figure 2.5: BMAL1 TAD mutations decrease affinity for CBP(p300) and CRY1 and influence circadian period.....46

Figure 2.6: Distinct sites on CLOCK and BMAL1 facilitate repression by CRY1.....48

Figure 2.7: Regulation of the BMAL1 TAD by CRY1 contributes to determination of circadian period..... 50

Supplemental Figure 2.1: Validation of genetic complementation assay in BMAL1–/–:Per2^{Luc} fibroblasts 63

Supplemental Figure 2.2: Domain structure, sequence alignment and structural features of BMAL1 and BMAL2..... 64

Supplemental Figure 2.3: The C-terminal regulatory domain of BMAL1 is critical for maintaining circadian period length and rhythm amplitude 65

Supplemental Figure 2.4: The BMAL1 TAD interacts directly with transcriptional coregulators and is required for CLOCK:BMAL1 activity..... 66

Supplemental Figure 2.5: The TAD undergoes dynamic structural rearrangement upon binding to the p300 KIX domain and CRY1 CC peptide to couple the TAD helix and C-terminus 67

Supplemental Figure 2.6: Comparison of BMAL1 and BMAL2 TAD domains by NMR spectroscopy 68

Supplemental Figure 2.7: Quantitative analysis of BMAL TAD interactions with coregulators 69

Supplemental Figure 2.8: CRY1 regulation of CLOCK:BMAL1 requires interaction with both CLOCK and BMAL1 70

Figure 3.1: Isomerization about a conserved W-P bond in the C-terminus of BMAL1 74

Figure 3.2: The proline switch tunes the period of circadian cycling.....77

Figure 3.3: Both isomers of the TAD switch interact with transcriptional activators and repressors.....78

Figure 3.4: Kinetic analysis of isomerization using ZZ-exchange Spectroscopy 80

Figure 3.5: Modulation of isomerization rate by PPIases.....82

Supplemental Figure 3.1: Identification of the BMAL1 TAD switch 98

Supplemental Figure 3.2: A *cis*/*trans* isomerization drives the TAD switch 99

Supplemental Figure 3.3: Assignment and cycling analysis of TAD switch mutants 100

Supplemental Figure 3.4: TAD switch mutants in BMAL1 constructs 101

Supplemental Figure 3.5: Quantitative analysis of BMAL1 TAD Switch isomers with transcriptional coregulators 102

Supplemental Figure 3.6: Kinetic analysis of *cis*/*trans* isomerization 103

Supplemental Figure 3.7: Build up curves from zz-exchange data.....104

Supplemental Figure 3.8: Kinetic analysis of isomerization in the presence of peptidyl-prolyl isomerases 105

Figure 4.1: Domain Architecture of CBP.....107

Figure 4.2: Structure of the KIX domain of CBP 110

Figure 4.3: Structure of TAZ1:STAT2. PDB 2ka4 113

Figure 4.4: Multivariate interactions of transcription factors with CBP KIX.....114

Figure 4.5: Interaction of BMAL1 TAD with 15N CBP KIX occurs in multiple exchange regimes 115

Figure 4.6: Chemical shift perturbations of the KIX domain upon titration of BMAL1 switch peptides.....117

Figure 4.7: Comparison of interactions of CBP KIX with BMAL1 TAD Δswitch and BMAL1 switch peptide.....118

Figure 4.8: Mapping interactions of BMAL1 TAD motifs onto CBP KIX 119

Figure 4.9: Mutation on CBP KIX c-Myb binding face
abolishes interactions with BMAL1 TAD 121

Figure 4.10: Differential interactions of *cis* and *trans*
isomers of BMAL1 TAD with CBP KIX. 123

Figure 4.11: Interaction of BMAL1 TAD Trp mutatnts with CBP KIX and CRY1 125

Figure 4.12: Interactions of BMAL1 TAD with TAZ1 domain of CBP 127

Figure 4.13: ITC analysis of BMAL1 TAD with CBP TAZ1
binding isotherm of BMAL1 titrated into CBP TAZ1. 129

Figure 4.14: Interactions of BMAL1 TAD with CBP TAZ2 129

Figure 4.15: Temperature stability of CBP KIX. 130

Figure 4.16: Modulation of chemical exchange regime for
NMR studies on CBP KIX and BMAL1 TAD 131

Figure 5.1: The multidimensional energy landscape dictates
the timescale of molecular motions 143

Figure 5.2: The BMAL1 TAD is an intrinsically disordered region 144

Figure 5.3: Fast timescale motions of the BMAL1 TAD 145

Figure 5.4: The BMAL1 TAD undergoes structural rearrangements upon binding 146

LIST OF TABLES

Table 1.1: List of clock protein structures.....7

Table 1.2: PAS domain boundaries in representative clock proteins 9

Table 2.1: Dissociation constants for the interaction of BMAL transactivation domains with transcriptional coregulators.....46

Table 3.1: Affinity measurements of BMAL1 TAD isomers for transcriptional regulators 78

Table 3.2: Kinetics of *cis* to *trans* isomerization measured by ZZ-exchange spectroscopy....81

Table 4.1: Interactions between KIX TADs and binding partners 107

Table 4.2: Mapping functional motifs and sites of interaction on the KIX domain. 109

Table 4.3: KIX interacting proteins and location of interaction 111

Table 4.4: Affinities of CBP KIX for BMAL1 TAD switch isomers. 122

Table 4.5: Affinities of CBP KIX to the W624 mutants. 124

ABSTRACT

MODULATION OF CIRCADIAN CYCLING BY THE C-TERMINAL TRANSACTIVATION DOMAIN OF BMAL1

Chelsea LeBrun Gustafson

Nearly all terrestrial organisms possess an intrinsic biological timekeeping system that functions to align key physiological processes with the solar day. In mammals, this circadian cycling is driven by temporally specific interactions between the heterodimeric transcription factor, CLOCK:BMAL1 and its cognate transcriptional regulators. The biochemical processes that drive the handoff between active and repressive complexes tunes the phase, period and robustness of circadian cycling. In this study, we show that the unstructured C-terminal transactivation domain (TAD) of BMAL1 is a regulatory hub where transcriptional activators and repressors compete for binding. Using NMR spectroscopy and real time monitoring of circadian cycling in mammalian cells we studied how interactions of the TAD with transcriptional regulators control the generation of circadian rhythms. We show that the KIX and TAZ1 domains of CBP and the CC helix of CRY1 interact with the BMAL1 TAD at overlapping sites. Perturbations of these regions of BMAL1 by site-directed mutagenesis have direct consequences for the balance of transcriptional activation and repression and elicit large changes the period of circadian oscillations. Using paramagnetic resonance spectroscopy we show that the BMAL1 TAD undergoes significant and differing conformational rearrangements upon binding CBP KIX and CRY CC. Furthermore, we identified a slow conformational change in the extreme C-terminus of BMAL1, a region of the TAD that is essential for normal circadian timekeeping. Using NMR spectroscopy, we performed structural and kinetic analysis of the conformational switch to identify a *cis*/*trans* isomerization about a Trp-Pro imide bond. Using NMR, fluorescence polarization and cell-based studies, we further characterized the switch to assess its role in circadian cycling and identified cyclophilins capable of regulating the rate of switch interconversion *in vitro*. Together, these data highlight the importance of structural dynamics of the BMAL1 TAD in tuning the molecular circadian clock.

ACKNOWLEDGEMENTS

DISSERTATION PROJECT ACKNOWLEDGEMENTS

I would like to express my special appreciation and thanks to my advisor Dr. Carrie Parch. Her constant support, excellent scientific guidance and enthusiasm for the subject matter facilitated my growth as a scientist and individual. Thank you for your brilliant comments, experimental suggestions, the countless brainstorm sessions and most of all, your patience. I deeply respect and admire your commitment to rigorous scientific investigation and am fortunate to have benefited from your extensive knowledge. I could not have asked for a better scientific mentor.

I would like to acknowledge the other members of my thesis committee, Dr. Seth Rubin and Dr. Michael Stone for their insightful comments and encouragement, and also for the probing scientific questions that incented me to think about my research in a larger context. In addition to being a tremendous source of technical knowledge, Jack Lee has been an unwavering pinnacle of positivity and encouragement-even when I called him with NMR questions in the middle of the night and on weekends. The members of the Rubin and Lokey labrotories were instrumental in my academic progress; thanks for all the great ideas, brainstorming sessions and technical assistance.

I thank my fellow lab-mates for the stimulating discussions, emotional support, creative ideas and super fun lab-cleanup parties. The stellar undergraduate researchers that I had the joy to mentor during my time in the Parch lab taught me invaluable life lessons, and I am so thankful the significant academic contributions they made to my dissertation. Specifically, Nicolette Goularte, Nicole Parsley and Kyle Franks made significant academic contributions to my projects; through their reciprocal mentorship, I gained a deeper understanding of how to effectively work as a team.

My sincere thanks also goes to Dr. Greg Miller and Dr. Hala Schepmann who, during my undergraduate career instilled in me a profound respect and enthusiasm for chemistry and the scientific method. I would like to give a special thanks to my family and friends who have provided me with encouragement, guidance and most importantly, perspective over the course

of my studies. My successes are a direct reflection of the support that I received from my parents and brother; thank you for teaching me the skills to succeed. My life partner, best friend and fellow graduate student, Alex Steely, has been a stalwart advocate of my career, academic aspirations and life choices. Thank you for believing in me, and consistently reminding me that I am good enough. Last but not least, a big thanks to a girls' best friend, my constant companion, adventuring buddy and emotional support system, Lotus.

There are countless others that have profoundly assisted me during the course of my studies. I wish I could name them all-please know you have my humble gratitude.

CHAPTER 1 ACKNOWLEDGEMENTS

The text of this dissertation includes a reprint from sections of the following previously published material:

Gustafson, C.L. and Partch, C.L. (2015). Emerging models for the molecular basis of mammalian circadian timing. Biochemistry 54, 134-149. DOI: 10.1021/bi500731f

This is an unofficial translation of an article that appeared in an ACS publication. ACS has not endorsed the content of this translation or the context of its use.

The following are a list of contributes that the candidate, Chelsea Gustafson performed for the development of this manuscript:

1. Idea development and outline writing
2. Assisted C.L.P. in the drafting of the manuscript
3. Identification and organization of appropriate references

Manuscript acknowledgements

We thank Eva Wolf for sharing coordinates of the mCRY1:PER2 CBD crystal structure (PDB: 4CT0) prior to its release in the Protein Databank. We apologize to colleagues whose work could not be cited due to space considerations.

CHAPTER 2 ACKNOWLEDGEMENTS

The text of this dissertation includes a reprint of the following previously published material:

Xu,H., Gustafson, C.L., Sammons, P.J., Khan, S.K., Parsley, N.C., Ramanathan, C., Lee, H.-W., Liu, A.C. and Partch, C.L. (2015). Cryptochrome 1 regulates the circadian clock through dynamic interactions with the BMAL1 C terminus. Nat. Struct. Mol. Biol. 22, 476-484. DOI: 10.1038/nsmb.3018

The following are a list of contributions that the candidate, Chelsea Gustafson performed for the development of this manuscript:

1. Designed the project in collaboration with C.L.P., J.S, H.X., A.C.L.

2. Wrote the manuscript in collaboration with C.L.P., H.X. and A.C.L

3. Performed protein growths and purifications for the experiments to generate the data found in figure 1, figure 4, figure 5, figure 6, figure 7, supplemental figure 4, supplemental figure 5, supplemental figure 6, supplemental figure 7 and supplemental figure 8 in collaboration with N.C.P and P.J.S.

4. Performed NMR experiments in figure 4, supplemental figure 4, supplemental figure 5, supplemental figure 6 in collaboration with C.L.P P.J.S and N.C.

5. Performed the ITC experiments to generate the data shown in figure 5, figure 7, supplemental figure 7 and Table 1

6. Performed fluorescence polarization studies used to generate the data shown in supplemental figure 7 and table1

Manuscript acknowledgements

We thank P.E. Wright (The Scripps Research Institute) and A. Sancar (University of North Carolina, Chapel Hill) for sharing reagents. We thank Jillian Miller and Glenn Millhauser (University of California, Santa Cruz) for technical assistance and access to instrumentation for automated peptide synthesis and purification, S.M. Rubin (University of California, Santa Cruz) for access to calorimetry instrumentation, critical discussions and advice, and the Chemical Screening Center (University of California, Santa Cruz) for access to other instrumentation.

CHAPTER 3 ACKNOWLEDGMENTS

A huge thanks to Nicole Parsley for her tireless work collecting ZZ-exchange data and to Owen Williams for his help with Matlab. Thanks to Nicolette Goularte for helping me with protein preps and as an amazing poster and figure editor. Thanks to Alicia Michael for tirelessly perfecting CRY1 protein preps and giving me egregious amounts of the precious protein for my experiments. Thanks to Hande Asimgil for your cell culture advice and all your work purifying PPIs. Thanks to Chris Ahlbach for your work on the PPI rate enhancements. Thanks to members of the R.S. Lokey lab and the G. Millhauser lab for your help with peptide synthesis and purification. Thanks to Walter Bray at the UCSC Chemical Screening Center for your advice and instrumentation training.

CHAPTER 4 ACKNOWLEDGMENTS

I would like to recognize Linnea Jansson for her contributions to the work published in this chapter during her rotation in the Partch lab. Thanks to Chris Ahlbach for your work on the PPI rate enhancements. Thanks to members of the R.S. Lokey lab and the G. Millhauser lab for your help with peptide synthesis and purification. Thanks to Eefei Chen for instrumentation training.

CHAPTER 1

EMERGING MODELS FOR THE MOLECULAR BASIS OF MAMMALIAN CIRCADIAN TIMING

ABSTRACT

Mammalian circadian timekeeping arises from a transcription-based feedback loop driven by a set of dedicated clock proteins. At its core, the heterodimeric transcription factor CLOCK:BMAL1 activates expression of *Period*, *Cryptochrome* and *Rev-Erb* genes, which feed back to repress transcription and create oscillations in gene expression that confer circadian timing cues to cellular processes. The formation of different clock protein complexes throughout this transcriptional cycle helps to establish the intrinsic ~24-hour periodicity of the clock; however, current models of circadian timekeeping lack the explanatory power to fully describe this process. Recent studies confirm the presence of at least three distinct regulatory complexes: a transcriptionally active state comprising the CLOCK:BMAL1 heterodimer with its coactivator CBP/p300, an early repressive state containing PER:CRY complexes, and a late repressive state marked by a poised but inactive, DNA-bound CLOCK:BMAL1:CRY1 complex. In this review we analyze high-resolution structures of core circadian transcriptional regulators and integrate biochemical data to suggest how remodeling of clock protein complexes may be achieved throughout the 24-hour cycle. Defining these detailed mechanisms will provide a foundation for understanding the molecular basis of circadian timing and help to establish new platforms for the discovery of therapeutics to manipulate the clock.

THE MOLECULAR OSCILLATOR AS A KEY MECHANISM IN HUMAN HEALTH

Predictable environmental changes arising from the rotation of Earth about its axis set the fundamental diurnal tempo of our lives. Intrinsic molecular clocks synchronize behavior and physiology into circadian (*about a day*) rhythms that are coordinated with the solar day to provide stability within an ever-changing environment. Nearly all cells in the human body contain an endogenous and cell-autonomous molecular clock[1] that regulate the expression of nearly 40% of the human genome in a tissue and time specific manner.[2] These so-called clock controlled genes (CCGs) are key components of important cellular processes including cell-cycle progression[3], energy homeostasis[4-10], xenobiotic metabolism[11], reproduction[12] and angiogenesis.[2]

Mammals possess a hierarchical circadian system that can be entrained through a host of environmental cues, called zeitgebers (from the German word “time giver”) including hormonal signals, exercise, food consumption and temperature.[13,14] The predominant zeitgeber is the absorption of blue light by the photo-sensing retinal melanopsin proteins[14-17]. Photoentrainment of the circadian system subsequently occurs as neural signals propagate along the retinohypothalamic (RHT) tract to the suprachiasmatic nucleus (SCN) [14,18] where kinase-based signaling pathways function to set the phase of the clock through the phosphorylation of CREB [19].Phosphorylated CREB induces the expression of the dedicated clock genes *Per1* and *Per2* by binding to cAMP response elements (CREs), thereby resetting the phase of the clock.[19] Commonly referred to as the master clock, the SCN is a highly networked bundle of neurons in the hypothalamus that maintains robust circadian oscillations through cellular coupling. Connections to the endocrine system allow the SCN to regulate circadian cycling at an organismal level through the thermal and hormonal triggered synchronization of the peripheral (cell-autonomous cellular) clocks.[14]

Proper circadian cycling is central to human health. Divergence between human behavior and the bodies’ circadian-controlled physiological processes have been shown to elicit adverse medical conditions such as cardiovascular disease, cancer, diabetes, depression, obesity and premature aging[3,20-23]. Understanding how circadian timekeeping occurs at the molecular level could inform new strategies for therapeutic discovery that aim to reinforce circadian systemic synchronization for its numerous health benefits. While the last fifteen years have seen major advances in our understanding of the genetic basis of circadian timing, we have not yet achieved a level of mechanistic insight comparable to other important global regulatory processes such as the cell cycle. A recent explosion of high-resolution structures of mammalian clock proteins, cistrome mapping and biochemical data support some aspects of the canonical model for clock function and challenge others.

TRANSCRIPTION FEEDBACK LOOPS DRIVE MOLECULAR OSCILLATIONS

All somatic cells possess cell-autonomous and endogenous molecular clock directed by a transcription/translation feedback loop (TTFL) with ~24 hour periodicity (**Fig. 1.1a**) The basic helix-loop-helix Per-Arnt-Sim (bHLH-PAS) proteins CLOCK and BMAL1 constitute a heterodimeric transcription factor that is the driving force behind the molecular clock in mammals.[24,25]

Transcriptional activation by CLOCK:BMAL1 at E/E' boxes in the promoters of the core clock genes *Period*, *Cryptochrome* and *Rev-Erb* initiates the beginning of negative feedback within the loop, which is ultimately closed when these factors enter the nucleus and repress transcription.[26-29] Subsequent cycles of activation and repression generate circadian oscillations (i.e. one peak per day) in the expression of clock proteins to determine the intrinsic timing of the molecular clock. In addition to the core clock genes, the TTFL regulates the expression of output genes to confer circadian timing to physiological processes in a tissue-specific manner (**Fig. 1.1b**).[30,31] Post-transcriptional regulation also plays an important role through RNA processing and stabilization to establish intrinsic circadian timing and clock-controlled output genes [32-35] .

The current model of the core feedback loop is defined by periodic regulation of CLOCK:BMAL1 activity from repressive complexes containing PER and CRY proteins. The intrinsic ~24-hour periodicity of the clock is regulated in large part by controlling the subcellular localization and stability of PER:CRY complexes through the opposing activity of kinases,

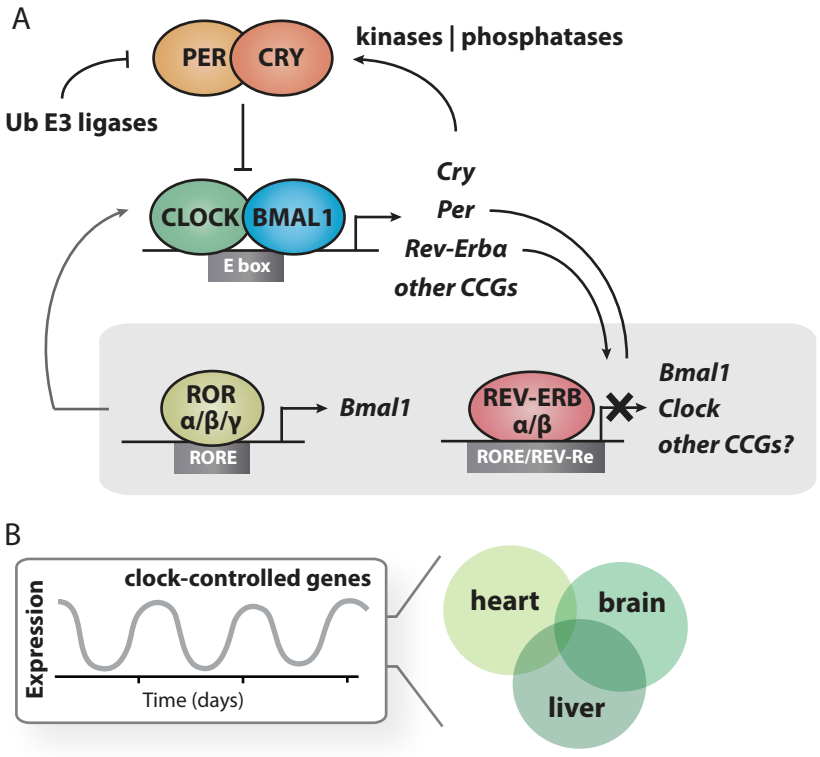

Figure 1.1: Transcription/translation feedback loops control mammalian circadian timing. (A) Core clock proteins interact with one another to regulate transcription (B) The circadian feedback loop creates oscillations in the tissue-specific expression of clock-controlled genes with 24-hour periodicity.

phosphatases and ubiquitin E3 ligases.[36-45] Loss of a single phosphoacceptor site within PER or modulation of kinase activity (by mutation or pharmacological inhibition) elicits periods ranging from ~20–44 hour,[46-49] underscoring an amazing flexibility that is inherent within the architecture of the circadian feedback loop. Therefore, post-translational regulation of PER and CRY helps to establish critical delays in feedback regulation that contribute to the 24-hour period of the clock.

A second, interlocked feedback loop involves the nuclear receptors ROR and REV-ERB, which generate oscillations in *Bmal1* expression and the cyclic repression of other gene targets.[50-52] Phenotypes of mice with deletions of individual genes within this interlocked feedback loop are mild;[53] however, deletion of both *Rev-Erb*α and *Rev-Erb*β genes disrupts circadian rhythms, demonstrating that cyclical repression at RORE and REV-Re elements by the REV-ERB proteins represents a critical component of circadian timekeeping.[54] In addition to ROR/REV-ERB, many other proteins work in concert with core clock proteins to regulate the epigenome and influence circadian transcriptional activity (MLL1, MLL3 SIRT1, EZH2, etc.).[55-59]

Determining how PER and CRY regulate CLOCK:BMAL1 activity will illuminate regulatory nodes within the feedback loop that can be further targeted for therapeutic intervention. A comprehensive mapping of the circadian cistrome in mouse liver shows that core circadian factors (CRY1/CRY2, PER1/PER2, CLOCK:BMAL1) are coordinately recruited to nearly 1500 sites in the genome. [33,34,60] The temporal pattern of their recruitment to clock-controlled genes such as *Dbp* (**Fig. 1.2a**) generally agrees with the canonical TTFL model where CLOCK:BMAL1 activity is repressed by a PER:CRY complex in the evening from CT12 – CT20. Analysis of native PER:CRY complexes by mass spectrometry and co-IP demonstrates that they contain additional proteins capable of eliciting transcription termination and epigenetic changes that reduce transcriptional activation (**Fig. 1.2c**).[61,62] PER:CRY complexes are very large, approaching several megadaltons in mass, and recent studies show that constituents of the complex can evolve over time,[63,64] expanding the initial, simplified view of a static PER:CRY repressive complex.

Perhaps the most striking conclusion to arise from recent studies is the clear evidence for a late repressive complex constituted by DNA-bound CLOCK:BMAL1 with CRY1, independent of PER proteins, that exists from CT0-CT4 (**Fig. 1.2b**).[60,65,66] The foundation for this emerging

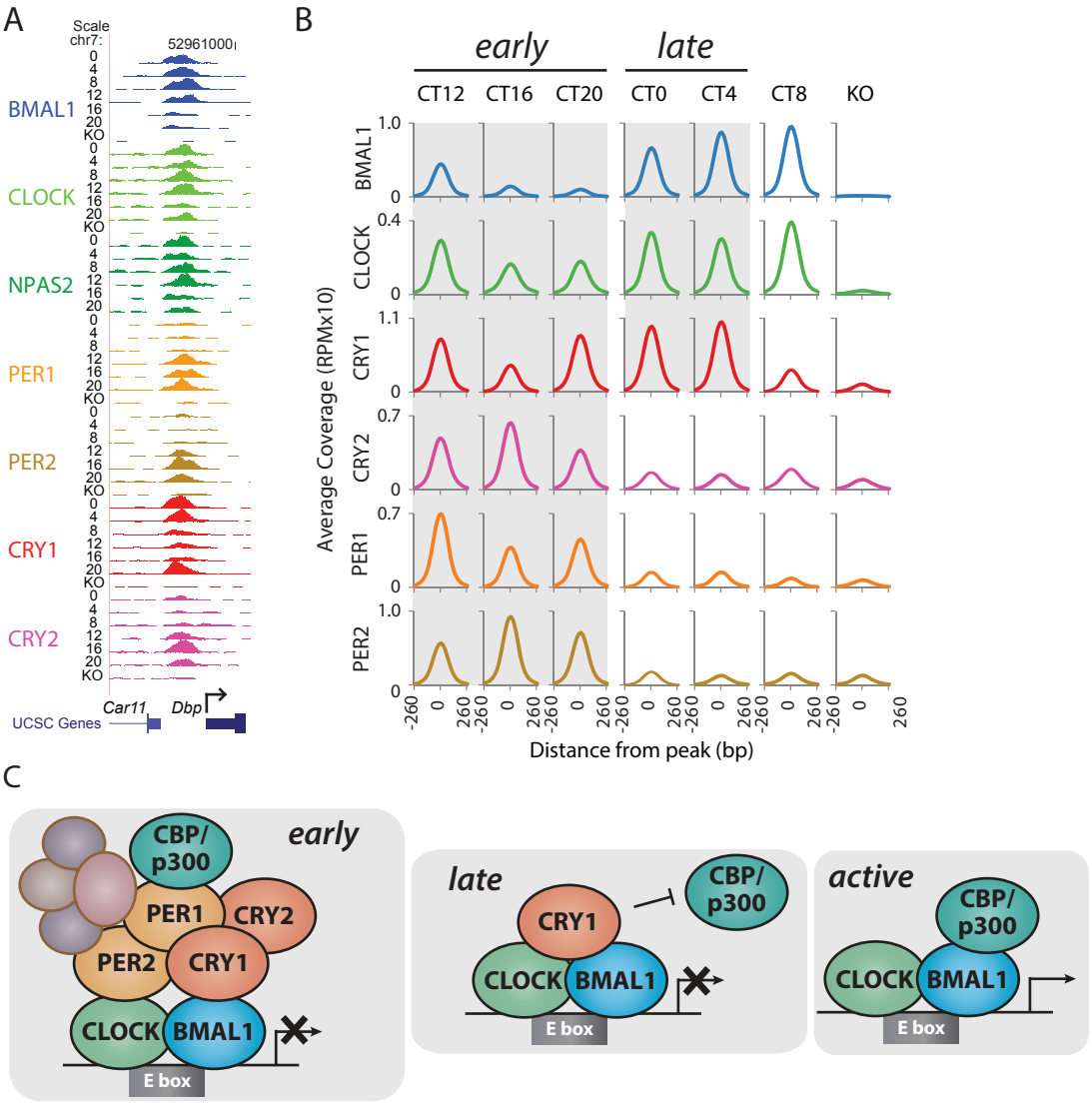

Figure 1.2: Multiple transcriptional regulatory complexes within the circadian feedback loop. (A) UCSC genome browser view of core clock protein occupancy at a portion of the Dbp locus on chromosome 7 (chr7), representing normalized chromatin immunoprecipitation and massively parallel sequencing read coverage at single time points within the circaidan cycle. Six timepoints are shown every 4 hours beginning at circadian time 0(CT0) and ending at CT20, with knockout (KO) mice as controls. (B) Binding coverage profiles [RPM (reads per million) x 10] from ChIP-Seq data illustrate the temporal basis of clock protein recruitment to their 1444 common sites. Gray boxes behind the data illustrate composition of the putative clock protein complexes. Parts A and B from Ref. 60. Reprinted with permission from AAAS. (C) Cartoon schematics of distinct clock regulatory complexes based on ChIP-Seq and proteomic data, including the large early repressive PER:CRY complexes, and the late ternary CLOCK:BMAL1:CRY complex.

model of the clock originates from biochemical studies in the Sancar lab providing the first evidence for a ternary CLOCK:BMAL1:CRY complex *in vitro* and *in vivo* that is incompatible with PER binding.[66] ChIP-Seq studies in mouse liver indicate that recruitment of the early repressive PER:CRY complex, the late repressive CRY1 complex and the transcriptional activators CBP/p300 to CLOCK:BMAL1 are three temporally distinct phases of the molecular cycle. Concomitant analysis of RNA Pol II complexes throughout the circadian cycle indicate that the late, CRY1-containing repressive complex most likely represents a poised but inactive form of CLOCK:BMAL1 (**Fig. 1.2c**). These studies suggest that binding of CRY1 to CLOCK:BMAL1 may hold off activation by coactivators CBP/p300 and thus transcriptional initiation until CT8.[60] This model is consistent with a critical role for the delayed expression of *Cry1* and its exclusive ability to support cycling in minimal cellular oscillators.[67-69] Accumulating evidence from genetic, chemogenetic and computational modeling studies further supports the spatiotemporal separation of key PER and CRY functions in the feedback loop.[70-72] Recent structural and biochemical data further support this exciting new role for CRY1 and will be discussed later in this review.

PROTEIN ARCHITECTURE OF CORE CIRCADIAN TRANSCRIPTIONAL REGULATORS

The repertoire of high-resolution structures of mammalian clock proteins has increased dramatically in the last three years to include most of the structured domains of the core positive and negative circadian regulators (**Table 1.1** and **Fig. 1.3**). These structures provide a foundation for understanding the biochemistry of clock proteins and yield insight into the disruptive power of mutations that arise from forward genetic screens. The conservation of domain architectures between positive and negative regulators suggests that they use common structural motifs to interact with DNA and/or core clock proteins (**Fig. 1.3**). For example, REV-ERB proteins share the same common nuclear receptor architecture as the RORs, although they bind different ligands within their LBDs and lack a specific helix that is needed to interact with transcriptional coactivators, thus designating them as constitutive repressors.[73] By contrast, CLOCK and BMAL1 are defined by their tandem PAS domains, which mediate heterodimerization[25], and disordered C-termini that regulate their activity.[55,74-76] PER proteins also have tandem PAS domains that control formation of PER homo- and heterodimers[77,78] followed by a long, disordered C-terminus that contains binding sites for kinases and cryptochrome.[79,80]

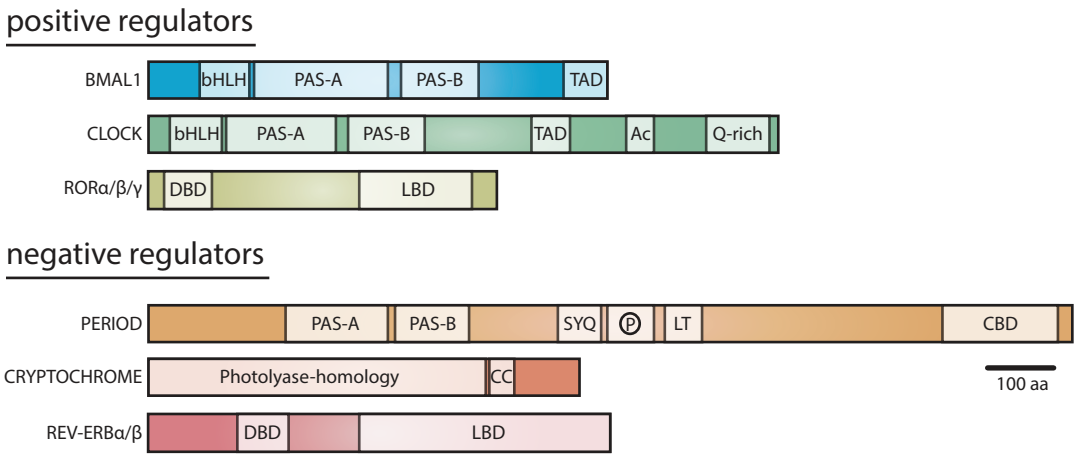

Figure 1.3: Domain architecture of core circadian transcriptional regulators. The location and size of conserved domains within core clock proteins is indicated according to scale bar.

Table 1.1: List of clock protein structures.

Protein[a]	Domain(s)	Ligand	Method	Resolution[b]	PDB ID	Year[c]
mCLOCK:mBMAL1	bHLH	DNA	xtal	2.27 Å	4H10	2012
mCLOCK:mBMAL1	bHLH-PAS-AB		xtal	2.40 Å	4F3L	2012
mBMAL2	PAS-B		NMR		2KDK	2011
mPER1	PAS-AB		xtal	2.75 Å	4DJ2	2012
mPER2	PAS-AB		xtal	2.40 Å	3GDI	2009
mPER3	PAS-AB		xtal	2.50 Å	4DJ3	2012
mCRY1	PHR-CC		xtal	2.65 Å	4K0R	2013
mCRY1	PHR-CC	PER2 CBD	xtal	2.45 Å	4CT0	2014
mCRY2	PHR-CC		xtal	2.70 Å	4I6E	2013
mCRY2	PHR-CC	FAD	xtal	2.20 Å	4I6G	2013
mCRY2	PHR-CC	FBXL3-SKP1	xtal	2.70 Å	4I6J	2013
mCRY2	PHR-CC	KL001	xtal	1.94 Å	4MLP	2013
hREV-ERBα	LBD	NCoR peptide	xtal	2.60 Å	3N00	2010
hREV-ERBα	DBD	DNA	xtal	2.80 Å	1HLZ	2001
hREV-ERBβ	LBD		xtal	2.40 Å	2V0V	2007
hREV-ERBβ	LBD	Heme	xtal	1.90 Å	3CQV	2008
hRORα	LBD	Cholesterol	xtal	1.63 Å	1N83	2002
rRORβ	LBD	Retinoic acid	xtal	1.50 Å	1NQ7	2003
hRORγ	LBD	Hydroxy-cholesterol	xtal	2.35 Å	3KYT	2010

[a] Core transcriptional regulators only

[b] NMR structure represents 10 lowest energy structures

[c] Release date

Cryptochromes have distinctly different protein architecture from the other core clock proteins as they lack PAS domains. Most of the protein is composed of a photolyase homology region (PHR) that bears strong structural similarity to photolyase.[81] In addition to the PHR, cryptochromes possess disordered C-termini that are not present in photolyase ancestors. Also unique to mammalian cryptochromes is a highly conserved helix just after the PHR that has a periodic spacing of nonpolar residues common to coiled coils, thus designated the CC helix.[82] The CC helix plays a central role in the biochemistry of the mammalian clock by facilitating competitive interactions between CRY and its E3 ubiquitin ligase FBXL3 and PER[83] to regulate its stability, and by mediating the ability of CRY to repress the CLOCK:BMAL1 complex.[82] The structural basis of competition for the cryptochrome CC helix will be discussed later in this review.

PAS DOMAINS

Present in tandem in three of the four core clock proteins, PAS domains have a central role in clock protein function.[84] Originally identified through conservation of a minimal sequence motif from *Drosophila* to mammals (**Fig. 1.4a**) [84], PAS domains function as sensors of chemicals and light, and act as oligomerization nodes. Since the original identification of the PAS motif, the definition of a PAS domain as been expanded to include the highly conserved secondary structure topology, consisting of a five-stranded antiparallel β-sheet flanked on one side by a series of α-helices. These strands are named alphabetically from the first (Aβ) to the final β-strand (Iβ) of the domain (**Fig. 1.4b**).[85] The original PAS motif is restricted to the conserved residues that form the short helices that run along the front of the PAS domain, and the accompanying PAS-associated C-terminal (PAC) motif encompasses part of the β-sheet. While acknowledging the historical significance and sequence conservation of PAS motifs, we argue that it is important to define PAS domains as their folded, biologically relevant domains rather than fragmented sequence motifs. A comparison of the boundaries of PAS domains identified in the recent crystal structures of mCLOCK to the bioinformatic PAS/PAC predictions is illustrated in Table 2.

Several features distinguish the PAS-A and PAS-B domains of tandem PAS-containing proteins although they share the same core PAS domain fold (**Fig. 1.4d**). PAS-A domains frequently possess an N-terminal helix termed A'α that docks onto the β-sheet to mediate PAS-PAS interactions (**Fig. 1.4b,d**).[85] PAS-A domains also tend to have longer flexible loops

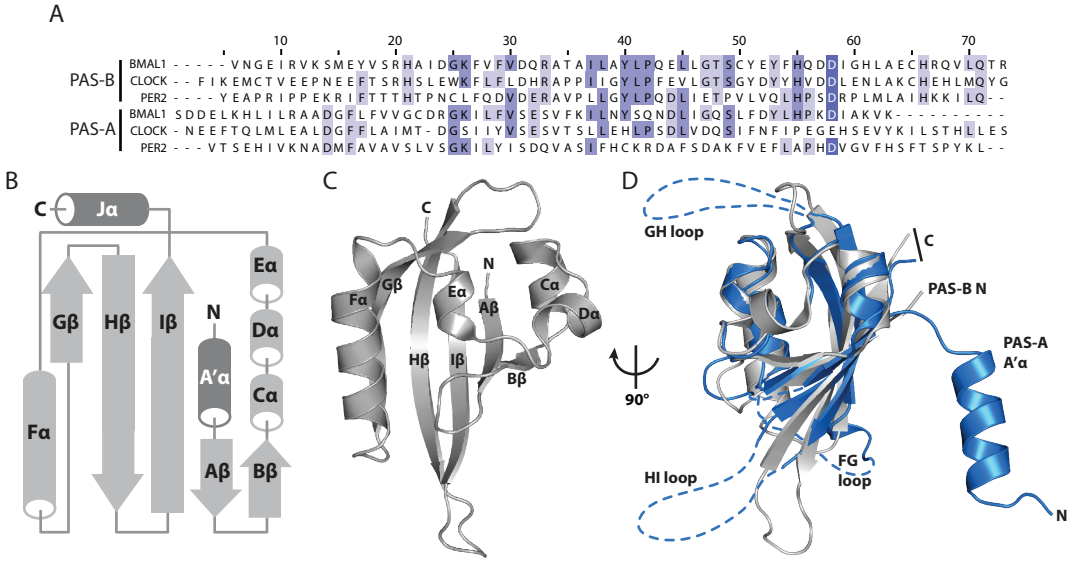

Figure 1.4: The PAS domain. (A) Alignment of UniPROT PAS motifs for mammalian CLOCK, BMAL1 and PER2. (B) Secondary structure topology of PAS domains. The core PAS fold in encoded by the structural elements in light gray, while the dark gray A'α and Jα helices represent structural elements associated with certain PAS domains. N, N-terminus; C, C-terminus. (C) Tertiary structure of a PAS domain. Secondary structure elements are labeled throughout the mouse BMAL1 PAS-B domain (PDB: 4F3L). (D) Conservation of the PAS domain core in PAS-A and PAS-B domains despite distinct changes in domain size. Gray, BMAL1 PAS-B domain; Blue, BMAL1 PAS-A domain (PDB: 4F3L). Note the lack of structured FG, GH, and HI loops (dashed blue lines) and the presence of an A'α helix for the PAS-A crystal structure.

Table 1.2: PAS domain boundaries in representative clock proteins

Protein[a]	Domain[b]	Residues	Motif[c]	Residues
CLOCK	PAS-A	106 – 258	PAS 1	107 – 177
	PAS-B	274 – 376	PAS 2	262 – 332
			PAC	336 – 379
BMAL1	PAS-A	142 – 320	PAS 1	143 – 215
	PAS-B	353 – 442	PAS 2	327 – 397
			PAC	402 – 445
PER2	PAS-A	191 – 315	PAS 1	179 – 246
	PAS-B	329 – 435	PAS 2	319 – 385
			PAC	393 – 436

[a] UniPROT accession: mCLOCK O08785, mBMAL1 Q9WTL8-4, mPER2 O54943)

[b] Determined from domain boundaries in crystal structures 4F3L and 3GDI; includes A'α helix (PAS-A) or Jα helix (PAS-B) where appropriate

[c] UniPROT database (www.uniprot.org)

(~25-35 residues) between the Gβ–Hβ or Hβ–Iβ strands (known as the GH and HI loops, respectively). The importance of these disordered loops within PAS-A domains is generally not well understood within the bHLH-PAS family. The loops could be regulated by posttranslational modification or mediate interactions with transcriptional regulatory proteins, both of which are facilitated by backbone flexibility.[86] Along these lines, the BMAL1 PAS-A is sumoylated at a conserved lysine in the GH loop to regulate CLOCK:BMAL1 activity through an unknown mechanism.[87] By contrast, PAS-B domains are generally much more compact than PAS-A domains with shorter loops (**Fig. 1.4d**). Some PAS-B domains have a C-terminal helix termed Jα (**Fig. 1.4b**) that can dock onto either the α-helical or β-sheet face of the PAS-B domain in a reversible manner to regulate PAS domain function.[88,89] Therefore, not all PAS domains are alike although they share a common core fold, suggesting that PAS-A and PAS-B domains could contribute to clock regulation through different mechanisms.

Both the α-helical and β-sheet interfaces of PAS domains can interact with PAS domains and other proteins in a variety of modes to control the architecture of transcriptional regulatory complexes.[25,90-92] For example, the ARNT PAS-B simultaneously mediates heterodimer formation with the PAS-B domain of its bHLH-PAS partner HIF-2α and recruits coactivators needed to activate gene expression for hypoxia adaptation.[93] Notably, the PAS domains of CLOCK, BMAL1 and PER have been implicated in recruitment of PER to the CLOCK:BMAL1 complex by truncation/co-IP studies from cells[94], but we still lack biochemical confirmation of direct interactions *in vitro*. Understanding how the PAS domains of mammalian clock proteins assemble transcriptional regulatory complexes will provide important insight into clock function.

The close relationship of mammalian PAS domains to those in plants and bacteria that bind small molecule ligands and possess direct sensory capabilities suggests the intriguing possibility that small molecule metabolites could regulate clock function through the PAS domains.[85] Indeed, the PAS domains of PER, CLOCK and NPAS2 are reported to bind heme *in vitro*[95-97], but there is some disagreement over heme binding[98] and the physiological relevance of these interactions has yet to be clearly demonstrated in cell-based assays or *in vivo*.[95-98] The general plasticity of PAS domains that allows this small conserved fold to accommodate chemically diverse ligands has been exploited to find small molecules that bind within the solvated cores of PAS domains in the mammalian hypoxia adaptation response pathway.[99] Ligand binding

within the PAS-B domains of HIF-2α and ARNT allosterically regulates protein interactions to inhibit transcriptional responses to hypoxia.[100-103] While researchers may have yet to identify endogenous ligands for PAS domains in circadian proteins, it should be possible to identify exogenous ligands that target PAS domains of the molecular clock to exploit them for regulation.

PERIOD: A PAS DIMER AT THE HEART OF THE CLOCK

PER proteins have a fundamentally important role within the mammalian circadian clock, as changes in their posttranslational modification state throughout the day exert exquisite control over the stability and localization of early PER:CRY repressive complexes.[104] Attenuating this process with kinase inhibitors can lengthen the period of the molecular clock[37,48,49,105,106], demonstrating that PER proteins help establish the rather long, circadian period of the feedback loop. Moreover, induction of *Per* mRNA by external stimuli known as zeitgebers (*time givers*) controls the phase of the molecular oscillator to synchronize internal clocks with the environment.[19,107] Because PER proteins are stoichiometrically limiting for assembly of clock protein complexes,[108] the introduction of naïve PER protein at different points within the feedback loop appears to advance or delay the molecular oscillator by controlling assembly of the early repressive complex. Therefore, understanding the biochemical basis of PER interactions with other clock proteins and transcriptional regulators will provide key insights into the molecular basis of circadian timing.

PER proteins exist as homo and heterodimers *in vivo*,[78] and given the observation of PAS dimers in other systems,[84] attention focused on the PAS domains as likely candidates for dimerization domains. Crystal structures have been solved for the tandem PAS domains of all three PER proteins, each displaying the same PAS-B-mediated dimer (**Fig. 1.5a-b**).[89,109] The PAS-B β-sheets interact in an antiparallel orientation (**Fig. 1.5e-f**) similar to the HIF-2α:ARNT PAS-B dimer,[90] using a highly conserved tryptophan in the HI loop (W419 in PER2) to pack onto a predominantly hydrophobic cleft on the β-sheet of its partner (**Fig. 1.5g**). This appears to be the predominant dimer interface within full-length proteins, and disruption of these interactions alters the mobility of full-length PER proteins in the cell.[109] Moreover, in-frame deletion of the PAS-B domain in the *Per2*^{Brdm} mutant disrupts clock function,[110] but it unclear whether the phenotype arises from loss of PER dimers or disruption of other functions. One such role could be subcellular localization, as each PAS-B domain has a C-terminal Jα helix that comprises

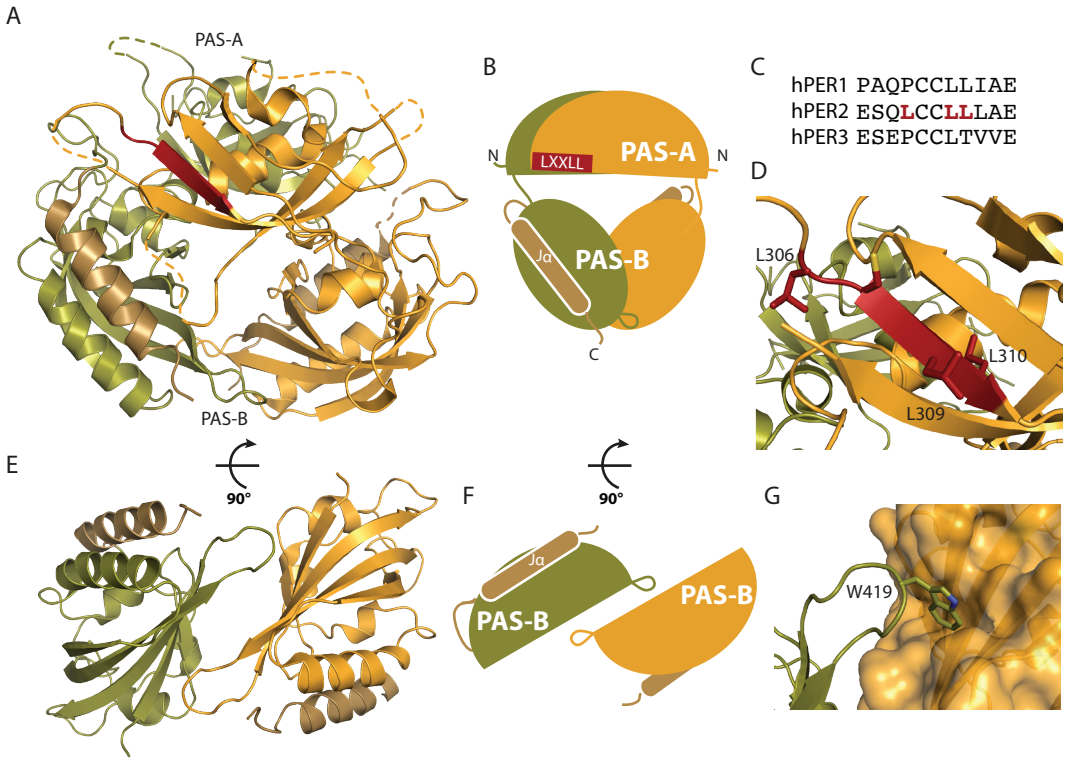

Figure 1.5: The PER2 PAS-AB dimer structure. (A) Crystal structure of the mouse PER2 tandem PAS-AB domains (PDB: 3GDI). Monomers colored in orange and olive with the Jα helices in tan. The conserved LXXLL motif in PER2 PAS-A is colored in red. Dashed lines represent disordered loops absent in the crystal structure. (B) A cartoon of the relative PAS domain orientations in the crystal structure. (C) PER2 has an LXXLL motif not conserved in PER1 or PER3. (D) A close-up view of the LXXLL motif in the PER2 PAS-A domain with sidechains of the motif leucines labeled. (E) Antiparallel orientation of the PAS-B dimer, shown without PAS-A domains for clarity. (F) A cartoon of the relative orientation of the PAS-B domains, illustrating contacts between the HI loop of one domain and the β-sheet of the other domain. (G) A close-up view of the HI loop with the sidechain of residue W419 shown docking into its hydrophobic cleft on the β-sheet of its partner PAS domain.

an active nuclear export signal.[111] Residues of the export motif also mediate direct interaction with the α-helical face of the PAS-B domain,[89,109] suggesting that the structure represents an inhibited NES and that the interaction is regulated and/or reversible in solution. Given that the β-TrCP-dependent PER2 phosphodegron is also located immediately downstream of the Jα helix,[43] these structural insights hint that there is still rich biochemistry to explore within the PAS domain structures.

The PAS-A domains sit above the PAS-B dimer and lack substantial contacts with either the PAS-B domains or each other, suggesting that they have the ability to assume various structures in solution. The PER2 PAS-A domain has an LXXLL motif that is needed to interact

with REV-ERBα and other nuclear receptors (**Fig. 1.5a-c**).[112] Canonical LXXLL motifs present the conserved leucine sidechains on one face of a helix to interact with a host of transcriptional regulators.[113,114] However, the LXXLL motif in PER2 is embedded with the Iβ strand of the PAS-A domain (**Fig. 1.5d**) suggesting that it may not have a role in direct binding, at least in terms of a canonical LXXLL motif. Nevertheless, mutational analyses of this region show that this PAS-AB interface is important for interaction with nuclear receptors.[112] Further study here will help to define how PERs could regulate transcription outside of the core clock loop, consistent with their recruitment to thousands of sites throughout the day outside of CLOCK:BMAL1 control, including nuclear receptor motifs.[60]

A region comprising the tandem PAS domains of PER has been found to interact with the PAS-containing regions of individual CLOCK and BMAL1 proteins by co-IP[75,94] and is generally presumed to represent the basis for recruitment of PER:CRY complexes to CLOCK:BMAL1 early in the repressive phase of the feedback loop. However, full-length PER2 purified from insect or mammalian cells either as a pure protein or in complex with CRY1, respectively, does not interact directly with the CLOCK:BMAL1 complex on DNA *in vitro*;[66,115] either the purified protein(s) lack essential post-translational modification(s) needed to interact with each other or other proteins are needed to bridge the interaction. While co-IP assays provide some insight into protein complexes, they lack the ability to elucidate direct protein interactions within complexes or discriminate possible heterogeneity of complexes in solution. Therefore, the question of how early repressive PER:CRY complexes are recruited to DNA-bound CLOCK:BMAL1 remains one of the central unanswered questions in the biochemistry of the mammalian clock.

Aside from the tandem PAS domains, PER proteins are largely unstructured, a feature that PER proteins share with their functional analog FRQ in *Neurospora*.[116] The lack of intrinsic structure in a protein with many interaction partners provides a thermodynamic advantage by allowing specificity and affinity to be tuned for multiple partners.[117,118] In addition to binding promiscuity, unstructured regions could allow for variable posttranslational modifications and rapid degradation when not in complex with their binding partners. Many examples of how intrinsic disorder modulates protein stability have been noted in other systems[119], including the immediate posttranslational degradation of the *Neurospora crassa* clock protein FRQ when not in complex with its partner, FRH.[116] Because the lack of tertiary structure removes purely

architectural constraints on conservation, alignment of intrinsically disordered regions tends to highlight functionally important residues. Algorithms such as PONDR use sequence biases to predict disorder,[120] but of particular interest are predictions for short regions of order within long stretches of disorder, represented as downward spikes in the PONDR prediction (**Fig. 1.6a**). These 'minima' represent regions with increased propensity to form secondary structure, typically α-helices, which often act to nucleate formation of protein interactions.[121] Aside from the ordered PAS domains, many of the minima in PER2 have weak predictions of secondary structure and high sequence conservation, serving as a useful guide for future biochemical studies of PER function.

Binding sites for the kinases CKIδ and CKIε represented by the SYQ and LT motifs are minima that are highly conserved in PER across phyla (**Fig. 1.6a-b**). [79] Conservation of these regions with the *C. elegans* PER homolog LIN-42,[122] which controls developmental timing,[123,124]

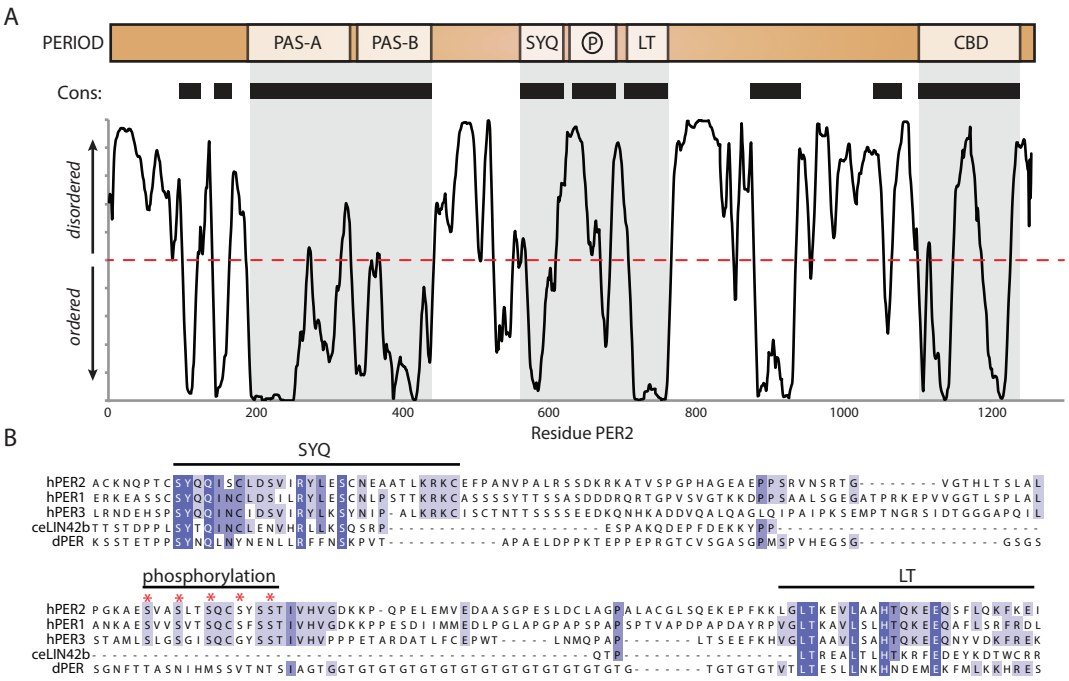

Figure 1.6: Conservation and disorder in PER2. (A) The domain architecture of PER2 is aligned above the PONDR prediction of disorder. Within this plot, curves below the red dashed line are predicted to be ordered, while those above the line are flexible; stretches longer than 30 residues classify as 'intrinsic disorder'. Regions exhibiting a high degree of conservation (cons.) between PER1 and PER2 are represented as black bars below the domain schematic. Gray boxes denote known regions of functional importance: PAS dimer, kinase-binding SYQ/LT regions, and the CRY-binding domain (CBD). (B) Alignment of the SYQ-phosphorylation-LT region shows conservation of key sequence motifs amongst human and *Drosophila* PER proteins and the *C. elegans* PER-homolog LIN-42, isoform b.

and in *Drosophila* where it impacts PER clock function[125] suggests that they represent an ancient site for regulation of PER activity. The multisite phosphorylation cassette that controls subcellular localization of mammalian PERs is located between the SYQ and LT motifs (**Fig. 1.6b**).[46] We speculate that additional conserved minima in PER2 may recruit other proteins to form the native megadalton transcriptional regulatory complexes seen *in vivo*.[61-63] The extreme C-terminus of PER1 and PER2, but not PER3, harbors a conserved CRY-binding domain (CBD) that is essential for clock function.[80,94,115] Control of CRY through its interaction with PER at this site represents a critical component of the mammalian feedback loop. Therefore, the absence this motif in PER3 may explain its nonessential role in the feedback loop,[126,127] while still allowing for modulation of circadian timing through heterodimer formation with PER1 or PER2 to titrate CRY recruitment from the early repressive complex.[128]

CRY1: THE CIRCADIAN REPRESSOR

Since their discovery fifteen years ago, CRY proteins have been acknowledged as a key negative regulator of the core circadian feedback loop. Cryptochromes repress CLOCK:BMAL1 transcriptional activation in reporter assays and their loss in *Cry1*$^{-/-}$*Cry2*$^{-/-}$ animals leads to increased expression of clock target genes and disruption of the feedback loop, consistent with global derepression of CLOCK:BMAL1.[27,28,129,130] However, the mechanism by which cryptochromes repress CLOCK:BMAL1 to 'close' the feedback loop on a daily basis is still not known. Early studies of native clock proteins by co-IP demonstrated that PER:CRY complexes interact with CLOCK:BMAL1 in the early phase of repression, helping to establish the canonical model for the feedback loop (**Fig. 1.1a**).[104] Concurrent with these studies, it was observed that CRY can repress CLOCK:BMAL1 after transient transfection in cell-based reporter assays without stoichiometric PER, including in heterologous systems that lack all mammalian PERs.[127] While these initial studies provided clear evidence that CRY does not need PER to assert its repressive function on CLOCK:BMAL1, concerns over artifacts from transfection studies proved the need for further studies to resolve the roles of PER and CRY in the clock

Recent biochemical, structural and genomic mapping studies highlight several lines of evidence that challenge the canonical feedback loop model. First, CRY interacts with the CLOCK:BMAL1 complex on DNA *in vitro* and *in vivo* to form what has been dubbed the 'late repressive complex' (**Fig. 1.2c**).[60,65,66] In the mouse liver, CRY is found at the CLOCK:BMAL1

complex on DNA in the early morning without PER; this ternary complex is suggested to represent a poised but repressed state that holds off activation by the histone acetyltransferases p300/CBP until the appropriate time of day.[60] Consistent with this, PER proteins are not needed for CRY to repress CLOCK:BMAL1 activation of the *Dbp* locus *in vivo.*[66] Second, PER proteins titrate CRY away from ternary CLOCK:BMAL1:CRY complexes *in vitro* and *in vivo.*[66,94,115] The C-terminal CRY-binding domain (CBD) of PER1 and PER2 is sufficient for this activity[94,115] and the feedback loop is disrupted when the PER2 CBD is constitutively expressed.[94] Thus, one function of early repressive complexes may be to protect and hold CRY stably in reserve bound to PER until initiation of the late repressive phase, when CRY interacts directly with CLOCK:BMAL1.[60,65] This model may explain the sensitivity of the circadian feedback loop to PER:CRY stoichiometry.[108,131,132] Given the body of evidence that points to both independent and combined roles for PER and CRY, it may be time to reevaluate the canonical model for the mammalian circadian feedback loop.

Cryptochrome structure is largely based on its homology to photolyase, encompassing a ~50 kDa photolyase homology region (PHR) with an N-terminal α/β domain and C-terminal α-helical domain that harbors the canonical flavin-binding site.[81] Mammalian CRYs bind FAD weakly due to structural variations that create much shallower flavin binding site than photolyases.[83,133] The predominant structural features that distinguish CRYs from photolyase are their disordered C-terminal tails.[134] The CRY C-termini are divergent from one another and dispensable for generating the molecular feedback loop, but their deletion alters the period and amplitude of cycling,[69,82] indicating that they can modulate clock protein function. Consistent with this regulatory role, the C-termini possess several phosphorylation sites and a nuclear localization signal.[135-137] To date, no CRY structures have included the C-terminal tails, most likely due to their intrinsic flexibility. However, the C-termini interact in trans with the PHR *in vitro* and are partially protected from proteolysis in the full-length protein, suggesting that interaction with the PHR may impart some order to the tails.[134,138] Understanding the cryptic role of CRY C-termini interactions with the PHR and other clock proteins represents a structural biology challenge that may require moving beyond x-ray crystallography.

Two highly conserved motifs on CRY are needed for its function in the clock: a hydrophobic motif adjacent to the flavin-binding site termed the interface loop or C-terminal lid[83,139] and the

CC helix.[82] The PER2 CBD[140] and the E3 ubiquitin ligase FBXL3[83] both engage these motifs, wrapping snugly around the CC helix (**Fig. 1.7a**). The overlapping nature of binding sites on the CRY CC helix nicely explains the stabilizing effect that PER has on CRY *in vivo;*[104,141] by interacting with the PER2 CBD, CRY is restricted from interacting with its E3 ubiquitin ligase.[83] Moreover, these structures demonstrate how the small molecule KL001 stabilizes CRY by competing with the FBXL3 C-terminus for binding at the flavin-binding cleft.[70,142] Altogether, an elegant integration of high-resolution structures, biochemistry and *in vivo* studies provides a solid model for regulation of CRY stability and localization predicated on antagonistic interactions at overlapping binding sites.

The elusive role of Timeless in the mammalian clock[143] may result from its involvement in this competitive, regulatory mechanism through its interactions with the CRY CC helix.[144] As

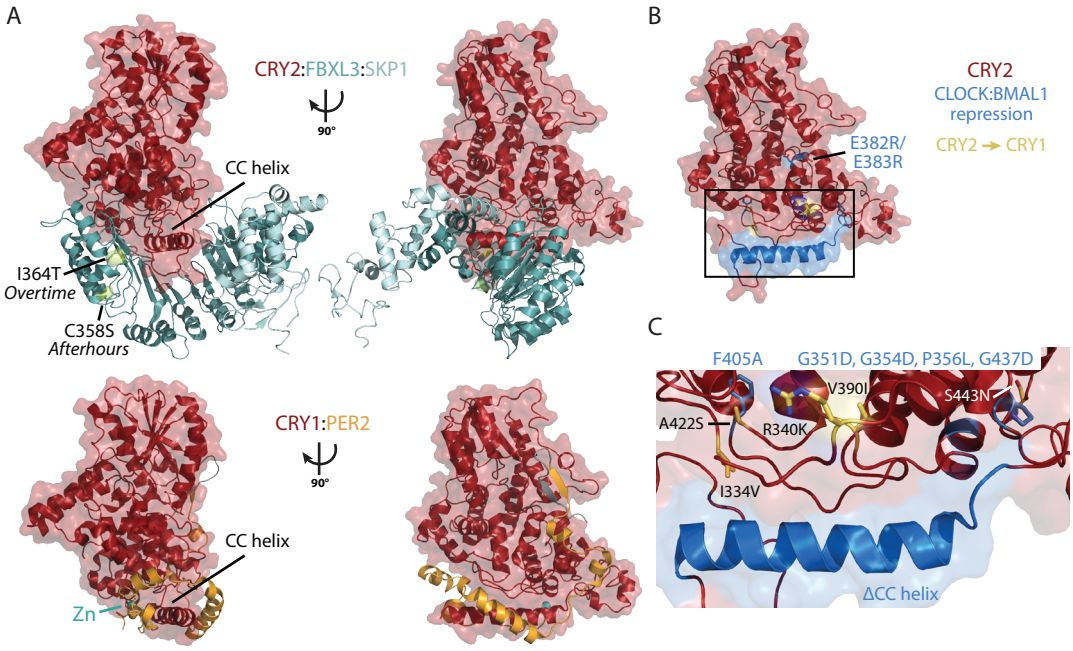

Figure 1.7 Competition for the CC helix controls CRY function in the feedback loop: (A) Crystal structures of mouse CRY2 in complex with FBXL3:SKP1 (top, PDB: 4I6J) and mouse CRY1 in complex with PER2 CBD (bottom, PDB: 4CT0) illustrate their overlapping binding sites. Location of FBXL3 *Afterhours* and *Overtime* mutations is depicted with the residues shown as spheres (citron). Location of CRY1:PER2–coordinated zinc is shown as a sphere (teal). (B) Crystal structure of apo mouse CRY2 (PDB: 4I6E) shown in red with residues needed for repression of CLOCK:BMAL1 highlighted in blue. Residues that confer CRY1 activity to CRY2 are shown in yellow. (C) A close-up view of one face of CRY illustrating residues needed for CLOCK:BMAL1 repression. Side chains for CRY1 residues that confer cycling ability to CRY2 in yellow, labels in black; side chains for residues needed to repress CLOCK:BMAL1 in blue, labels in blue above box.

a replication fork-associated factor[145], Timeless is involved in DNA damage repair and checkpoint activation, and its expression is strictly controlled by the cell cycle. [143,145-149] Therefore, its interaction with CRY suggests that it may serve to connect the circadian clock with cellular proliferation.[146] Exciting studies also suggest that Timeless could play a role in conveying phase-resetting *zeitgebers* arising from DNA damage to the core feedback loop.[144,150-152] Finally, like PER, cryptochromes also interact with nuclear receptors[21] and are recruited to thousands of sites outside of CLOCK:BMAL1 regulation each day to expand the scope of circadian transcriptional regulation.[60] Defining the molecular basis of these interactions with CRY will provide further insight into its regulation and activity in the core clock feedback loop and beyond.

Underscoring the importance of competition for CRY regulation, the same interface used as a hot-spot to regulate CRY localization and stability is also needed to regulate CLOCK:BMAL1 activity.[69,82] The CC helix interacts directly with the transcriptional activation domain (TAD) of BMAL1 *in vitro*[139] and mutations of the BMAL1 TAD or CRY CC decrease repression by CRY.[75,76,153] Additional residues needed to repress CLOCK:BMAL1 activity and drive the feedback loop surround the CC helix (**Fig. 1.7b-c**). Some of these residues are unique to CRY1 and can confer the ability to drive cycling in minimal cellular oscillators to CRY2, a property it otherwise lacks without compensation from systemic properties.[67,69] The presence of distinctive residues within the CRY1 PHR required for repression that do not overlay the PER2 CBD binding site[140] suggest they may be involved in interactions with CLOCK:BMAL1. While the model that CRY may function by antagonizing coactivators to hold off transcription has been slowly emerging over the last few years, the mechanism by which cryptochromes interact with and repress CLOCK:BMAL1 has not yet been elucidated.

CLOCK:BMAL1—THE PRINCIPAL CIRCADIAN TRANSCRIPTION FACTOR

Although a detailed model of the core circadian feedback loop is beginning to emerge, many questions still remain. Recent structures of the CLOCK:BMAL1 heterodimer provide a solid foundation for these models by elucidating the protein architecture of the primary circadian transcription factor and how it binds DNA. Functional studies augment the crystal structure models and demonstrate that intrinsically disordered regions in both CLOCK and BMAL1 (**Fig. 1.8a**) play critical roles in regulation of CLOCK:BMAL1 activity *in vivo,*[24,74-76,154,155] as they do within the larger bHLH-PAS family of transcription factors.[156]

During the active phase of the circadian complex, the transcriptional coactivators CBP/p300 interact directly with BMAL1 to initiate transcription through acetylation of histone H3 and recruitment of basal transcriptional machinery at E-box promoter regions.[60,157-160] Somewhat perplexingly, CBP/p300 also interact with PER and are found in the early repressive PER:CRY complex, while they are absent from the late repressive complex that contains CRY1.[60] CLOCK:BMAL1 also recruits additional coactivators during the active phase of transcription including MLL and TRAP150.[55,56,161] The molecular mechanisms that lead to transcriptional activation at CLOCK:BMAL1 sites, and therefore reinitiation of the feedback loop, are still relatively poorly defined but play an important role in the feedback loop mechanism.

A structure of the bHLH heterodimer in complex with its cognate E-box recognition sequence provides the first detailed view of interactions that determine the specificity of CLOCK:BMAL1 recruitment to DNA and its regulation by phosphorylation.[162,163] In contrast to studies showing a dramatic effect of the redox state of NAD cofactors on DNA binding *in vitro,*[164,165] this new study finds no effect of NAD cofactors on the conformation of the bHLH heterodimers or their affinity for DNA.[162] Moreover, the redox ratios of NAD cofactors previously found to influence the CLOCK:BMAL1 complex are not likely to occur in cells,[166] indicating that DNA binding is probably not regulated directly by changes in NAD redox status. The structure of the isolated bHLH domains bound to DNA is highly similar to bHLH domains within the larger bHLH-PAS-AB heterodimer structure obtained in the absence of DNA (**Fig. 1.8a**)[25], suggesting that large changes in conformation of the bHLH domains upon DNA binding are unlikely.

CLOCK and BMAL1 PAS domains form the major basis for heterodimer recognition and stability of the complex.[25] Within the complex, both BMAL1 PAS domains are presented on one face and the CLOCK PAS domains on the other (**Fig. 1.8a**). The PAS-A domains form the heart of the heterodimer complex by swapping their A'α helices to interact with the β-sheet of the opposing PAS-A domain (**Fig. 1.8b**) and disruption of this helical embrace significantly disrupts heterodimer stability in cells.[25] A mutation in the linker between CLOCK PAS-A and PAS-B (I254N) found in a zebrafish ENU screen causes a short period;[167] Ile254 is buried under the CLOCK:BMAL1 PAS-B domains and relatively inaccessible to solvent, suggesting that the mutation may influence the packing or flexibility of the two PAS-B domains in relation to the bHLH-PAS-A core of the complex. The BMAL1 PAS-B domain β-sheet sits atop the α-helical

face of the CLOCK PAS-B domain in a parallel orientation (**Fig. 1.8c**). One consequence of this tandem arrangement is that the β-sheet of CLOCK PAS-B remains largely exposed, in contrast to most other PAS domains studied to date, which seem to have an obligate requirement engage their β-sheets in protein interactions.[85]

In addition to mediating heterodimerization of bHLH-PAS proteins, PAS domains can also recruit regulatory proteins to control transcription.[93,102,168,169] As noted earlier, it is unclear if PER proteins can interact directly with the CLOCK:BMAL1 complex on DNA.[66,94] CRY interacts with CLOCK PAS-B by yeast two-hybrid and mutation of two residues within the HI loop of the PAS-B domain disrupts binding.[170] Other mutations within the HI loop or directly adjacent to it on CLOCK PAS-B reduce CRY repression of the CLOCK:BMAL1 complex *in vivo* (**Fig. 1.8c**).[76,170] Furthermore, mutation of the BMAL1 TAD disrupts interactions with the CRY1 CC helix and synergistically decreases repression by CRY when assayed with CLOCK PAS-B mutants.[75,76]

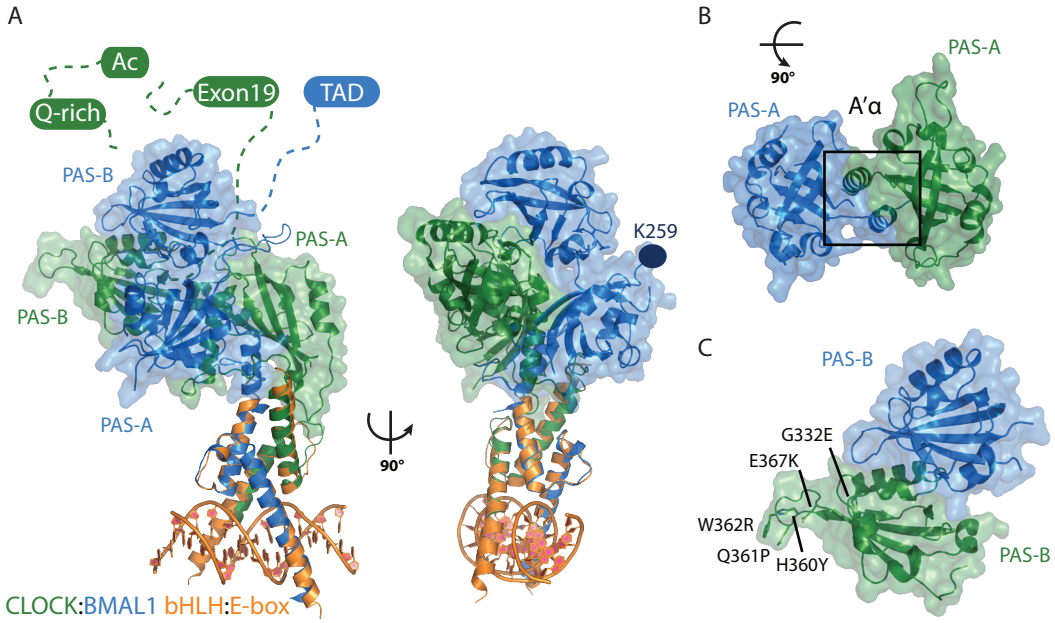

Figure 1.8: The CLOCK:BMAL1 bHLH-PAS dimer structure. (A) Crystal structures of the bHLH dimer:E-box complex in orange (PDB: 4H10) and the bHLH-PAS-AB dimer (PDB: 4F3L) overlaid with CLOCK in green and BMAL1 in blue. Dashed lines indicate intrinsically disordered C-terminal regions containing functionally important regions including the CLOCK Exon 19, Acetyl-CoA-binding motif (Ac), and glutamine-rich (Q-rich) region and the BMAL1 transcriptional activation domain (TAD). K259 (dark blue) is the SUMOylation site on BMAL1 PAS-A. (B) Depiction of interactions between the PAS-A domains, shown in isolation at 90° rotation relative to the left structure in part A. (C) Depiction of interactions between the PAS-B domains, shown in isolation, with mutations within CLOCK PAS-B that decrease CRY binding and/or repression of the CLOCK:BMAL1 complex.

These data suggest that CRY interacts with multiple distinct sites on CLOCK:BMAL1, likely a component of its potent repressive activity towards the complex.

Regions downstream of the PAS domains lack ordered structure, and few *in vitro* biochemical or biophysical studies have been done on the isolated CLOCK or BMAL1 C-termini.[139] However, we believe that the C-termini represent an exciting frontier that is rich with unexplored biology because they are essential for regulating the activity of CLOCK:BMAL1. [24,74-76,154,155,171,172] The activity of the CLOCK:BMAL1 complex is not simply predicated on DNA binding as it bound to E-boxes throughout much of the day (**Fig. 1.2b**).[34,60] Therefore, describing the mechanisms by which positive and negative acting factors are recruited via the C-termini to control activity of the complex should yield important insight into clock function. As noted earlier, flexibility of the C-termini is likely an important aspect of CLOCK:BMAL1 function, a property that is common to other 'malleable machines' involved in transcriptional regulation.[117] For example, how the acetyl CoA-binding motif of CLOCK confers acetylation to clock proteins[154,155] in the absence of a canonical MYST-family HAT domain structure[173] remains to be shown. Moreover, short regions of predicted order such as the 51-residue α-helical Exon 19 are essential for clock function[74] by interacting with positive and negative transcriptional regulators,[55,170] yet exist within a sea of disordered protein. The intrinsic flexibility of these regions may allow them to interact with a host of binding partners in a temporally dependent manner, allowing intrinsic timekeeping of the circadian clock to be finely tuned by interactions between regulatory proteins, possibly in a tissue-specific manner.

MODELING CIRCADIAN OSCILLATORS

The ring oscillator is a model commonly used in systems biology to study the parametric basis of biological feedback mechanisms. This model system is comprised of an odd number of inverter gates (also called logic or NOT gates) that feedback on one another[174] as either an activator (positive node) or repressor (negative node) (**Fig. 1.9a,b**). Transcriptional-based feedback loops can be modeled as ring oscillators using various bioinformatic methods, such as Monte Carlo simulations. Altering the number and organization of gates, or the presence or absence of auto-regulation, can modulate cycling phenotypes generated by the models. These models can provide insight into the mechanisms necessary to support circadian cycling.

The Goodwin model[175,176] is a three-ring oscillator that can be used to describe a number of multi-step biological feedback loops including expression of p53, somitogenesis, production of NF-kB and circadian rhythms.[174,177,178] The basic concept of a Goodwin oscillator is displayed in (**Fig. 1.9c**) where A is the mRNA product of a clock-controlled gene, B is the transcribed, nascent protein and C the functional repressor protein (once active via PTMs and correctly localized). A simple mathematical model of this system (equations 1.1-1.3) results in a cycle with a period much shorter than the observed 24-hours of circadian cycle. Therefore, a delay in the form of a Hill function is added to the negative feedback step in the model (equation 1.1); in order to obtain a model with circadian-like timing, the value of n must be larger than 8.[176,179,180] Hill functions are commonly used to describe the kinetics of cooperative interactions and in these instances n is greater than 1, but usually no larger than 4. The high n value in the circadian system elegantly predicts the presence of a multi-step process that active PER and CRY, of which many have been biochemically validated over the past decade.[36,40,42,43,46,48,72,83,87,105,135,136,181,182] While negative feedback loops increase robustness of cycling, the addition of delayed feedback is an inherent source of instability.[179]

$$\frac{dX}{dT} = k_1 \frac{K^n}{K^n + Z^n} - k_2 X \qquad (1.1)$$

$$\frac{dY}{dT} = k_3 X - k_4 Y \qquad (1.2)$$

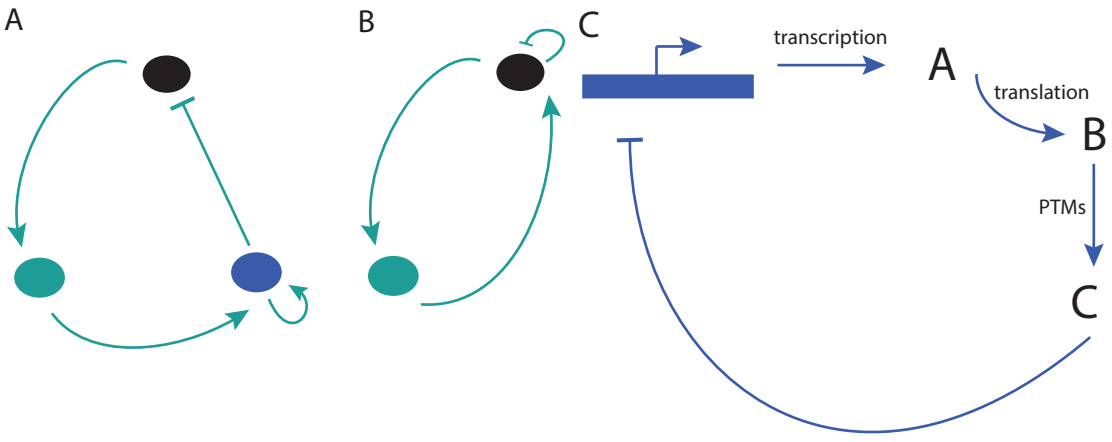

Figure 1.9: Organization of ring oscillators. (A) A simple three ring oscillator with negative feedback and positive auto-regulation. (B) A simple two ring oscillator with negative auto-regulation. (C) A model of the generic Goodwin oscillator.

$$\frac{dZ}{dT} = k_5 Y - k_6 Z \qquad (1.3)$$

Investigations into the robustness of cycling show that it is directly proportional to the number of feedback mechanisms within a system.[174] It is possible that the ROR and Rev-erbα/β auxiliary loop of the circadian system evolved as a method to increase robustness of cycling.[54,183] Intriguingly, the presence of a single auto-regulatory mechanism increased the robustness of a ring oscillator by an order of magnitude.[174] It is important to note that in both modeling and biology, the need for robustness must be weighed against economy and plasticity.

CONCLUSION

The molecular circadian clock is a dynamic system that can maintain homeostatic balance with high fidelity, yet is capable of being altered in a tissue specific or whole-organism manner in response to behaviors. The dynamic molecular interactions, post-translational modifications, translocation and degradation of the dedicated core clock proteins described in this chapter work in concert to tune the system and establish circadian timing in mammals.

We believe that continuing to integrate *in vivo* and *in vitro* studies will provide deep insight into the fundamental, biochemical processes that drive these processes. The recent abundance of high-resolution structures has provided a much-needed visualization of clock proteins and their interactions at the atomic level. However, many important regions of clock proteins are not depicted in these crystal structures because they lack a single, static structure. Protein flexibility is inherent to transcriptional regulators because it dramatically expands their repertoire of protein interactions,[117,118] even helping to establish the timescale and/or magnitude of gene activation.[184] Therefore, it is important that a wide range of techniques (crystallography, NMR, SAXS, EM, HDX and native MS) is utilized to fully describe protein interactions and their dynamics that give rise to circadian timing.

Looking forward, this is a truly exciting time for the field of circadian biology. We now possess the tools to probe clock protein function from complex animal models down to the resolution of structural details to learn how the clock sets intrinsic timing and interfaces with metabolism, tissue-specific factors, and pathophysiological states. There is no shortage of surprises at the complex and elegant biochemistry of the clock. The recent discovery of ancient,

redox-based posttranslational circadian oscillators conserved from archaebacteria to humans [185,186] highlights that we are still learning ways in which living organisms have evolved to coordinate their activity with the environment.

THESIS SUMMARY

Biological systems are comprised of macromolecules with numerous intricate and highly tuned molecular motions. From picosecond side chain motions to posttranslational modifications and conformational changes that occur on the milliseconds to seconds timescale, collective protein motions work in synergy to achieve precise mechanistic timing *in vivo*. Protein stoichiometry[94], phosphorylation[36,43,46,48,72,105,135,136,181], ubiquitination[40,42,83], sumoylation[87,157,182], and translocation have all been suggested as chronometric determinants that function to set the intrinsic period of the molecular clock. Yet, we still do not have a full mechanistic model describing the multitude of dynamic processes that contribute to maintain periodicity and robustness of circadian cycling.

Over the last two decades, intrinsically disordered proteins (IDPs) and intrinsically disordered regions (IDRs) have gained recognition as crucial components of cellular processes.[86,187-192] These dynamic regions of protein are commonly molecular hubs that have the capacity to interact with a variety of binding partners in differing orientations. The thermodynamics and kinetics that define the conformational heterogeneity of both IDPs and folded proteins are mechanistic determinates in physiology. This dissertation is a compilation of the published and unpublished works that highlight the role of the unstructured C-terminal BMAL1 TAD in the regulation of the mammalian circadian clock. We investigate the various binding modes of the BMAL1 TAD to multiple transcriptional regulators and investigate the thermodynamics and kinetics that drive a slow conformational switch in this hub-like region of the protein.

In chapter 2 we propose a model where competition between CRY and CBP/p300 for binding the BMAL1 TAD helps set the circadian period. We used luciferase reporter assays of chimeric BMAL1-BMAL2 proteins and biophysical techniques on point mutations of BMAL1 to study the mechanism of interaction between the BMAL1 TAD and its binding partners. We find that the C-terminal TAD of BMAL1 is the distinctive region of the protein that differentiates its ability to support circadian cycling *in vitro* from its homolog, BMAL2, which is unable to do

so. Furthermore, by tuning the relative affinity of CBP and CRY for the BMAL1 TAD, we can modulate the circadian period in cycling mammalian cell cultures.

In chapter 3 we introduce the discovery and characterization of a slow conformational change in the form of a *cis/trans* isomerization about an imide bond in the extreme C-terminus of the BMAL1 TAD. Both isomers can interact with transcriptional regulators *in vitro* and we find that this slow switch modulates circadian rhythms in cycling cells. To our knowledge, this is the first in-depth report and direct evaluation of native *cis/trans* isomerization kinetics of a protein by ZZ-exchange spectroscopy. Furthermore, we show that the kinetics of isomerization can be modulated *in vitro* by the cyclophilin family of peptidyl prolyl isomerases, suggesting the potential for regulation of switch kinetics *in vivo*.

In chapter 4, we further characterize the interactions of the BMAL1 TAD with two domains of the transcriptional co-activator CBP. Mechanistic insight into BMAL1 TAD interactions with the KIX and TAZ1 domains will allow us to tease apart the differing roles of CBP and its homolog p300 in the circadian cycle. Finally, in Chapter 5 we review the results of our studies in the context of the larger circadian system and look forward to the future of mechanistic circadian biochemistry.

REFERENCES

1. Yoo, S.-H. *et al.* PERIOD2::LUCIFERASE real-time reporting of circadian dynamics reveals persistent circadian oscillations in mouse peripheral tissues. *Proc. Natl. Acad. Sci. U.S.A.* **101,** 5339–5346 (2004).
2. Zhang, R., Lahens, N. F., Ballance, H. I., Hughes, M. E. & Hogenesch, J. B. A circadian gene expression atlas in mammals: implications for biology and medicine. *Proceedings of the National Academy of Sciences* **111,** 16219–16224 (2014).
3. Feillet, C., van der Horst, G. T. J., Levi, F., Rand, D. A. & Delaunay, F. Coupling between the Circadian Clock and Cell Cycle Oscillators: Implication for Healthy Cells and Malignant Growth. *Front. Neurol.* **6,** 201–7 (2015).
4. Hodge, B. A. *et al.* The endogenous molecular clock orchestrates the temporal separation of substrate metabolism in skeletal muscle. *Skelet Muscle* **5,** 17 (2015).
5. Patel, V. R. *et al.* The pervasiveness and plasticity of circadian oscillations: the coupled circadian-oscillators framework. *Bioinformatics* **31,** 3181–3188 (2015).
6. Perelis, M., Ramsey, K. M. & Bass, J. The molecular clock as a metabolic rheostat. *Diabetes* (2015). doi:10.1111/dom.12521
7. Coomans, C. P. *et al.* Plasticity of circadian clocks and consequences for metabolism. *Diabetes Obes Metab* **17 Suppl 1,** 65–75 (2015).
8. Saini, C., Petrenko, V. & Pulimeno, P. A functional circadian clock is required for proper insulin secretion by human pancreatic islet cells. *Diabetes* (2015). doi:10.1002/dom.12616
9. Eckel-Mahan, K. & Sassone-Corsi, P. Metabolism and the Circadian Clock Converge. *Physiol. Rev.* **93,** 107–135 (2013).

10. Eckel-Mahan, K. L. *et al.* Coordination of the transcriptome and metabolome by the circadian clock. *Proceedings of the National Academy of Sciences* **109,** 5541–5546 (2012).

11. Librodo, P., Buckley, M., Luk, M. & Bisso, A. Chronotherapeutic Drug Delivery. *Journal of Infusion Nursing* **35,** 329–334 (2012).

12. Simonneaux, V. & Bahougne, T. A Multi-Oscillatory Circadian System Times Female Reproduction. *Front. Endocrinol.* **6,** 188–15 (2015).

13. Roenneberg, T., Daan, S. & Merrow, M. The art of entrainment. *Journal of Biological Rhythms* (2003). doi:10.1177/0748730403253393

14. Hughes, S., Jagannath, A., Hankins, M. W., Foster, R. G. & Peirson, S. N. *Photic Regulation of Clock Systems*. *Circadian Rhythms and Biological Clocks Part B* **552,** 125–143 (Elsevier Inc., 2015).

15. Berson, D. M., Dunn, F. A. & Takao, M. Phototransduction by retinal ganglion cells that set the circadian clock. *Science* **295,** 1070–1073 (2002).

16. Sekaran, S., Foster, R. G., Lucas, R. J. & Hankins, M. W. Calcium Imaging Reveals a Network of Intrinsically Light-Sensitive Inner-Retinal Neurons. *Current Biology* **13,** 1290–1298 (2003).

17. Hattar, S. Melanopsin-Containing Retinal Ganglion Cells: Architecture, Projections, and Intrinsic Photosensitivity. *Science* **295,** 1065–1070 (2002).

18. Moore, R. Y., Speh, J. C. & Card, J. P. The retinohypothalamic tract originates from a distinct subset of retinal ganglion cells. *J. Comp. Neurol.* **352,** 351–366 (1995).

19. Meijer, J. H. & Schwartz, W. J. In search of the pathways for light-induced pacemaker resetting in the suprachiasmatic nucleus. *Journal of Biological Rhythms* (2003). doi:10.1177/0748730403253370

20. Takahashi, J. S., Hong, H.-K., Ko, C. H. & McDearmon, E. L. The genetics of mammalian circadian order and disorder: implications for physiology and disease. *Nat Rev Genet* **9,** 764–775 (2008).

21. Lamia, K. A. *et al.* Cryptochromes mediate rhythmic repression of the glucocorticoid receptor. *Nature* **480,** 552–556 (2011).

22. Brum, M. C. B., Filho, F. F. D., Schnorr, C. C., Bottega, G. B. & Rodrigues, T. C. Shift work and its association with metabolic disorders. *Diabetol Metab Syndr* **7,** 45 (2015).

23. Kripke, D. F., Elliott, J. A., Welsh, D. K. & Youngstedt, S. D. Photoperiodic and circadian bifurcation theories of depression and mania. *F1000Res* **4,** 107 (2015).

24. Gekakis, N. *et al.* Role of the CLOCK protein in the mammalian circadian mechanism. *Science* **280,** 1564–1569 (1998).

25. Huang, N. *et al.* Crystal Structure of the Heterodimeric CLOCK:BMAL1 Transcriptional Activator Complex. *Science* **337,** 189–194 (2012).

26. Zheng, B. *et al.* Nonredundant roles of the mPer1 and mPer2 genes in the mammalian circadian clock. *Cell* **105,** 683–694 (2001).

27. van der Horst, G. T. *et al.* Mammalian Cry1 and Cry2 are essential for maintenance of circadian rhythms. *Nature* **398,** 627–630 (1999).

28. Vitaterna, M. H. *et al.* Differential regulation of mammalian period genes and circadian rhythmicity by cryptochromes 1 and 2. *Proc. Natl. Acad. Sci. U.S.A.* **96,** 12114–12119 (1999).

29. Preitner, N. *et al.* The orphan nuclear receptor REV-ERBalpha controls circadian transcription within the positive limb of the mammalian circadian oscillator. *Cell* **110,** 251–260 (2002).

30. Storch, K.-F. *et al.* Extensive and divergent circadian gene expression in liver and heart. *Nature* **417,** 78–83 (2002).

31. Panda, S., Hogenesch, J. B. & Kay, S. A. Circadian rhythms from flies to human. *Nature* **417,** 329–335 (2002).

32. Morf, J. *et al.* Cold-inducible RNA-binding protein modulates circadian gene expression posttranscriptionally. *Science* **338,** 379–383 (2012).

33. Le Martelot, G. *et al.* Genome-wide RNA polymerase II profiles and RNA accumulation reveal kinetics of transcription and associated epigenetic changes during diurnal cycles. *Plos Biol* **10,** e1001442 (2012).

34. Menet, J. S., Rodriguez, J., Abruzzi, K. C. & Rosbash, M. Nascent-Seq reveals novel features of mouse circadian transcriptional regulation. *Elife* **1,** e00011–e00011 (2012).

35. Kojima, S., Sher-Chen, E. L. & Green, C. B. Circadian control of mRNA polyadenylation dynamics regulates rhythmic protein expression. *Genes & Development* **26,** 2724–2736 (2012).

36. Hirota, T. *et al.* A chemical biology approach reveals period shortening of the mammalian circadian clock by specific inhibition of GSK-3beta. *Proceedings of the National Academy of Sciences* **105,** 20746–20751 (2008).

37. Isojima, Y. *et al.* CKIepsilon/delta-dependent phosphorylation is a temperature-insensitive, period-determining process in the mammalian circadian clock. *Proceedings of the National Academy of Sciences* **106,** 15744–15749 (2009).

38. Lamia, K. A. *et al.* AMPK regulates the circadian clock by cryptochrome phosphorylation and degradation. *Science* **326,** 437–440 (2009).

39. Yoo, S.-H. *et al.* Competing E3 ubiquitin ligases govern circadian periodicity by degradation of CRY in nucleus and cytoplasm. *Cell* **152,** 1091–1105 (2013).

40. Hirano, A. *et al.* FBXL21 Regulates Oscillation of the Circadian Clock through Ubiquitination and Stabilization of Cryptochromes. *Cell* **152,** 1106–1118 (2013).

41. Siepka, S. M. *et al.* Circadian mutant Overtime reveals F-box protein FBXL3 regulation of cryptochrome and period gene expression. *Cell* **129,** 1011–1023 (2007).

42. Busino, L. *et al.* SCFFbxl3 controls the oscillation of the circadian clock by directing the degradation of cryptochrome proteins. *Science* **316,** 900–904 (2007).

43. Shirogane, T., Jin, J., Ang, X. L. & Harper, J. W. SCFbeta-TRCP controls clock-dependent transcription via casein kinase 1-dependent degradation of the mammalian period-1 (Per1) protein. *J. Biol. Chem.* **280,** 26863–26872 (2005).

44. Partch, C. L., Shields, K. F., Thompson, C. L., Selby, C. P. & Sancar, A. Posttranslational regulation of the mammalian circadian clock by cryptochrome and protein phosphatase 5. *Proc. Natl. Acad. Sci. U.S.A.* **103,** 10467–10472 (2006).

45. Lee, H., Chen, R., Lee, Y., Yoo, S. & Lee, C. Essential roles of CKIdelta and CKIepsilon in the mammalian circadian clock. *Proceedings of the National Academy of Sciences* **106,** 21359–21364 (2009).

46. Toh, K. L. *et al.* An hPer2 phosphorylation site mutation in familial advanced sleep phase syndrome. *Science* **291,** 1040–1043 (2001).

47. Xu, Y. *et al.* Functional consequences of a CKIdelta mutation causing familial advanced sleep phase syndrome. *Nature* **434,** 640–644 (2005).

48. Hirota, T. *et al.* High-throughput chemical screen identifies a novel potent modulator of cellular circadian rhythms and reveals CKIα as a clock regulatory kinase. *Plos Biol* **8,** e1000559 (2010).

49. Chen, Z. *et al.* Identification of diverse modulators of central and peripheral circadian clocks by high-throughput chemical screening. *Proceedings of the National Academy of Sciences* **109,** 101–106 (2012).

50. Ueda, H. R. *et al.* A transcription factor response element for gene expression during circadian night. *Nature* **418,** 534–539 (2002).

51. Sato, T. K. *et al.* A functional genomics strategy reveals Rora as a component of the mammalian circadian clock. *Neuron* **43,** 527–537 (2004).

52. Crumbley, C. & Burris, T. P. Direct regulation of CLOCK expression by REV-ERB. *PLoS ONE* **6,** e17290 (2011).

53. Liu, A. C. *et al.* Redundant function of REV-ERBalpha and beta and non-essential role for BMAL1 cycling in transcriptional regulation of intracellular circadian rhythms. *PLoS Genet.* **4,** e1000023 (2008).

54. Cho, H. *et al.* Regulation of circadian behaviour and metabolism by REV-ERB-α and REV-ERB-β. *Nature* **485,** 123–127 (2012).

55. Katada, S. & Sassone-Corsi, P. The histone methyltransferase MLL1 permits the oscillation of circadian gene expression. *Nat. Struct. Mol. Biol.* **17,** 1414–1421 (2010).

56. Valekunja, U. K. *et al.* Histone methyltransferase MLL3 contributes to genome-scale circadian transcription. *Proceedings of the National Academy of Sciences* **110,** 1554–1559 (2013).

57. Nakahata, Y. *et al.* The NAD+-dependent deacetylase SIRT1 modulates CLOCK-mediated chromatin remodeling and circadian control. *Cell* **134,** 329–340 (2008).

58. Asher, G. *et al.* SIRT1 regulates circadian clock gene expression through PER2 deacetylation. *Cell* **134,** 317–328 (2008).

59. Etchegaray, J.-P. *et al.* The polycomb group protein EZH2 is required for mammalian circadian clock function. *J. Biol. Chem.* **281,** 21209–21215 (2006).

60. Koike, N. *et al.* Transcriptional architecture and chromatin landscape of the core circadian clock in mammals. *Science* **338,** 349–354 (2012).

61. Duong, H. A., Robles, M. S., Knutti, D. & Weitz, C. J. A molecular mechanism for circadian clock negative feedback. *Science* **332,** 1436–1439 (2011).

62. Padmanabhan, K., Robles, M. S., Westerling, T. & Weitz, C. J. Feedback regulation of transcriptional termination by the mammalian circadian clock PERIOD complex. *Science* **337,** 599–602 (2012).

63. Duong, H. A. & Weitz, C. J. Temporal orchestration of repressive chromatin modifiers by circadian clock Period complexes. *Nat. Struct. Mol. Biol.* **21,** 126–132 (2014).

64. Brown, S. A. *et al.* PERIOD1-associated proteins modulate the negative limb of the mammalian circadian oscillator. *Science* **308,** 693–696 (2005).

65. Stratmann, M., Stadler, F., Tamanini, F., van der Horst, G. T. J. & Ripperger, J. A. Flexible phase adjustment of circadian albumin D site-binding protein (DBP) gene expression by CRYPTOCHROME1. *Genes & Development* **24,** 1317–1328 (2010).

66. Ye, R., Selby, C. P., Ozturk, N., Annayev, Y. & Sancar, A. Biochemical analysis of the canonical model for the mammalian circadian clock. *Journal of Biological Chemistry* **286,** 25891–25902 (2011).

67. Liu, A. C. *et al.* Intercellular coupling confers robustness against mutations in the SCN circadian clock network. *Cell* **129,** 605–616 (2007).

68. Ukai-Tadenuma, M. *et al.* Delay in feedback repression by cryptochrome 1 is required for circadian clock function. *Cell* **144,** 268–281 (2011).

69. Khan, S. K. *et al.* Identification of a novel cryptochrome differentiating domain required for feedback repression in circadian clock function. *Journal of Biological Chemistry* **287,** 25917–25926 (2012).

70. Hirota, T. *et al.* Identification of small molecule activators of cryptochrome. *Science* **337,** 1094–1097 (2012).

71. Maywood, E. S. *et al.* Tuning the period of the mammalian circadian clock: additive and independent effects of CK1εTau and Fbxl3Afh mutations on mouse circadian behavior and molecular pacemaking. *J. Neurosci.* **31,** 1539–1544 (2011).

72. St John, P. C., Hirota, T., Kay, S. A. & Doyle, F. J. Spatiotemporal separation of PER and CRY posttranslational regulation in the mammalian circadian clock. *Proceedings of the National Academy of Sciences* **111,** 2040–2045 (2014).

73. Kojetin, D. J. & Burris, T. P. REV-ERB and ROR nuclear receptors as drug targets. *Nat Rev Drug Discov* **13,** 197–216 (2014).

74. King, D. P. *et al.* Positional cloning of the mouse circadian clock gene. *Cell* **89,** 641–653 (1997).

75. Kiyohara, Y. B. *et al.* The BMAL1 C terminus regulates the circadian transcription feedback loop. *Proc. Natl. Acad. Sci. U.S.A.* **103,** 10074–10079 (2006).

76. Sato, T. K. *et al.* Feedback repression is required for mammalian circadian clock function. *Nat. Genet.* **38,** 312–319 (2006).

77. Tei, H. *et al.* Circadian oscillation of a mammalian homologue of the Drosophila period gene. *Nature* **389,** 512–516 (1997).

78. Yagita, K. *et al.* Dimerization and nuclear entry of mPER proteins in mammalian cells. *Genes & Development* **14,** 1353–1363 (2000).

79. Lee, C., Weaver, D. R. & Reppert, S. M. Direct association between mouse PERIOD and CKIepsilon is critical for a functioning circadian clock. *Molecular and Cellular Biology* **24,** 584–594 (2004).

80. Miyazaki, K., Mesaki, M. & Ishida, N. Nuclear entry mechanism of rat PER2 (rPER2): role of rPER2 in nuclear localization of CRY protein. *Molecular and Cellular Biology* **21,** 6651–6659 (2001).

81. Sancar, A. Structure and function of DNA photolyase and cryptochrome blue-light photoreceptors. *Chem. Rev.* **103,** 2203–2237 (2003).

82. Chaves, I. *et al.* Functional evolution of the photolyase/cryptochrome protein family: importance of the C terminus of mammalian CRY1 for circadian core oscillator performance. *Molecular and Cellular Biology* **26,** 1743–1753 (2006).

83. Xing, W. *et al.* SCF(FBXL3) ubiquitin ligase targets cryptochromes at their cofactor pocket. *Nature* **496,** 64–68 (2013).

84. Huang, Z. J., Edery, I. & Rosbash, M. PAS is a dimerization domain common to Drosophila period and several transcription factors. *Nature* **364,** 259–262 (1993).

85. Möglich, A., Ayers, R. A. & Moffat, K. Structure and signaling mechanism of Per-ARNT-Sim domains. *Structure* **17,** 1282–1294 (2009).

86. Oldfield, C. J. & Dunker, A. K. Intrinsically disordered proteins and intrinsically disordered protein regions. *Annu. Rev. Biochem.* **83,** 553–584 (2014).

87. Cardone, L. *et al.* Circadian clock control by SUMOylation of BMAL1. *Science* **309,** 1390–1394 (2005).

88. Harper, S. M., Neil, L. C. & Gardner, K. H. Structural basis of a phototropin light switch. *Science* **301,** 1541–1544 (2003).

89. Hennig, S. *et al.* Structural and functional analyses of PAS domain interactions of the clock proteins Drosophila PERIOD and mouse PERIOD2. *Plos Biol* **7,** e94 (2009).

90. Erbel, P. J. A., Card, P. B., Karakuzu, O., Bruick, R. K. & Gardner, K. H. Structural basis for PAS domain heterodimerization in the basic helix--loop--helix-PAS transcription factor hypoxia-inducible factor. *Proc. Natl. Acad. Sci. U.S.A.* **100,** 15504–15509 (2003).

91. Wu, D., Potluri, N., Kim, Y. & Rastinejad, F. Structure and dimerization properties of the aryl hydrocarbon receptor PAS-A domain. *Molecular and Cellular Biology* **33,** 4346–4356 (2013).

92. Razeto, A. *et al.* Structure of the NCoA-1/SRC-1 PAS-B domain bound to the LXXLL motif of the STAT6 transactivation domain. *J. Mol. Biol.* **336,** 319–329 (2004).

93. Partch, C. L. & Gardner, K. H. Coactivators necessary for transcriptional output of the hypoxia inducible factor, HIF, are directly recruited by ARNT PAS-B. *Proceedings of the National Academy of Sciences* **108,** 7739–7744 (2011).

94. Chen, R. *et al.* Rhythmic PER abundance defines a critical nodal point for negative feedback within the circadian clock mechanism. *Mol. Cell* **36,** 417–430 (2009).

95. Dioum, E. M. *et al.* NPAS2: a gas-responsive transcription factor. *Science* **298,** 2385–2387 (2002).

96. Kaasik, K. & Lee, C. C. Reciprocal regulation of haem biosynthesis and the circadian clock in mammals. *Nature* **430,** 467–471 (2004).

97. Lukat-Rodgers, G. S., Correia, C., Botuyan, M. V., Mer, G. & Rodgers, K. R. Heme-Based Sensing by the Mammalian Circadian Protein CLOCK. *Inorg. Chem.* **49,** 6349–6365 (2010).

98. Airola, M. V., Du, J., Dawson, J. H. & Crane, B. R. Heme binding to the mammalian circadian clock protein period 2 is nonspecific. *Biochemistry* (2010).

99. Amezcua, C. A., Harper, S. M., Rutter, J. & Gardner, K. H. Structure and interactions of PAS kinase N-terminal PAS domain: model for intramolecular kinase regulation. *Structure* (2002).

100. Scheuermann, T. H. *et al.* Artificial ligand binding within the HIF2alpha PAS-B domain of the HIF2 transcription factor. *Proceedings of the National Academy of Sciences* **106,** 450–455 (2009).

101. Scheuermann, T. H. *et al.* Allosteric inhibition of hypoxia inducible factor-2 with small molecules. *Nat. Chem. Biol.* **9,** 271–276 (2013).

102. Guo, Y. *et al.* Regulating the ARNT/TACC3 axis: multiple approaches to manipulating protein/protein interactions with small molecules. *ACS Chem. Biol.* **8,** 626–635 (2013).

103. Key, J., Scheuermann, T. H., Anderson, P. C., Daggett, V. & Gardner, K. H. Principles of ligand binding within a completely buried cavity in HIF2alpha PAS-B. *J. Am. Chem. Soc.* **131,** 17647–17654 (2009).

104. Lee, C., Etchegaray, J. P., Cagampang, F. R., Loudon, A. S. & Reppert, S. M. Posttranslational mechanisms regulate the mammalian circadian clock. *Cell* **107,** 855–867 (2001).

105. Eide, E. J. *et al.* Control of mammalian circadian rhythm by CKIepsilon-regulated proteasome-mediated PER2 degradation. *Molecular and Cellular Biology* **25,** 2795–2807 (2005).

106. Meng, Q.-J. *et al.* Entrainment of disrupted circadian behavior through inhibition of casein kinase 1 (CK1) enzymes. *Proceedings of the National Academy of Sciences* **107,** 15240–15245 (2010).

107. Schibler, U., Ripperger, J. & Brown, S. A. Peripheral circadian oscillators in mammals: time and food. *Journal of Biological Rhythms* **18,** 250–260 (2003).

108. Lee, Y., Chen, R., Lee, H.-M. & Lee, C. Stoichiometric relationship among clock proteins determines robustness of circadian rhythms. *Journal of Biological Chemistry* **286,** 7033–7042 (2011).

109. Kucera, N. *et al.* Unwinding the differences of the mammalian PERIOD clock proteins from crystal structure to cellular function. *Proceedings of the National Academy of Sciences* **109,** 3311–3316 (2012).

110. Zheng, B. *et al.* The mPer2 gene encodes a functional component of the mammalian circadian clock. *Nature* **400,** 169–173 (1999).

111. Vielhaber, E. L., Duricka, D., Ullman, K. S. & Virshup, D. M. Nuclear export of mammalian PERIOD proteins. *J. Biol. Chem.* **276,** 45921–45927 (2001).

112. Schmutz, I., Ripperger, J. A., Baeriswyl-Aebischer, S. & Albrecht, U. The mammalian clock component PERIOD2 coordinates circadian output by interaction with nuclear receptors. *Genes & Development* **24,** 345–357 (2010).

113. Heery, D. M., Kalkhoven, E., Hoare, S. & Parker, M. G. A signature motif in transcriptional co-activators mediates binding to nuclear receptors. *Nature* **387,** 733–736 (1997).

114. Plevin, M. J., Mills, M. M. & Ikura, M. The LxxLL motif: a multifunctional binding sequence in transcriptional regulation. *Trends Biochem. Sci.* **30,** 66–69 (2005).

115. Akashi, M. *et al.* A Positive Role for PERIOD in Mammalian Circadian Gene Expression. *Cell Rep* **7,** 1056–1064 (2014).

116. Hurley, J. M., Larrondo, L. F., Loros, J. J. & Dunlap, J. C. Conserved RNA helicase FRH acts nonenzymatically to support the intrinsically disordered neurospora clock protein FRQ. *Mol. Cell* **52,** 832–843 (2013).

117. Fuxreiter, M. *et al.* Malleable machines take shape in eukaryotic transcriptional regulation. *Nat. Chem. Biol.* **4,** 728–737 (2008).

118. Cortese, M. S., Uversky, V. N. & Dunker, A. K. Intrinsic disorder in scaffold proteins: getting more from less. *Prog. Biophys. Mol. Biol.* **98,** 85–106 (2008).

119. Dyson, H. J. & Komives, E. A. Role of disorder in IκB-NFκB interaction. *IUBMB Life* **64,** 499–505 (2012).

120. Romero, D. P., Obradovic, Z. & Dunker, A. K. Natively Disordered Proteins. *Appl-Bioinformatics* **3,** 105–113 (2004).

121. Fuxreiter, M., Simon, I., Friedrich, P. & Tompa, P. Preformed structural elements feature in partner recognition by intrinsically unstructured proteins. *J. Mol. Biol.* (2004).

122. Tennessen, J. M., Gardner, H. F., Volk, M. L. & Rougvie, A. E. Novel heterochronic functions of the< i> Caenorhabditis elegans</i> period-related protein LIN-42. *Developmental biology* (2006).

123. Joen, M., Gardner, H. F., Miller, E. A., Deshler, J. & Rougvie, A. E. Similarity of the C. elegans developmental timing protein LIN-42 to circadian rhythm proteins. *Science* **286,** 1141–1146 (1999).

124. Monsalve, G. C., Van Buskirk, C. & Frand, A. R. LIN-42/PERIOD controls cyclical and developmental progression of C. elegans molts. *Curr. Biol.* **21,** 2033–2045 (2011).

125. Nawathean, P., Stoleru, D. & Rosbash, M. A small conserved domain of Drosophila PERIOD is important for circadian phosphorylation, nuclear localization, and transcriptional repressor activity. *Molecular and Cellular Biology* **27,** 5002–5013 (2007).

126. Bae, K. *et al.* Differential functions of mPer1, mPer2, and mPer3 in the SCN circadian clock. *Neuron* **30,** 525–536 (2001).

127. Shearman, L. P. *et al.* Interacting molecular loops in the mammalian circadian clock. *Science* **288,** 1013–1019 (2000).

128. Pendergast, J. S., Niswender, K. D. & Yamazaki, S. Tissue-specific function of Period3 in circadian rhythmicity. *PLoS ONE* **7,** e30254 (2012).

129. Griffin, E. A., Staknis, D. & Weitz, C. J. Light-independent role of CRY1 and CRY2 in the mammalian circadian clock. *Science* **286,** 768–771 (1999).

130. Kume, K. *et al.* mCRY1 and mCRY2 are essential components of the negative limb of the circadian clock feedback loop. *Cell* **98,** 193–205 (1999).

131. Oster, H., Yasui, A., van der Horst, G. T. J. & Albrecht, U. Disruption of mCry2 restores circadian rhythmicity in mPer2 mutant mice. *Genes & Development* **16,** 2633–2638 (2002).

132. Kim, J. K. & Forger, D. B. A mechanism for robust circadian timekeeping via stoichiometric balance. *Mol. Syst. Biol.* **8,** 630 (2012).

133. Ozgur, S. & Sancar, A. Purification and properties of human blue-light photoreceptor cryptochrome 2. *Biochemistry* **42,** 2926–2932 (2003).

134. Partch, C. L., Clarkson, M. W., Ozgur, S., Lee, A. L. & Sancar, A. Role of structural plasticity in signal transduction by the cryptochrome blue-light photoreceptor. *Biochemistry* **44,** 3795–3805 (2005).

135. Kurabayashi, N., Hirota, T., Sakai, M., Sanada, K. & Fukada, Y. DYRK1A and glycogen synthase kinase 3beta, a dual-kinase mechanism directing proteasomal degradation of CRY2 for circadian timekeeping. *Molecular and Cellular Biology* **30,** 1757–1768 (2010).

136. Gao, P. *et al.* Phosphorylation of the Cryptochrome 1 C-terminal Tail Regulates Circadian Period Length. *Journal of Biological Chemistry* **288,** 35277–35286 (2013).

137. Zhu, H., Conte, F. & Green, C. B. Nuclear localization and transcriptional repression are confined to separable domains in the circadian protein CRYPTOCHROME. *Curr. Biol.* **13,** 1653–1658 (2003).

138. Czarna, A. *et al.* Structures of Drosophila cryptochrome and mouse cryptochrome1 provide insight into circadian function. *Cell* **153,** 1394–1405 (2013).

139. Czarna, A. *et al.* Quantitative analyses of cryptochrome-mBMAL1 interactions: mechanistic insights into the transcriptional regulation of the mammalian circadian clock. *Journal of Biological Chemistry* **286,** 22414–22425 (2011).

140. Schmalen, I. *et al.* Interaction of Circadian Clock Proteins CRY1 and PER2 Is Modulated by Zinc Binding and Disulfide Bond Formation. *Cell* **157,** 1203–1215 (2014).

141. Yagita, K. *et al.* Nucleocytoplasmic shuttling and mCRY-dependent inhibition of ubiquitylation of the mPER2 clock protein. *EMBO J.* **21,** 1301–1314 (2002).

142. Nangle, S., Xing, W. & Zheng, N. Crystal structure of mammalian cryptochrome in complex with a small molecule competitor of its ubiquitin ligase. *Cell Research* **23,** 1417–1419 (2013).

143. Gotter, A. L. A Timeless debate: resolving TIM's noncircadian roles with possible clock function. *Neuroreport* **17,** 1229–1233 (2006).

144. Engelen, E. *et al.* Mammalian TIMELESS is involved in period determination and DNA damage-dependent phase advancing of the circadian clock. *PLoS ONE* **8,** e56623 (2013).

145. Gotter, A. L., Suppa, C. & Emanuel, B. S. Mammalian TIMELESS and Tipin are evolutionarily conserved replication fork-associated factors. *J. Mol. Biol.* **366,** 36–52 (2007).

146. Unsal-Kaçmaz, K., Mullen, T. E., Kaufmann, W. K. & Sancar, A. Coupling of human circadian and cell cycles by the timeless protein. *Molecular and Cellular Biology* **25,** 3109–3116 (2005).

147. Chou, D. M. & Elledge, S. J. Tipin and Timeless form a mutually protective complex required for genotoxic stress resistance and checkpoint function. *Proc. Natl. Acad. Sci. U.S.A.* **103,** 18143–18147 (2006).

148. Leman, A. R., Noguchi, C., Lee, C. Y. & Noguchi, E. Human Timeless and Tipin stabilize replication forks and facilitate sister-chromatid cohesion. *J. Cell. Sci.* **123,** 660–670 (2010).

149. Local and global functions of Timeless and Tipin in replication fork protection. *Cell Cycle* **11,** 3945–3955 (2012).

150. Oklejewicz, M. *et al.* Phase resetting of the mammalian circadian clock by DNA damage. *Curr. Biol.* **18,** 286–291 (2008).

151. Gamsby, J. J., Loros, J. J. & Dunlap, J. C. A phylogenetically conserved DNA damage response resets the circadian clock. *Journal of Biological Rhythms* **24,** 193–202 (2009).

152. Kang, T.-H. & Leem, S.-H. Modulation of ATR-mediated DNA damage checkpoint response by cryptochrome 1. *Nucleic Acids Research* **42,** 4427–4434 (2014).

153. Ozber, N. *et al.* Identification of two amino acids in the C-terminal domain of mouse CRY2 essential for PER2 interaction. *BMC Mol. Biol.* **11,** 69 (2010).

154. Doi, M., Hirayama, J. & Sassone-Corsi, P. Circadian Regulator CLOCK Is a Histone Acetyltransferase. *Cell* **125,** 497–508 (2006).

155. Hirayama, J., Sahar, S., Grimaldi, B. & Tamaru, T. CLOCK-mediated acetylation of BMAL1 controls circadian function. *Nature* (2007).

156. Michael, A. K. & Partch, C. L. bHLH-PAS proteins: functional specification through modular domain architecture. *OA Biochemistry* **1,** 1–6 (2014).

157. Lee, Y. *et al.* Coactivation of the CLOCK-BMAL1 complex by CBP mediates resetting of the circadian clock. *J. Cell. Sci.* **123,** 3547–3557 (2010).

158. Takahata, S. *et al.* Transactivation mechanisms of mouse clock transcription factors, mClock and mArnt3. *Genes to Cells* **5,** 739–747 (2000).

159. Hosoda, H. *et al.* CBP/p300 is a cell type-specific modulator of CLOCK/BMAL1-mediated transcription. *Mol Brain* **2,** 34 (2009).

160. Etchegaray, J.-P., Lee, C., Wade, P. A. & Reppert, S. M. Rhythmic histone acetylation underlies transcription in the mammalian circadian clock. *Nature* **421,** 177–182 (2003).

161. Lande-Diner, L., boyault, C., Kim, J. Y. & Weitz, C. J. A positive feedback loop links circadian clock factor CLOCK-BMAL1 to the basic transcriptional machinery. *Proceedings of the National Academy of Sciences* **110,** 16021–16026 (2013).

162. Wang, Z., Wu, Y., Li, L. & Su, X. D. Intermolecular recognition revealed by the complex structure of human CLOCK-BMAL1 basic helix-loop-helix domains with E-box DNA. *Cell Research* (2013).

163. Tamaru, T., Hirayama, J., Isojima, Y. & Nagai, K. CK2α phosphorylates BMAL1 to regulate the mammalian clock. *Nature structural & …* (2009).

164. Rutter, J., Reick, M., Wu, L. C. & McKnight, S. L. Regulation of clock and NPAS2 DNA binding by the redox state of NAD cofactors. *Science* **293,** 510–514 (2001).

165. Yoshii, K., Ishijima, S. & Sagami, I. Effects of NAD (P) H and its derivatives on the DNA-binding activity of NPAS2, a mammalian circadian transcription factor. *Biochemical and biophysical research …* (2013).

166. Wise, D. D. & Shear, J. B. Circadian tracking of nicotinamide cofactor levels in an immortalized suprachiasmatic nucleus cell line. *Neuroscience* (2004).

167. Tan, Y., DeBruyne, J., Cahill, G. M. & Wells, D. E. Identification of a mutation in the Clock1 gene affecting zebrafish circadian rhythms. *J. Neurogenet.* **22,** 149–166 (2008).

168. Partch, C. L., Card, P. B., Amezcua, C. A. & Gardner, K. H. Molecular basis of coiled coil coactivator recruitment by the aryl hydrocarbon receptor nuclear translocator (ARNT). *J. Biol. Chem.* **284,** 15184–15192 (2009).

169. Labrecque, M. P., Prefontaine, G. G. & Beischlag, T. V. The aryl hydrocarbon receptor nuclear translocator (ARNT) family of proteins: transcriptional modifiers with multi-functional protein interfaces. *Curr. Mol. Med.* **13,** 1047–1065 (2013).

170. Zhao, W.-N. *et al.* CIPC is a mammalian circadian clock protein without invertebrate homologues. *Nat. Cell Biol.* **9,** 268–275 (2007).

171. Annayev, Y. *et al.* Gene Model 129 (Gm129) Encodes a Novel Transcriptional Repressor That Modulates Circadian Gene Expression. *Journal of Biological Chemistry* **289,** 5013–5024 (2014).

172. Anafi, R. C. *et al.* Machine learning helps identify CHRONO as a circadian clock component. *Plos Biol* **12,** e1001840 (2014).

173. Yuan, H. *et al.* MYST protein acetyltransferase activity requires active site lysine autoacetylation. *EMBO J.* **31,** 58–70 (2012).

174. Woods, M. L., Leon, M., Perez-Carrasco, R. & Barnes, C. P. A Statistical Approach Reveals Designs for the Most Robust Stochastic Gene Oscillators. *ACS Synth. Biol.* acssynbio.5b00179–12 (2016). doi:10.1021/acssynbio.5b00179

175. Ruoff, P., Vinsjevik, M., Monnerjahn, C. & Rensing, L. The Goodwin oscillator: on the importance of degradation reactions in the circadian clock. *Journal of Biological Rhythms* **14,** 469–479 (1999).

176. Woller, A., Gonze, D. & Erneux, T. The Goodwin model revisited: Hopf bifurcation, limit-cycle, and periodic entrainment. *Phys. Biol.* **11,** 045002–15 (2014).

177. Forger, D. B. Signal processing in cellular clocks. in (2011). doi:10.1073/pnas.1004720108/-/DCSupplemental

178. Yamada, Y. R. & Forger, D. B. Multiscale complexity in the mammalian circadian clock. *Current Opinion in Genetics & Development* **20,** 626–633 (2010).

179. Sarkar, R. R., Maithreye, R. & Sinha, S. Design of regulation and dynamics in simple biochemical pathways. *J. Math. Biol.* **63,** 283–307 (2010).

180. DeWoskin, D., Geng, W., Stinchcombe, A. R. & Forger, D. B. It is not the parts, but how they interact that determines the behaviour of circadian rhythms across scales and organisms. *Interface Focus* **4,** 20130076–20130076 (2014).

181. Virshup, D. M., Eide, E. J., Forger, D. B., Gallego, M. & Harnish, E. V. Reversible protein phosphorylation regulates circadian rhythms. *Cold Spring Harb. Symp. Quant. Biol.* **72,** 413–420 (2007).

182. Lee, J. *et al.* Dual Modification of BMAL1 by SUMO2/3 and Ubiquitin Promotes Circadian Activation of the CLOCK/BMAL1 Complex. *Molecular and Cellular Biology* **28,** 6056–6065 (2008).

183. Buhr, E. D. & Takahashi, J. S. Molecular components of the Mammalian circadian clock. *Handb Exp Pharmacol* **217,** 3–27 (2013).

184. Parker, D. *et al.* Role of secondary structure in discrimination between constitutive and inducible activators. *Molecular and Cellular Biology* **19,** 5601–5607 (1999).

185. Edgar, R. S. *et al.* Peroxiredoxins are conserved markers of circadian rhythms. *Nature* **485,** 459–464 (2012).

186. O'Neill, J. S. & Reddy, A. B. Circadian clocks in human red blood cells. *Nature* **469,** 498–503 (2011).

187. Dunker, A. K., Bondos, S. E., Huang, F. & Oldfield, C. J. Intrinsically disordered proteins and multicellular organisms. *Seminars in Cell and Developmental Biology* **37,** 44–55 (2015).

188. Tompa, P. *et al.* Close encounters of the third kind: disordered domains and the interactions of proteins. *BioEssays* **31,** 328–335 (2009).

189. van der Lee, R. *et al.* Classification of Intrinsically Disordered Regions and Proteins. *Chem. Rev.* **114,** 6589–6631 (2014).

190. Fuxreiter, M. *et al.* Malleable machines take shape in eukaryotic transcriptional regulation. *Nat. Chem. Biol.* **4,** 728–737 (2008).

191. Fuxreiter, M. *et al.* Disordered Proteinaceous Machines. *Chem. Rev.* **114,** 6806–6843 (2014).

192. Fuxreiter, M. & Tompa, P. Fuzzy complexes: a more stochastic view of protein function. *Adv. Exp. Med. Biol.* **725,** 1–14 (2012).

CHAPTER 2

CRYPTOCHROME 1 REGULATES THE CIRCADIAN CLOCK THROUGH DYNAMIC INTERACTIONS WITH THE BMAL1 C-TERMINUS

ABSTRACT

The molecular circadian clock in mammals is generated from transcriptional activation by the bHLH-PAS transcription factor CLOCK–BMAL1 and subsequent repression by PERIOD and CRYPTOCHROME (CRY). The mechanism by which CRYs repress CLOCK–BMAL1 to close the negative feedback loop and generate 24-hour timing is not known. Here we show that CRY1 competes for binding with coactivators to the intrinsically unstructured C-terminal transactivation domain (TAD) of BMAL1 to establish a functional switch between activation and repression of CLOCK–BMAL1. Mutations within the TAD that alter binding affinities for coregulators change the balance of repression and activation to consequently change intrinsic circadian period or eliminate cycling altogether. Our results suggest that CRY1 fulfills its role as an essential circadian repressor by sequestering the TAD from coactivators and highlight regulation of the BMAL1 TAD as a critical mechanism for establishing circadian timing.

INTRODUCTION

Mammalian circadian rhythms integrate behavior, physiology and metabolism into daily cycles that are coordinated with the solar day.[1] Circadian timing arises from a genetically encoded oscillator that uses transcriptional feedback loops to generate a self-sustaining clock and control the output of clock-controlled genes with near 24-hour periodicity.[2] At the core of this molecular circadian clock, the heterodimeric basic helix-loop-helix PER-ARNT-SIM (bHLH-PAS) transcription factor CLOCK–BMAL1 drives expression of the *Period* (*Per*) and *Cryptochrome* (*Cry*) genes. PER and CRY proteins form complexes that are posttranslationally modified to control stability and translocation into the nucleus where they repress CLOCK–BMAL1-mediated transcription, thereby closing the transcriptional feedback loop[3-5]. However, the mechanisms by which PER and CRY fulfill their roles as negative transcriptional regulators are still not fully understood. In addition to its role in early repressive PER–CRY complexes, CRY1 also interacts directly with CLOCK–BMAL1 *in vitro*[6] and on chromatin later in the circadian cycle[7,8], and it can potently repress CLOCK–BMAL1 activity in the absence of PER.[9,10] Therefore, identifying

how CRY1 regulates CLOCK–BMAL1 will provide valuable insight into its essential role in the molecular circadian clock.

Because many factors contribute to robustness of circadian behavior at the organismal level (e.g., intercellular coupling in the suprachiasmatic nucleus and other systemic cues), delineating the biochemical mechanisms needed to establish circadian cycling from *in vivo* studies has been challenging.[11,12,13] For example, BMAL1 (also known as ARNTL) and its partner CLOCK interact through their N-terminal bHLH and tandem PAS domains[14]; these core bHLH-PAS domains are largely conserved in the paralog BMAL2 (also known as ARNTL2). However, *Bmal1*$^{-/-}$ mice lack all behavioral and molecular circadian rhythms, establishing its essential role in the molecular circadian clock.[15] While overexpression of *Bmal2* in *Bmal1*$^{-/-}$ mice can partially rescue circadian behavior, paradoxically, it does not restore circadian rhythms in most tissues.[16] Therefore, we still lack a fundamental understanding of how core clock proteins function to generate the transcription-based circadian clocks in mammals.

The distinct functions of the two *Bmal* paralogs offer a heuristic opportunity to uncover properties of CLOCK–BMAL1 that are needed to generate circadian oscillations. To define the circadian function of BMAL1, we employed cell-based genetic complementation in *Bmal1*$^{-/-}$ fibroblasts derived from mice harboring the *Per2*^{Luc} transgenic reporter.[17] Domain-based swapping of *Bmal1* and *Bmal2* revealed the oscillatory function of the BMAL1 C-terminus that functionally distinguishes it from its non-circadian paralog, BMAL2. We found that CRY1 binds to the transactivation domain (TAD) of BMAL paralogs at sites that overlap with binding of the coactivator, CBP (CREB-binding protein) and its homolog, p300. Mutations within the TAD markedly altered affinities for CRY1 and caused large changes in period length. These findings provide new insights into transcriptional regulation by CRY1 and demonstrate that the BMAL1 TAD plays an important role in establishing 24-hour timing.

ONLY BMAL1 CAN GENERATE CELL-AUTONOMOUS CIRCADIAN RHYTHMS

Fibroblasts derived from *Bmal1*$^{-/-}$ *Per2*^{Luc} mice are completely arrhythmic, but circadian rhythms can be restored through genetic complementation of *Bmal1* under control of the constitutive *UBC* promoter.[17] *Bmal2* was unable to restore circadian rhythms in these cells, even when its transcript and protein were expressed to similar levels as *Bmal1* (**Fig. 2.1a-c** and

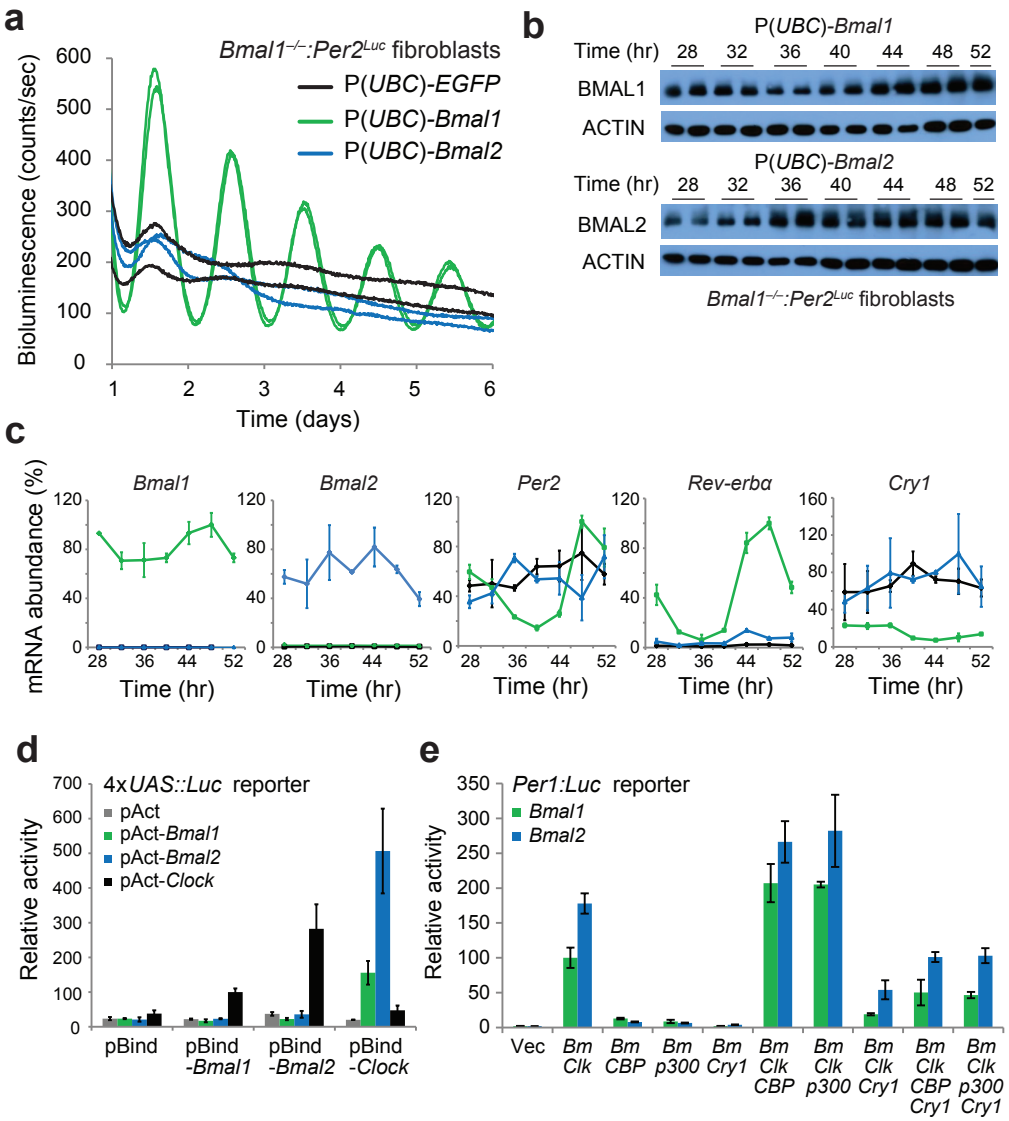

Figure 2.1: Only BMAL1 can restore circadian rhythms in *Bmal1*$^{-/-}$ *Per2*^{Luc} fibroblasts. **(a)** Luminescence records from *Bmal1*$^{-/-}$ *Per2*^{Luc} fibroblasts expressing EGFP, *Bmal1* or *Bmal2*. Traces from replicate cell cultures are shown from one representative experiment (*n* = 3 clonal lines). **(b)** Western blot of Flag-tagged *Bmal* paralog expression in *Bmal1*$^{-/-}$ *Per2*^{Luc} fibroblasts. **(c)** Expression of clock-controlled genes in *Bmal1*$^{-/-}$ *Per2*^{Luc} fibroblasts determined by quantitative reverse transcription PCR. Values are expressed as percentage of maximum expression, set to 100% for each gene except for *Bmal2*, which was normalized to *Bmal1* Points represent mean expression ± s.d. of triplicate measurements from two independent timecourses. **(d)** Luciferase-based mammalian two-hybrid assay in HEK293T cells transiently transfected with the indicated plasmid pairs. pBind, fusion with Gal4 DNA-binding domain; pAct, fusion with VP16 transactivation domain. Luminescence values are expressed as mean ± s.d. of triplicate measurements from one representative experiment (*n* = 3). Relative activity normalized to pAct-*Clock*–pBind-*Bmal1* set to 100. **(e)** *Per1-Luc* assay of CLOCK–BMAL activity in HEK293T cells transiently transfected with indicated plasmids. Vec, vector; *Bm*, *Bmal1* or *Bmal2*; *Clk*, *Clock*. Luminescence values are expressed as mean ± s.d. of triplicate measurements from one representative experiment (*n* = 3). Relative activity normalized to *Clock*–*Bmal1* set to 100.

Supplemental Fig. 2.1). Moreover, *Bmal2* was neither upregulated in *Bmal1*$^{-/-}$ cells nor upon ectopic expression of *Bmal1* (**Fig. 2.1c**) to display a lack of paralog compensation, a common network feature of genes involved in molecular circadian clocks.[18] Compared to high amplitude oscillations of *Per2* and *Rev-erbα* mRNA expression in *Bmal1*-rescued cells, we observed constitutive expression of *Per2* and *Rev-erbα* in cells expressing *Bmal2* but with lower overall mRNA levels, perhaps caused by increased expression of *Cry1* in these cells (**Fig. 2.1c**). Overall, these data demonstrate that E-box-mediated circadian transcription is substantially attenuated in the absence of *Bmal1*. Therefore, *Bmal1* and *Bmal2* are not functionally redundant; while *Bmal1* is an essential clock component, *Bmal2* is not sufficient to support the circadian clock at the cellular level.

BMAL PARALOGS HAVE SIMILAR STEADY-STATE ACTIVITIES

To begin to explore differences in the BMAL paralogs, we compared biochemical activities known to be critical for circadian function. Using a mammalian two-hybrid assay, we showed that BMAL2 had a slightly higher intrinsic affinity for CLOCK than BMAL1 (**Fig. 2.1d**). Steady-state transcription assays showed that CLOCK–BMAL2 also activated transcription of the *Per1*-luciferase (*Per1-Luc*) reporter to higher levels than CLOCK–BMAL1 (**Fig. 2.1e**), all consistent with previous observations.[19,20] Increased transcriptional activation by BMAL2 may correlate with its higher affinity for CLOCK, as mutations that decrease affinity of BMAL1 for CLOCK lead to decreased transactivation.[14] Moreover, complexes of CLOCK with either BMAL1 or BMAL2 were both capable of further activation by CBP or p300, and repression by CRY1 (**Fig. 2.1e**). Therefore, even though BMAL2 is unable to support the molecular circadian clock in *Bmal1*$^{-/-}$ cells, its steady-state activities appear to be comparable to BMAL1. These apparently paradoxical data suggest that a balance of affinities for transcriptional coregulators may be important for establishing the appropriate strength of activation and repression needed to establish circadian oscillations.

THE C-TERMINUS OF BMAL1 IS NEEDED FOR CIRCADIAN CYCLING

To identify specific sequences in BMAL1 that confer circadian function, we generated a series of domain-swapping chimeras by systematically substituting regions of *Bmal1* with corresponding sequences from *Bmal2* (**Fig. 2.2a**). To minimize issues with protein misfolding, we used highly conserved or identical sequences at swap junctions (**Supplemental Fig. 2.2**) and

tested the ability of chimeras to express full-length proteins (**Supplemental Fig. 2.3**). We then examined the ability of the chimeras to restore circadian rhythms in *Bmal1*$^{-/-}$ *Per2*^{Luc} fibroblasts following lentiviral transduction and stable selection.

The *Bmal1*-A2 mutant, harboring substitution of the distal N-terminus of *Bmal2* into *Bmal1*, rescued circadian rhythms of the same period (**Fig. 2.2b,c**) albeit with significantly lower amplitude than wild type *Bmal1* (**Supplemental Fig. 2.3**) possibly arising from the lack of an NLS in the BMAL2 N-terminus.[21] Chimeras based on swaps of other individual regions within the core bHLH-PAS domains of BMAL2 (i.e., *Bmal1*-B2, -C2, -D2, -E2 and -F2) were all able to restore circadian rhythms**,** albeit with some changes in period (-D2) or amplitude (-D2, -E2) depending on the individual region (**Fig. 2.2b,c** and **Supplemental Fig. 2.3**). A *Bmal1* chimera containing the intact, tandem PAS domains from *Bmal2* was also able to reconstitute circadian rhythms (**Fig. 2.2d**). By contrast, substitution of the PAS domain core of *Bmal1* into *Bmal2* (the *Bmal2*-PAS1 mutant) did not confer the ability to generate rhythms to *Bmal2* (**Fig. 2.2d**). Together, these data demonstrate that the distal N-terminus and bHLH-PAS core domains do not define the distinct ability of BMAL1 to generate circadian rhythms.

Next we examined the divergent C-termini, focusing on the H region that encompasses a transcriptional activation domain (TAD) at the distal C-terminus[22], and an upstream G region that contains the intervening sequence after the PAS domains (**Fig. 2.2a**). Swaps of either the G or H region (*Bmal1*-G2 and *Bmal1*-H2) rescued circadian rhythms, but exhibited a significantly shorter period and lower amplitude compared to *Bmal1* (**Fig. 2.2e,f** and **Supplemental Fig. 2.3**). Strikingly, a *Bmal1* chimera fused to the entire C-terminus of *Bmal2* (*Bmal1*-G2H2) was unable to restore circadian rhythms of the *Per2*^{Luc} reporter (**Fig. 2.2e**) or mRNA expression of clock-controlled genes (**Supplemental Fig. 2.3**). Therefore, the sequence determinants that distinguish the circadian functions of the two BMAL paralogs lie in their divergent and poorly characterized C-termini.

BMAL1 C-TERMINAL TAD DETERMINES CIRCADIAN PERIOD

To begin to dissect how the BMAL1 C-terminus regulates circadian function, we focused our attention on the transactivation domain of the H region. The ability of the TAD to interact with both negative[22-25] and positive[26] transcriptional coregulators provides a clear first step towards

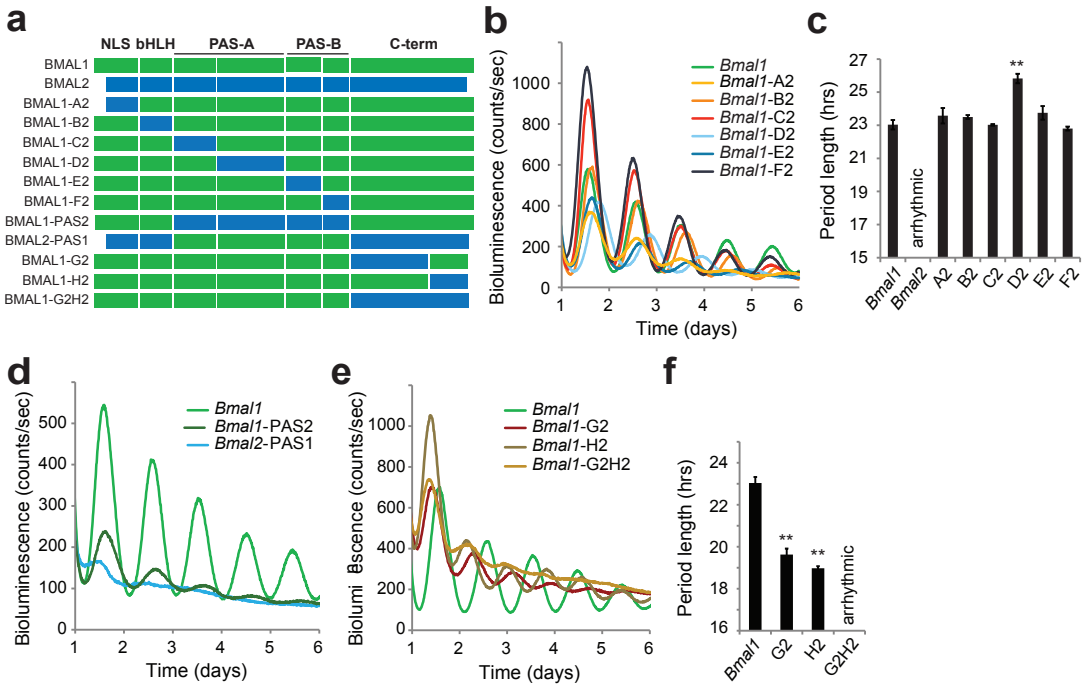

Figure 2.2: The BMAL1 C-terminus is needed for circadian function. **(a)** Domain organization of BMAL proteins and diagram of chimeric constructs. Chimera boundaries can be found in Supplemental **Fig. 2.2**. **(b)** Luminescence records from *Bmal1*$^{-/-}$ *Per2*^{Luc} fibroblasts expressing WT *Bmal1* or *Bmal1* chimeras with *Bmal2* substitutions of the N-terminal core domains. One trace per chimera is shown from a representative experiment (*n* = 3 clonal lines with 2 cell culture replicates each). **(c)** Mean period of rescued circadian luminescence rhythms ± s.d. (*n* = 3 clonal lines with 2 cell culture replicates each). **(d)** Luminescence records from *Bmal1*$^{-/-}$ *Per2*^{Luc} fibroblasts expressing WT *Bmal1* or PAS-swapping chimeras. One trace per chimera is shown from a representative experiment (*n* = 3 clonal lines with 2 cell culture replicates each). **(e)** Luminescence records from *Bmal1*$^{-/-}$ *Per2*^{Luc} fibroblasts expressing WT *Bmal1* or C-terminal chimeras. One trace per chimera is shown from a representative experiment (*n* = 3 clonal lines with 2 cell culture replicates each). **(f)** Mean period of rescued circadian luminescence rhythms ± s.d. (*n* = 3 clonal lines with 2 cell culture replicates each). *** $P < 0.001$ compared to WT *Bmal1*, two-tailed paired *t* test.

understanding how the BMAL1 C-terminus may control protein interactions and progression of circadian transcription. We began by confirming that the TAD is both required for transcriptional activation by CLOCK–BMAL1[22] and necessary to rescue circadian cycling in *Bmal1*$^{-/-}$ *Per2*^{Luc} fibroblasts (**Supplemental Fig. 2.3**).

In our chimera studies, substitution of the *Bmal2* TAD (H domain) into *Bmal1* gave rise to a circadian period that was more than three hours shorter than wild-type (WT) *Bmal1* (**Fig. 2.2f**). Nearly half of the C-terminal 30 residues in the TAD are divergent between BMAL1 and BMAL2 (**Supplemental Fig. 2.2**), particularly within the predicted α-helix (**Fig. 2.3a**). To identify the

sequence determinants that give rise to this dramatic change in period length, we performed site-directed mutagenesis to mutate groups of *Bmal1* TAD residues to their corresponding sequences in *Bmal2* and tested their ability to rescue circadian rhythms in *Bmal1*$^{-/-}$ *Per2*^{Luc} fibroblasts. Two *Bmal1* mutants, E597S A598I A599D and V602A I603F, exhibited significantly shorter period lengths (~22.5 and ~22.0 h, respectively) compared to WT *Bmal1* (~23.5 h) (**Fig. 2.3b,e**). The effect of these mutations was nearly additive, as the combined *Bmal1* mutant (E597S A598I A599D V602A I603F) led to a substantially shorter period length (~20.6 h) (**Fig. 2.3c,e**).

The *Bmal1* V602A I603F mutant may interfere with function of the TAD IxxLL recognition motif (**Fig. 2.3a**), a helical sequence known to recruit proteins associated with transcriptional regulation such as the KIX domain of CBP or p300 (refs. 27,28). Mutation of the first leucine within the IxxLL motif in the *Bmal1* S605N L606Y mutant led to a significantly longer period

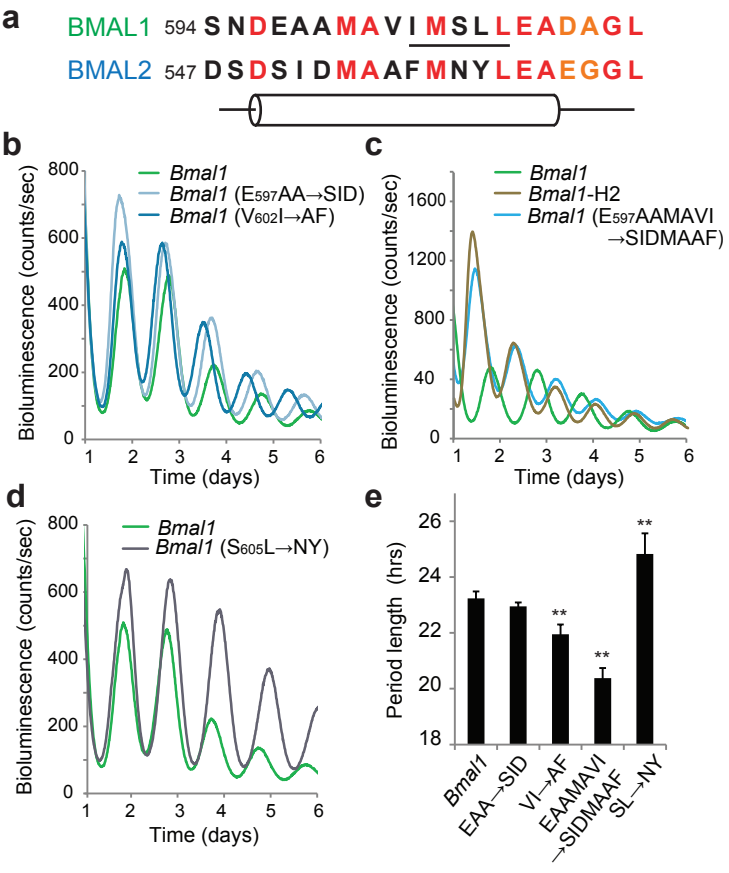

Figure 2.3: A helical motif within the BMAL1 H domain controls circadian period length. **(a)** Comparison of BMAL paralog sequence and predicted secondary structure near the H domain α-helix. Underlined, KIX-binding IxxLL motif. Residue coloring: red, conserved; orange, similar; black, non-conserved. Cylinder, predicted α-helix. **(b-d)** Luminescence records from *Bmal1*$^{-/-}$ *Per2*^{Luc} fibroblasts expressing WT *Bmal1* or *Bmal1* chimeras with substitutions from the *Bmal2* H domain α-helix, including mutants of the N-terminal **(b-c)** or C-terminal half of the α-helix **(d)**. One trace per chimera is shown from a representative experiment (n = 3 clonal lines with 2 cell culture replicates each). **(e)** Mean period of rescued circadian luminescence rhythms ± s.d. (n = 3 clonal lines with 2 cell culture replicates each). ** P < 0.01, *** P < 0.001 compared to WT *Bmal1*, two-tailed paired t test.

and higher amplitude cycling compared to *Bmal1* (**Fig. 2.3d,e**). Therefore, we observed large changes in period length of the molecular circadian clock (~5 h from shortest to longest) upon incorporation of BMAL2 residues into the BMAL1 TAD α-helix. These data suggest that modulation of TAD structure and/or interactions with transcriptional coregulators can fine-tune the balance of activation and repression to control progression of the circadian clock.

THE BMAL1 TAD IS INTRINSICALLY UNSTRUCTURED

Striking changes in circadian period elicited by TAD mutations prompted us to investigate the biochemical basis by which the TAD regulates CLOCK–BMAL1 function. The last 30 residues of the TAD are highly conserved between vertebrates and insects that possess a vertebrate-like clock (**Supplemental Fig. 2.4**), in which transcriptional repression is driven by CRY[29]. Aside from the single α-helix, the BMAL1 TAD (residues 579-626) is predicted to be intrinsically disordered, typical of transactivation domains found in other transcription factors.[30] Given the predicted flexibility of this essential domain, we turned to solution NMR spectroscopy to study the TAD. A heteronuclear single quantum coherence (HSQC) spectrum of the ^{15}N-labeled TAD protein backbone displayed the modest chemical shift dispersion expected for a disordered protein. The lack of structure was verified by chemical shift analyses of Cα and Cβ assignments[31,32], which confirmed modest helical propensity localized only to the predicted α-helical region (**Supplemental Fig. 2.4**).

CRY1 AND CBP(P300) COMPETE FOR BMAL1 TAD BINDING

To examine binding of transcriptional coregulators on the BMAL1 TAD, we used a CRY1 CC peptide representing a monomeric, surface-exposed α-helix on CRY1 needed for CLOCK–BMAL1 repression[33], or the isolated CBP(p300) KIX domain, one of several TAD-binding modular domains from CBP and p300 proteins (**Supplemental Fig. 2.4**). Both the CRY1 CC and CBP(p300) KIX domain have been reported to interact with the BMAL1 TAD.[24,26] To identify binding sites on the TAD, we collected ^{15}N HSQC spectra of ^{15}N-labeled TAD alone or in the presence of coregulators. Titration of ^{15}N TAD with either the CRY1 CC, CBP or p300 KIX domains led to chemical shift perturbations at similar residues, confirming their interaction and further demonstrating that their binding sites overlap on the TAD (**Supplemental Fig. 2.4**). Marked differences in the linewidth of ^{15}N TAD crosspeaks occurred upon binding to coregulators, particularly at residues in or near the IxxLL motif (e.g. V602 and S605, **Supplemental**

Fig. 2.4). As other TADs can undergo a coupled folding and binding process to form helical complexes with KIX domains[34], the observed changes in linewidth upon coregulator binding reflect different rates of chemical exchange that could arise from changes in affinity, conformational exchange, or both.

Chemical shift mapping revealed that the shared binding sites center on the canonical KIX-binding IxxLL motif within the TAD α-helix, as well as a second cluster of seven residues in the distal C-terminus (**Fig. 2.4a,b**). The CRY1 binding sites we identify here agree with previous studies that indicate 1:1 stoichiometry of the complex[23-25]. To determine if CRY1 and p300 could compete for binding to the TAD, we performed a ^{15}N HSQC titration with ^{15}N TAD and CRY1 CC to a 1:1 stoichiometric ratio, and then added an equivalent amount of the p300 KIX domain (**Fig. 2.4c**). ^{15}N TAD crosspeaks are expected to fall somewhere between the binary ^{15}N TAD–CRY1 or ^{15}N TAD–KIX complexes, representing a population-weighted average of complexes present in solution. Our data showed that addition of p300 KIX domain to ^{15}N TAD–CRY complexes resulted in relocalization of ^{15}N TAD crosspeaks to the ^{15}N TAD–KIX complex (**Fig. 2.4c**), reporting that the p300 KIX domain effectively competes CRY1 CC off the TAD *in vitro*.

DYNAMIC INTERACTIONS OF TAD WITH CRY1 AND CBP(P300)

To investigate coupling between the TAD α-helix and distal C-terminus, we took advantage of paramagnetic relaxation enhancement (PRE) with manganese, a paramagnetic cation that induces loss of peak intensities when brought into close proximity (~20-25 Å) of NMR-active nuclei. We acquired ^{15}N HSQC spectra of ^{15}N TAD possessing a C-terminal cysteine covalently coupled to EDTA (^{15}N TAD–EDTA) in the presence and absence of chelated Mn^{2+}. Covalent modification of the TAD with EDTA via the added cysteine does not impact complex formation with p300 KIX or CRY1 CC (**Supplemental Fig. 2.5**). We found no evidence that the distal C-terminus interacts appreciably with the α-helix in the free TAD, as Mn^{2+}-dependent broadening was confined to residues proximal to the labeling site (**Fig. 2.4d**), consistent with localized PRE effects seen in other disordered proteins.[35]

To determine if the TAD undergoes dynamic conformational rearrangement upon complex formation, we collected ^{15}N HSQC spectra of the ^{15}N TAD–EDTA ± Mn^{2+} titrated with either p300

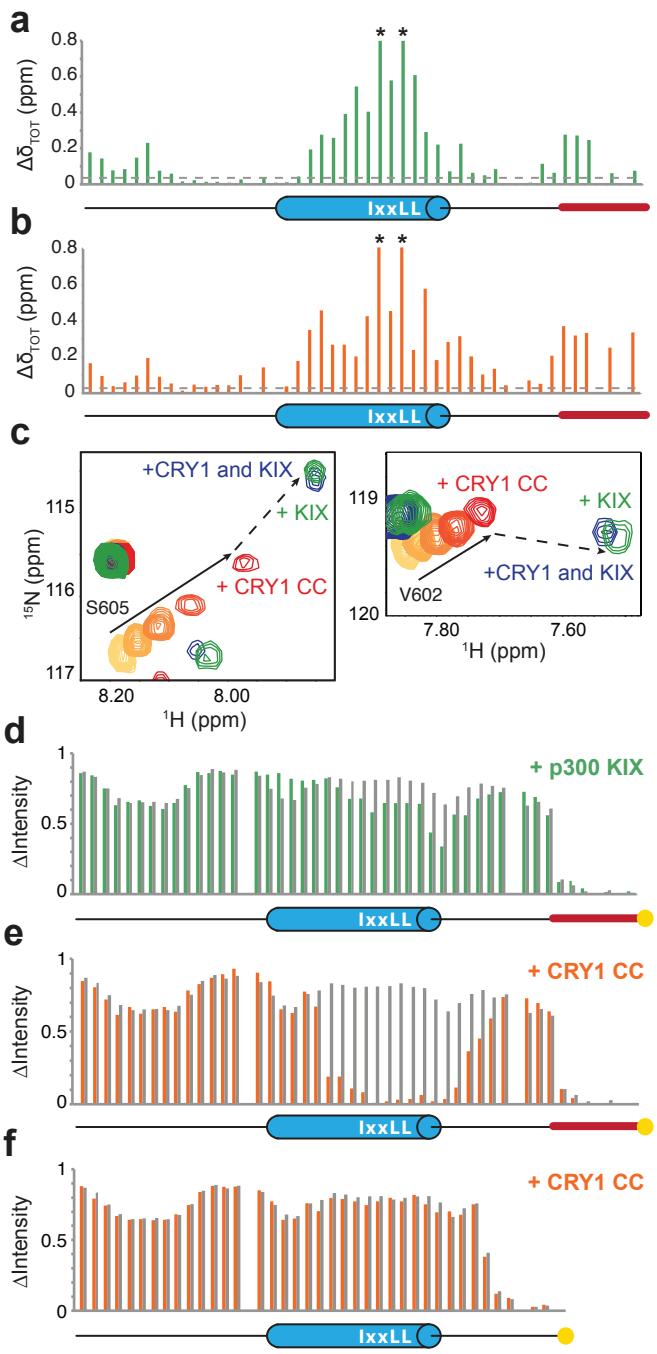

Figure 2.4: CBP(p300) and CRY1 interact with BMAL1 TAD. **(a-b)** Backbone chemical shift perturbations of ^{15}N BMAL1 TAD with stoichiometric p300 KIX **(a)** or CRY1 CC **(b)**. p.p.m., parts per million. Dashed line, $\Delta\delta_{TOT}$ significance cutoff = 0.04 p.p.m. *residues broadened beyond detection. **(c)** Highlighted regions of ^{15}N HSQC spectra showing titration of ^{15}N BMAL1 TAD with CRY1 CC to 1:1 stoichiometry (light to dark purple; solid arrow); at 1:1 stoichiometry with p300 KIX (green); or in the presence of both CRY1 CC and p300 KIX (brown). Dashed line shows transition of ^{15}N TAD–CRY1 to ^{15}N TAD–p300 KIX upon competition. **(d-e)** Relative^{15}N TAD–EDTA peak intensities from PRE experiments as ratio of Mn^{2+} chelation by the C-terminal EDTA (black circle) in the free protein (gray), or upon complex formation with p300 KIX (green) **(d)** or CRY1 CC (purple) **(e)**. **(f)** Relative^{15}N TAD 619X–EDTA peak intensities from PRE experiments as ratio of Mn^{2+} chelation by the C-terminal EDTA (black circle) in the free protein (gray), or upon complex formation with CRY1 CC (purple).

KIX or CRY1 CC (**Supplemental Fig. 2.5**). Quantitative analysis of Mn^{2+}-dependent changes in peak intensity identified regions near the TAD helix that are decreased upon formation of both ^{15}N TAD–p300 KIX (**Fig. 2.4d**) and ^{15}N TAD–CRY1 CC complexes (**Fig. 2.4e**). We observed a striking, near complete loss of signal intensity at the TAD α-helix upon binding to CRY1 CC (**Fig. 2.4e**), suggesting that the distal C-terminus is brought into close proximity to the TAD

α-helix in a CRY1-dependent manner. A ^{15}N TAD mutant lacking the seven residues at the distal C-terminus lost this CRY1- and Mn^{2+}-dependent broadening of the TAD α-helix (**Fig. 2.4f**), demonstrating the dependence of the conformational rearrangement on the distal C-terminus. Thus, the BMAL1 TAD is highly dynamic in its interactions with transcriptional coregulators.

TAD MUTATIONS ALTER AFFINITY FOR CRY1 AND CBP(P300)

To explore functional differences in the TADs of BMAL1 and BMAL2, we generated a suite of mutant proteins to quantitatively compare against WT TAD interactions with transcriptional coregulators. Like BMAL1, the BMAL2 TAD (residues 540-579) is intrinsically disordered with a weakly formed α-helix, and it interacts with both p300 KIX and CRY1 CC at the α-helix as well as the C-terminal seven residues (**Supplemental Fig. 2.6**). We focused on two substitution mutants of the BMAL1 TAD α-helix (the short period V602A I603F mutant and long period S605N L606Y mutant) (see **Fig. 2.3**), and two structure-based mutants, the L606A L607A mutant, designed to interfere with the IxxLL motif, and the 619X truncation mutant that removed the C-terminal seven residues. In all cases, mutation-induced backbone chemical shift perturbations localized to the site of mutation, demonstrating that we can selectively perturb either the α-helix or the distal C-terminus (**Supplemental Fig. 2.6**).

We determined affinities of the TADs for the CBP KIX domain or CRY1 CC using isothermal titration calorimetry (ITC, **Supplemental Fig. 2.7**). Due to relatively low heats evolved in the TAD–CRY1 CC ITC experiments, we also determined affinities for CRY1 CC using a fluorescence polarization (FP) assay (**Supplemental Fig. 2.7**) and obtained comparable affinities to our ITC data (**Table 2.1**). The L606A L607A mutant disrupted interaction with the CBP KIX domain or CRY1 CC under our assay conditions (**Fig. 2.5a,b**). We found that the other TADs had relatively similar affinities for the CBP KIX domain while affinities for CRY1 CC varied by an order of magnitude. Notably, the short period V602A I603F mutant decreased affinity for CRY1 CC by about three-fold compared to the WT BMAL1 TAD, while the long period S605N L606Y mutant increased affinity by about three-fold (**Table 2.1**). These opposing phenotypes result from substitution of different residues from BMAL2; however, affinity of the intact BMAL2 TAD was similar to BMAL1 (**Table 2.1**), suggesting a complicated interplay of sequence context and structural dynamics in recognition of transcriptional coregulators by BMAL paralog TADs. Moreover, truncation of the C-terminal seven residues (619X) decreased affinity for CRY1 CC

Table 2.1: Dissociation constants for the interaction of BMAL transactivation domains with transcriptional coregulators

Construct	CBP KIX (μM)	CRY1 CC (μM)	
	ITC*	ITC*	FP**
BMAL1	2.05 ± 0.11	6.13 ± 0.82	6.80 ± 1.00
BMAL1 V603A I604F	1.17 ± 0.09	nd	17.3 ± 0.30
BMAL1 S605N L606Y	0.98 ± 1.18	2.16 ± 0.28	2.9 ± 1.50
BMAL1 619X	4.44 ± 0.23	19.67 ± 2.57	nd
BMAL1 L606A L607A	nd	nd	nd
BMAL2	5.59 ± 0.81	6.10 ± 1.50	6.00 ± 0.80

*K_D values from one representative ITC experiment with standard error for fit (*n* = 2 or 3).

**Mean K_D values (calculated from *n* = 4 replicates with s.d.) from one representative FP experiment (*n* = 3).

nd, binding not detectable under experimental conditions

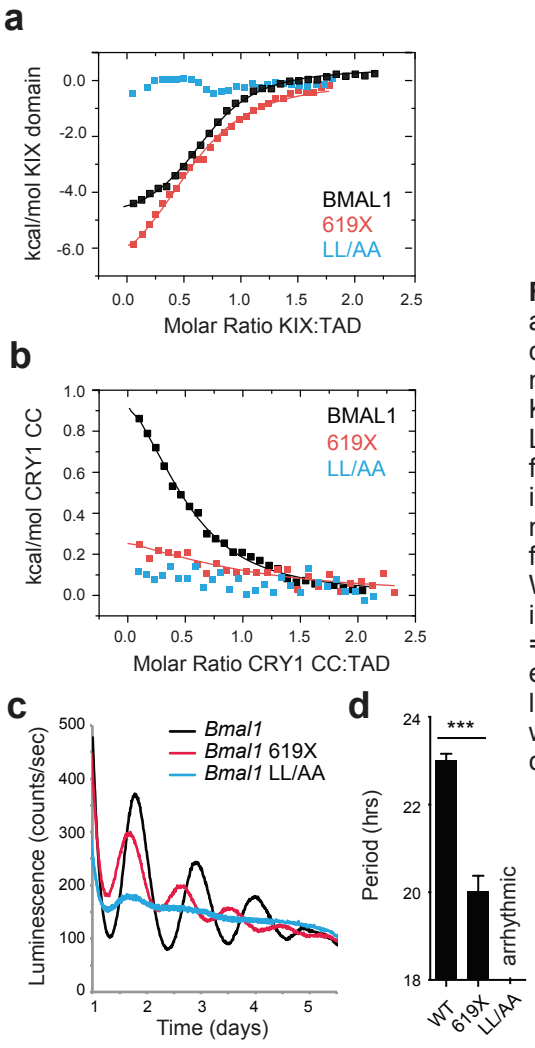

Figure 2.5: BMAL1 TAD mutations decrease affinity for CBP(p300) and CRY1 and influence circadian period. **(a)** Isothermal titration calorimetric (ITC) profiles for the interaction of CBP KIX domain with WT or mutant BMAL1 TADs. Line, one-site binding model representing best fit to data; see Table 1. **(b)** ITC profile for the interaction of CRY1 CC peptide with WT or mutant BMAL1 TADs. **(c)** Luminescence records from *Bmal1*$^{-/-}$ *Per2*^{Luc} fibroblasts expressing WT or mutant *Bmal1*. One trace per chimera is shown from a representative experiment (*n* = 3 clonal lines with 2 cell culture replicates each). **(d)** Mean period of rescued circadian luminescence rhythms ± s.d. (*n* = 3 clonal lines with 2 cell culture replicates each). *** $P < 0.001$ compared to WT *Bmal1*, two-tailed paired *t* test.

to an extent similar to the V602A I603F mutation. Collectively, these data suggest that the IxxLL motif in the TAD α-helix is the major binding site for both CRY1 CC and CBP(p300) KIX domains, although the distal C-terminus also makes an important contribution. The preferential effect of mutations on CRY1 binding relative to CBP(p300) suggests that modulating affinity for CRY1 may elicit the changes in circadian periodicity we measured in the mutants.

TAD MUTATIONS PERTURB CIRCADIAN TIMEKEEPING

To test our prediction that BMAL1 TAD interactions play an important role in period determination, we complemented *Bmal1*$^{-/-}$ *Per2*^{Luc} cells with either the C-terminal truncation (619X) or the L606A L607A mutant of *Bmal1.* Truncation of the C-terminus shortened the intrinsic period by nearly three hours, while the L606A L607A mutant abolished cycling (**Fig. 2.5c,d** and **Supplemental Fig. 2.7**). Given that these TAD mutations substantially reduce affinity for CRY1 (**Table 2.1**), we sought to measure CRY1 repression of CLOCK–BMAL1 mutants in *Per1-Luc* reporter assays. CLOCK–BMAL1 complexes harboring either the L606A L607A or 619X mutation exhibited decreased steady-state activity, although BMAL1 proteins were expressed to similar levels (**Fig. 2.6a** and **Supplemental Fig. 2.8**). Repression by CRY1 was significantly reduced with both mutants, but to a greater extent with the L606A L607A mutant (**Fig. 2.6b**), consistent with our observation that this mutation leads to a greater reduction in apparent affinity for CRY1 (**Table 2.1**).

CRY1 BINDS TO MULTIPLE SITES ON CLOCK–BMAL1

Formation of a stable ternary complex consisting of CLOCK, BMAL1, and CRY1 lies at the heart of CRY1-dependent negative feedback in the clock.[6,7,10,36] Given the modest affinities that we measured for the BMAL1 TAD and isolated CRY1 CC peptide, we reasoned that there are likely other interactions between the CLOCK–BMAL1 complex and CRY1. Mutations that localize in or adjacent to the solvent-exposed HI loop of the CLOCK PAS-B domain (named for its location between the Hb and Ib strands of the PAS domain; **Fig. 2.6c**)[14] in CLOCK also reduce repression by CRY1 (refs. 22,25,37). To determine if mutation of the CLOCK HI loop (Q361P W362R) affects complex formation with CRY1, we performed coimmunoprecipitation assays to examine interaction of CRY1-myc with WT or HI mutant Flag-tagged CLOCK and WT BMAL1. We showed that, while WT CLOCK and BMAL1 coimmunoprecipitated with CRY1-myc, mutation of the CLOCK HI loop rendered CLOCK and BMAL1 unable to stably interact with

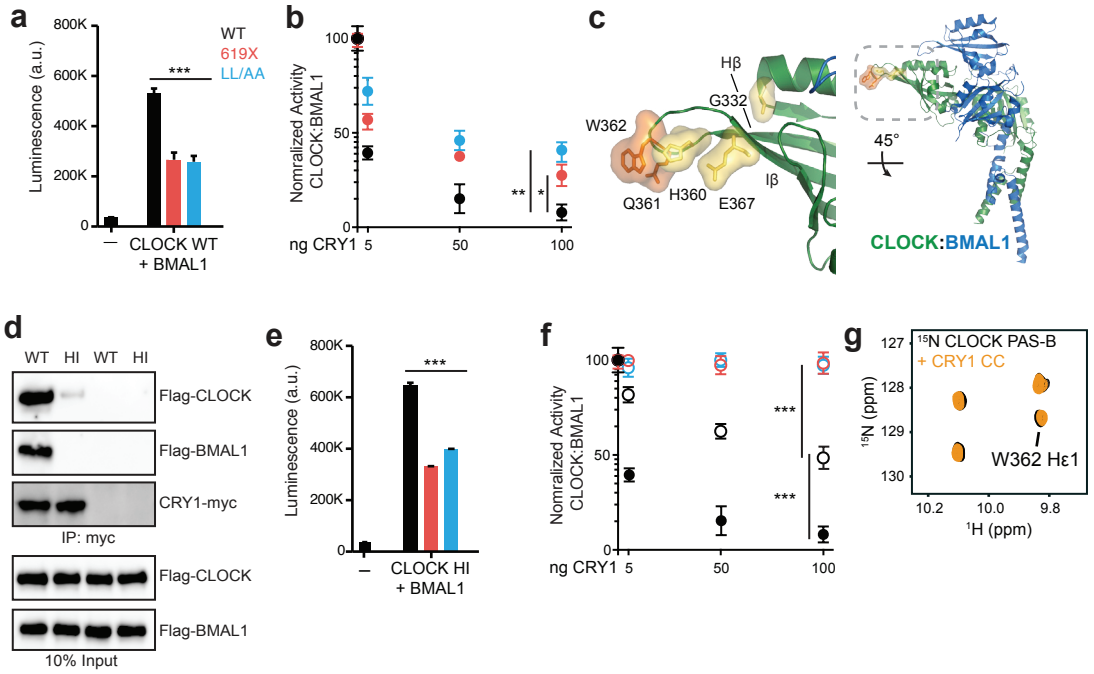

Figure 2.6: Distinct sites on CLOCK and BMAL1 facilitate repression by CRY1. (a) *Per1-Luc* assay in HEK293T cells transiently transfected with plasmids encoding *Clock* WT and *Bmal1* WT, 619X or L606A L607A. Relative light units (RLU) are scaled down by 10^3 and expressed as mean ± s.d. of triplicate measurements from one representative experiment (n = 3). (b) *Per1-Luc* assay with increasing amounts of plasmids encoding *Cry1* with *Clock* WT and *Bmal1* WT, 619X or L606A L607A. Relative activity normalized to *Clock* WT–*Bmal1* WT set to 100. (c) Residues in the Hβ-Iβ (HI) loop on CLOCK PAS-B (PDB 4F3L)[14] that reduce CRY1 repression when mutated (yellow[25] or orange[37]). (d) Coimmunoprecipitation (IP) of Flag-CLOCK WT or HI (Q361P W362R) and Flag-BMAL1 by CRY1-myc from HEK293T cells with anti-myc antibody. Western blots (IB) were performed using indicated antibodies. Uncropped images can be found in Supplementary Data Set 1. (e) *Per1-Luc* assay with plasmids encoding *Clock* WT and *Bmal1* WT, 619X or L606A L607A. RLU represented as in panel (a). (f) *Per1-Luc* assay with increasing amounts of plasmid encoding *Cry1* with *Clock* HI and *Bmal1* WT, 619X or L606A L607A. Relative activity normalized to *Clock* HI–*Bmal1* WT set to 100. (g) Tryptophan indole region of ^{15}N HSQC spectra showing ^{15}N CLOCK PAS-B in the absence (black) and presence (orange) of CRY1 CC. The full spectrum can be found in Supplemental F**ig. 2.8**. ** $P < 0.01$; ***$P < 0.001$ compared to *Bmal1* WT by two-tailed paired *t* test.

CRY1-myc (**Fig. 2.6d** and **Supplemental Fig. 2.8**). Taken together, complex formation between CRY and CLOCK–BMAL1 occurs through interactions with both the BMAL1 C-terminus and CLOCK PAS-B.

To explore how the interaction of CRY1 with CLOCK PAS-B impacts regulation of CLOCK–BMAL1, we assayed *Per1-Luc* activity. Transcriptional activation by CLOCK HI–BMAL1 complexes is similar to WT CLOCK–BMAL1 (**Fig. 2.6a, e**), but repression by CRY1 is significantly reduced (**Fig. 2.6f**). Strikingly, we found that mutation of the CLOCK PAS-B HI loop

in conjunction with BMAL1 L606A L607A or 619X eliminated repression by CRY1 (**Fig. 2.6f**), even when CRY1 was overexpressed to suprastoichiometric levels relative to CLOCK–BMAL1 (**Supplemental Fig. 2.8**). We could not detect a direct interaction between CRY1 CC and ^{15}N CLOCK PAS-B by NMR spectroscopy (**Fig. 2.6g** and **Supplemental Fig. 2.8**), indicating that the CLOCK PAS-B domain mediates interactions with CRY1 through a site distinct from the CRY1 CC α-helix. Therefore, simultaneous disruption of CRY-interacting interfaces on CLOCK PAS-B and the BMAL1 TAD eliminates CRY1 regulation of CLOCK–BMAL1, demonstrating the importance of multivalent interactions for CRY1 repression.

DISCUSSION

Our study leveraged the finding that although BMAL1 and its close paralog BMAL2 share similar steady-state biochemical activities, BMAL2 is unable to sustain circadian cycling[15,17], allowing us to discover that the C-terminus of BMAL1 holds the key to generating circadian oscillations. By integrating data from biophysical and cell-based assays, we now identify the important role the BMAL1 TAD plays in the clock and identify two distinct binding sites on CLOCK–BMAL1 that are required for CRY1 function. The first site on the CLOCK PAS-B domain presumably functions as a docking site to localize CRY1 to the complex, and the second site on the BMAL1 TAD controls the circadian activity of CLOCK–BMAL1. From the mutations studied here, we find that affinity of the TAD for CRY1 appears to correlate with period; decreasing affinity leads to shorter periods while increasing affinity leads to longer periods (**Fig. 2.7a**). We find it compelling that substitution of only a few residues within the BMAL1 TAD α-helix can elicit circadian rhythms with shorter or longer than normal periods (**Fig. 2.7b**), demonstrating that the TAD plays an important role in establishing intrinsic circadian timekeeping. Our observation of opposing period phenotypes encoded by adjacent sequences within the α-helix of the BMAL2 TAD may explain why it is an outlier when comparing CRY1 affinity and period (**Fig. 2.7a**). Additional studies of BMAL1 and BMAL2 TADs that also take into consideration the G region identified in this study will be needed to understand the biochemical properties of BMAL1 that enable dynamic interactions with coregulators that underlie generation of self-sustaining circadian rhythms.

CRY1 appears to fulfill part of its essential role as a negative regulator by interacting directly with CLOCK–BMAL1 to sequester the BMAL1 TAD from coactivators (**Fig. 2.7c**). Here we

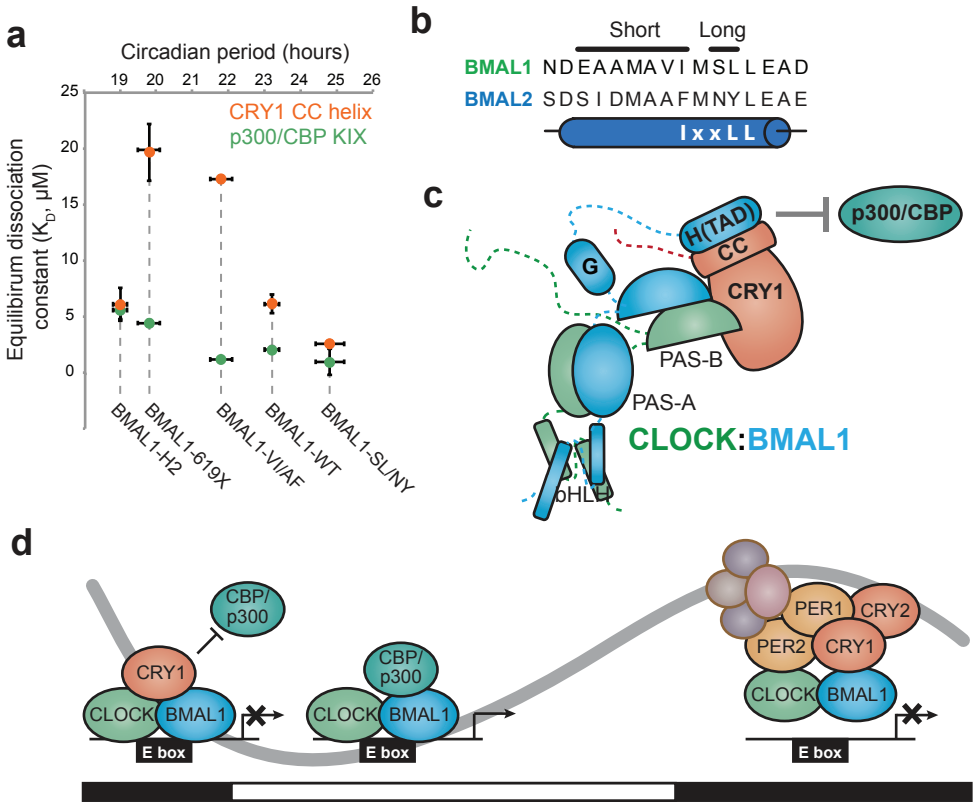

Figure 2.7: Regulation of the BMAL1 TAD by CRY1 contributes to determination of circadian period. (a) Correlation of coregulator affinities for isolated TADs with period lengths from circadian rescue experiments. Not shown: *Bmal1* L606A L607A mutant, which has no observable affinity for either CBP(p300) KIX or CRY1 CC and does not rescue circadian rhythms in *Bmal1*$^{-/-}$ *Per2*^{Luc} fibroblasts. **(b)** Location of long and short period substitution mutants in the TAD α-helix. **(c)** Model of CRY1 interactions with the CLOCK–BMAL1 complex. **(d)** Model for regulation of the circadian transcriptional feedback loop by the ternary CLOCK–BMAL1–CRY1 complex. Black and white bars underneath indicate night or day, respectively. See text for more details.

examined interactions of the BMAL1 TAD with the CBP(p300) KIX domain as a proxy for coactivator recruitment. We expect that our proposed mechanism for CRY1, linking inhibition to TAD sequestration, will hold true for other coactivators and other domains from CBP(p300) that may interact with the BMAL1 TAD. It is worth noting that the related bHLH-PAS transcription factor HIF (hypoxia-inducible factor) uses both TAD-dependent and -independent modes to recruit transcriptional regulators[38-40], suggesting the potential for additional regulatory mechanisms that control CLOCK–BMAL1 activity. In this context, we note that our model is compatible with studies showing that CRY1 may also interact with additional epigenetic regulators to help achieve complete repression *in vivo*.[41]

The CRY1 mechanism we propose here occurs independently of the direct involvement of PER proteins (**Fig. 2.7d**). Recent studies show that PER2 titrates CRY1 away from direct interactions with CLOCK–BMAL1 *in vitro* and in cells.[6,42,43] Two recent CRY structures provide evidence for a possible CLOCK–BMAL1 binding site in the antenna chromophore-binding pocket, distinct from the PER2 binding site centered on the CRY1 CC α-helix.[23,44] Because both PER2 and BMAL1 interact with the CRY1 CC α-helix[23,24,33,44], our data suggest that a timely handoff between early repressive PER2–CRY1 complexes[3-5,45] to the late repressive CLOCK–BMAL1–CRY1 complexes[7,8] may represent a critical control mechanism for the molecular circadian clock. We do not discount the importance of PER2 in regulating the stability and timing of nuclear entry of the PER2–CRY1 complexes and the resultant temporal progression of circadian transcriptional repression[46,47], or roles that CRY1 may play in the PER2–CRY1 complexes.[10]

Precedence for regulation of protein function based on competition for mutually exclusive binding sites exists throughout biology.[38,48] Competitive mechanisms can make the conversion between inactive and active states more switch-like instead of graded[49], and switch-like responses that exhibit a high degree of cooperativity amplify rhythms in the molecular circadian clock, preventing them from reaching an equilibrium that terminates oscillation.[50] Furthermore, computational models suggest that tight binding of repressors and activators along with control over protein stoichiometry is key for generation of a robust circadian clock.[51] The remarkable decrease in CRY1 repression we observed upon disruption of the stable CLOCK–BMAL1–CRY1 complex (**Fig. 2.6f**) illustrates how important ternary complex formation is for repression when CRY is expressed to near stoichiometric levels with the CLOCK–BMAL1 complex *in vivo.*[52]

It is well recognized that changes in clock protein abundance, posttranslational modifications and subcellular localization play critical roles in circadian timekeeping.[36] Our data suggest that conformational dynamics also play a critical role in period determination, as disordered regions can easily coordinate protein interactions with diverse coregulators by coupling folding to binding.[34,53] Modest changes in the intrinsic secondary structure of other TADs affect the thermodynamics of binding to CBP(p300) to influence the temporal basis (i.e., transient or constitutive) of coactivation.[54,55] Therefore, the structural dynamics we observe within the

BMAL1 TAD could play an interesting role in setting the timescale of activation and repression to ultimately contribute to circadian timing.

METHODS

Lentiviral DNA Constructs, Preparation And Transduction

Bmal1 and *UBC* promoters were cloned into the pENTR-5'-TOPO vector (Life Technologies) as before.[17] Mouse *Bmal1*, *Bmal2* and various chimeras or mutants were first subcloned to p3xFlag-CMV-10 or -14 vectors to obtain 3xFlag tags at the N- or C-terminus, respectively, and then cloned to the pENTR/D-TOPO vector (Life Technologies). The promoter and cDNA pENTR vectors were recombined with pLV7 destination vector[56] using Clonase (Life Technologies) to generate the lentiviral expression constructs. All constructs were verified by sequencing of the entire open reading frame.

Recombinant lentiviral particles were produced by transient transfection in human embryonic kidney HEK293T cells (ATCC) using the calcium-phosphate method as previously described.[56,57] *Bmal1*$^{-/-}$ *Per2*^{Luc} mouse fibroblast cell line was generated in our previous studies.[17] Cells were cultured in DMEM supplemented with 10% FBS and 1x penicillin-streptomycin-glutamine mixture. All cell culture reagents were from HyClone. For infection of *Bmal1*$^{-/-}$ *Per2*^{Luc} fibroblasts, culture medium containing viral particles (~10^6 viral particles/ml) were harvested at 48 hr post-transfection and used for subsequent infection of cells. Transduced cells were selected with 10 μg/ml blasticidin (InvivoGen) as previously done.[17]

Luminescence Recording And Data Analysis

We used a LumiCycle luminometer (Actimetrics) for luminescence recording as previously described.[56] Cells were grown to confluence in 35 mm dishes prior to recording. The recording medium contained 1x DMEM, 25 mM HEPES (pH 7.4), 1% FBS, 1x B-27 and 1 mM luciferin as previously.[17] Three independent clonal lines and 2-3 dishes for each clone were tested to validate phenotypes. Raw luminescence data (counts/sec) as a function of time (days) in culture were analyzed using the LumiCycle Analysis program (version 2.53, Actimetrics) to determine circadian parameters. Due to high transient luminescence upon medium change, the first cycle was excluded from analysis. Briefly, raw data were fitted to a linear baseline, and the baseline-subtracted data were fitted to a damped sine wave, from which period length,

goodness of fit, and damping constants were determined. A goodness-of-fit of >80% was usually achieved from samples that showed persistent rhythms. Damping rate is described by the value of 1/damping constant. For amplitude analysis, raw data from days 3-5 were fitted to a linear baseline (polynomial number = 1), and the baseline-subtracted data were fitted to a sine wave, from which amplitude was determined.

Transient Transfection And Reporter Assays

Reporter assays investigating steady-state differences between *Bmal1* and *Bmal2* function were performed using HEK293T cells in triplicate on 384-well plates. For mammalian two-hybrid assays, 12.5 ng of pGL4P-4x*UAS*::*Luc*, 2.5 ng *Renilla luciferase* (*RLuc*), 25 ng pACT and 25 ng pBIND plasmids were used in each well as previously described.[25] The *Per1-Luc* reporter assay was performed as reported elsewhere with minor modifications.[25] For each well, 12.5 ng *Per1- Luc* reporter, 25 ng pLV7-P(*UBC*)-mouse *Bmal*, 25 ng pLV7-P(CAG)-mouse *Clock*, 25 ng pcDNA-CMV-mouse *p300* or *Cbp*, 25 ng pLV156-P(CMV)-mouse *Cry1*, and 2.5 ng *RLuc* were used. When needed, empty vectors were included to make up to 115 ng of total plasmid amount. *RLuc* was used for reporter normalization. In assays with *Cry1*, indicated amounts of pLV156-P(CMV)-*Cry1* were compensated with empty pLV7 destination vector to a total of 50 ng. Lipofectamine 2000 (Life Technologies) were used with a reverse transfection protocol. Reporter assay was performed 24 hr post transfection using DualGlo luciferin reagent (Promega) and luciferase reporter activity was normalized with *Renilla* luciferase.

To compare expression of Flag-tagged *Bmal1* genes, cells were lysed in RIPA buffer containing complete protease and phosphatase inhibitors (Sigma). Immunoblotting was done using the following primary antibodies: mouse anti-Flag antibody (M2) (Sigma cat. # F3165) and goat anti-β actin (C-11) (Santa Cruz Biotechnology cat. # sc-1615), and the following secondary antibodies: anti-mouse IgG-HRP (Santa Cruz Biotechnology cat. # sc-2005) and anti-goat IgG-HRP (Santa Cruz Biotechnology cat. # sc-2020). SuperSignal West Pico substrate (Pierce) was used for chemiluminescent detection on autoradiograph film.

For coimmunoprecipitation assays, plasmids were transfected into HEK293T cells in a 35 mm dish using LT-1 transfection reagent (Mirus) with the indicated plasmid ratios: 1.5 mg each pSG5 mouse Flag-BMAL1 and pSG5 mouse His6Flag-Clock, plus 50 ng pcDNA3 mouse Cry1

(no tag; used for anti-Flag IP) or 250 ng pcDNA4 Cry1 (C-terminal Flag, myc, His6-tagged; used for anti-myc IP). Cells were harvested 48 hours later for coimmunoprecipitation with anti-myc (9E10) (distributed by the Developmental Studies Hybridoma Bank at the University of Iowa, IA, cat. # 9E 10-a) or anti-Flag antibody (Sigma). Briefly, cells were lysed on ice for 15 min in 250 ml 50 mM HEPES pH 7.5, 150 mM NaCl, 5% (v/v) glycerol, 0.5% (v/v) NP-40 and EDTA-free protease inhibitors (RPI Biochemicals). Clarified extracts were added to 300 ml lysis buffer containing 1 mg of anti-myc monoclonal antibody plus 15 ml Protein A/G resin (Santa Cruz biotechnology) or 15 ml anti-Flag M2 affinity resin (Sigma cat. #A2220) after retaining 25 ml as the input sample. Tubes were rotated end over end for 4 hours, and resin was washed three times with 400 ml lysis buffer. Proteins were eluted from resin by addition of 30 ml 2X SDS Laemmli buffer and boiled for 3 minutes. Complexes were resolved by 7.5% SDS-PAGE after transfer to nitrocellulose. Proteins were detected by immunoblotting using the following primary antibodies: mouse anti-myc, mouse anti-Flag, rat anti-CRY1 (a gift from A. Sancar)58, mouse anti-BMAL1 (B-1) (Santa Cruz Biotechnology cat. # sc-365645), or rabbit anti-CLOCK (H-276) (Santa Cruz Biotechnology cat. # sc-25361), and secondary antibodies: anti-mouse IgG-HRP (Sigma cat. # A9917), anti-rabbit IgG-HRP (Sigma cat. # A0545), and anti-rat IgM-HRP (Thermo Fisher cat. # 31476). Clarity reagent (Bio-Rad) was used for chemiluminescent detection on a ChemiDoc XRS+ imager (Bio-Rad). All data shown are representative from three independent experiments.

For Per1-Luc reporter gene assays investigating CRY1 repression, plasmids were transfected in duplicate into HEK293T cells in a 48-well plate using LT-1 transfection reagent (Mirus) with the indicated plasmids: 5 ng pGL3 Per1-Luc reporter[59], 100 ng each pSG5 Flag-BMAL1 and pSG5 His6Flag-Clock, and pcDNA3 Cry1 (untagged) in increasing amounts as indicated; empty pcDNA4 vector was used to normalize total plasmid to 800 ng/well. Cells were harvested 30 hours after transfection using Passive Lysis Buffer (NEB) and luciferase activity assayed with Bright-Glo luciferin reagent (Promega). Each reporter assay was repeated at least three independent times. To compare relative expression of CLOCK, BMAL1, and CRY1 proteins, a 12-well plate of HEK293T cells was transfected with 400 ng each pSG5 His6Flag-Clock and Flag-BMAL1 with pcDNA4B Cry1 (C-terminal Flag, myc, His6 epitope tags)[60] as indicated, using empty pcDNA4 vector to normalize plasmid concentration to 1 mg total DNA. Cells were

harvested 48 hours later for immunoblotting with anti-Flag antibody, anti-BMAL1 (B-1), and anti-CLOCK (H-276) antibodies. Immunoblot of relative expression in **Supplemental Fig. 2.8** shown is representative of two independent experiments.

qPCR Analysis

Cells were synchronized with 200 nM dexamethasone and the first time point was collected 24 hours later as previously described.[17] Total RNAs were prepared using the RNeasy 96 kit (Qiagen). High-capacity RNA to cDNA kit (Applied Biosystems) was used for reverse transcription, and qPCR was performed using SYBR Green PCR master mix (Thermo Scientific) on an iCycler thermal cycler (BioRad). Transcript levels for each gene were normalized to *Gapdh* and values were expressed as percentage of expression as indicated.

Expression And Purification Of Recombinant Proteins

Proteins were expressed in *E. coli* Rosetta2 (DE3) cells from a pET22b vector backbone (EMD Millipore). Mouse BMAL1 TAD (residues 579-626), BMAL2 TAD (residues 540-579), and p300 KIX (residues 565-653) domains all possessed an N-terminal TEV-cleavable His_6-GST or His_6-SUMO tag. Mutations were introduced by site-directed mutagenesis and confirmed by sequencing. The plasmid encoding untagged mouse CBP KIX was a gift from Peter Wright. CBP KIX protein was expressed in Rosetta (DE3) cells overnight at 18°C after IPTG induction and the soluble fraction was purified on Ni-NTA resin as described above using native His residues on CBP KIX. Cells were either grown in LB medium or M9 minimal medium containing 1 g/L $^{15}NH_4Cl$ for uniform ^{15}N labeling as described before[40]; for triple resonance experiments, uniformly ^{13}C, ^{15}N-labeled samples were made using 1 g/L $^{15}NH_4Cl$ and 3g/L ^{13}C-glucose as the sole nitrogen and carbon sources in M9 medium. Protein expression was induced at OD_{600} ~0.8-1.0 with 0.5 mM IPTG for ~16 h at 18°C. Cells were lysed in buffer containing 50 mM Tris (pH 7.5), 300 mM NaCl and 20 mM imidazole. Affinity purification was carried out with Ni-NTA resin (Qiagen), and eluted protein was buffer exchanged to a low imidazole buffer by desalting column or by diafiltration with an Amicon stirred cell concentrator under nitrogen pressure, followed by proteolysis with TEV protease overnight at 4°C. Cleaved protein was retained from flow-through from an Ni-NTA column and further purified by size exclusion chromatography on Superdex 75 16/600 (GE Life Sciences) in NMR buffer (20 mM MES pH 6.5, 50 mM NaCl). Site-specific labeling of the BMAL1 TAD with the added C-terminal cysteine was performed

with S-methanethiosulfonylcysteaminyl-EDTA (MTS-EDTA; Toronto Research Chemicals) as previously indicated.[40] Protein identities and/or covalent labeling were confirmed by ESI-MS on a Micromass ZMD mass spectrometer (Wythenshawe, UK).

Peptide Synthesis And Purification

The mouse CRY1 CC peptide (residues 470-503, sequence MVNHAEASRLNIERMKQI-YQQL SRYRGLGLLASV) or a CC peptide containing an N-terminal cysteine (N-Cys CRY1 CC; residues 471-505, sequence CNHAEASRLNIERMKQIYQQLSRYRGLGLLASVPS) were synthesized on a CEM Liberty1 microwave peptide synthesizer using standard Fmoc chemistry. Amino acids were purchased from NovaBiochem and assembled on Rink-amide-MBHA resin; all other reagents were purchased from Sigma-Aldrich. Fmoc deprotection was achieved using 20% piperidine with 0.1 M hydroxybenzotriazole (HOBt) in dimethylformamide (DMF). Couplings used 5 molar equivalents of Fmoc-amino acid, 5 molar equivalents of Diisopropylcarbodiimide and 10 molar equivalents of HOBt in DMF. Fully synthesized peptide resins were washed with dichloromethane and dried. Cleavage of the peptide from the resin was performed in a trifluoroacetic acid/thioanisole/ethanedithiol/phenol (90:4:4:2) solution for 90 minutes. Peptides were purified by RP-HPLC (Vydac) on preparative C18 columns. Fractions were collected and analyzed by ESI-MS on a Micromass ZMD mass spectrometer to confirm the correct molecular weight. In each case the major peak was found to be the peptide, and fractions that contained the peptide as a major constituent (≥95% purity) were combined and lyophilized.

NMR Spectroscopy

NMR experiments were conducted at 25°C on a Varian INOVA 600-MHz spectrometer equipped with ^{1}H, ^{13}C, ^{15}N triple resonance, Z-axis pulsed field gradient probes. All NMR data were processed using NMRPipe and NMRDraw.[61] Chemical shift assignments were made with SPARKY[62] using NMR data obtained from standard 3D triple resonance experiments acquired on 300 mM uniformly ^{13}C,^{15}N labeled TAD protein, including: HNCO, HNCACB, CBCA(CO) NH, HCCH-TOCSY, H(CCO)NH-TOCSY and C(CO)NH-TOCSY and HCCH-TOCSY spectra. Chemical shifts of mutant TADs were re-assigned by using triple resonance data in NMRViewJ RunAbout or, when warranted from minor chemical shift perturbations, by minimal chemical shift analysis in NMRViewJ[63]. Secondary structure predictions were validated by TALOS+[64] and by comparison to the Chemical Shift Index.[31,32] ^{15}N HSQC titration of 100 μM ^{15}N TAD proteins

was done by stepwise addition of CRY1 CC peptide, CBP or p300 KIX domain in 20 mM MES pH 6.5, 50 mM NaCl. Samples were concentrated to 300 µl final volume and adjusted to a final concentration of 10% (v/v) D_2O. ^{15}N HSQC titration data were analyzed with NMRViewJ[63] using chemical shift perturbations defined by the equation: $\Delta\delta_{TOT} = [(\Delta\delta^1H)^2 + (\chi(\Delta\delta^{15}N)^2]^{½}$ and normalized with the scaling factor $\chi = 0.17$, established from estimates of atom-specific chemical shift ranges in a protein environment.[65] For PRE NMR experiments, peak intensities from ^{15}N HSQC spectra were determined using the Rate Analysis tool in NMRViewJ to extract normalized peak intensities. Minor broadening at negatively charged residues throughout the TAD is likely due to interaction with trace amounts of unchelated Mn^{2+}, as acquisition of NMR data under moderately higher salt conditions (100 mM vs. 50 mM NaCl) alleviated this non-specific broadening (data not shown).

Isothermal Titration Calorimetry (ITC)

Proteins were extensively dialyzed at 4°C in 10 mM MES pH 6.5, 50 mM NaCl using 2 kDa molecular weight cutoff filter dialysis tubing (Spectrum Labs) prior to collecting ITC data. CBP KIX was used for analysis of TAD binding by ITC due to increased stability over p300 KIX, which was slightly more prone to precipitation under our ITC experimental conditions. ITC was performed on a MicroCal VP-ITC calorimeter at 25°C with a stir speed of 177 rpm, reference power of 10 mCal/sec and 10 mL injection sizes. Protein ratios for the cell and syringe for the ITC assays (2 or 3 independent ITC experiments were performed for each complex) are as follows: 223 mM CBP KIX titrated into 23 mM BMAL1 TAD (Stoichiometry, N = 0.74), 225 mM CBP KIX titrated into 18 mM BMAL2 TAD (N = 0.70), 223 mM CBP KIX titrated into 18 mM BMAL1 SL/NY (N = 1.06), 223 mM CBP KIX titrated into 22 mM BMAL1 VI/AF (N = 0.82), 252 mM CBP KIX titrated into 29 mM LL/AA TAD (N = not determined), 221 mM CBP KIX titrated into 25 mM 619X TAD (N = 0.78), or 225 mM CRY1 CC titrated into 22 mM BMAL1 TAD (N = 0.68), 220 mM CRY1 CC titrated into 25 mM BMAL2 TAD (N = 0.7), 225 mM CRY1 CC titrated into 18 mM BMAL1 SL/NY (N = 0.90), 225 mM CRY1 CC titrated into 20 mM BMAL1 VI/AF (N = not determined), 230 mM CRY1 CC titrated into 22 mM LL/AA TAD (N = not determined), and 221 mM CBP KIX titrated into 25 mM 619X TAD (N = 0.78). All data were best fit by a one-site binding model.

Fluorescence Polarization (FP)

The tetramethylrhodamine 5-maleimide fluorophore (Molecular Probes) was reacted with N-Cys CRY1 CC peptide at a 2-5 fold molar excess for 1.5 – 4 hours at 4°C in 25 mM MES, pH 5.0 with 25 mM NaCl and 10 % DMSO. The low pH of the labeling reaction was essential to avoid non-specific attachment of the TMR group to the lysine amide in the CRY CC peptide as determined by mass spectrometry. Fluorescently labeled TMR-CRY1 CC was purified by reverse phase HPLC and electrospray ionization mass spectrometry was used to verify the labeling and assess purity. Samples with greater than 95% purity were lyophilized and reconstituted in 10 mM MES pH 6.5, 50 mM NaCl and stored at -80 °C until needed.

Equilibrium binding assays between TMR-CRY1 CC and BMAL TADs were performed in 40 mM Tris, pH 8.0, 150 mM NaCl, 0.05% (v/v) Tween-20, 1 mM DTT at 25°C. Binding was monitored by changes in fluorescence polarization using an Perkin Elmer EnVision 2103 Multilabel plate reader with excitation at 531 nm and emission at 595 nm. 10 nM TMR-CRY1 CC peptide was preincubated with buffer alone or increasing concentrations of BMAL TAD constructs (27 nM-300 μM) for 150 minutes at room temperature in the dark prior to FP analysis. The equilibrium dissociation constant (K_D) was calculated by fitting the dose-dependent change in milli-polarization level (Δmp) to a one-site specific binding model in the GraphPad Prism software package, using averaged Δmp values from quadruplicate assays. Data shown are from one representative experiment of three independent assays.

Accession Codes

Chemical shift assignments have been deposited with the Biological Magnetic Resonance Bank for the BMAL1 TAD (25280) and BMAL2 TAD (25549).

REFERENCES

1. Bass, J. Circadian topology of metabolism. *Nature* **491**, 348-356 (2012).
2. Partch, C.L., Green, C.B. & Takahashi, J.S. Molecular architecture of the mammalian circadian clock. *Trends in cell biology* **24**, 90-99 (2014).
3. Brown, S. et al. PERIOD1-associated proteins modulate the negative limb of the mammalian circadian oscillator. *Science* **308**, 693-696 (2005).
4. Duong, H., Robles, M., Knutti, D. & Weitz, C. A molecular mechanism for circadian clock negative feedback. *Science* **332**, 1436-1439 (2011).
5. Lee, C., Etchegaray, J., Cagampang, F., Loudon, A. & Reppert, S. Posttranslational mechanisms regulate the mammalian circadian clock. *Cell* **107**, 855-867 (2001).

6. Ye, R., Selby, C., Ozturk, N., Annayev, Y. & Sancar, A. Biochemical analysis of the canonical model for the mammalian circadian clock. *J Biol Chem* **286**, 25891-25902 (2011).
7. Koike, N. et al. Transcriptional architecture and chromatin landscape of the core circadian clock in mammals. *Science* **338**, 349-354 (2012).
8. Stratmann, M., Stadler, F., Tamanini, F., van der Horst, G. & Ripperger, J. Flexible phase adjustment of circadian albumin D site-binding protein (DBP) gene expression by CRYPTOCHROME1. *Genes Dev* **24**, 1317-1328 (2010).
9. Shearman, L. et al. Interacting molecular loops in the mammalian circadian clock. *Science* **288**, 1013-1019 (2000).
10. Ye, R. et al. Dual modes of CLOCK:BMAL1 inhibition mediated by Cryptochrome and Period proteins in the mammalian circadian clock. *Genes Dev* **28**, 1989-1998 (2014).
11. Liu, A. et al. Intercellular coupling confers robustness against mutations in the SCN circadian clock network. *Cell* **129**, 605-616 (2007).
12. Evans, J., Pan, H., Liu, A. & Welsh, D. Cry1-/- circadian rhythmicity depends on SCN intercellular coupling. *J Biol Rhythms* **27**, 443-452 (2012).
13. Khan, S. et al. Identification of a novel cryptochrome differentiating domain required for feedback repression in circadian clock function. *J Biol Chem* **287**, 25917-25926 (2012).
14. Huang, N. et al. Crystal structure of the heterodimeric CLOCK:BMAL1 transcriptional activator complex. *Science* **337**, 189-194 (2012).
15. Bunger, M. et al. Mop3 is an essential component of the master circadian pacemaker in mammals. *Cell* **103**, 1009-1017 (2000).
16. Shi, S. et al. Circadian clock gene BMAL1 is not essential; functional replacement with its paralog, BMAL2. *Curr Biol* **20**, 316-21 (2010).
17. Liu, A.C. et al. Redundant function of REV-ERBalpha and beta and non-essential role for BMAL1 cycling in transcriptional regulation of intracellular circadian rhythms. *PLoS Genet* **4**, e1000023 (2008).
18. Baggs, J.E. et al. Network features of the mammalian circadian clock. *PLoS Biol* **7**, e52 (2009).
19. Hogenesch, J.B. et al. The basic helix-loop-helix-PAS protein MOP9 is a brain-specific heterodimeric partner of circadian and hypoxia factors. *J Neurosci* **20**, RC83 (2000).
20. Schoenhard, J.A. et al. Regulation of the PAI-1 promoter by circadian clock components: differential activation by BMAL1 and BMAL2. *J Mol Cell Cardiol* **35**, 473-81 (2003).
21. Kwon, I. et al. BMAL1 shuttling controls transactivation and degradation of the CLOCK/BMAL1 heterodimer. *Mol Cell Biol* **26**, 7318-30 (2006).
22. Kiyohara, Y. et al. The BMAL1 C terminus regulates the circadian transcription feedback loop. *Proc Natl Acad Sci U S A* **103**, 10074-10079 (2006).
23. Czarna, A. et al. Structures of Drosophila cryptochrome and mouse cryptochrome1 provide insight into circadian function. *Cell* **153**, 1394-1405 (2013).
24. Czarna, A. et al. Quantitative analyses of cryptochrome-mBMAL1 interactions: mechanistic insights into the transcriptional regulation of the mammalian circadian clock. *J Biol Chem* **286**, 22414-22425 (2011).
25. Sato, T. et al. Feedback repression is required for mammalian circadian clock function. *Nature genetics* **38**, 312-319 (2006).
26. Takahata, S. et al. Transactivation mechanisms of mouse clock transcription factors, mClock and mArnt3. *Genes to cells* **5**, 739-747 (2000).
27. Heery, D., Kalkhoven, E., Hoare, S. & Parker, M. A signature motif in transcriptional co-activators mediates binding to nuclear receptors. *Nature* **387**, 733-736 (1997).
28. Radhakrishnan, I. et al. Solution structure of the KIX domain of CBP bound to the transactivation domain of CREB: a model for activator:coactivator interactions. *Cell* **91**, 741-752 (1997).

29. Yuan, Q., Metterville, D., Briscoe, A. & Reppert, S. Insect cryptochromes: gene duplication and loss define diverse ways to construct insect circadian clocks. *Molecular biology and evolution* **24**, 948-955 (2007).

30. Wells, M. et al. Structure of tumor suppressor p53 and its intrinsically disordered N-terminal transactivation domain. *Proc Natl Acad Sci U S A* **105**, 5762-5767 (2008).

31. Wang, Y. & Jardetzky, O. Probability-based protein secondary structure identification using combined NMR chemical-shift data. *Protein science* **11**, 852-861 (2002).

32. Wishart, D. & Sykes, B. The 13C chemical-shift index: a simple method for the identification of protein secondary structure using 13C chemical-shift data. *J Biomol NMR* **4**, 171-180 (1994).

33. Chaves, I. et al. Functional evolution of the photolyase/cryptochrome protein family: importance of the C terminus of mammalian CRY1 for circadian core oscillator performance. *Mol Cell Biol* **26**, 1743-1753 (2006).

34. Sugase, K., Dyson, H. & Wright, P. Mechanism of coupled folding and binding of an intrinsically disordered protein. *Nature* **447**, 1021-1025 (2007).

35. Felitsky, D., Lietzow, M., Dyson, H. & Wright, P. Modeling transient collapsed states of an unfolded protein to provide insights into early folding events. *Proc Natl Acad Sci U S A* **105**, 6278-6283 (2008).

36. Gustafson, C.L. & Partch, C.L. Emerging models for the molecular basis of mammalian circadian timing. *Biochemistry* **54**, 134-49 (2015).

37. Zhao, W.-N. et al. CIPC is a mammalian circadian clock protein without invertebrate homologues. *Nature cell biology* **9**, 268-275 (2007).

38. Freedman, S. et al. Structural basis for negative regulation of hypoxia-inducible factor-1alpha by CITED2. *Nature structural biology* **10**, 504-512 (2003).

39. Partch, C., Card, P., Amezcua, C. & Gardner, K. Molecular basis of coiled coil coactivator recruitment by the aryl hydrocarbon receptor nuclear translocator (ARNT). *J Biol Chem* **284**, 15184-15192 (2009).

40. Partch, C. & Gardner, K. Coactivators necessary for transcriptional output of the hypoxia inducible factor, HIF, are directly recruited by ARNT PAS-B. *Proc Natl Acad Sci U S A* **108**, 7739-7744 (2011).

41. Etchegaray, J.-P. et al. The polycomb group protein EZH2 is required for mammalian circadian clock function. *J Biol Chem* **281**, 21209-21215 (2006).

42. Akashi, M. et al. A positive role for PERIOD in mammalian circadian gene expression. *Cell reports* **7**, 1056-1064 (2014).

43. Chen, R. et al. Rhythmic PER abundance defines a critical nodal point for negative feedback within the circadian clock mechanism. *Mol Cell* **36**, 417-430 (2009).

44. Nangle, S.N. et al. Molecular assembly of the period-cryptochrome circadian transcriptional repressor complex. *eLife* (2014).

45. Padmanabhan, K., Robles, M., Westerling, T. & Weitz, C. Feedback regulation of transcriptional termination by the mammalian circadian clock PERIOD complex. *Science* **337**, 599-602 (2012).

46. Etchegaray, J.-P. et al. Casein kinase 1 delta regulates the pace of the mammalian circadian clock. *Mol Cell Biol* **29**, 3853-3866 (2009).

47. Lee, H.-m. et al. The period of the circadian oscillator is primarily determined by the balance between casein kinase 1 and protein phosphatase 1. *Proc Natl Acad Sci U S A* **108**, 16451-16456 (2011).

48. Hirschi, A. et al. An overlapping kinase and phosphatase docking site regulates activity of the retinoblastoma protein. *Nature structural & molecular biology* **17**, 1051-1057 (2010).

49. Rossi, F., Kringstein, A., Spicher, A., Guicherit, O. & Blau, H. Transcriptional control: rheostat converted to on/off switch. *Mol Cell* **6**, 723-728 (2000).

50. Forger, D. Signal processing in cellular clocks. *Proc Natl Acad Sci U S A* **108**, 4281-4285 (2011).

51. Kim, J. & Forger, D. A mechanism for robust circadian timekeeping via stoichiometric balance. *Molecular systems biology* **8**, 630 (2012).

52. Lee, Y., Chen, R., Lee, H.-m. & Lee, C. Stoichiometric relationship among clock proteins determines robustness of circadian rhythms. *J Biol Chem* **286**, 7033-7042 (2011).

53. Fuxreiter, M. et al. Malleable machines take shape in eukaryotic transcriptional regulation. *Nature chemical biology* **4**, 728-737 (2008).

54. Parker, D. et al. Analysis of an activator:coactivator complex reveals an essential role for secondary structure in transcriptional activation. *Mol Cell* **2**, 353-359 (1998).

55. Parker, D. et al. Role of secondary structure in discrimination between constitutive and inducible activators. *Mol Cell Biol* **19**, 5601-5607 (1999).

56. Ramanathan, C., Khan, S., Kathale, N., Xu, H. & Liu, A. Monitoring cell-autonomous circadian clock rhythms of gene expression using luciferase bioluminescence reporters. *Journal of visualized experiments : JoVE* **67**, e4234 (2012).

57. Levin, R.D. et al. Circadian function in patients with advanced non-small-cell lung cancer. *Br J Cancer* **93**, 1202-8 (2005).

58. Ozturk, N., Lee, J., Gaddameedhi, S. & Sancar, A. Loss of cryptochrome reduces cancer risk in p53 mutant mice. *Proc Natl Acad Sci U S A* **106**, 2841-2846 (2009).

59. Gekakis, N. et al. Role of the CLOCK protein in the mammalian circadian mechanism. *Science* **280**, 1564-1569 (1998).

60. Partch, C., Shields, K., Thompson, C., Selby, C. & Sancar, A. Posttranslational regulation of the mammalian circadian clock by cryptochrome and protein phosphatase 5. *Proc Natl Acad Sci U S A* **103**, 10467-10472 (2006).

61. Delaglio, F. et al. NMRPipe: a multidimensional spectral processing system based on UNIX pipes. *J Biomol NMR* **6**, 277-293 (1995).

62. Goddard, T.D. & Keneller, D.G. Sparky3. *University of California, San Francisco* (2006).

63. Johnson, B. Using NMRView to visualize and analyze the NMR spectra of macromolecules. *Methods in molecular biology* **278**, 313-352 (2004).

64. Shen, Y., Delaglio, F., Cornilescu, G. & Bax, A. TALOS+: a hybrid method for predicting protein backbone torsion angles from NMR chemical shifts. *J Biomol NMR* **44**, 213-223 (2009).

65. Farmer, B. et al. Localizing the NADP+ binding site on the MurB enzyme by NMR. *Nature structural biology* **3**, 995-997 (1996).

66. Ozber, N. Baris, I., Tatlici, G., Kilinc, S., Unal, E.B., Kavakli, I.H. Identification of two amino acids in the C-terminal domain of mouse CRY2 essential for PER2 interaction. *BMC Mol Biol* **11**, 69 (2010).

SUPPLEMENTAL FIGURES FOR CHAPTER 2

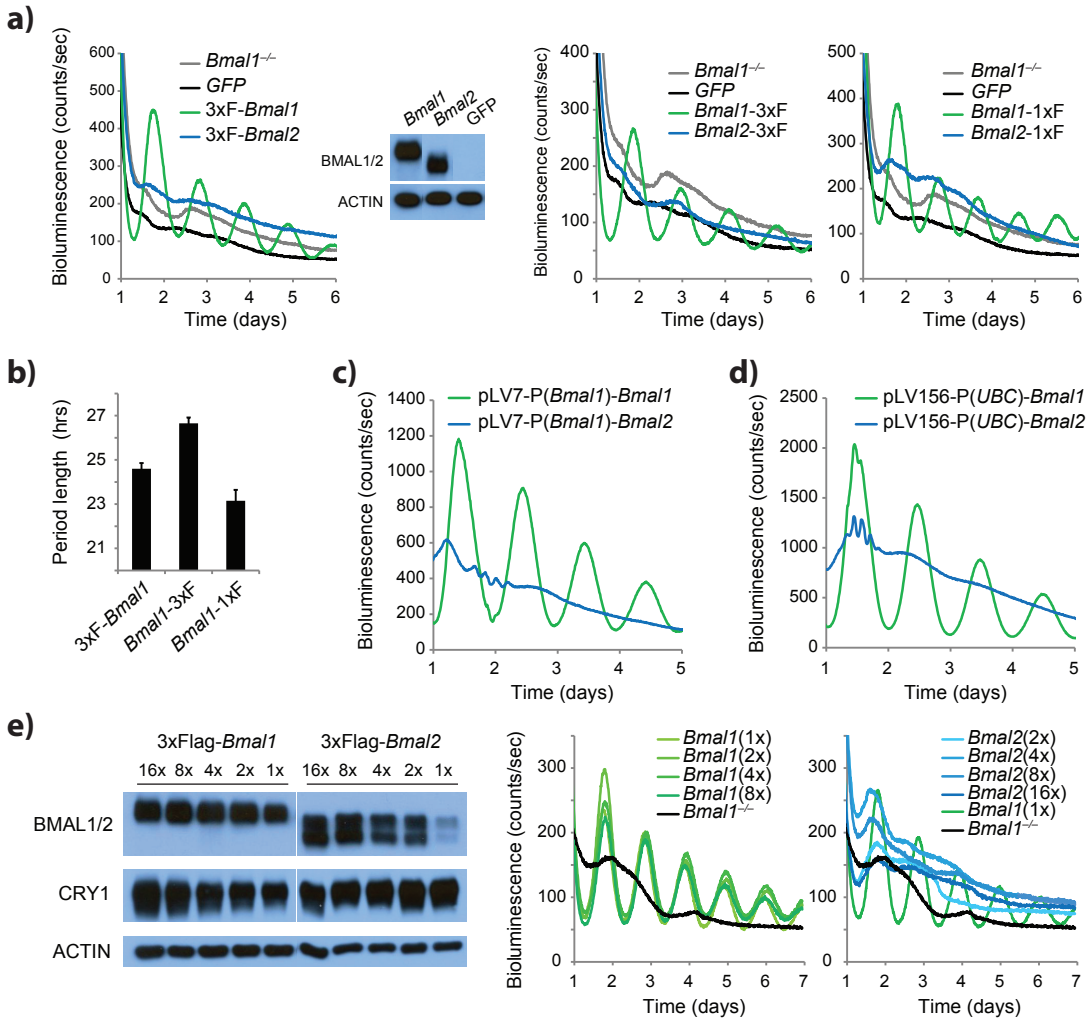

Supplemental Figure 2.1: Validation of genetic complementation assay in BMAL1–/–:Per2^{Luc} fibroblasts. a) Only *Bmal1*, but not *Bmal2*, rescues circadian rhythms from cells. Cells expressing various BMAL constructs (Flag-tagged at either the N- or- C-terminus) were subjected to cycling analysis: 3xF-*Bmal, Bmal* tagged with 3xFlag at the N-terminus; *Bmal*-3xF, 3xFlag tag at the C-terminus; *Bmal*-1xF, 1xFlag at the C-terminus. A representative western blot of 3xF-BMAL proteins (inset) shows that *Bmal1* and *Bmal2* were expressed to similar levels off the plasmid. b) Period length analysis of rescued rhythms in part a). Data are plotted as mean ± SD error bars from 3 independent clonal lines. Placement of Flag tags impact period length. We tested both 3xF-*Bmal* and *Bmal1*-1xF constructs throughout the study and similar results from domain swaps/mutants were obtained. c) Cyclic expression of *Bmal1*, but not *Bmal2*, rescues circadian rhythms in *Bmal1–/–:Per2*^{Luc} fibroblasts. A fragment of the *Bmal1* promoter that contains RORE *cis*-elements was used to drive transcription. Expression of *Bmal2* under control of the *Bmal1* promoter was unable to rescue rhythms. d) The ability of *Bmal1* to rescue rhythms does not depend on the expression vector used. The pLV156 vector expresses an IRES-mediated GFP while the recombination-based pLV7 vector confers high efficiency cloning. Expression of *Bmal1* off the pLV7 plasmid reconstituted cycling was used throughout this study. e) The ability of *Bmal1* to rescue rhythms is dosage independent. Protein expression levels at various levels of infection were determined by Western blot (left panel). *Bmal1* rescued circadian rhythms under all expression regimes tested (center), *Bmal2* failed to rescue levels (right panel). CRY1 displayed a modest dose response to titration of BMAL1, but demonstrated no effect upon BMAL2 titration.

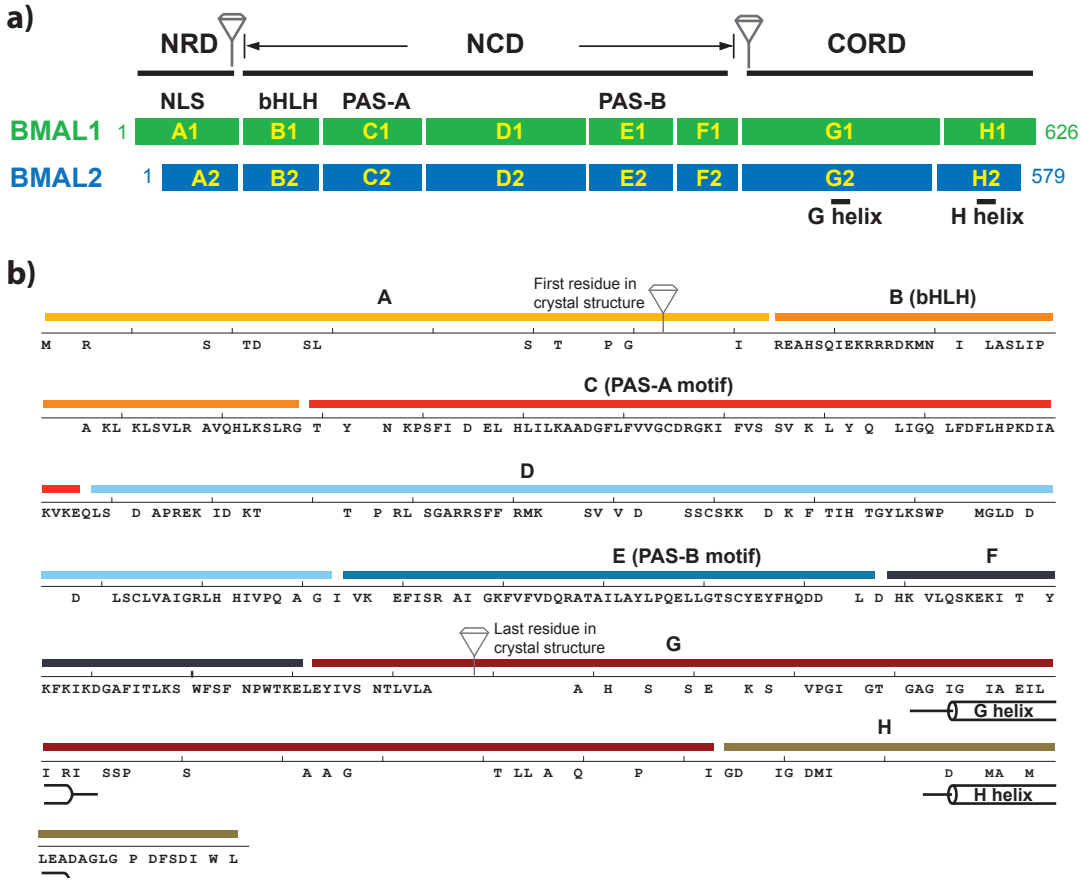

Supplemental Figure 2.2: Domain structure, sequence alignment and structural features of BMAL1 and BMAL2. a) Schematic diagram of domain structure of BMAL1 (green) and BMAL2 (blue); cartoons are drawn to scale. NRD, N-terminal regulatory domain; NCD, N-terminal core domain; CORD, C-terminal oscillator regulatory domain. The BMAL1-NRD (region A) contains a nuclear localization signal (NLS) that is not conserved in BMAL2. The NCD contains the bHLH DNA-binding domain (region B), PAS-A motif (region C), and PAS-B motif (E). The CORD contains regions G and H. Diamonds indicate the protein fragment for which a crystal structure is available (PDB: 4F3L). b) Sequence alignment of BMAL1 and BMAL2 demonstrates divergence of CORD sequences. Mouse BMAL protein sequences were aligned in Vector NTI. Consensus sequence is shown in black. Barrels indicate JPred-predicted secondary structure (alpha helices) in the CORD.

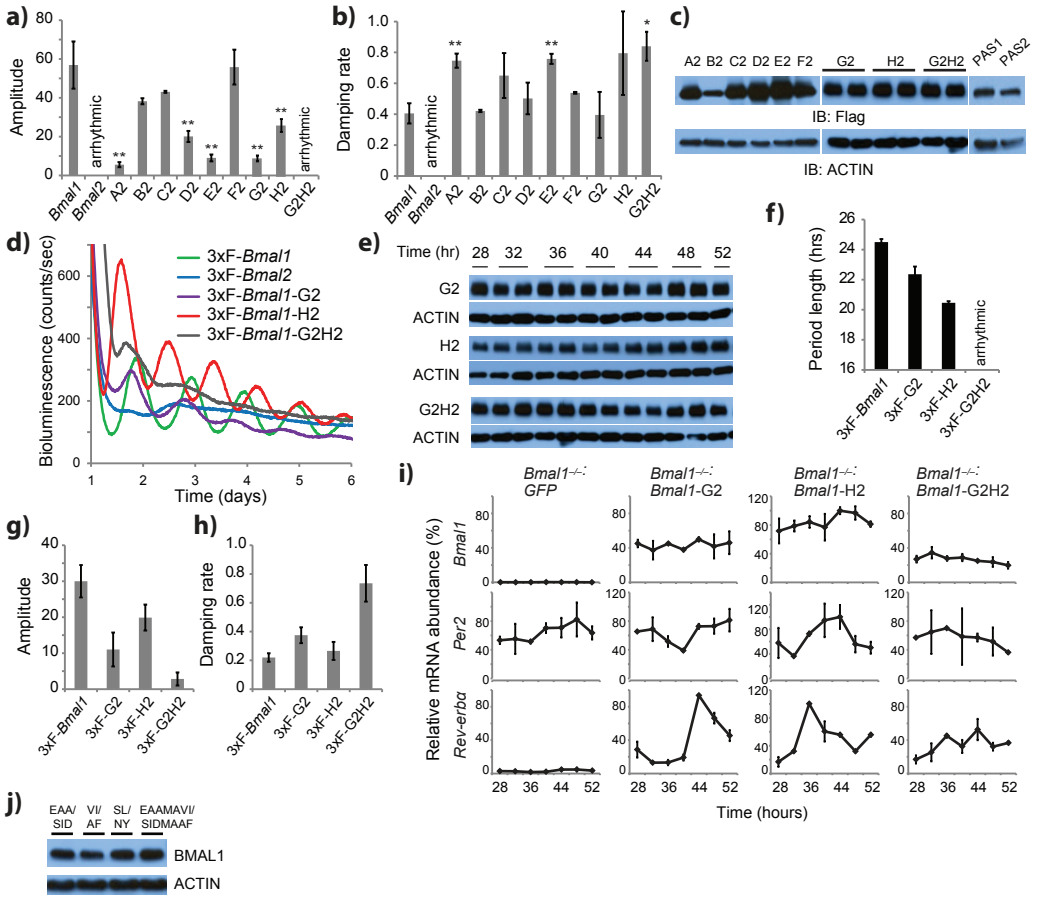

Supplemental Figure 2.3: The C-terminal regulatory domain of BMAL1 is critical for maintaining circadian period length and rhythm amplitude. a-b) Analysis of (a) amplitude and (b) damping rates and (c) expression of *Bmal1*, *Bmal2*, and chimeric *Bmal1-Bmal2* constructs from **Fig. 2.2**. Data are plotted as mean ± SD error bars from 3 independent clonal lines. Relative protein expression levels were determined by western blot using indicated antibodies. d) Both G and H regions of the BMAL1 CORD are required to reconstitute circadian cycling in *Bmal1–/–:Per-2^{Luc}* fibroblasts. Experimental details are the same as in **Fig. 2.2,** except that 3xFlag-*Bmal* constructs were used here (while *Bmal*-1xF constructs were used throughout the main figures of the paper). e) Relative expression levels of mutant chimeric proteins were determined by Western blot over a time course after synchronization of clocks by dexamethasone treatment (time = 0). Expression of *Bmal1*-G2, H2, or G2H2 chimeric proteins was determined using Flag antibody; actin is shown as a loading control. f-h) Analysis of (f) period length, (g) amplitude, (h) and damping rates for 3xF-BMAL constructs shown in part d. Data are plotted as mean ± SD error bars from 3 independent clonal lines. i) Temporal expression profiles of clock gene mRNA in *Bmal1–/–:Per2^{Luc}* fibroblasts expressing *Bmal1*-G2, H2, or G2H2. Values are expressed as percentage of maximum expression for each gene and can be directly compared with those in **Fig. 2.1c**. Error bars represent SD of expression levels from two independent culture samples for each cell line. Time, hours after dexamethasone synchronization. j) Western blot analysis of chimeric and mutant BMAL1 expression in 293T cells detected by Flag antibody. Similar results were obtained from *Bmal1−/−:Per2^{Luc}* fibroblasts expressing various forms of the chimeric/mutant BMAL1 proteins corresponding to cell lines shown in **Fig. 2.3** (data not shown).

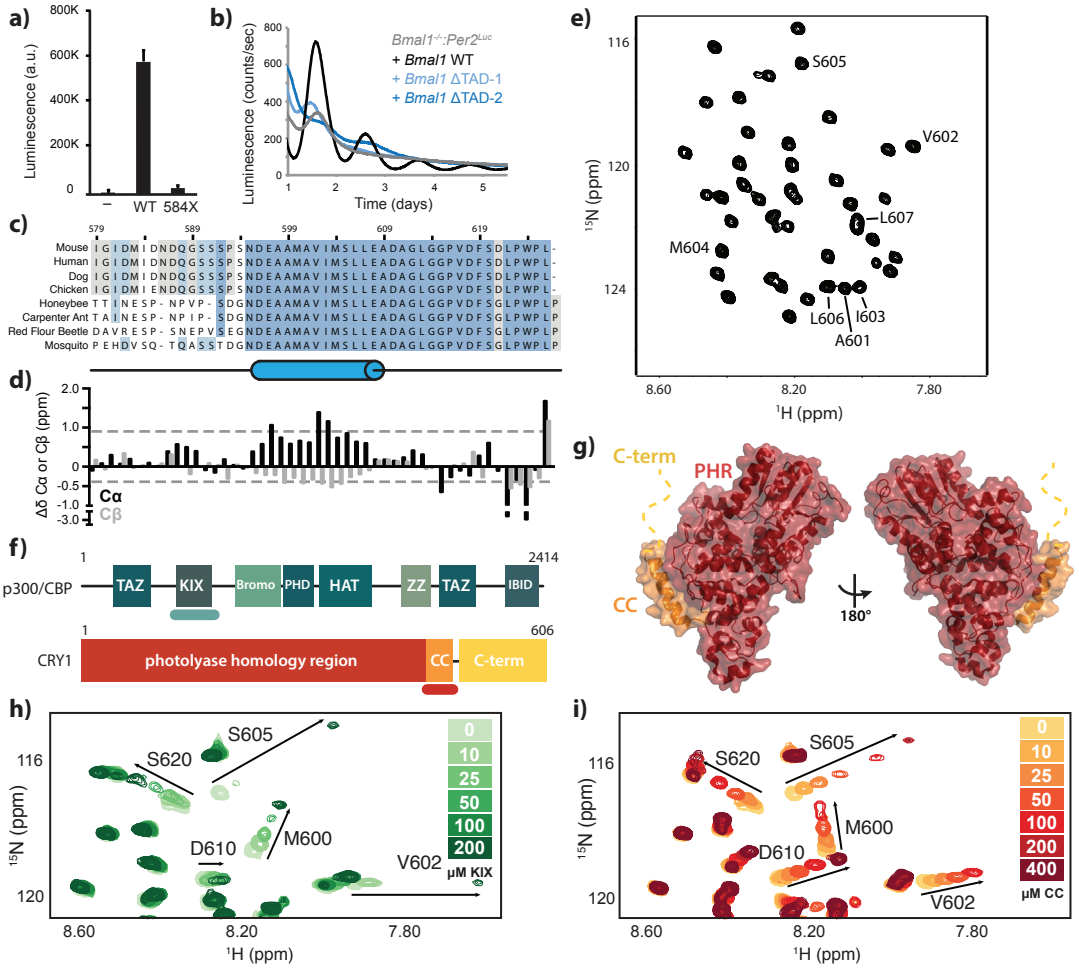

Supplemental Figure 2.4: The BMAL1 TAD interacts directly with transcriptional coregulators and is required for CLOCK:BMAL1 activity. a) Deletion of the BMAL1 TAD by truncation at residue 584 (584X) eliminates CLOCK:BMAL1 activation of a Per1:luc reporter gene in 293T cells. Data are plotted as mean luminescence counts ± SD error bars for three independent replicates. b) Representative bioluminescence records from BMAL1−/−:Per2Luc fibroblasts complemented with the indicated BMAL1 constructs (ΔTAD indicates truncation of H region). c) Conservation of TAD primary sequence and secondary structure across metazoan species with a vertebrate-like clock. Blue barrel, predicted α-helix (JPred); black line, no predicted structure. d) Comparison of Cα/Cβ chemical shifts to the chemical shift index of random coil shifts (Δδ) (Wishart, D. 1994; Wang, Y. 2002). Residues correspond to alignment and secondary structure prediction in part c. Dashed line: significance cutoff for helical prediction from Δδ. e) Region of the $^{15}N/^{1}H$ HSQC spectrum of the BMAL1 TAD displays the modest chemical shift dispersion typical of unfolded/partly helical proteins. Assignments for residues of the IxxLL motif in the α-helix are indicated. f) Modular domain architecture of p300/CBP (green) and CRY1 (red), with domains used in the present study underlined. g) Crystal structure of mouse CRY1 (PDB: 4K0R) displayed with domain coloring from part f. The PHR domain of CRY1, and the CC helix (orange). h-i) The p300/CBP KIX domain and CRY1 CC helix bind overlapping regions on the BMAL1 TAD. A highlighted region of $^{15}N/^{1}H$ HSQC spectra from 100 μM ^{15}N BMAL1 TAD titrated with increasing concentrations of either p300 KIX (h) or the monomeric CRY1 CC peptide (i) show perturbation of the same residues. Quantification of chemical shift perturbations at the 1:1 molar ratio for p300 KIX and CRY1 CC are depicted in **Fig. 2.4a** and b, respectively.

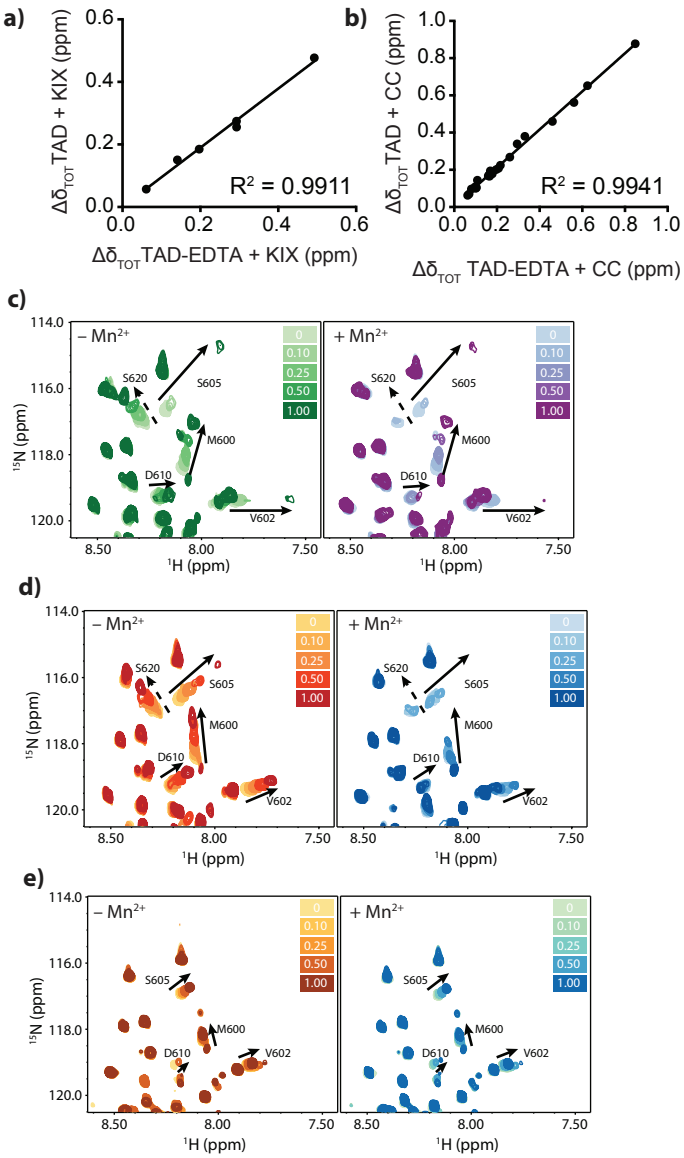

Supplemental Figure 2.5: The TAD undergoes dynamic structural rearrangement upon binding to the p300 KIX domain and CRY1 CC peptide to couple the TAD helix and C-terminus. a-b) Covalent coupling of the MTS-EDTA moiety at a C-terminal Cysteine (TAD-EDTA) does not perturb interactions with p300 KIX or CRY1 CC. Correlation of chemical shift perturbations in WT TAD or TAD-EDTA ^{15}N BMAL1 TAD upon complex formation at 1:1 stoichiometry with p300 KIX domain (a) or CRY1 CC peptide (b). c-d) ^{15}N/^{1}H HSQC spectra of ^{15}N TAD-EDTA ±Mn2+ titrated with p300 KIX (c) or CRY1 CC (d) up to 1:1 stoichiometry. Legends represent various steps of stoichiometry of p300 KIX or CRY CC relative to ^{15}N BMAL1 TAD-EDTA in the absence (left panel) or presence (right panel) of chelated Mn2+. Arrow lengths and orientation are maintained within all panels to illustrate changes (or lack thereof) in chemical shift perturbation upon chelation of paramagnetic Mn^{2+}. Dashed arrow for residue Ser620 illustrates a residue in the TAD C-terminus that undergoes complex-independent broadening due to its proximity to the C-terminal PRE label (see **Fig. 2.4d**). e) ^{15}N/^{1}H HSQC spectra of ^{15}N TAD 619X-EDTA ±Mn^{2+} titrated with CRY1 CC peptide demonstrate the lack of CRY1-dependent broadening at the TAD helix in the absence of the C-terminal seven residues.

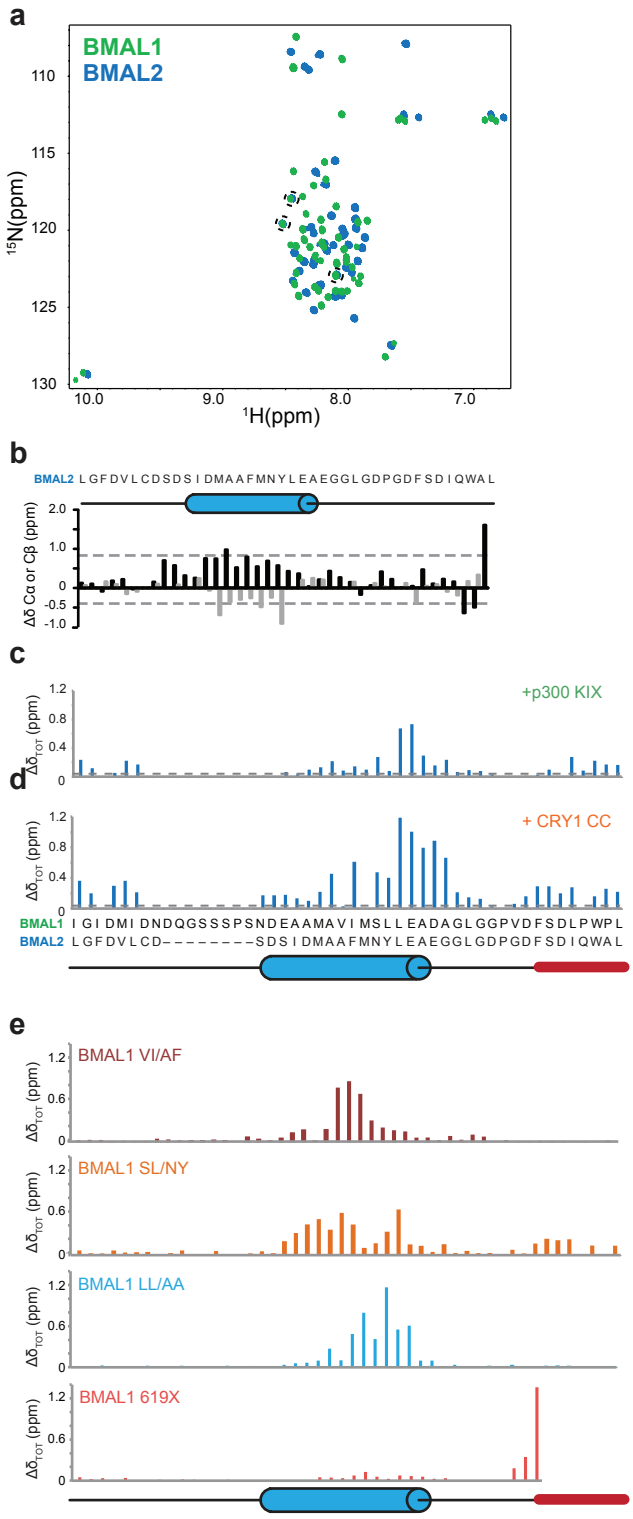

Supplemental Figure 2.6: Comparison of BMAL1 and BMAL2 TAD domains by NMR spectroscopy. a) $^{15}N/^{1}H$ HSQC spectra of 100 μM ^{15}N BMAL1 TAD (green) or ^{15}N BMAL2 TAD (blue) demonstrate minimal overlap of chemical shifts. Dashed circles indicate the only residues that have similar chemical shifts; these residues represent the conserved N-terminal vector artifact left after TEV cleavage. b) The BMAL2 TAD has a modest propensity for α-helix formation, demonstrated by comparison of Cα/Cβ chemical shifts to the chemical shift index of random coil shifts (Δδ) (Wishart, D. 1994; Wang, Y. 2002). Dashed-line line: significance cutoff for helical prediction from Δδ analysis. c-d) Comparison of BMAL TAD interactions with the p300/CBP KIX domain and CRY1 CC peptide. Chemical shift changes (ΔδTOT) on ^{15}N BMAL2 TAD for the 1:1 molar ratio of either p300/CBP KIX domain (c) or the CRY1 CC peptide (d). Dashed line: significance cutoff (0.04 ppm) for chemical shift perturbations. The BMAL TAD sequences are aligned underneath NMR data with predicted secondary structure: blue barrel, predicted α-helix; red line, C-terminal seven residues; black line, no predicted structure. e) Mutations in BMAL1 TAD induce local chemical shift perturbations. Bar graphs plot total chemical shift perturbation ($\Delta\delta_{TOT}$) of backbone shifts from $^{15}N/^{1}H$ HSQC spectra of mutant TADs compared to WT TAD. Mutations in the α-helix largely perturb just the helix and truncation of the C-terminal seven residues gives rise to large chemical shift perturbations only at the new C-terminus.

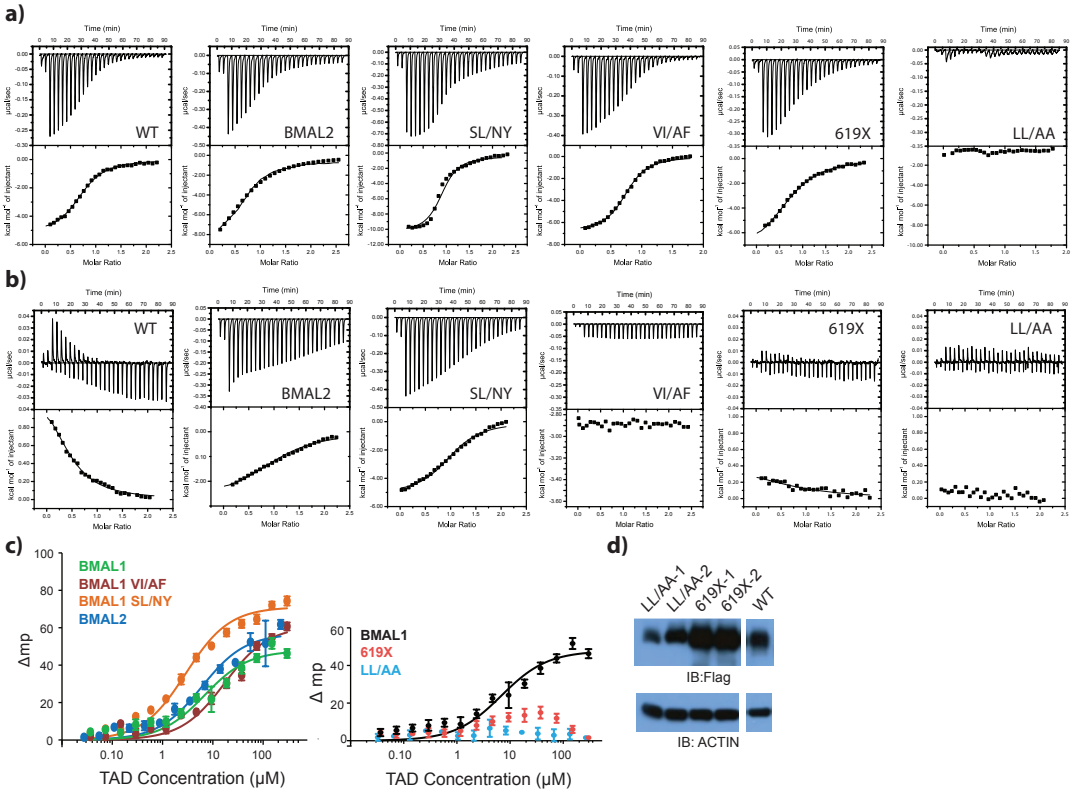

Supplemental Figure 2.7: Quantitative analysis of BMAL TAD interactions with coregulators. a-b) Data from isothermal titration calorimetry (ITC) experiments of BMAL TAD (BMAL1, BMAL2, or BMAL1 mutants, as indicated above) with either CBP KIX domain (a) or the CRY1 CC peptide (b). All ITC experiments were set up with 15-30 μM TAD in the cell and 220-250 μM KIX or CRY1 CC peptide in the syringe and run at 25°C. Data shown are representative of at least two independent ITC runs. Thermodynamic parameters from ITC data were fit to a one-site binding model and populate Table 1, with representative N values of 0.7-1.0 indicating 1:1 stoichiometry. c) Fluorescence polarization-based titration of rhodamine-labeled CRY1 CC peptide against BMAL1, BMAL2 or BMAL1 mutant TADs. Data are shown as mean change in milli-polarization units (Δmp) from free CC peptide ± SD error bars from four independent experiments. Curves were fitted by non-linear regression to a one-site binding model to determined KD values in Table 1. d) Relative protein expression of BMAL1 WT and mutant constructs within the complemented lines were determined by western blot using indicated antibodies.

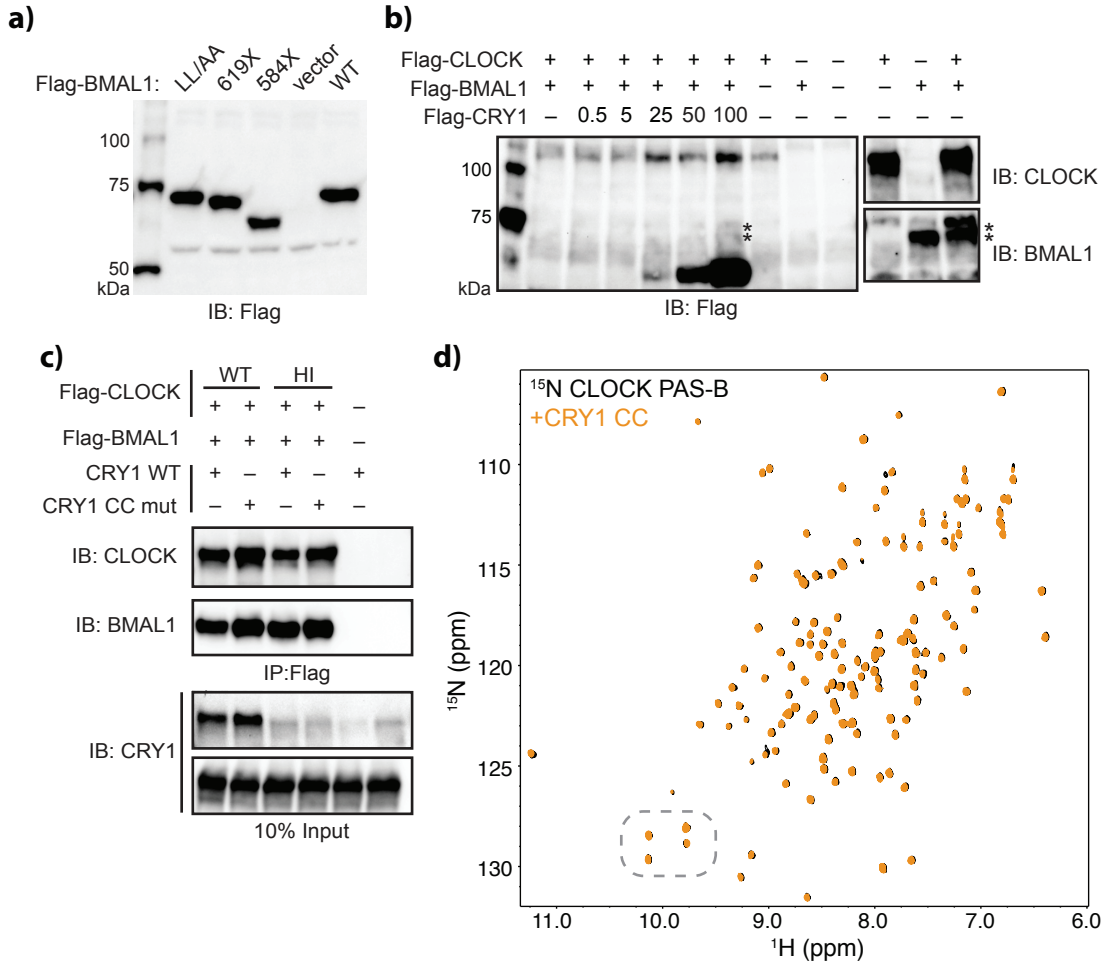

Supplemental Figure 2.8: CRY1 regulation of CLOCK:BMAL1 requires interaction with both CLOCK and BMAL1. a) Wild-type and mutant Flag-BMAL1 clones are expressed to similar levels in 293T cells as determined by western blot using Flag antibody. *, non-specific band that serves as a loading control. b) Relative expression levels of CLOCK, BMAL1 *and* CRY1 with plasmid ratios used in luciferase assays. 293T cells were transfected with plasmid ratios used in *Per1:luc* assay (100 ng each *Clock* and *Bmal1*, and *Cry1* plasmid as indicated, scaled 4X for increase in culture dish area). Relative protein expression levels are shown by western blotting using indicated antibodies. Under these experimental conditions, BMAL1 expression is just at the detection limit with the Flag antibody. Expression of CLOCK and BMAL1 was verified by blotting with CLOCK and BMAL1 antibodies, which provide greater sensitivity of detection compared to the Flag antibody. **, migration of the CLOCK-dependent phosphorylated BMAL1 species in the Flag blot relative to its detection with the BMAL1 antibody. c) Mutation of the CLOCK PAS-B HI loop (Q361P/W362R) disrupts interaction with CRY1 by Flag Co-IP when co-expressed with Flag-BMAL1 in 293T cells. The CRY1 CC mut (R501Q/K503R) (Ozber, N. 2010) does not affect interaction of CRY1 with co-expressed Flag-CLOCK and Flag-BMAL1. d) The CRY1 CC helix does not bind directly to the CLOCK PAS-B domain. $^{15}N/^{1}H$ HSQC spectra of 60 μM ^{15}N CLOCK PAS-B in the absence (black) and presence (orange) of 240 μM CRY1 CC peptide show no chemical shift perturbations upon addition of CC peptide. Dashed box: tryptophan indole region shown in **Fig. 2.6g**. Assignment of the CLOCK PAS-B W362 indole peak was made by mutagenesis.

CHAPTER 3

A SLOW CONFORMATIONAL SWITCH IN THE BMAL1 TRANSACTIVATION DOMAIN MODULATES CIRCADIAN CYCLING

SUMMARY

The C-terminal transactivation domain (TAD) of BMAL1 is a regulatory hub where transcriptional activators and repressors compete for binding to contribute to period determination of the mammalian circadian clock. Here, we report the discovery of two distinct conformational states that slowly exchange within the dynamic TAD. This binary switch results from *cis/trans* isomerization about a highly conserved Trp-Pro imide bond in a region of the TAD that is essential for normal circadian timekeeping. Both *cis* and *trans* isomers interact with transcriptional regulators to suggest that isomerization may serve a role in assembling regulatory complexes *in vivo*. Towards this end, we show that complementation of *trans*-locked *Bmal1* mutants in *Bmal1*$^{-/-}$*PER2*^{Luc} cells leads to shortened circadian periods. Furthermore, switch kinetics are accelerated *in vitro* by cyclophilins, highlighting a potential new role for regulation of BMAL1 protein dynamics in period determination.

INTRODUCTION

Mammalian circadian clocks are intrinsic molecular timekeeping systems that coordinate physiological processes with external environmental cues to appropriately time daily activities. This coordination is achieved by two interlocked transcription feedback loops that control the temporal basis of expression for over 40% of the mammalian genome.[1,2] The heterodimeric transcription factor CLOCK:BMAL1 sits at the core of the primary feedback loop to direct the chronometric transcription of clock-controlled genes.[3] Intrinsic timekeeping is established as a result of the coordinate regulation of CLOCK:BMAL1 by transcriptional co-activators CBP/p300 and repressors PER and CRY. Many processes contribute to the timing of activation and repression, such as the localization[4-9], phosphorylation[9-19], degradation[17,18,20-22] and stoichiometry[23,24] of repressors in the nucleus. However, mechanisms that regulate changes in the architecture of CLOCK:BMAL1 transcriptional regulatory complexes throughout the day are still poorly understood. The highly dynamic BMAL1 transactivation domain (TAD) is a hub for these interactions, as it interacts with both activators and repressors[25-31] and is necessary

for circadian cycling.[32-35] Modulating affinity of the BMAL1 TAD for its regulators elicits large changes in period, demonstrating its critical role in the transcription-based clock. Identification of processes that modulate interactions between the BMAL1 TAD and transcriptional regulators will shed light on the mechanism by which animals measure time and use it to control biology.

Chemical processes such as post-translational modifications can act as biological switches to regulate protein function, inducing changes in conformation, protein-protein interactions, or subcellular localization. However, proteins also possess a range of dynamic behaviors on different timescales that can also control function. Temporally specific processes abound in mechanistic biology; from the timescales of protein folding and stochastic motions of intrinsically disordered regions (IDRs) to posttranslational modifications and subcellular localization, organisms possess an arsenal of biochemical tools to regulate the timescale of biological processes. One such process is isomerization about a proline-containing imide peptide bond (Xaa-Pro). Popularly dubbed a *molecular timer,* proline isomerization is an intrinsically slow process (~10^{1}-10^{-3} s^{-1}), the timescale of which can also be enzymatically modulated by peptidyl prolyl isomerases (PPIases) by up to 4-5 orders of magnitude.[36,37] Proline isomerization is relatively rare (only ~1-5% of imide bonds undergo isomerization[37]), yet these slow 'molecular timers' [38-40] have a broad impact on diverse biological processes. Through regulation of protein folding or inter/intramolecular interactions, proline isomerization has been shown to modulate ion channel gating, protein degradation, transcription, and signal transduction.[41,42] Likewise, PPIases are pivotal components in many biological pathways[43-47]. Dysfunctional regulation of proline isomerization and/or PPIase activity has been implicated in cancer, Alzheimer's disease [48] and disruption of circadian cycling in *Drosophila*.[49]

Here, we report the discovery of a slow conformational switch in the BMAL1 TAD that modulates circadian cycling. NMR spectroscopy identified that *cis/trans* isomerization about a conserved Trp-Pro imide bond controls the conformational exchange, which we have dubbed the 'TAD switch'. Using site-directed mutagenesis and solid phase peptide synthesis (SPPS), we developed locked *cis* and *trans* isomers to study the individual roles of the isomers in interactions with circadian transcriptional regulators. Locking the TAD into its *trans* isomer shortens the circadian period in cell-based assays to show that slow conformational exchange is important for circadian timekeeping. Both isomers interact with transcriptional regulators

with similar affinities. Isomerization of the TAD switch occurs on a timescale of minutes, over 3 orders of magnitude slower than the lifetimes of the transcriptionally active and repressive complexes. Finally, we discovered selective and potent enhancement of isomerization rates by some PPIases within the cyclophilin family *in vitro*. Broad inhibition of the cyclophilin family leads to period lengthening in cell, suggesting that modulation of slow dynamics at the TAD may play a role in tuning circadian period.

RESULTS

A Proline Isomerization Actis As A Molecular Switch In The C-terminus Of BMAL1

The BMAL1 TAD acts as a regulatory hub, interacting with positive and negative transcriptional regulators as a function of circadian time (CT). We previously mapped interactions of the transcriptional co-activator CBP/p300 KIX and the CC domain of the repressor CRY to two distinct and regions in the BMAL1 TAD: the predicted alpha helical region and the extreme C-terminus (**Fig. 3.1a**) [50]. ^{15}N-HSQC spectra of dynamic domains such as BMAL1 consist of single resonances for each of the constituent N-H bonds that is representative of the population-weighted averages of all conformers. Surprisingly, the ^{15}N-HSQC of the BMAL1 TAD revealed two distinct resonances for each of the 8 C-terminal residues (**Fig. 3.1b, Supplemental Fig. 3.1a**), indicating that a localized slow conformational exchange occurs in the extreme C-terminus of BMAL1, a region that we have dubbed the TAD switch. Mass spectrometry confirmed the presence of a single peptide species of expected molecular weight and truncation of the TAD switch residues resulted in a ^{15}N HSQC spectrum devoid of peak doubling (**Supplemental Fig. 3.1b-e**).

In order to identify the structural change responsible for the conformational heterogeneity, we turned to 3-dimentional CCONH TOCSY experiments. Characteristic proline $^{13}C_{\beta}$ and $^{13}C_{\gamma}$ shifts indicate that the Trp624–Pro625 bond is found in two distinct conformations, a *cis* and a *trans* form (**Fig. 3.1c**), distinguished by a 180-degree rotation about the imide bond (**Fig. 3.1d**). No significant isomerization was detected for the other four imide bonds in the BMAL1 TAD construct (**Fig. 3.1c** and **Supplemental Fig. 3.1d**). The relative abundance of the two isomers can be determined through peak volume measurements. We chose to average the peak volumes from the W624 indole, W624 backbone and L626 backbone and found that the TAD switch is comprised of about 65% *trans* and 35% *cis* (**Supplemental Fig. 3.1h**).

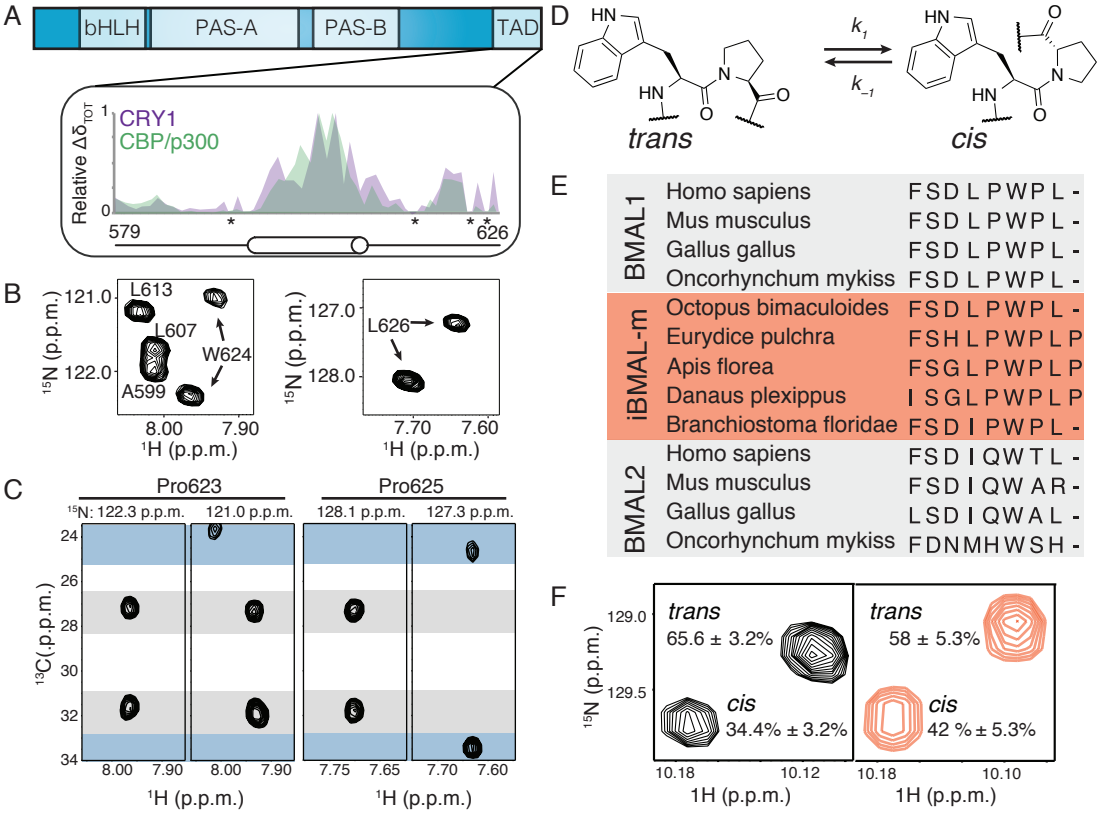

Figure 3.1: Isomerization about a conserved W-P bond in the C-terminus of BMAL1 (A) Domain schematic of BMAL1 highlighting the binding locations of CRY CC and CBP KIX on the C-terminal TAD (residues 579-626) (B) Regions of the ^{15}N HSQC spectra of the BMAL1 TAD displaying the backbone amide bond resonances of the two conformers of Trp624 and Leu626 (C) strips from the ^{15}N ^{13}C (H)C(CO)NH TOCSY of the BMAL1 TAD at the ^{1}H and ^{15}N chemical shifts of the backbone amide from Trp624 and Leu626 (x- and z-axes, respectively) and the ^{13}C shifts of Pro623 and P625 C_β and C_γ residues (y axis). Grey region is accepted ^{13}C shifts for proline C_β and C_γ found in *trans* and blue region is accepted ^{13}C shifts for proline C_β and C_γ in *cis* (D) chemical drawing of the W624-P625 bond in the *cis* and *trans* conformations. (E) Sequence alignment BMAL1, BMAL2 and CYCLE in insects with a mammalian-like clock (F) Regions of the natural abundance ^{15}N HSQC of the switch peptides FSDLPWPL (black, left panel) and FSGLPWPLP (peach, right panel) showing the *cis* and *trans* resonances for Trp624 indole. Relative abundance of each of the peaks was calculated using peak volumes.

Conservation Of TAD Switch In BMAL1 And iBMAL

Phylogenetic analysis of the insect ortholog of BMAL1, CYCLE shows that a profound divergence occurred from the ancestral insect resulting in two distinct proteins: the drosophila CYCLE (dCYC) that possesses PAS-A, PAS-B, bHLH and Pac domains only and a BMAL1 like CYCLE that also contains a C-terminal TAD.[51,52] These BMAL1 like CYCLE proteins occur in insects that possess a mammalian-like cytochrome (CRY-m) and while phylogenically related

to dCYC, it has higher functional and structural homology to mammalian BMAL1 than dCYC [53]. Therefore, we will refer to this protein as insect-BMAL (iBMAL).

All eight residues in the BMAL1 TAD switch are fully conserved throughout all animal species investigated. Furthermore, the primary sequence of iBMAL is highly conserved with that of BMAL1; residues F619 and D621 in BMAL1 are variable in some species and a C-terminal P is sometimes observed (**Fig. 3.1e**). This high level of conservation indicates biological importance. In order to determine if these deviations in primary sequence affect the isomer ratios we synthesized switch peptides using SPPS with the mammalian BMAL1 and the *apis florea* BMAL (apBMAL) sequences and analyzed the peak intensities using natural abundance ^{15}N HSQCs.

The wild-type switch peptide (FSDLPWPL) displayed equilibrium populations of isomers only slightly different than the full length BMAL1 TAD (**Fig. 3.1f** left panel and **Supplemental Fig. 3.2c**). The differences between the 34.4% *cis* for the BMAL1 TAD and the 40.5% observed in the switch peptide is likely due to experimental variability, as a significant change in peak integration of longer switch peptides was not observed (**Supplemental Fig. 3.2d**). The *ap*BMAL1 switch peptide FSGLPWPLP, displaced *cis* content of 42.3 ±2.72%, not a significant difference from the wild type FSDLPWPL peptide (**Fig. 3.1f**). These data indicate that the deviations in primary sequence of iBMAL and mammalian BMAL1 do not affect steady-state isomerization ratios and insects with a mammalian-like clock share similar *cis/trans* ratios and switch functionality with their mammalian ortholog BMAL1.

Intriguingly, BMAL2 does not share conservation of the isomerizing proline (**Fig. 3.1e**) and it is due to these variations from BMAL1 and the change in the predicated alpha helical region BMAL2 cannot support circadian cycling.[54] Replacement of the BMAL1 TAD with the BMAL2 TAD abolishes circadian cycling in MEFs and truncation of the TAD at the switch region results in a 3 hour shortening of the circadian period.[34,55]

Trp And Pro Are The Key Residues Comprising The TAD Switch

In order to develop tools with which to probe the importance of the two isomers on circadian systems, we proceeded with an investigation of the effect of point mutations on Trp624 and Pro625 on isomer equilibrium populations. As expected, mutation of Pro625 to Ala resulted in no identifiable *cis* conformer, providing us with a *trans*-locked BMAL1. Integration of the

proline analog 5,5-dimethyl proline (dmP) in place of Pro625 produced the opposite effect, a TAD switch that appears to sample the *cis* conformer exclusively (**Fig. 3.2a,b**). The absolute backbone geometry was verified by chemical shift values using natural abundance ^{13}C HSQCs and ^{1}H-^{1}H TOCSYs on the peptides (**Supplemental Fig. 3.3a,b**). The *trans* locked switch was integrated into ^{15}N BMAL1 TAD to verify the congruence between the TAD switch peptides and full TAD (**Supplemental Fig. 3.4a**).

The identity of the residue preceding the proline (i-1) has a profound impact on the equilibrium populations of isomers.[34] Aromatic amino acids increase an imide bond's propensity to sample the *cis* conformation by stabilizing the electron poor proline Hα, while small electron poor amino acids in the i-1 position decrease the stability of a *cis* conformer. Long range interactions affecting the equilibrium population of isomers have been reported in highly structured systems[32], however for IDRs such as the BMAL1 TAD, long rage structural constraints are unlikely to affect the isomerization. The replacement of Trp624 to an Ala resulted in a peptide with no observable *cis* configuration (**Fig. 3.2a,b** and **Supplemental Figs. 3.3a,b** and **3.4a**). A decrease in aromaticity of the i-1 residue by mutating the Trp to Phe and Tyr resulted in a slight decrease in *cis* propensity (**Fig. 3.2a, Supplemental Fig. 3.3a,b**). Together, these data indicated that the high degree of conservation of W-P is due to the specific *cis/trans* ratio that the Trp-Pro interaction sustains.

The *Trans* Locked Tad Switch Drives A Short Circadian Phenotype In Cycling Mef Cells

Point mutations in the predicted alpha helical region of BMAL1 TAD have been shown to elicit extreme changes in cycling metrics. In one instance, substitution of two key resides with those in BMAL2 (L606A/L607A) rendered $PER2^{Luc}$ cycling MEF cells completely arrhythmic.[56] To examine the importance of the TAD switch in circadian cycling we incorporated the *trans* locked BMAL1 mutants into the *Bmal*$^{-/-}$ *Per2*^{Luc} cycling MEF system. In our hands, genetic complementation with wild type BMAL1 resulted in periods of ~22.7 hours (**Fig. 3.2c** left panel, **3.2d** and **Supplemental Fig. 3.4b**), near the previously reported 23.5 hours.[33] Genetic complementation with full length P625A BMAL1 TAD decreased the circadian period by over 1 hour (**Fig. 3.2c** middle panel and **3.2d** and **Supplemental Fig. 3.4b**). Upon incorporation of the W624A mutation, we observed ~3 hour decrease in period and a significant increase in damping

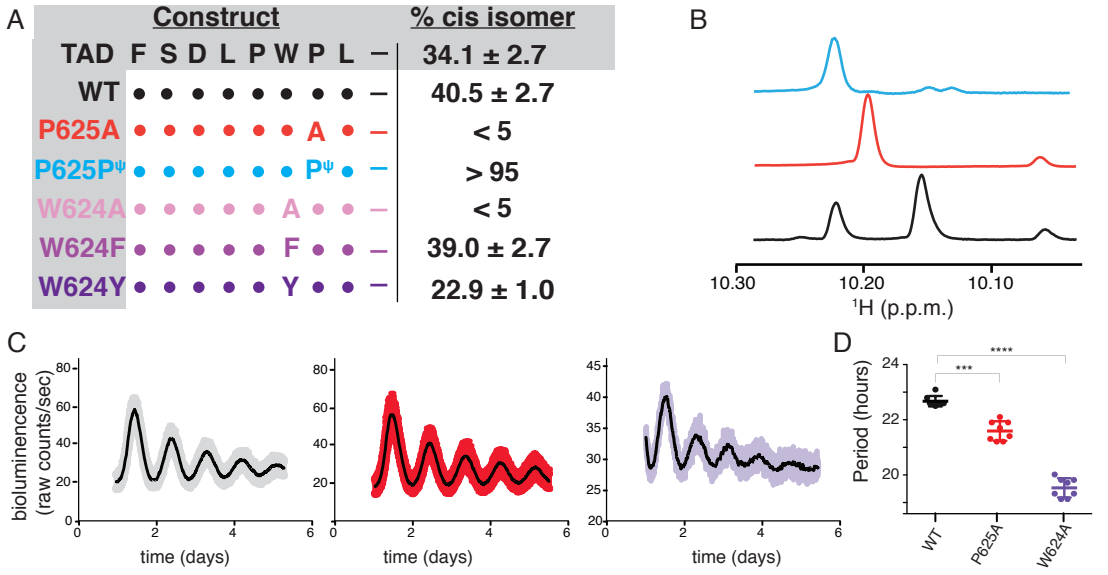

Figure 3.2: The proline switch tunes the period of circadian cycling: (A) Representation of the *cis* content of the TAD switch peptides for P625 and W624 mutants compared to the ^{15}N BMAL1 TAD. *Cis* content was calculated from the average of the peak volumes from residues 624 and 626 in the ^{15}N HSQC and ^{1}H-^{1}H TOCSY spectra (B) Region of the ^{1}H NMR spectra from the FSDLPWPL (black), FSDLPWAL (red) and FSDLPW dmP L (blue) TAD switch peptides highlighting the NH indole from W624 (C) Luminescence records from BMAL1$^{-/-}$ *Per2*^{Luc} mouse fibroblasts genetically complemented with WT (grey), P525A (red) or W624A (purple) BMAL1. D) Mean period of genetically complemented fibroblasts in (C) with same color scheme. ***P=0.003 compared to WT and ****P<0.0001 compared to WT BMAL1 by two tailed paired t test.

rate (**Fig. 3.2c** right panel and 2D and **Supplemental Fig. 3.4b**), a phenotype as extreme as that observed upon removal of the entire switch region.[35]

Both Isomers Of The Tad Switch Interact With Transcriptional Activators And Repressors

In order to probe the molecular mechanism responsible for the phenotypic change observed in BMAL1/1 P625A BMAL1 TAD MEF cells, we analyzed the interactions of the *cis* and *trans* isomers to transcriptional regulators using NMR and fluorescence anisotropy. Analysis of the previously reported ^{15}N HSQC titrations with CC helix and CBP KIX [41] show that both the *cis* and *trans* peaks interact with the repressor (**Fig. 3.3a** left panels) in fast to intermediate exchange. The same experiment was performed using ^{15}N BMAL1 TAD P625A (**Fig. 3.3a** right panels) and nearly identical shifts were observed for the *trans*-locked TAD as the wild-type *trans* peak, indicating that P625A is a good representation of the *trans* isomer of W624-P625.

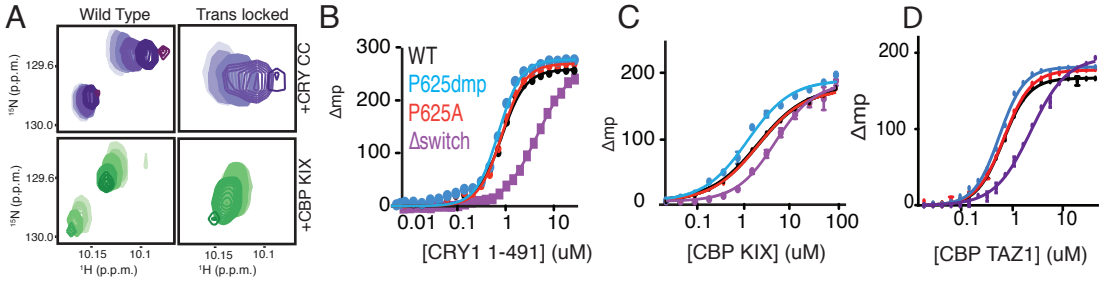

Figure 3.3: Both isomers of the TAD switch interact with transcriptional activators and repressors(A) Regions of the ^{15}N HSQC spectra showing WT ^{15}N BMAL1 TAD WT (left panels) or ^{15}N BMAL1 TAD P625A (right panels) with increasing concentrations of CRY CC (purple, top panels) or CBP KIX (green, bottom panels), increasing concentration is indicated by darker colors. Fluorescence anisotropy data for B) CRY1 1-491 and C) CBP KIX and D) CBP TAZ1 for wild type (black), P625A (red), P625dmP (blue) and ΔSwitch (purple) short BMAL1 TAD (594-626). Traces are representative from 3 independent experiments with N=2 or N=3. (F) ITC profile of CBP KIX and wild type (black), P625A (red) and P625dmP (blue) BMAL1 TAD (G) Thermodynamic parameters calculated from the ITC data in (F) Traces are representative from 3 independent experiments

We determined affinities of the TAD switch variations with CRY1 and CBP KIX using fluorescence anisotropy with 5,6-TAMRA labeled WT, P625A, P625dmP BMAL1 TADs. In order to promote the largest change in milipolarization unites (mP), we elected to use CRY1 1-491 instead of the small CC helix as was used in the NMR studies. The CBP KIX domain elicited a sufficient change in mP value to be used in this assay without modification. Wild Type BMAL1 TAD appeared to interact with CRY 1-491 with an affinity of 0.9 μM (**Fig. 3.2b** and **Table 3.1**) and CBP KIX with an affinity of 1.34 μM (**Fig. 3.2c** and **Table 3.1**). These data correlate well with the previously reported ITC data of wild type BMAL1 TAD with CRY1 [57].

The *cis* and *trans* locked isomers displayed affinities for CRY1 and CBP KIX identical to that of WT TAD, indicating that differential interactions between transcriptional activators and

Table 3.1: Affinity measurements of BMAL1 TAD isomers for transcriptional regulators. All measurements were performed using fluorescence polarization. Values are averages of three or four independent experiments with n=2 or n=3.

BMAL1 TAD types	Cry1 (1-491)		CBP TAZ1		CBP KIX	
	KD	Hill	KD	Hill	KD	Hill
Wild Type	0.90 ±0.27	1.6 ±0.1	0.75 ±0.15	1.0 ±0.1	1.34 ±0.40	1.6 ±026
P625A	0.99 ±0.27	1.8 ±0.1	0.75 ±0.06	1.0 ±0.3	1.59 ±0.66	1.6 ±0.1
P625dmP	0.86 ±0.17	1.9 ±0.1	0.54 ±0.12	1.0 ±0.5	1.16 ±0.44	1.7 ±0.2
ΔSwitch	4.28 ±0.33	0.9 ±0.04	2.39 ±0.23	0.9 ±0.2	4.63 ±1.05	1.1 ±0.2

repressors is not the mechanism by which the TAD switch regulates the period of cycling. The slope of the binding curves indicated positive cooperativity of binding, potentially due to the multi-variant interactions of the TAD with CRY1 [58-61]. In order to test this hypothesis, we performed the assay with TAMRA-labeled Δswitch and indeed, the hill coefficient suggested no cooperativity of binding and a four-fold increase in K_D. The affinities of the *trans* locked and WT TADs to CBP KIX were identical, however the *cis* locked TAD had a slightly shifted curve; all three constructs displayed positive cooperativity. As expected the Δswitch mutant displayed a 3-fold decrease in affinity and no cooperativity. Furthermore, we assayed the interactions of the BMAL1 TAD with other TAD interacting domains of CBP and found that TAZ1 binds to the isolated BMAL1 TAD with nM affinity (**Fig. 3.3d, Table 3.1**). Further analysis with the Δswitch, P625A and P625dmP TAMRA labeled TADs showed that while the TAD switch is important for interactions with TAZ1 the *cis* and *trans* isomers did not display significantly differing affinities for TAZ1 (**Fig. 3.3d, Table 3.1**).

Isomerization Of The Switch Is Much Slower Than The Lifetimes Of The Complexes

Isomerization about an imide bond is an inherently slow process due to the relatively high thermodynamic barrier of ~20 KJ/mol[62-64]. We used ZZ-exchange spectroscopy to measure the kinetics of conformational exchange between *cis* and *trans* isomers of the BMAL1 TAD. However, when performed at 25 °C, the characteristic cross peaks that indicate chemical exchange were absent (**Fig. 3.4a** top left panel) even out to a 3 s delay. These data indicate that the isomerization process is slower than can be detected using normal ZZ-exchange.

Unstructured proteins usually exhibit increased thermostability compared to their natively folded counterparts. Integrity of the BMAL1 TAD was retained after ~20 hour incubations a temperatures up to 70 °C (**Fig. 3.4b**), allowing us to perform ZZ-exchange experiments at increased temperature. Cross peaks were observed between 55° and 70 °C. Intensities for peaks representing the W625 and L626 *cis*, *trans*, *cis* to *trans* and *trans* to *cis* conformations were plotted as a function of delay time (**Fig. 3.4c**), and kinetic parameters calculated for each temperature using equations 1-3 (methods). Eyring analysis was performed in order to interpolate the kinetics of exchange back to 25 °C (**Fig. 3.4c** and **Table 3.2**). At 25 °C, the isomerization of a single molecule of the *cis* conformer to *trans* takes 3.64 minutes while the reverse isomerization takes 6.30 minutes. Based upon these data, the thermodynamic barrier of the Trp624-Pro624

transition is about 21 Kcal/mol and the difference in stability between the two states in around 0.5 Kcal/mol (**Fig. 3.4d**). Compared to the calculated lifetimes of the TAD regulatory complexes [64]the TAD switch, the excursions between *cis* and *trans* constitute generations; the timescales measured for the BMAL1 TAD isomerization are greater than 3 orders of magnitude larger than the lifetimes of the BMAL1 TAD:KIX or BMAL1 TAD:CRY complexes. These data indicate that isomerization does not routinely occur during complex formation.

Peptidyl-Prolyl Isomerases Can Modulate The TAD Switch

Members of the Cyclophilin (Cyp) family of peptidyl-prolyl isomerases enhance the rate of *cis/trans* isomerization about Xaa-Pro imide bonds. These ubiquitous enzymes are known to regulate transcription of numerous genes though (1) modulation of transcription factor activity

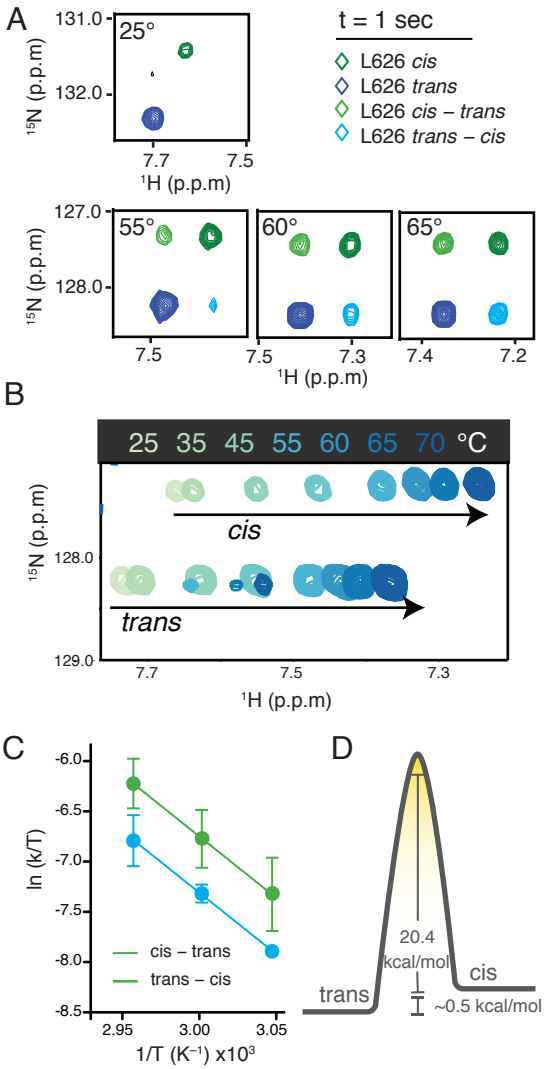

Figure 3.4: Kinetic analysis of isomerization using ZZ-exchange Spectroscopy (A) Region of an ^{15}N HSQC of the BMAL1 TAD displaying the *cis* (dark green), *trans* (dark blue), *cis* to *trans* (light green) and *trans* to *cis* (light blue) peaks for Leu626 with dso=1 s from ZZ-exchange experiments performed at various temperatures (B) Overlay of ^{15}N HSQC spectra regions, showing the *cis* and *trans* peaks of Leu 626 at various temperatures (C) Eyring analysis comparing K_{ex} and temperature using equation 7 (methods). (D) Free energy plot showing the calculated the activation energy of isomerization.

Table 3.2: Kinetics of *cis* to *trans* isomerization measured by ZZ-exchange spectroscopy

Temperature (°C)	Rate of isomerization (s^{-1})		Time per Isomerization (sec)	
	cis to *trans*	*trans* to *cis*	*cis* to *trans*	*trans* to *cis*
25*	$4.583x10^{-3}$	$2.644x10^{-3}$	218.22	378.18
37*	$2.33x10^{-2}$	$1.345x10^{-2}$	42.86	74.34
55	$2.15x10^{-1}$	$1.238x10^{-1}$	4.652	8.077
60	$3.819x10^{-1}$	$2.199x10^{-1}$	2.603	4.55
65	$6.672x10^{-1}$	$3.841x10^{-1}$	1.4986	2.603

*Rates were determined at 55-65 °C and extrapolated back to 25 °C using the Eyring equation.

and localization[43,44,65,66]; (2) association with splicesomal complexes[67,68] and (3) the recruitment and modulation of histone modifying proteins [69]. Notably, the drosophila PPIase, Dodo (a homologue of the human PPIase Pin1) has been implicated in circadian timing.[62]

In order to determine if PPIases can catalyze the rate of isomerization of the TAD switch, we performed a ZZ-exchange experiment on the BMAL1 TAD in the presence of the most highly promiscuous Cyp, PPIA. We found that PPIA binds to the BMAL1 TAD *in vitro* and increases the rate of isomerization by greater than 200-fold (**Fig. 3.5a,b**). We subsequently assayed the nuclear Cyps, PPIE, PPIG and PPIH the mitochondrial Cyp PPIF and the poorly characterized PPIL2, PPIL3, PPWD and SDCCAG for activity against the TAD switch. We found that PPIF, PPILE, PPIG and PPIH all possess the ability to modulate the kinetics of isomerization in BMAL1 to varying extents (**Fig. 3.5a,b**).

DISCUSSION

In this study, we introduce a slow conformational switch in the C-terminal TAD of BMAL1 that participates in the molecular regulation of the finely tuned circadian clock. *A cis/trans* isomerization about the highly conserved Trp624-Pro625 imide affects the chemical environment of the terminal eight residues of BMAL1, a region that has previously been shown to modulate interactions with transcriptional regulators. By coupling cell cycling studies with biophysical techniques, we show that the TAD switch is a central component of the regulatory mechanism that drives the formation of transcriptional complexes. The competition between transcriptional activators and repressors for binding at the eight residues affected by the isomerization (619-626) [57] suggests that the TAD switch is poised to play a pivotal role in circadian cycling.

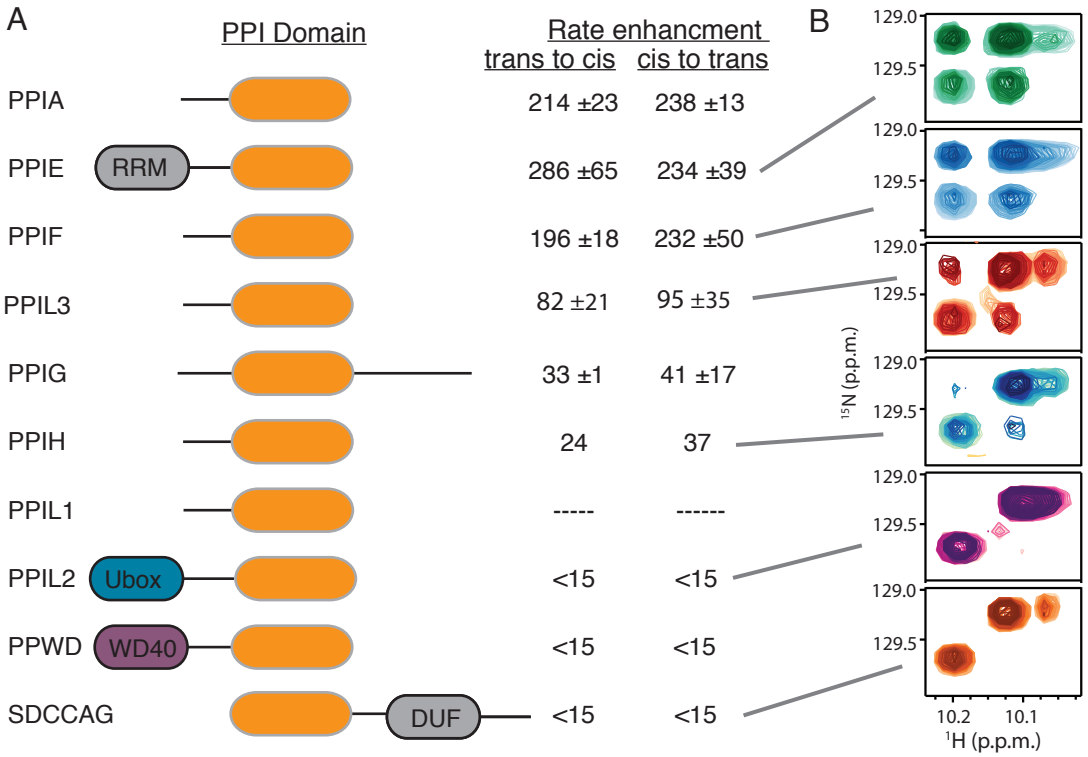

Figure 3.5: Modulation of isomerization rate by PPIases (A) domain schematics of the PPIases analyzed for activity against the BMAL1 TAD switch and their relative rate enhancement compared to the apo BMAL1 TAD isomerization rate and (B) regions of the ZZ-exchange spectra from select experiments with PPIases displaying the W624 indole region.

At equilibrium about 40% of the BMAL1 TAD reside in the higher energy *cis* form (**Fig. 3.1d,f**). Both the W624 and P625 of BMAL1 are 100% conserved in all species and even into iBMAL1 (Cycle, in insects with a mammalian-like clock), indicating a specific functional role for this region (**Fig. 3.1e**). Notably, the few deviations in local sequence of the TAD switch region (619-626) present in some species of insects do not affect the ratio of isomers at equilibrium (**Fig. 3.1f**). Proline isomerization is a rare occurrence and has been shown to modulate a host of biological processes from signaling cascades to splicing and protein degradation[43,47,70-83]. Strikingly, the *trans* locked BMAL1 TAD drives circadian rhythms with an altered phenotype; the P625A *trans* locked TAD results in a one hour shortened period

Both *cis* and *trans* isomers were found to interact with the transcriptional activator CBP KIX and repressor CRY1 with similar affinities by fluorescence anisotropy (**Fig. 3.3b-d**). NMR studies confirmed that the chemical shift perturbations elicited upon titrations of CRY CC or

CBP KIX into ^{15}N BMAL1 TAD were of similar magnitude and direction for the *trans* isomer of WT BMAL1 as for the *trans* locked P625A BMAL1 (**Fig. 3.3a**). While it is possible that the proline to alanine mutation can change the functionality of the BMAL1 TAD, these data indicate that the two resides behave in a similar manner when interaction with identified binding partners. The *trans* locked W624A mutant displays a phenotype nearly identical to the Δswitch mutant[57], indicating that the Trp, in addition to stabilizing the important *cis* conformation has another role in the molecular mechanism of the circadian clock (**Fig. 3.2**).

The rate of uncatalyzed proline isomerization is extremely slow on the timescale of macromolecular functions–in other systems *cis/trans* isomerization is considered a molecular timer, toggling between two biologically different functions on a timescale of minutes.[84] Kinetic analysis of the switch shows that it takes 6.3 minutes to transition from *trans* to *cis* and 3.6 minutes to transition from *cis* to *trans (***Fig. 3.4**). The lifetimes of the BMAL1 TAD:CRY CC and BMAL1 TAD:KIX complexes can be calculated from the dissociation constants (assuming a K_{on} of $1x10^7$); a comparison of these values with the timescale of isomerization shows that the difference in timescale is over 3 orders of magnitude. In the molecular clock the timescale of interactions is profoundly important and it is possible that dynamic motions of the BMAL1 TAD that drive the handoff between transcriptional activators and repressors.

There are a multitude of potential mechanisms through which the TAD switch can regulate circadian cycling; from differential interactions with binding partners to modulating K_{off} rates upon isomerization and temporal regulation by PPIases. Our data showing that a number of PPIases are capable of interacting with the BMAL1 TAD *in vitro* suggest that it is possible that PPI modulation of the switch could affect circadian cycling *in vivo*. Intriguingly, PPIA is the cellular ligand for the immunosuppressive drug cyclosporine A (CsA) [85,86] and patients dosed with cyclosporine report circadian disruptions.[87] Furthermore, PPIA was found to associate with BMAL1 in the cytoplasm[88] and could have a role in either transcription or translation.

Cooperative binding of numerous transcription factors to the KIX domain is regulated through a central hydrophobic network that link the two independent binding sites in KIX in a Monod-Wyman-Shageux (MWC) like model of allostery.[60,61,63,89,90] The decrease in affinity for the KIX domain upon truncation of the switch region of the BMAL1 TAD (Δswitch) (**Fig. 3.3**)

suggests that similar interactions may contribute to BMAL1 TAD:KIX interactions.[57] The difference in hill coefficients (**Table 3.1**) that we observed for KIX interaction with the BMAL1 TAD versus the Δswitch TAD support this hypothesis. Intriguingly, the same shift in hill coefficients and affinity is observed with CRY1 binding to the BMAL1 TAD (WT versus Δswitch), indicating that cooperative binding either through allostery or more likely, through avidity help to tune interactions of BMAL1 with the repressor CRY. An additional method of cooperativity is suggested by our finding that a second domain of CBP interacts with the BMAL1 TAD. It is possible that the increased transcriptional efficiency observed for promoter regions containing tandem Ebox elements is due to the presence of two BMAL1 TADs in sequence that can capture CBP through two different binding mechanisms.

Mammalian circadian rhythms are multifaceted regulatory processes that are central to human health. The finely tuned molecular mechanism is regulated through a host of dynamic biochemical processes that function to maintain robust, yet plastic oscillatory behavior. The activation and degradation rates of the repressors CRY and PER through PTMs are the most highly studied forms of circadian regulation, yet we know very little about the mechanism that drives the transition between transcriptionally active and repressive complexes on the E-box promoter elements. The identification of a slow switch in the BMAL1 that regulates circadian rhythms highlights the critical role of the dynamic interactions of the intrinsically disordered BMAL1 TAD with transcriptional activators and repressors. The possibility of *in vivo* enzymatic regulation of this molecular timer holds the possibility of previously unrecognized regulatory components and offers a new perspective on how fast and slow conformational changes in core clock proteins set the timescale of circadian cycling.

EXPERIMENTAL PROCEDURES

Lentiviral DNA Constructs, Preparation And Transduction

Flag tagged Mouse BMAL1 and BMAL1 P625A were cloned into pENTR/D-TOPO vector (Life Technologies) then recombined with pLV7 destination vector[91] as previously described.[57] All constructs were verified by sequencing.

The *Bmal1*$^{-/-}$ *Per2*^{Luc} cell lines that had been previously generated[92] were cultured in DMEM (Hyclone) with 10% FBS (Hyclone) and 1x penicillin-streptomycin (Hyclone). Recombinant

lentiviral particles production and infection of BMAL1 -/- Per2:Luc was performed as described previously.[57]

Bioluminescence Recording And Data Analysis

Cells were grown to confluence in 35 mm dishes and synchronized with 200 nM dexamethasone. Recording medium contained DMEM, 25 mM HEPES, pH7.4, 1% FBS 1 mM luciferin and B-27 supplement. A LumiCycle luminometer (Actimetrics) was used to monitor the luminance signal (counts/s) as a function of time; data were analyzed using the LumiCycle Analysis program (version 2.53, Actimetics). Raw data were baseline corrected and fit to a damped sine wave, from which period length, goodness of fit, amplitude and damping rate were determined. Data acquired from the first 24 hours of recording were omitted from the processing. Three dishes per clonal line were tested, experiments were performed on two independent dates with differing cell passage numbers for each clonal line. Data were deemed acceptable if the goodness of fit exceeded 80% and a representative trace from each clonal line was reported.

Expression And Purification Of Recombinant Proteins

Mouse BMAL1 TAD (579-626) was cloned from full length mBMAL1 and placed into a pet22b[93] vector backbone (EMD Millpore) under the control of the T7 promoter; BMAL1 TAD 594-626 was codon optimized (GeneWiz, South Plainfield, NJ) and cloned into the same vector. Both constructs possessed an N-terminal TEV cleavable His_6-GST solubilizing tag and ampicillin resistance. The mammalian expression vector for mouse CBP was kindly provided by Andrew Liu (University of Memphis). The TAZ1 (340-439) and TAZ2 (1764-1855) domains were amplified and cloned into a pet22b vector backbone devoid of an affinity tag. The plasmid encoding mouse CBPKIX (585-672) was a kind gift from the laboratory of P.E. Wright. CBPKIX has native histadine residues that allow for the purification of the protein using Nickel resin. Mutations were introduced using site directed mutagenesis[94] and confirmed with sequencing.

The Rosetta DE3 stain of E. Coli containing plasmids with either BMAL1 TAD or CBP KIX were grown to an OD_{600} of ~0.6-0.9 in the presence of ampicillin (0.1 mg/mL) and chloramphenicol (0.035 mg/mL). Protein expression was induced with IPTG and allowed to proceed for 16-18 hours at 18 °C in either Luria Broth Medium or M9 minimal medium containing 1g/L $^{15}NH_4Cl$.

Cells were lysed in buffer containing 50 mM Tris pH 7.5, 300 mM NaCl and 20 mM imidazole. The soluble fraction of E. coli lysates were passed over Ni-NTA resin and the protein of interest eluted using 250 mM imidazole. Eluted protein was buffer exchanged into 20 mM imidazole using a stirred-cell pressure concentrator with 3 KDa MWCO filters from Amicon. Proteolysis was performed with His_6-tagged TEV protease overnight at 4 °C and cleaved protein was retained from the flow-through of a Ni-NTA column. The purified protein was injected onto a Superdex 75 16/600 (GE Life Sciences) size-exclusion column, pre-equilibrated with NMR buffer (10 mM MES, pH 6.5 and 50 mM NaCl).

The Rosetta DE3 stain of E. Coli containing plasmids with TAZ1 were grown to an OD_{600} of ~0.6-0.9 in the presence of ampicillin (0.1 mg/mL) and chloramphenicol (0.035 mg/mL). Protein expression was induced with IPTG and allowed to proceed for 4 hours at 37 °C in Luria Broth Medium supplemented with 50 μM $ZnSO_4$.

Cells were lysed in a buffer containing 50 mM Tris pH 7.5, 300 mM NaCl, 20 mM DTT, 50 μM $ZnSO_4$. The insoluble fraction of E. coli lysates were suspended and washed 2X in the same buffer to remove impurities. The final insoluble pellet was resuspended in 10 mM Tris pH 7.5, 50 μM $ZnSO_4$, 20 mM NaCl, 20 mM DTT, and 6 M urea by sequential sonication and homogenization. The insoluble particulates were removed via centrifugation and the supernatant passed over a 1 mL HiTrap SP XL sepharose cation exchange column. Bound TAZ1 or TAZ2 was washed with 50 mM Tris pH 7.5, 50 μM $ZnSO_4$, 20 mM NaCl and 20 mM DTT and eluted in the same buffer with 50 mM Tris pH 7.5, 50 μM $ZnSO_4$, 1 M NaCl and 20 mM DTT. Eluted protein was quantified and 3 molar equivalent of ZNSO4 titrated into the solution with concurrent pH monitoring. Precipitated DTT•Zn was removed via centrifugation and the TAZ1 was further purified on a onto a Superdex 75 16/600 (GE Life Sciences) size-exclusion column, pre-equilibrated with NMR buffer (10 mM MES, pH 6.5 and 50 mM NaCl).

All of the bacterial expression constructs of human cyclophilins used in this study have been kindly gifted by Tara Davis (University of Drexel, Drexel, USA) except isomerase domain of PPIE and PPIH. The detailed cloning protocol is in reference Adams BM., 2015[68]. PPIH and PPIase domain of PPIE were cloned into pet22b based parallel vector system between BamH1 and Not1 cut sites with HISGST and HIS tags, respectively. PPIG was cloned into pet22b based parallel

vector system between EcoR1 and BamH1 cut sites with HIS tag. The accession numbers for cyclophilins cDNAs of cyclophilins from the Mammalian Gene Collection are as follows :

PPIA: BC003026, PPIE:BC008451, PPIG: BC001555, PPIH: BC003412, PPIL1: BC003048, PPIL2: BC000022, PPIL3: BC007693, PPWD1: BC015385, CWC27: BC012117.

For the multidomain cyclophilins (PPWD, PPIG, CWC27/SDCCAG) we cloned the isomerase domain due to solubility problems with the full length proteins.

The expression constructs were transformed into BL21 (DE3) cells. The cells were grown at 37 °C until they reached OD600 0.8-1 and were induced with 500μM IPTG and growth in Luria Broth at 16 °C overnight. The cells were resuspended in buffer A (50mM Tris-Cl pH 7.5, 300 mM NaCl, 20mM imidazole) and lysed in a cell disrupter. Initially, cyclophilins were purified by Ni-NTA column according to manufacturer's protocol (Promega, Madison, WI). The N terminal HIS6 tags of the cyclophilins were allowed to remain during analysis with the exception of HISGST-PPIH, which was subjected to overnight incubation with TEV protease at 4 °C. The HISGST tag was removed by Ni/NTA resin. Further purification was achieved for all cylophilins except PPIL3 and the isomerase domain of PPIE (ΔRRM-PPIE) with a Superdex 75 16/600 (GE Life Sciences) size-exclusion column, pre-equilibrated with 20mm Hepes pH 7.0, 100mM NaCl, and 2mM TCEP). The HEPES buffer pH increased to pH 7.6 and 8.0, when we worked with PPIL3 and the isomerase domain of PPIE, respectively.

Using the baculovirus expression system (Invitrogen) His-tagged mouse CRY1 (amino acids 1–491) was expressed in SF9 suspension insect cells (Expression Systems). Cells were infected with a P3 virus at 1.5 *10^6 cells/mL and grown for 72 hours. Following brief centrifugation at 4K rpm, cells were resuspended in 50 mM Tris pH 7.5, 200 mM NaCl, 20mM imidazole, 10% glycerol, 0.2% triton x-100, 0.1% NP40, 0.4% Tween-20, 5mM β-mercaptoethanol and EDTA-free protease inhibitors (Pierce). Cells were lysed using a microfluidizer followed by brief sonication for 15 sec. on/30 sec. off for 3 pulses. Lysate was clarified at 37K rpm, 4 °C for 1 hour. The protein was then isolated by Ni-NTA agarose affinity chromatography. The eluted protein was further purified by size-exclusion chromatography into 20 mM HEPES pH 7.5, 125 mM NaCl, 5% glycerol and 2 mM TCEP. Prior to fluorescence polarization experiments the purified protein

was buffer exchanged into FP buffer: 50 mM bis-tris propane, 100 mM NaCl, 2 mM TCEP and 0.05% Tween-20.

Peptide Synthesis And Purification

Switch peptides FSDLPWPL, FSDLPAPL, FSDLPWPL, SDLPWPL, DLPWPL, LPWPL, and PWPL were synthesized using solid phase peptide synthesis on 3-chlortrityl resin with standard FMOC chemistry, one or two 1:4:4:4:6 molar ratio of resin:HBTU:HOAT:Fmoc-AA-OH:DiPEA coupling reactions were performed in DMF for each amino acid addition. Switch peptide FSDLPWdmPL was synthesized using solid phase peptide synthesis using standard FMOC chemistry, coupling of dmP onto the Leu-Resin was performed using 1:2:2:4 molar ratio of Resin:HATU:Fmoc- dmP -OH:DiPEA, coupling of the Trp onto the Resin-Leu- dmP was performed using 1:3.8:4:6 molar ratio of Rsin:COMU:Fmoc-Trp-Boc-OH:DiPEA, all other coupling reactions were performed using HBTU/HOAT as described above. All Fmoc protected amino acids were purchased from Fluka, Nova Biochem, AAPPTec, or Sigma Aldrich. Fmoc- dmP was purchased from PolyPeptide Group (San Diego, California). Peptides were purified by reverse phase C18 HPLC, purity and identity were verified by MS/MS on a waters HPLC-MS/MS system.

BMAL1 TAD P625dmP and switch peptides FSDLPFPL, FSDLPYPL, FSDLPAPL and FSDLPWAL were purchased from Bio-Synthesis Inc (Lewisville, Tx). The mouse CRY1 CC peptide (resiudes 471-503 sequence MVNHAEASRLNIERMKQIYQQL SRYRGLGLLASV) was synthesized as described previously.[57]

NMR Spectroscopy

NMR experiments were conducted on a Varian INOVA 600-MHz spectrometer equipped with ^{1}H, ^{13}C, ^{15}N triple resonance, Z-axis pulsed filed gradient probe. All NMR data were processed using NMRPipe/NMRDraw.[95] Assignments of mBMAL1 TAD were reported elsewhere.[57] ^{15}N HSQC titrations of BMAL1 TAD with CBP KIX or CRY CC were performed using 300 uL ^{15}N BMAL1 TAD and 10% D2O with a stepwise addition of CBP KIX or CC peptide in 10 mM MES pH 6.5, 50 mM NaCl. Titration data were analyzed with NMRViewJ using chemical shift perturbations defied by the equation $\Delta\delta_{TOT} = [(\Delta\delta^{1}H)^{2} + (\chi(\Delta\delta^{15}N)^{2}]^{½}$ and normalized with the scaling factor $\chi = 0.5$. All titration data were collected at 25 °C.

ZZ-exchange experiments[96] in the form of 24 ^{15}N HSQCs with interleaved mixing times ranging from 0-3 seconds were used to measure the rate constant of the *cis*-*trans* interconversion at 55, 60 and 65 °C. Integration of the auto and cross peaks for each mixing time were extracted using SPARKEY [27,59,97-105] and NMRviewJ [106]. Cross peak intensities were normalized to the small cross peak intensities at t=0 and total intensity was set to the sum of the integrations of the *cis* and *trans* peaks at t=0. The exchange constant was calculated by fitting integration data to an exchange model for two state intercoversion as described by equations 3.1-3.4 [107,108] using MATLAB Student software (http://www.mathworks.com/products/matlab/index-b.html).

$$I_{AA} = \frac{1}{2} P_A \left[\left(\frac{1 - R_{1A}^0 - R_{1B}^0 + K_{ex}(r_B - r_A)}{l_+ - l_-} \right) e^{-(-t)} + \left(1 + \left(\frac{1 - R_{1A}^0 - R_{1B}^0 + K_{ex}(r_B - r_A)}{l_+ - l_-} \right) e^{-(+t)} \right) \right] \quad (3.1)$$

$$I_{AA} = \frac{1}{2} P_B \left[\left(\frac{1 - R_{1A}^0 - R_{1B}^0 + K_{ex}(r_B - r_A)}{l_+ - l_-} \right) e^{-(-t)} + \left(1 + \left(\frac{1 - R_{1A}^0 - R_{1B}^0 + K_{ex}(r_B - r_A)}{l_+ - l_-} \right) e^{-(+t)} \right) \right] \quad (3.2)$$

$$I_{AB} = P_B \left[\left(\frac{K_{ex} P_A}{l_+ - l_-} \right) \left(e^{-(-t)} - e^{-(+t)} \right) \right] \quad (3.3)$$

$$I_{AB} = P_A \left[\left(\frac{K_{ex} P_A}{l_+ - l_-} \right) \left(e^{-(-t)} - e^{-(+t)} \right) \right] \quad (3.4)$$

Where, I is the time dependence of the transfer amplitudes (represented by the build up curves) for the *cis* (AA), *trans* (BB) and *cis* to *trans* (AB), P refers to the population of the indicated state, K_{ex} is the stochastic exchange of molecules between the two states per second, t is time in seconds, T is temperature in kelvin and R_{1A} and R_{1B} are the longitudinal relaxation rate constant in the absence of exchange.

The interconversion rates of *cis* to *trans* (K_{-1}) and *trans* to *cis* (K_1) were then calculated using the relative populations of the two isomers taken from the SPARKEY integrations, using equations 3.5-3.7.

$$K_{ex} = K_1 + K_{-1} \tag{3.5}$$

$$K_1 = K_{ex} P_{trans} \tag{3.6}$$

$$K_{-1} = K_{ex} P_{cis} \tag{3.7}$$

The rates of isomerization were interpolated to 25 °C and 37 °C using an Eyring-Polanyi equation (equation 3.8)[109]. Based upon transition state theory, the free energy of isomerization was calculated using equation 3.9 and the difference in free energy between the two isomers calculated using equation 3.10.

$$\ln \frac{K}{T} = -\frac{\Delta H}{RT} + \ln\left(\frac{k_B}{h}\right) + \frac{\Delta S}{R} \tag{3.8}$$

$$\Delta G^{\neq} = -RT \ln\left(\frac{hK_{CT}}{k_B T}\right) \tag{3.9}$$

$$\Delta G = \left|\Delta G^{\neq}_{CT} - \Delta G^{\neq}_{TC}\right| \tag{3.10}$$

Where T is temperature, R is the gas constant, k_B is the Boltzmann constant, h is Plank's constant and ΔH and ΔS are the activation enthalpy and entropy, respectively of *cis* to *trans* and *trans* to *cis* isomerization.

Fluorescence Anisotropy Experiments

The BMAL1 TAD WT, P625A P625 dmP and Δswitch peptide probes were purchased from Bio-Synthesis Inc (Lewisville, Tx) with a 5,6-TAMRA fluorescent probe covalently attached to the N-terminus. The C-terminus of the Δswitch peptide was amidated, the others were left as a free carboxyl group. Equilibrium binding assays with CRY1 1-491 were performed in 50 mM Bis-Tris propane pH, 7.5 with 100 mM NaCl, 2mM TCEP and 0.05% Tween-20; with KIX and TAZ1, the assay was performed in 10 mM MES, pH 6.5, with 50 mM NaCl and 0.05% Tween-20. Concentrated stocks of BMAL1 TAD probe peptides were stored between 15-200 μM at -70 °C

and diluted into assay buffer to 50 nM alone and in the presence of increasing concentrations of test protein. Plates were incubated at room temperature for 10-20 minutes prior to analysis. Binding was monitored by changes in fluorescence polarization with a Perkin Elmer En Vision 2103 Multilabel plate reader with excitation at 531 nm and emission at 595 nm. The hill coefficient, equilibrium binding dissociation constant and maximum velocity of binding were calculated by fitting the dose-dependent change in milliporaization (Δmp) to a one-site specific binding model in GraphPad Prism, with averaged Δmp values from duplicate or triplicate assays. Data shown are from one representative experiment of three independent assays.

REFERENCES

1. Thomas, M. C. & Chiang, C.-M. The general transcription machinery and general cofactors. *Crit. Rev. Biochem. Mol. Biol.* **41,** 105–178 (2006).
2. Zehavi, Y., Kedmi, A., Ideses, D. & Juven-Gershon, T. TRF2: TRansForming the view of general transcription factors. *Transcription* **6,** 1–6 (2015).
3. Czudnochowski, N., Bösken, C. A. & Geyer, M. Serine-7 but not serine-5 phosphorylation primes RNA polymerase II CTD for P-TEFb recognition. *Nature Communications* **3,** 842 (2012).
4. Kume, K. *et al.* mCRY1 and mCRY2 are essential components of the negative limb of the circadian clock feedback loop. *Cell* **98,** 193–205 (1999).
5. Yagita, K. *et al.* Dimerization and nuclear entry of mPER proteins in mammalian cells. *Genes & Development* **14,** 1353–1363 (2000).
6. Yagita, K. *et al.* Nucleocytoplasmic shuttling and mCRY-dependent inhibition of ubiquitylation of the mPER2 clock protein. *EMBO J.* **21,** 1301–1314 (2002).
7. Zhu, H., Conte, F. & Green, C. B. Nuclear localization and transcriptional repression are confined to separable domains in the circadian protein CRYPTOCHROME. *Curr. Biol.* **13,** 1653–1658 (2003).
8. Vielhaber, E. L., Duricka, D., Ullman, K. S. & Virshup, D. M. Nuclear export of mammalian PERIOD proteins. *J. Biol. Chem.* **276,** 45921–45927 (2001).
9. Chaves, I. *et al.* Functional evolution of the photolyase/cryptochrome protein family: importance of the C terminus of mammalian CRY1 for circadian core oscillator performance. *Molecular and Cellular Biology* **26,** 1743–1753 (2006).
10. Isojima, Y. *et al.* CKIepsilon/delta-dependent phosphorylation is a temperature-insensitive, period-determining process in the mammalian circadian clock. *Proceedings of the National Academy of Sciences* **106,** 15744–15749 (2009).
11. Virshup, D. M., Eide, E. J., Forger, D. B., Gallego, M. & Harnish, E. V. Reversible protein phosphorylation regulates circadian rhythms. *Cold Spring Harb. Symp. Quant. Biol.* **72,** 413–420 (2007).
12. Lee, C., Etchegaray, J. P., Cagampang, F. R., Loudon, A. S. & Reppert, S. M. Posttranslational mechanisms regulate the mammalian circadian clock. *Cell* **107,** 855–867 (2001).
13. Hirota, T. *et al.* A chemical biology approach reveals period shortening of the mammalian circadian clock by specific inhibition of GSK-3beta. *Proceedings of the National Academy of Sciences* **105,** 20746–20751 (2008).
14. Toh, K. L. *et al.* An hPer2 phosphorylation site mutation in familial advanced sleep phase syndrome. *Science* **291,** 1040–1043 (2001).

15. Hirota, T. *et al.* High-throughput chemical screen identifies a novel potent modulator of cellular circadian rhythms and reveals CKIα as a clock regulatory kinase. *Plos Biol* **8,** e1000559 (2010).

16. St John, P. C., Hirota, T., Kay, S. A. & Doyle, F. J. Spatiotemporal separation of PER and CRY posttranslational regulation in the mammalian circadian clock. *Proceedings of the National Academy of Sciences* **111,** 2040–2045 (2014).

17. Eide, E. J. *et al.* Control of mammalian circadian rhythm by CKIepsilon-regulated proteasome-mediated PER2 degradation. *Molecular and Cellular Biology* **25,** 2795–2807 (2005).

18. Kurabayashi, N., Hirota, T., Sakai, M., Sanada, K. & Fukada, Y. DYRK1A and glycogen synthase kinase 3beta, a dual-kinase mechanism directing proteasomal degradation of CRY2 for circadian timekeeping. *Molecular and Cellular Biology* **30,** 1757–1768 (2010).

19. Gao, P. *et al.* Phosphorylation of the Cryptochrome 1 C-terminal Tail Regulates Circadian Period Length. *Journal of Biological Chemistry* **288,** 35277–35286 (2013).

20. Busino, L. *et al.* SCFFbxl3 controls the oscillation of the circadian clock by directing the degradation of cryptochrome proteins. *Science* **316,** 900–904 (2007).

21. Shirogane, T., Jin, J., Ang, X. L. & Harper, J. W. SCFbeta-TRCP controls clock-dependent transcription via casein kinase 1-dependent degradation of the mammalian period-1 (Per1) protein. *J. Biol. Chem.* **280,** 26863–26872 (2005).

22. Reischl, S. *et al.* Beta-TrCP1-mediated degradation of PERIOD2 is essential for circadian dynamics. *Journal of Biological Rhythms* **22,** 375–386 (2007).

23. Kim, J. K. & Forger, D. B. A mechanism for robust circadian timekeeping via stoichiometric balance. *Mol. Syst. Biol.* **8,** 630 (2012).

24. Lee, Y., Chen, R., Lee, H.-M. & Lee, C. Stoichiometric relationship among clock proteins determines robustness of circadian rhythms. *Journal of Biological Chemistry* **286,** 7033–7042 (2011).

25. Lee, C. W., Arai, M., Martinez-Yamout, M. A., Dyson, H. J. & Wright, P. E. Mapping the Interactions of the p53 Transactivation Domain with the KIX Domain of CBP †. *Biochemistry* **48,** 2115–2124 (2009).

26. Lee, C. W., Martinez-Yamout, M. A., Dyson, H. J. & Wright, P. E. Structure of the p53 Transactivation Domain in Complex with the Nuclear Receptor Coactivator Binding Domain of CREB Binding Protein. *Biochemistry* **49,** 9964–9971 (2010).

27. Ferreon, J. C. *et al.* Cooperative regulation of p53 by modulation of ternary complex formation with CBP/p300 and HDM2. *Proceedings of the National Academy of Sciences* **106,** 6591–6596 (2009).

28. Borcherds, W. *et al.* Disorder and residual helicity alter p53-Mdm2 binding affinity and signaling in cells. *Nat. Chem. Biol.* **10,** 1000–1002 (2014).

29. Lai, Z., Auger, K. R., Manubay, C. M. & Copeland, R. A. Thermodynamics of p53 binding to hdm2(1-126): effects of phosphorylation and p53 peptide length. *ARCHIVES OF BIOCHEMISTRY AND BIOPHYSICS* **381,** 278–284 (2000).

30. Uesugi, M. & Verdine, G. L. The alpha-helical FXXPhiPhi motif in p53: TAF interaction and discrimination by MDM2. *Proc. Natl. Acad. Sci. U.S.A.* **96,** 14801–14806 (1999).

31. Teufel, D. P., Freund, S. M., Bycroft, M. & Fersht, A. R. Four domains of p300 each bind tightly to a sequence spanning both transactivation subdomains of p53. *Proc. Natl. Acad. Sci. U.S.A.* **104,** 7009–7014 (2007).

32. Hosoda, H. *et al.* CBP/p300 is a cell type-specific modulator of CLOCK/BMAL1-mediated transcription. *Mol Brain* **2,** 34 (2009).

33. Lee, Y. *et al.* Coactivation of the CLOCK-BMAL1 complex by CBP mediates resetting of the circadian clock. *J. Cell. Sci.* **123,** 3547–3557 (2010).

34. Koike, N. *et al.* Transcriptional architecture and chromatin landscape of the core circadian clock in mammals. *Science* **338,** 349–354 (2012).

35. Takahata, S. *et al.* Transactivation mechanisms of mouse clock transcription factors, mClock and mArnt3. *Genes to Cells* **5,** 739–747 (2000).

36. Goodman, R. H. & Smolik, S. CBP/p300 in cell growth, transformation, and development. *Genes & Development* (2000). doi:10.1101/gad.14.13.1553

37. Giles, R. H., Peters, D. J. & Breuning, M. H. Conjunction dysfunction: CBP/p300 in human disease. *Trends Genet.* **14,** 178–183 (1998).

38. Kee, B. L., Arias, J. & Montminy, M. R. Adaptor-mediated recruitment of RNA polymerase II to a signal-dependent activator. *J. Biol. Chem.* **271,** 2373–2375 (1996).

39. Nakajima, T. *et al.* RNA helicase A mediates association of CBP with RNA polymerase II. *Cell* **90,** 1107–1112 (1997).

40. Cho, H. *et al.* A human RNA polymerase II complex containing factors that modify chromatin structure. *Molecular and Cellular Biology* **18,** 5355–5363 (1998).

41. Wang, N. & Mapp, A. K. KINETIC AND CONFORMATIONAL CHARACTERIZATION OF TRANSCRIPTIONAL ACTIVATOR- COACTIVATOR INTERACTIONS. 1–178 (2013).

42. Ogryzko, V. V., Schiltz, R. L., Russanova, V., Howard, B. H. & Nakatani, Y. The transcriptional coactivators p300 and CBP are histone acetyltransferases. *Cell* **87,** 953–959 (1996).

43. Rycyzyn, M. A. & Clevenger, C. V. The intranuclear prolactin/cyclophilin B complex as a transcriptional inducer. *Proc. Natl. Acad. Sci. U.S.A.* **99,** 6790–6795 (2002).

44. Ansari, H., Greco, G. & Luban, J. Cyclophilin A Peptidyl-Prolyl Isomerase Activity Promotes Zpr1 Nuclear Export. *Molecular and Cellular Biology* **22,** 6993–7003 (2002).

45. Pastorino, L. *et al.* The prolyl isomerase Pin1 regulates amyloid precursor protein processing and amyloid-β production. *Nature* **440,** 528–534 (2006).

46. Ratajczak, T., Cluning, C. & Ward, B. K. Steroid Receptor-Associated Immunophilins: A Gateway to Steroid Signalling. *Clin Biochem Rev* **36,** 31–52 (2015).

47. Wang, Z. *et al.* Pro Isomerization in MLL1 PHD3-Bromo Cassette Connects H3K4me Readout to CyP33 and HDAC-Mediated Repression. *Cell* **141,** 1183–1194 (2010).

48. Kawasaki, H. *et al.* Distinct roles of the co-activators p300 and CBP in retinoic-acid-induced F9-cell differentiation. *Nature* **393,** 284–289 (1998).

49. Kasper, L. H. *et al.* A transcription-factor-binding surface of coactivator p300 is required for haematopoiesis. *Nature* **419,** 738–743 (2002).

50. Yuan, Z. M. *et al.* Function for p300 and not CBP in the apoptotic response to DNA damage. *Oncogene* **18,** 5714–5717 (1999).

51. Kalkhoven, E. CBP and p300: HATs for different occasions. *Biochemical Pharmacology* **68,** 1145–1155 (2004).

52. Yao, T. P. *et al.* Gene dosage-dependent embryonic development and proliferation defects in mice lacking the transcriptional integrator p300. *Cell* **93,** 361–372 (1998).

53. Chen, W. *et al.* Distinct Roles for CBP and p300 on the RA-Mediated Expression of the Meiosis Commitment Gene Stra8 in Mouse Embryonic Stem Cells. *PLoS ONE* **8,** e66076–8 (2013).

54. Waltzer, L. & Bienz, M. Drosophila CBP represses the transcription factor TCF to antagonize Wingless signalling. *Nature* **395,** 521–525 (1998).

55. Etchegaray, J.-P., Lee, C., Wade, P. A. & Reppert, S. M. Rhythmic histone acetylation underlies transcription in the mammalian circadian clock. *Nature* **421,** 177–182 (2003).

56. Curtis, A. M. *et al.* Histone acetyltransferase-dependent chromatin remodeling and the vascular clock. *J. Biol. Chem.* **279,** 7091–7097 (2004).

57. Xu, H. *et al.* Cryptochrome 1 regulates the circadian clock through dynamic interactions with the BMAL1 C terminus. *Nat. Struct. Mol. Biol.* **22,** 476–484 (2015).

58. Arai, M., Dyson, H. J. & Wright, P. E. Leu628 of the KIX domain of CBP is a key residue for the interaction with the MLL transactivation domain. *FEBS Lett.* **584,** 4500–4504 (2010).

59. De Guzman, R. N., Wojciak, J. M., Martinez-Yamout, M. A., Dyson, H. J. & Wright, P. E. CBP/p300 TAZ1 domain forms a structured scaffold for ligand binding. *Biochemistry* **44,** 490–497 (2005).

60. Palazzesi, F., Barducci, A. & Tollinger, M. The allosteric communication pathways in KIX domain of CBP. in (2013). doi:10.1073/pnas.1313548110/-/DCSupplemental

61. Brüschweiler, S., Konrat, R. & Tollinger, M. Allosteric Communication in the KIX Domain Proceeds through Dynamic Repacking of the Hydrophobic Core. *ACS Chem. Biol.* **8,** 1600–1610 (2013).

62. Law, S. M., Gagnon, J. K., Mapp, A. K. & Brooks, C. L. Prepaying the entropic cost for allosteric regulation in KIX. *Proc. Natl. Acad. Sci. U.S.A.* **111,** 12067–12072 (2014).

63. Brüschweiler, S. *et al.* Direct Observation of the Dynamic Process Underlying Allosteric Signal Transmission. *J. Am. Chem. Soc.* **131,** 3063–3068 (2009).

64. Goto, N. K., Zor, T., Martinez-Yamout, M., Dyson, H. J. & Wright, P. E. Cooperativity in Transcription Factor Binding to the Coactivator CREB-binding Protein (CBP). *J. Biol. Chem.* **277,** 43168–43174 (2002).

65. Galigniana, M. D., Morishima, Y., Gallay, P. A. & Pratt, W. B. Cyclophilin-A Is Bound through Its Peptidylprolyl Isomerase Domain to the Cytoplasmic Dynein Motor Protein Complex. *J. Biol. Chem.* **279,** 55754–55759 (2004).

66. Smith, D. F. & Toft, D. O. Minireview: The Intersection of Steroid Receptors with Molecular Chaperones: Observations and Questions. *Molecular Endocrinology* **22,** 2229–2240 (2008).

67. TEIGELKAMP, S. *et al.* The 20kD protein of human [U4/U6.U5] tri-snRNPs is a novel cyclophilin that forms a complex with the U4/U6-specific 60kD and 90kD proteins. *RNA* **4,** 127–141 (1998).

68. Adams, B. M., Coates, M. N., Jackson, S. R., Jurica, M. S. & Davis, T. L. Nuclear cyclophilins affect spliceosome assembly and function in vitro. *Biochem. J.* **469,** 223–233 (2015).

69. Grow, E. J. & Wysocka, J. Flipping MLL1's switch one proline at a time. *Cell* **141,** 1108–1110 (2010).

70. Kang, S. W. *et al.* Drosophila peptidyl-prolyl isomerase Pin1 modulates circadian rhythms via regulating levels of PERIOD. *Biochemical and Biophysical Research Communications* 1–6 (2016). doi:10.1016/j.bbrc.2015.05.033

71. Reimer, U., Drewello, M., Jakob, M., Fischer, G. & Schutkowski, M. Conformational state of a 25-mer peptide from the cyclophilin-binding loop of the HIV type 1 capsid protein. *Biochem. J.* **326 (Pt 1),** 181–185 (1997).

72. Zhan, Y. A. & Ytreberg, F. M. The *cis* conformation of proline leads to weaker binding of a p53 peptide to MDM2 compared to *trans*. *ARCHIVES OF BIOCHEMISTRY AND BIOPHYSICS* **575,** 22–29 (2015).

73. Schmid, F. X. Prolyl isomerase: enzymatic catalysis of slow protein-folding reactions. *Annu Rev Biophys Biomol Struct* **22,** 123–142 (1993).

74. Nelson, C. J., Santos-Rosa, H. & Kouzarides, T. Proline Isomerization of Histone H3 Regulates Lysine Methylation and Gene Expression. *Cell* **126,** 905–916 (2006).

75. Dumy, P. *et al.* Pseudo-prolines as a molecular hinge: reversible induction of *cis* amide bonds into peptide backbones. *Journal of the …* **119,** 918–925 (1997).

76. Martin, A. & Schmid, F. X. A Proline Switch Controls Folding and Domain Interactions in the Gene-3-protein of the Filamentous Phage fd. *J. Mol. Biol.* **331,** 1131–1140 (2003).

77. Fassolari, M. *et al.* Minute time scale prolyl isomerization governs antibody recognition of an intrinsically disordered immunodominant epitope. *Journal of Biological Chemistry* **288,** 13110–13123 (2013).

78. Dugave, C. & Demange, L. *Cis−Trans* Isomerization of Organic Molecules and Biomolecules: Implications and Applications †. *Chem. Rev.* **103,** 2475–2532 (2003).

79. Hanes, S. D. Prolyl isomerases in gene transcription. *BBA - General Subjects* **1850,** 1–18 (2014).

80. Driver, J. A., Zhou, X. Z. & Lu, K. P. Regulation of protein conformation by Pin1 offers novel disease mechanisms and therapeutic approaches in Alzheimer's disease. *Discov Med* **17,** 93–99 (2014).

81. Sarkar, P., Reichman, C., Saleh, T., Birge, R. B. & Kalodimos, C. G. Proline *cis-trans* Isomerization Controls Autoinhibition of a Signaling Protein. *Mol. Cell* **25,** 413–426 (2007).

82. Sarkar, P., Saleh, T., Tzeng, S.-R., Birge, R. B. & Kalodimos, C. G. Structural basis for regulation of the Crk signaling protein by a proline switch. *Nat. Chem. Biol.* **7,** 51–57 (2010).

83. Greenwood, A. I., Kwon, J. & Nicholson, L. K. Isomerase-Catalyzed Binding of Interleukin-1 Receptor-Associated Kinase 1 to the EVH1 Domain of Vasodilator-Stimulated Phosphoprotein. *Biochemistry* **53,** 3593–3607 (2014).

84. Lu, K. P., Finn, G., Lee, T. H. & Nicholson, L. K. Prolyl *cis-trans* isomerization as a molecular timer. *Nat. Chem. Biol.* **3,** 619–629 (2007).

85. Takahashi, N., Hayano, T. & Suzuki, M. Peptidyl-prolyl *cis-trans* isomerase is the cyclosporin A-binding protein cyclophilin. *Nature* **337,** 473–475 (1989).

86. Fischer, G., Wittmann-Liebold, B., Lang, K., Kiefhaber, T. & Schmid, F. X. Cyclophilin and peptidyl-prolyl *cis-trans* isomerase are probably identical proteins. *Nature* **337,** 476–478 (1989).

87. KATZ, M., SIMONETTA, S., RALPH, M. & GOLOMBEK, D. Immunosuppressant calcineurin inhibitors phase shift circadian rhythms and inhibit circadian responses to light. *Pharmacology Biochemistry and Behavior* **90,** 763–768 (2008).

88. Lipton, J. O. *et al.* The Circadian Protein BMAL1 Regulates Translation in Response to S6K1-Mediated Phosphorylation. *Cell* **161,** 1138–1151 (2015).

89. Toto, A., Giri, R., Brunori, M. & Gianni, S. The mechanism of binding of the KIX domain to the mixed lineage leukemia protein and its allosteric role in the recognition of c-Myb. *Protein Sci.* **23,** 962–969 (2014).

90. Dyson, H. J. & Wright, P. E. Role of Intrinsic Protein Disorder in the Function and Interactions of the Transcriptional Coactivators CREB-binding Protein (CBP) and p300. *J. Biol. Chem.* **291,** 6714–6722 (2016).

91. Ramanathan, C., Khan, S. K., Kathale, N. D., Xu, H. & Liu, A. C. Monitoring cell-autonomous circadian clock rhythms of gene expression using luciferase bioluminescence reporters. *J Vis Exp* e4234–e4234 (2012). doi:10.3791/4234

92. Liu, A. C. *et al.* Redundant function of REV-ERBalpha and beta and non-essential role for BMAL1 cycling in transcriptional regulation of intracellular circadian rhythms. *PLoS Genet.* **4,** e1000023 (2008).

93. Sheffield, P., Garrard, S. & Derewenda, Z. Overcoming expression and purification problems of RhoGDI using a family of 'parallel' expression vectors. *Protein Expr. Purif.* **15,** 34–39 (1999).

94. Liu, H. & Naismith, J. H. An efficient one-step site-directed deletion, insertion, single and multiple-site plasmid mutagenesis protocol. *BMC Biotechnol* **8,** 91 (2008).

95. Delaglio, F. *et al.* NMRPipe: a multidimensional spectral processing system based on UNIX pipes. *J. Biomol. NMR* **6,** 277–293 (1995).

96. Farrow, N. A., Zhang, O., Forman-Kay, J. D. & Kay, L. E. A heteronuclear correlation experiment for simultaneous determination of 15N longitudinal decay and chemical exchange rates of systems in slow equilibrium. *J. Biomol. NMR* **4,** 727–734 (1994).

97. Miller Jenkins, L. M. *et al.* Characterization of the p300 Taz2–p53 TAD2 Complex and Comparison with the p300 Taz2–p53 TAD1 Complex. *Biochemistry* **54,** 2001–2010 (2015).

98. Miller, M., Dauter, Z., Cherry, S., Tropea, J. E. & Wlodawer, A. Structure of the Taz2 domain of p300: insights into ligand binding. *Acta Cryst (2009). D65, 1301-1308 [doi:10.1107/S0907444909040153]* 1–8 (2009). doi:10.1107/S0907444909040153

99. Wojciak, J. M., Martinez-Yamout, M. A., Dyson, H. J. & Wright, P. E. Structural basis for recruitment of CBP/p300 coactivators by STAT1 and STAT2 transactivation domains. *EMBO J.* **28,** 948–958 (2009).

100. Franks, K. M. Clockwork: exploring activation mechanisms of the circadian transcription factor CLOCK:BMAL1. 1–27 (2016).

101. Krois, A. S., Ferreon, J. C., Martinez-Yamout, M. A., Dyson, H. J. & Wright, P. E. Recognition of the disordered p53 transactivation domain by the transcriptional adapter zinc finger domains of CREB-binding protein. *Proc. Natl. Acad. Sci. U.S.A.* **113,** E1853–E1862 (2016).

102. De Guzman, R. N., Martinez-Yamout, M. A., Dyson, H. J. & Wright, P. E. Interaction of the TAZ1 domain of the CREB-binding protein with the activation domain of CITED2: regulation by competition between intrinsically unstructured ligands for non-identical binding sites. *J. Biol. Chem.* **279,** 3042–3049 (2004).

103. De Guzman, R. N., Liu, H. Y., Martinez-Yamout, M., Dyson, H. J. & Wright, P. E. Solution structure of the TAZ2 (CH3) domain of the transcriptional adaptor protein CBP. *J. Mol. Biol.* **303,** 243–253 (2000).

104. De Guzman, R. N., Goto, N. K., Dyson, H. J. & Wright, P. E. Structural Basis for Cooperative Transcription Factor Binding to the CBP Coactivator. *J. Mol. Biol.* **355,** 1005–1013 (2006).

105. McManus, K. J. & Hendzel, M. J. CBP, a transcriptional coactivator and acetyltransferase. *Biochem. Cell Biol.* **79,** 253–266 (2001).

106. Johnson, B. A. Using NMRView to visualize and analyze the NMR spectra of macromolecules. *Methods Mol. Biol.* **278,** 313–352 (2004).

107. Kleckner, I. R. & Foster, M. P. An introduction to NMR-based approaches for measuring protein dynamics. *Biochim. Biophys. Acta* **1814,** 942–968 (2011).

108. Palmer, A. G., Kroenke, C. D. & Loria, J. P. Nuclear magnetic resonance methods for quantifying microsecond-to-millisecond motions in biological macromolecules. *Meth. Enzymol.* **339,** 204–238 (2001).

109. Eyring, H. The Activated Complex in Chemical Reactions. *J. Chem. Phys.* **3,** 107–10 (1935).

SUPPLEMENTAL FIGURES FOR CHAPTER 3

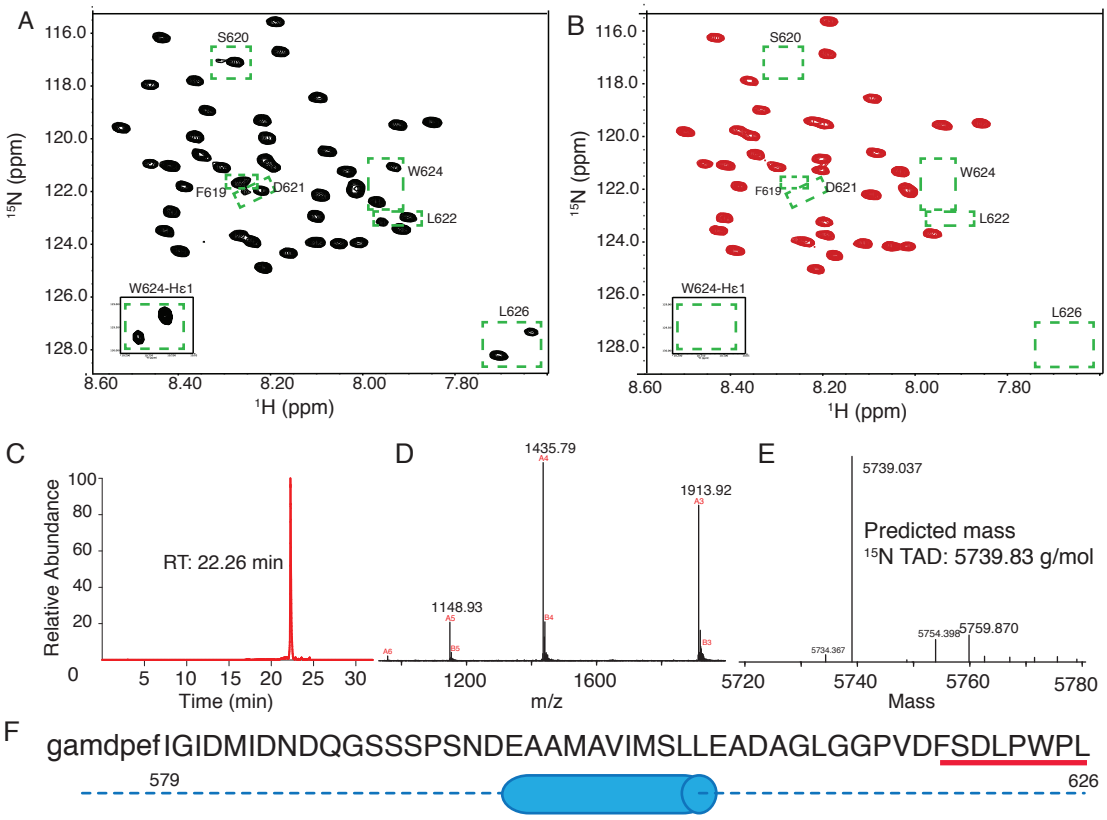

Supplemental Figure 3.1: Identification of the BMAL1 TAD switch. (A) ^{15}N HSQC of BMAL1 TAD (579-626) with peak doubling boxed in green (B) ^{15}N HSQC of ΔSwitch BMAL1 TAD (579-619) with green boxes indicating the lack of peak doubling (C) HPLC trace of ^{15}N BMAL1 TAD with elution from a C4 reverse phase column (D) mass spectrum of ^{15}N BMAL1 TAD (E) deconvolution of BMAL1 TAD mass spectrum in D. (F) Primary sequence of BMAL1 TAD with N-terminal vector tag indicated in lower case letters and the predicted α-helical region indicated below the sequence. Residues for which peak doubling was observed are underlined in red.

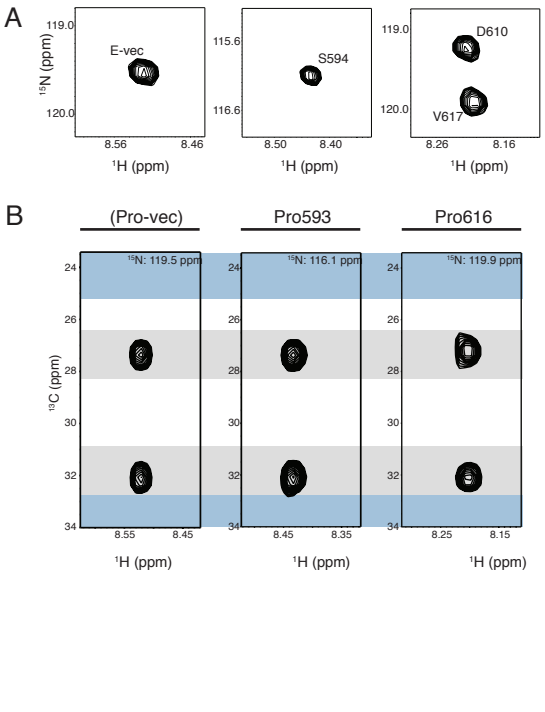

C

Resonance	% cis	% trans
W624NH	38.1	61.9
W624Hε1	32.8	67.2
L626	32.3	67.7
Average	34.4 ±3.2	65.6 ±3.2

D

Resonance	% cis	% trans
W624NH	37.9	62.1
W624Hε1	43.3	56.7
L626	40.2	59.8
Average	40.5 ± 2.7	59.5 ±2.7

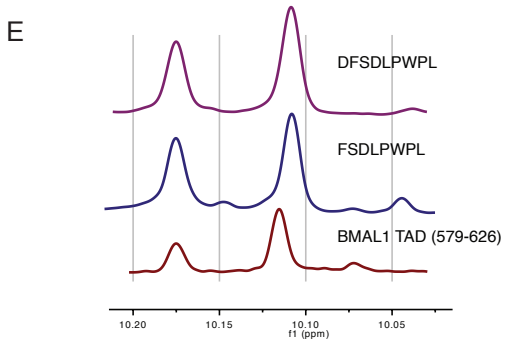

Supplemental Figure 3.2: A *cis*/*trans* isomerization drives the TAD switch. (A) Regions of the ^{15}N HSQC spectra of the BMAL1 TAD displaying the backbone amide bond resonances of the two conformers of Val617, Ser694 and Glu(vector) (B) strips from the ^{15}N ^{13}C (H)C(CO)NH TOCSY of the BMAL1 TAD at the ^{1}H and ^{15}N chemical shifts of the backbone amide from Val617 and Ser594 and Glu(vector tag) (x- and z-axes, respectively) and the ^{13}C shifts of Pro623 and P625 Cβ and Cγ residues (y axis). Grey region is accepted ^{13}C shifts for proline Cβ and Cγ found in *trans* and blue region is accepted ^{13}C shifts for proline Cβ and Cγ in *cis*. Ratios of *cis* and *trans* isomers in (C) ^{15}N BMAL1 TAD and (D) WT switch peptide calculated from the peak volumes of the indicated residues. (E) ^{1}H 1D spectra of the indole region taken from natural abundance WT switch peptides FSDLPWPL and DFSDLPWPL compared to ^{15}N BMAL1 TAD.

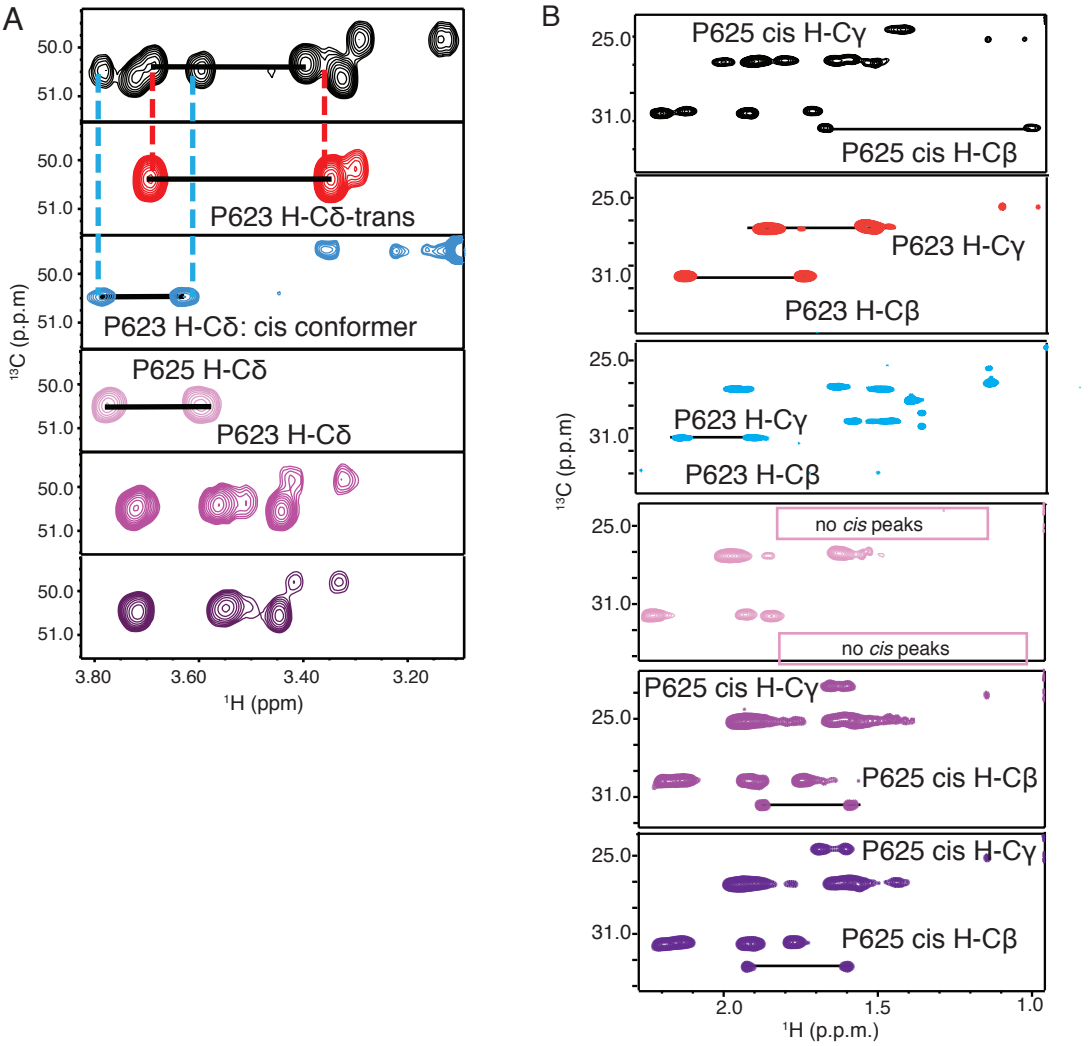

Supplemental Figure 3.3: Assignment and cycling analysis of TAD switch mutants. Regions of the ^{1}H-^{1}H TOCSY of FSDLPWPL (black) FSDLPWPL (red), FSDLPWdmPL (blue), FSDLPAPL (light pink), FSDLPFPL (violet) and FSDLPYPL (purple) showing the (A) Proδ chemical shifts and (B) Pro γ and Proβ chemical shifts.

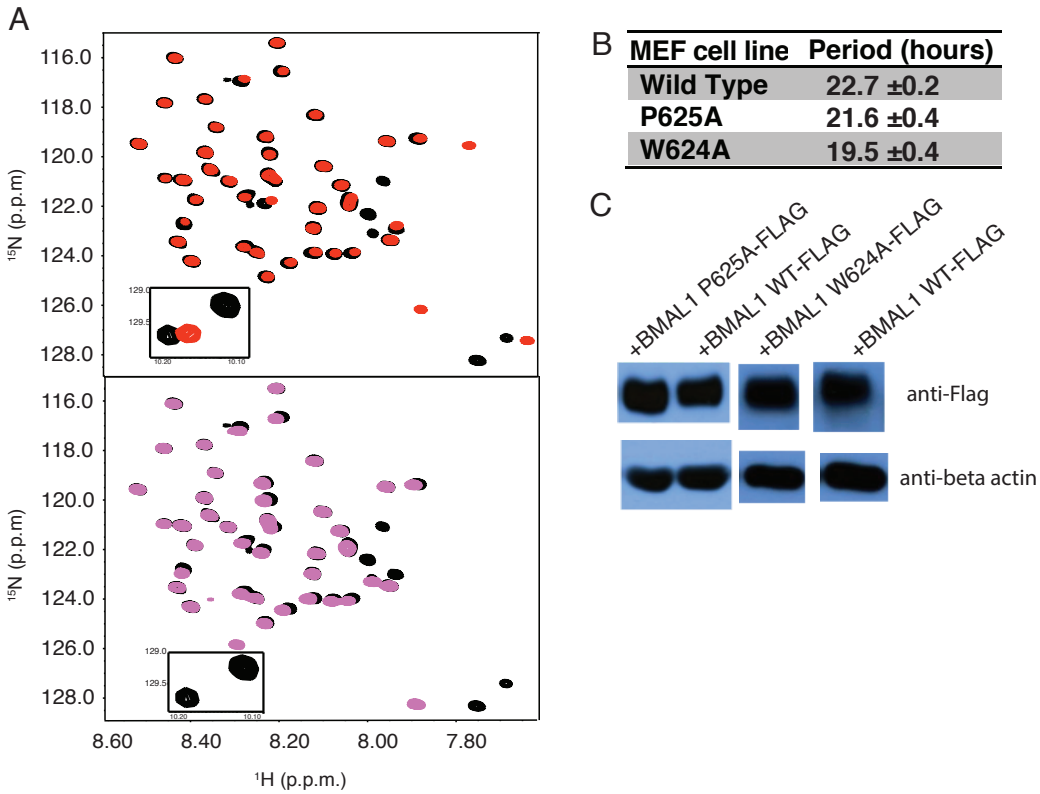

Supplemental Figure 3.4: TAD switch mutants in BMAL1 constructs. (C) ^{15}N HSQCs of the BMAL1 TAD wild type (black) overlaid with BMAL1 TAD harboring the P625A mutation (upper panel, red) and the W624A mutation (lower panel, pink). (D) Measured periods Per2Luc MEFs with BMAL1 WT, P625A and W624A from lumicycle analysis. Three independent experiments were performed in quadruplicate. (E) Western blot analysis of relative BMAL1 levels is WT, P625A and W624A Per2Luc MEFs.

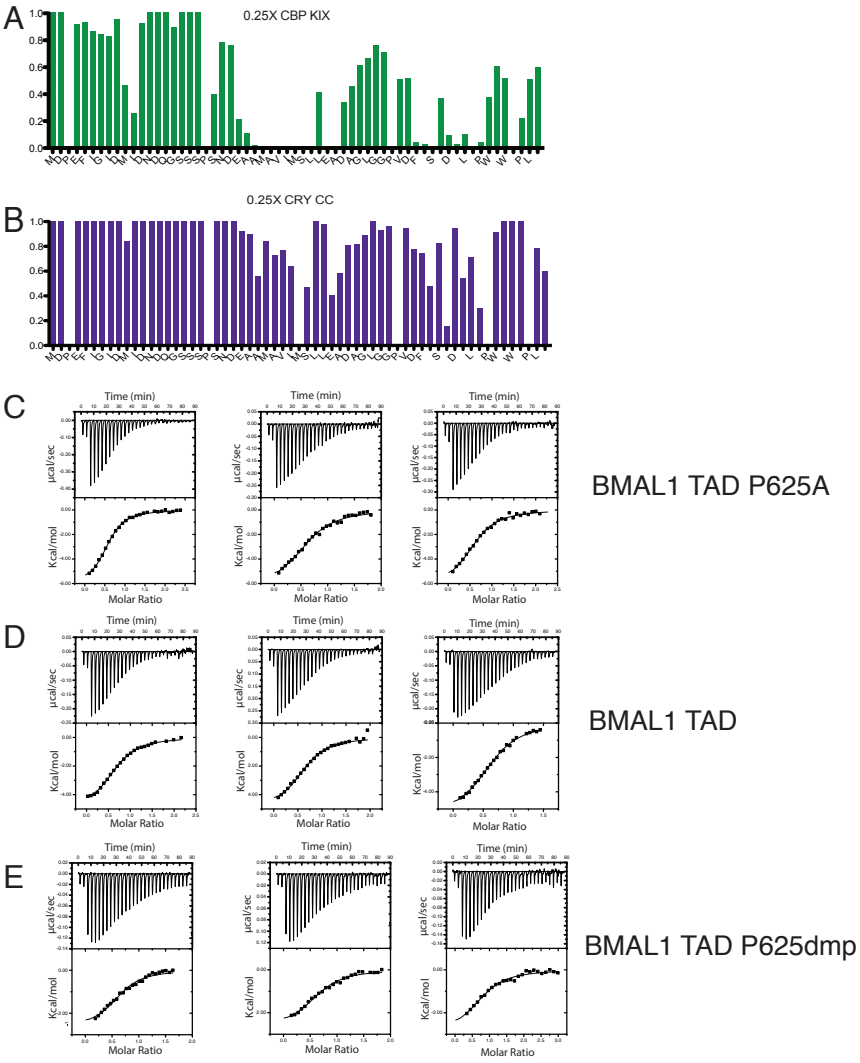

Supplemental Figure 3.5: Quantitative analysis of BMAL1 TAD Switch isomers with transcriptional coregulators Δvolume plots for ^{15}N BMAL1 TAD with A) 0.25X CBP KIX and B) 0.25X CRY CC. Isotherm plots from isothermal titration calorimetry (ITC) experiments of CBP KIX titrated into BMAL1 TAD (C) P625A (D) WT and (E) P625dmP. All ITC experiments were set up with 15-30 uM TAD in the cell and 220-250 uM KIX in the syringe and run at 25° C with 177 stir speed. ITC data were fit to a one-site binding model in Origin software to derive parameters that populate Table 3.1 with representative N values 0.6-0.8.

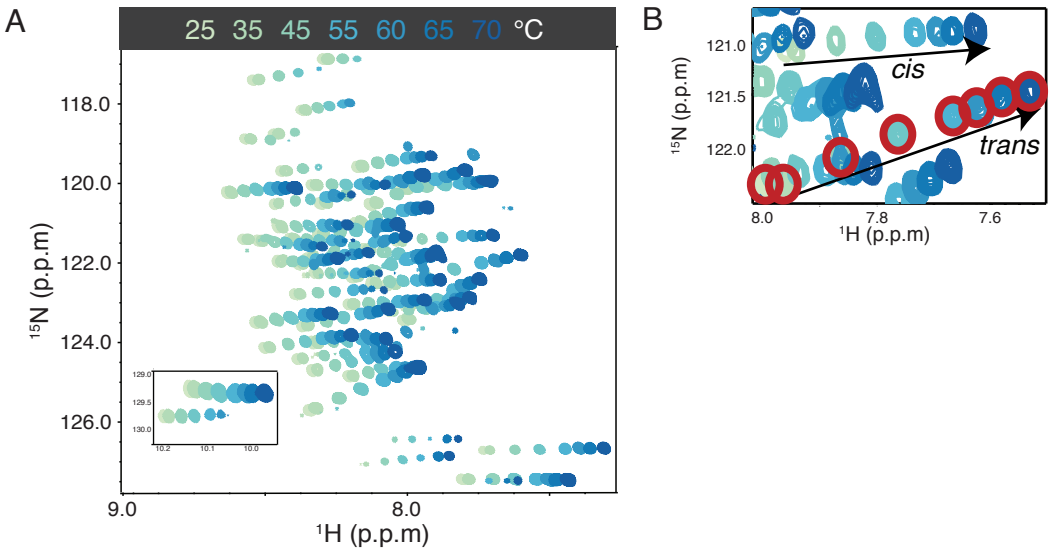

Supplemental Figure 3.6: Kinetic analysis of *cis*/*trans* isomerization. Overlaid ^{15}N HSQC spectra of WT BMAL1 TAD at various temperatures B) Region of the overlaid ^{15}N HSQC spectra showing the W624 backbone peaks at various temperatures.

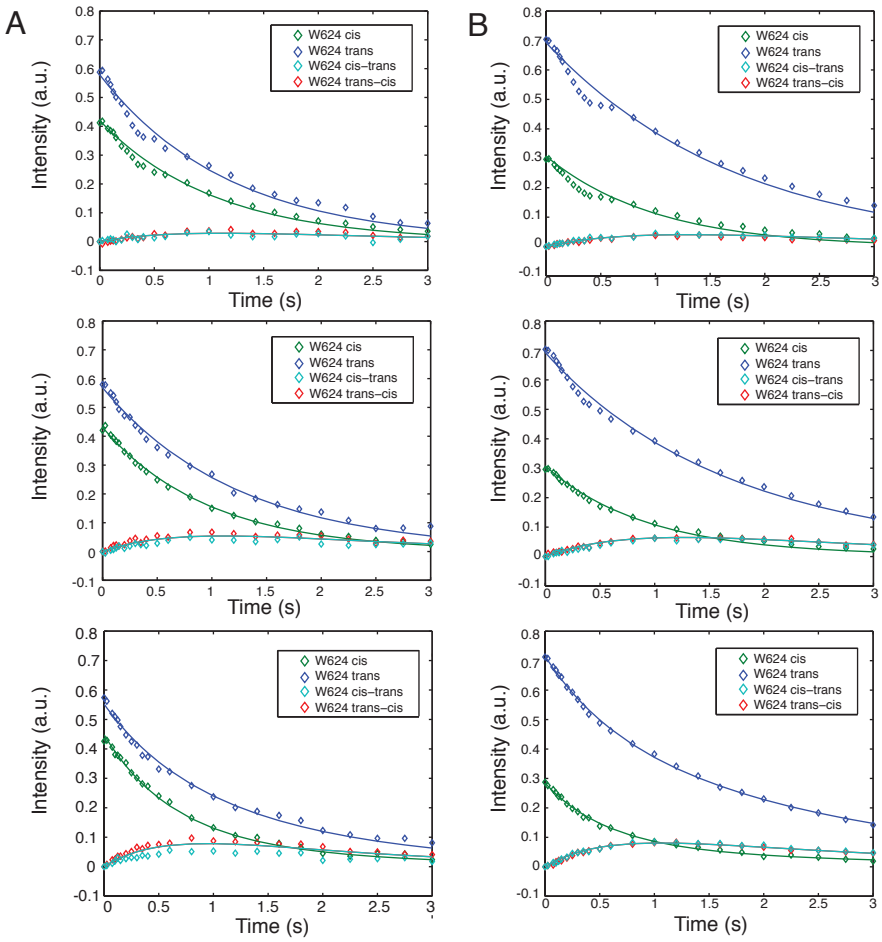

Supplemental Figure 3.7: Build up curves from zz-exchange data. Build up curves for C) W624 and D) L626 at 55 °C (top panels) 60 °C (middle panels) and 65 °C (bottom panels).

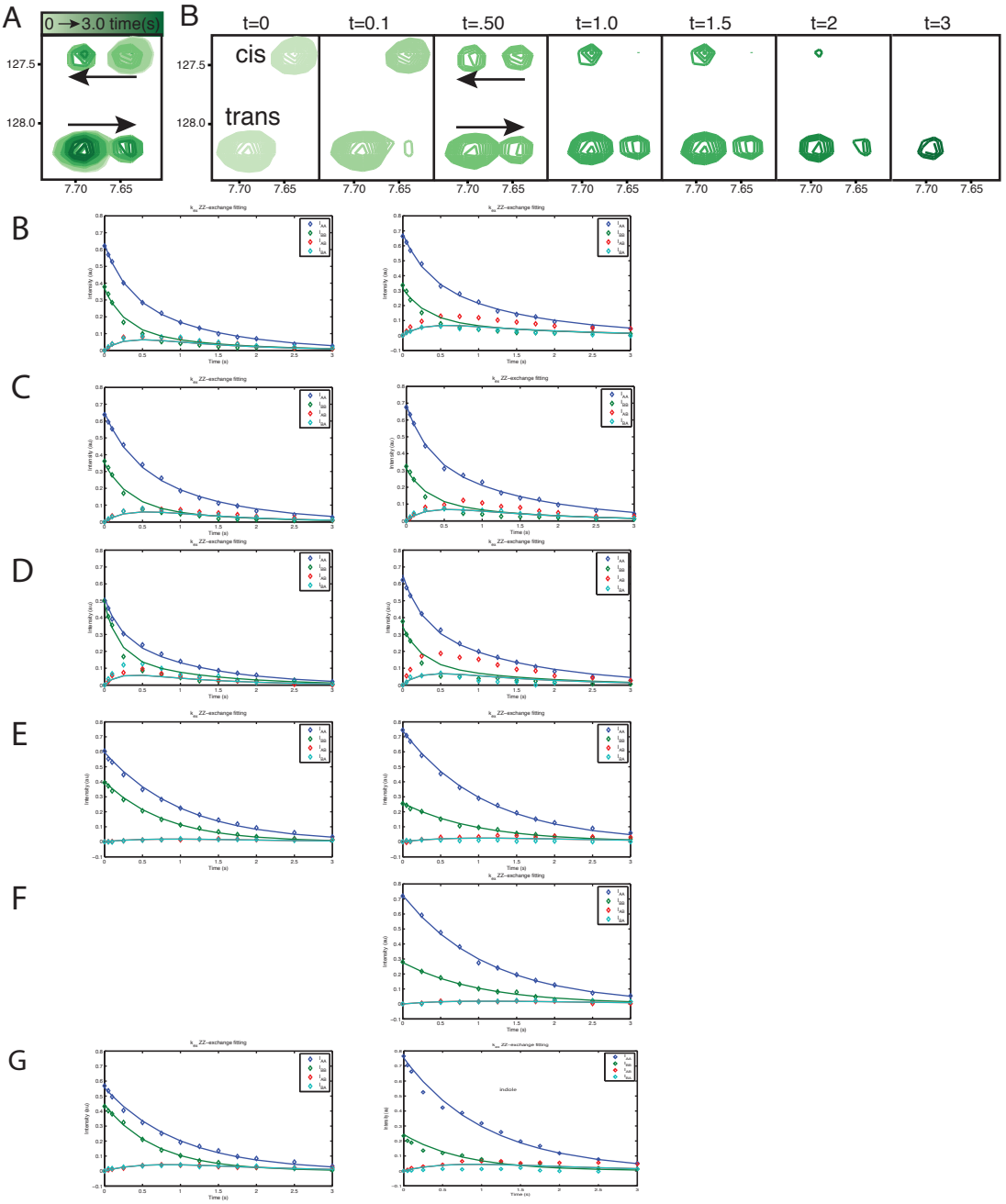

Supplemental Figure 3.8: Kinetic analysis of isomerization in the presence of peptidyl-prolyl isomerases. (A) Regions of the individual zz-exchange spectra, dso delay time is indicated above each spectra. Build up curves for L626 (left panels) and W624 (right panels) of ^{15}N BMAL1 TAD in the presence of (B) PPIA (C) PPIE (D) PPIF (E) PPIG (F) PPIH (G) PPIL3

CHAPTER 4

TRANSCRIPTIONAL ACTIVATION AT E-BOX ELEMENTS: INTERACTIONS OF THE BMAL1 TAD WITH TRANSCRIPTIONAL ACTIVATORS

INTRODUCTION

The Generic Process Of Transcriptional Activation

The production of mRNA transcripts from specific genes is a multistep process requiring coordinated efforts from a variety of proteins. In a generic transcription event, the general transcription factor IID (TFIID) binds a TATA box element ~25 base pairs upstream of the transcription start site (TSS) on the DNA; the subsequent step-wise recruitment of TFIIB, RNA polymerase II, TFIIF, TFIIE and TFIIH forms the pre-initiation complex (PIC).[1,2] Once the PIC is constructed, phosphorylation of RNA Pol II activates the complex leading to transcriptional elongation and the production of mRNA transcripts.[3] Site-specific transcription is regulated through modulation of chromatin structure and the binding of sequence-specific transcription factors to promoter elements upstream from the TSS. Coordination between site-specific transcription factors and the basal transcriptional machinery is moderated by transcriptional coactivators, which bind to transactivation domains of the transcription factors and subsequently recruit members of the PIC as well as histone acetyltransferases (HATs). In some cases, coactivators are able to act as HATs themselves.

CBP/p300 Are Promiscuous Co-Activators

The highly conserved CREB-binding protein (CBP) and its homolog E1A-binding protein (p300) are promiscuous transcriptional coactivators known to participate in the formation of the PIC through at a variety of different promoter regions.[4] In addition to acting as a bridge between transcription factors and basal machinery, CBP and p300 possess intrinsic aceyltransferase activity and are able to recruit other HATs to promoter regions[5-7]. Nearly 30 different DNA-bound transcription factors are known to interact with CBP and/or p300[8-17] and the co-activators are instrumental in processes such as hematopoiesis[18-20], cell cycle regulation, apotosis[10,15,16,21-24] and circadian rhythms.[25-28] Point mutations and ectopic expression of CBP and p300 have been linked to Rubinstein-Tabi syndrome, Acute Myeloid Leukemia and other hematological abnormalities while homozygous deletion of *CBP* or *p300* in mice is embryonic lethal.[18,29]

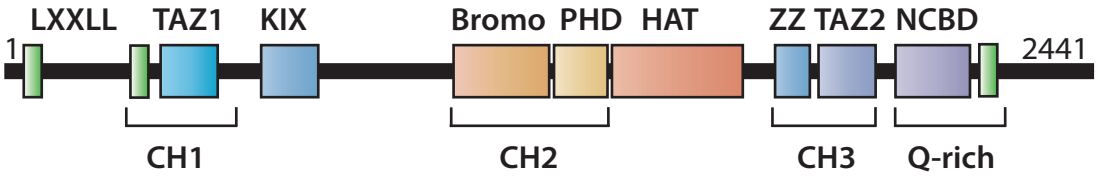

Figure 4.1: Domain Architecture of CBP. Mouse CREB-binding protein (CBP) Accession number Q6GQV9. The transactivation domains TAZ1, KIX, TAZ2 and NCBD interact with transcription factors and members of the preinitiation complex of basal transcriptional machinery. The HAT domain has acetyltransferase activity and the nearby Bromo domain is capable of recognizing acetylated histones.

While CBP and p300 share only 63% sequence identity[18], their modular domains are highly conserved (up to 93%). Additionally, the homologs have a significant amount of functional overlap and therefore are commonly referred to as CBP/p300. The two proteins are modular with many different domains that posses independent and overlapping functionalities (**Fig. 4.1**). The transactivation-binding domains TAZ1, KIX, TAZ2 and NCBD facilitate interactions with basal transcriptional machinery including the TATA-box binding protein (TBP), TFIIB and possibly even RNA Pol II [30-32] and promoter-specific transcription factors such as p53, c-Myb, CREB, MLL,HIF-1α, FOXO3a, C-Jun and others (**Table 4.1**).The Bromo domain recognizes acetylated histones and the adjacent HAT domain is capable of acetylating all four histones and a variety of non-histone proteins, including p53.[33,34]

In most systems, CBP and p300 are relatively redundant in their function as transcriptional co-activators, there is precedence for their distinct and sometimes antagonistic roles[4,19,35-38]. The cell cycle inhibitors $p21^{Cip1}$ and $p27^{Kip1}$ interact selectively with p300 and CBP, respectively.[39] p300, not CBP has been found to be imperative for haematopoiesis[19] and the apoptotic response to DNA damage.[40] Homozygous $p300^{-/-}$ or $CBP^{-/-}$ knockouts are both embryonic lethal however each display differing physiological abnormalities.[35,38] Transcription of the mouse STR8 gene

Table 4.1: Interactions between KIX TADs and binding partners

CBP/p300 Domain	Interacting proteins/ligands
N-terminus	STAT-1, SF-1, Nuclear hormone receptors
TAZ1	TAL1, p73, Mdm2, Hif-1α, Ets-1, RXT, p65f, Pit-1, HNF-4, Stat-2, TBP, p53
KIX	HPV E2, BRCA1, p45, c-Jun, c-Myb, TAX, Sap1, YY1, SREBP, ATF-1, ATF-4, p53
TAZ2	JMY, Mad, HPV E6, Tat, SF-1, E2F, Ets-1, GATA-1, Neuro-D, E1A, MyyoD, p90(RSK), cFo, SV40, YY1, p53
Q-Rich	pCIP, SRC-1

is enhanced by CBP and repressed by p300, showing that not only can the two co-activators possess differing roles, but they can also function as transcriptional repressors.[37] Likewise, in drosophila CBP acts as a transcriptional repressor through the acetylation of the LEF/TCF-1 gene which blocks binding of the co-activator beta-catenin.[36]

CBP/p300 In Circadian Rythyms

The CLOCK:BMAL1 mediated transcription that underlies circadian oscillations is dependent on the temporally specific interactions of CBP/p300 with the transcription factor at its cognate E-box complexes.[27,41] Intriguingly, the two co-activators interact with the CLOCK:BMAL1:E-box complex at differing circadian times. The time metric by which free running circadian oscillations are measured is circadian time (CT), where CT0 indicates the onset of activity for diurnal organisms (ex. Onset of activity for nocturnal organisms is CT12); p300 displays its major peak of occupancy at CT4-6 during transcriptional activation, while CBP occupancy peaks at CT16-18 during the early repressive phase and to a lesser extent at CT4-6 during active transcription. These data suggest that the two co-activators may have disparate and possibly antagonistic roles within the circadian system. It is possible CBP and/or p300 can act as both activator and repressor as a function of circadian time. The observation that peak CBP occupancy at CLOCK:BMAL1:E-Box sites occurs during the early repressive phase and is concomitant with CRY2, PER1 and PER2 occupancy[27] supports data published by Hosoda et. al.[25] that suggest that CBP can mediate transcriptional repression at E-box elements. These findings are contradictory however, to studies that have shown a direct increase in CLOCK:BMAL1 mediated transcription upon addition of CBP[42]. Moreover, CBP, and not p300, is required for CLOCK:BMAL1 mediated transcriptional activation upon serum synchronization, suggesting that it may play a special role in transducing phase-resetting cues from zeitgebers to the transcription-based clock.[26] Clearly, the role of CBP and p300 in maintaining circadian cycling is a complex, time dependent process, with differing roles for the two independent co-activators.

The N-terminal regions of CBP (452-721) and p300 (437-699) were identified by yeast two-hybrid to be sufficient and necessary for interaction with BMAL1[28]. This region contains one of CBP's three LXXLL motifs, which are known to interact with nuclear receptors[33] and the well-studied kinase-inducible domain interacting (KIX) domain. Subsequently, we used NMR spectroscopy to map KIX-binding motifs on the BMAL1 C-terminus.[43] Recent studies by our

lab have built upon this initial model of CBP interactions with the BMAL1 TAD by showing that the TAZ1 domain of CBP also interacts with the TAD with nanomolar affinity (chapter 2 of this dissertation). In the current study, we sought to elucidate the binding mechanism of the BMAL1 TAD with both the KIX and TAZ domains of CBP.

The KIX Domain Structure And Function

The KIX domain is a three-helix bundle with two 3_{10} helices and two independent TAD binding sites (**Fig. 4.2a,b**). The c-Myb and the MLL sites, named for the two transcription factors that exhibit specificity for each site, are connected through a central allosteric network of hydrophobic residues that runs up the center of the helical bundle. The c-Myb binding site is a shallow hydrophobic groove located between helices α1 and α3 helix and the MLL site is located on the open end of the 3-helix bundle and incorporates residues from all three helices (**Fig. 4.2** and **Table 4.2**).[14,44-46] The central allosteric network allows for a redistribution of conformational ensembles in the KIX domain upon interaction with a ligand at one of its two binding sites. The higher energy form of the KIX domain, with "preformed tertiary structure" that is ready to bind TADs at both sites, displays increased rigidity of the G_2 helix and C-terminal α3 helix and is only present in ~0.5% of unbound KIX molecules.[20,47,48] The population of this preformed state is stabilized in the binary MLL:KIX complex, where it is observed in 7% of the molecules leading to a 2-fold increase in binding affinity for pKID[20] compared to the apo KIX domain, due to the decreased entropic cost of interaction.[47] The interaction between the KIX domain and its ligands is therefore a highly dynamic process.

In addition to the internal dynamics of the KIX domain, many of its TAD ligands also undergo a coupled folding and binding process.[49,50] While theories regarding the benefits of coupled

Table 4.2: Mapping functional motifs and sites of interaction on the KIX domain.

α1	α2	G1	G2	MLL		c-Myb		Allosteric	
597-611	623-640	591-594	617-621	L664	T614	L599	L653	Leu 603	612
				Y631	L628	H602	A654	Leu 607	Y650
				R624	L620	L603	I657	Ile 611 t	H651
				F612	E626	K606	Y658	Leu 628	A654
				R668	V629	L607	Q661	Leu 653	Y658
				L628	K659	A610	K662	Ile 657	K659
				D622	Q661	Y650	Y640	Ile 660	
				N627	K662				
				L620	E665				
				M625					

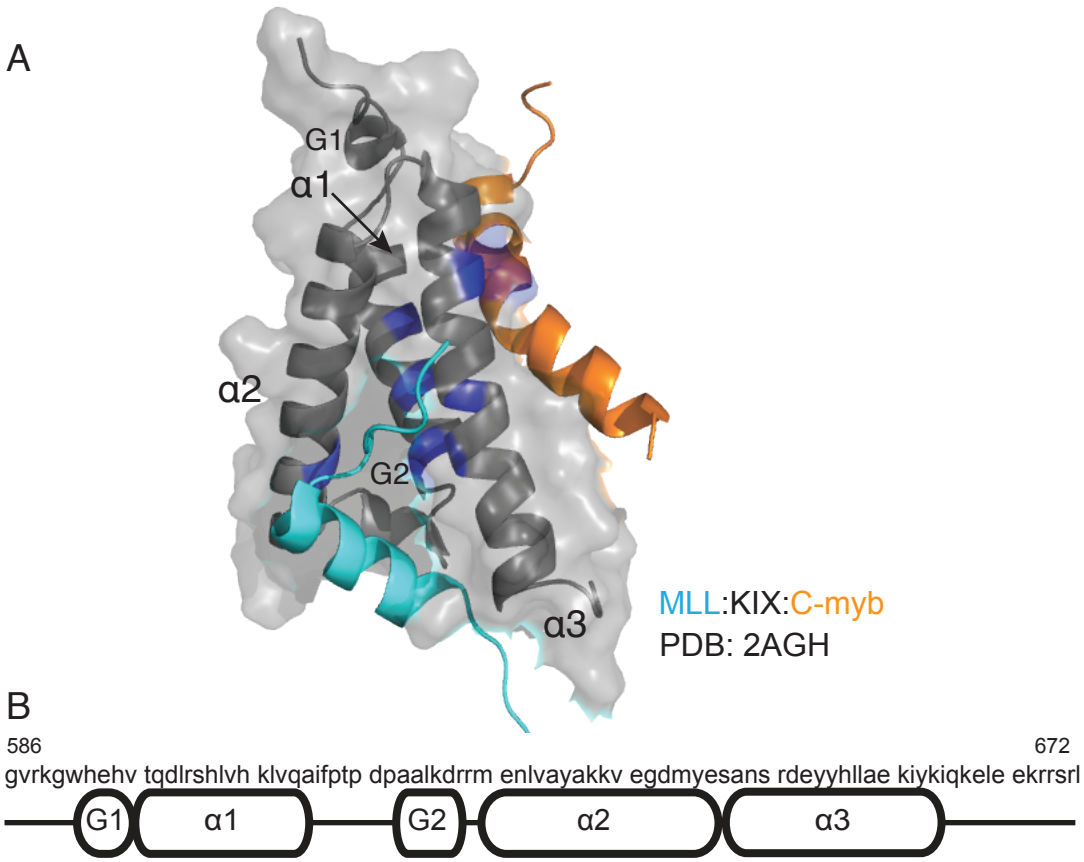

Figure 4.2: Structure of the KIX domain of CBP. (A) NMR structure of KIX (grey) in complex with c-Myb (orange) and MLL (cyan) peptides. Amino acids in the allosteric network are highlighted in dark blue. B) Primary sequence and secondary structure of the KIX domain.

folding and binding mechanism abound, and many are contradictory[51-53], it is clear that the dynamics and thermodynamics of these interactions are finely tuned to elicit the proper affinity and timescale of interactions. Stopped flow anisotropy studies and molecular modeling studies suggest that the association rate of the partially folded c-Myb with CBP KIX exceeds the predicted rates of interaction for a fully pre-folded c-Myb[47,50], indicating that a fast initial encounter with the partially folded c-Myb that undergoes a coupled folding and binding mechanism is faster than conformational selection. Furthermore, the relative helical content prior to interaction significantly alters the thermodynamic prolife of interactions of TADs with the KIX domain. For example, the fully unstructured KID domain interacts with KIX at low affinity in the unphosphorylated state due to the large entropic cost due to folding, but is capable of overcoming the entropic barrier when phosphorylated (pKID) due to the large heats evolved

from the electrostatic interactions. Conversely, the partially folded c-Myb displays favorable entropy changes upon binding. It has been proposed that these differing entropic profiles may be the cause of the constitutive vs inducible interaction of c-Myb and the pKID of CREB, respectively, with KIX[54].

The dynamic nature of the KIX domain has led to difficulties obtaining a crystal structure. Indeed, the only reported crystal structure of the KIX domain was obtained through the covalent tethering of a small molecule ligand near the MLL site.[55] However, the small well-folded structure of KIX lends itself well to NMR, and solution structures of the KIX domain in complex with a number of its binding partners have been reported.[33,44,46,48,56-59] A large number of TADs on a host of transcription factors have been shown to interact with the KIX domain with a high degree of heterogeneity (**Table 4.3**). The commonality between all the KIX interacting TADs is the presence of small amphipathic helices containing a characteristic Φ-X-X-Φ-Φ, sequence where Φ is any bulky hydrophobic residue. In the bound state, it is these hydrophobic residues of a TAD that make contacts with the binding grooves on either the MLL or c-Myb binding sites.[50,60]

TAZ1 Structure And Function

The putative zinc finger motifs TAZ1 (residues 340-439) and TAZ2 (residues 1764-1855) are also TAD binding domains. Both TAZ domains are comprised of four amphipathic helices

Table 4.3: KIX interacting proteins and location of interaction

Protein	Domain	c-Myb	MLL	Reference
CREB	pKID	X		Goodman 2000, Goto 2002, Bruschweiler 2013
c-Myb	TAD	X		Zor J. 2004, Goto 2002
p53	AD1	X	X	Lee biochem 2009
p53	AD2	X	X	Lee biochem 2009
MLL	TAD		X	De Guzmann 2006, Bruschweiler 2013
FOXO3a	CR2C	X		Wang PNAS 2012
FOXO3	CR3		X	Wang PNAS 2012
TAX	AD		X	Ramirez J 2007
c-Jun	AD		X	Campbell 2002
BRCA1	BRCT	X		Lee 2011
SREBP	AD	X		Yang 2006
HIV TAT	AD		X	Vendel 2004
HIV-1	TAT		X	Vendel 2004

are organized around 3 zinc clusters bound by repeating His-Cys-Cys-Cys motifs (**Fig. 4.3**). While structurally similar, the two domains differ significantly in amino acid composition at their three TAD-binding grooves. Highly selective in their interactions, the TAZ1 domain usually binds long intrinsically disordered regions with multiple amphipathic regions that can form helices and TAZ2 domain prefers short amphipathic helices[61-63]. While over 40 different transcription factors interact with the two TAZ domains, only a small number of them (<5) have overlapping specificity for both domains[9,23,44,61,62,64-69]. The free and bound structures of TAZ1 demonstrate that the domain does not rearrange significantly upon ligand binding.[44] Conversely, a significant number of the TADs known to interact with TAZ1 also undergo coupled folding and binding mechanisms.[61,67]

Multivalent And Coopoerative Interactions Of TAD To CBP/p300 Domains

The broad role that CBP/p300 have in transcriptional activation, suggests that competition for CBP/p300 binding by transcription factors may be a mechanism for transcriptional regulation.[4,70] Therefore, it could be advantageous for transcription factors to utilize cooperativity by interacting with multiple domains of CBP/p300 and/or multiple discrete binding sites within a single domain of the co-activators. As we showed earlier[43], the BMAL1 TAD interacts with CBP KIX through two distinct linear sequence motifs, the predicted α-helical region and the extreme C-terminal TAD switch and truncation of the TAD switch resulted in a decreased affinity for the KIX domain. These data suggest that it is possible that the two interaction motifs on the BMAL1 TAD interact with the MLL and c-Myb sites on KIX respectively.

Some transcription factors utilize multivalent interactions with CBP/p300 to achieve cooperative regulation. It is thought that the tumor suppressor protein p53 binds DNA as a tetramer and uses two motifs in its TAD (AD1 and AD2) to interact with TAZ1, TAZ2, KIX and NCBD to coordinate four molecules of CBP/p300 (**Fig. 4.4a**).[23,24] A number of CCG promoter regions possess the CLOCK:BMAL1 binding E-box elements in tandem (E1-E2, or EE-elements) [71-73]. These dual sites are enriched in core clock genes and have been correlated with a more robust CLOCK:BMAL1 binding.[71,72] While previous studies have focused on the KIX-containing region of CBP/p300 as the primary interaction site with BMAL1[28,43], it is possible that additional domains of the co-activator interact with BMAL1 to produce multivalent interactions similar to those with p53. It is likely that cooperativity of this nature would increase the robustness of the

transcription based feedback loop that drives circadian oscillatory behavior. Interactions of CBP TAZ1 with the BMAL1 TAD that are reported in chapter 2 of this dissertation lend credence to the idea that DNA-bound tandem CLOCK:BMAL1 heterodimers could bind a single molecule of CBP cooperatively or recruit multiple coactivators through interactions with the KIX and TAZ1 domains. A model of this hypothesis was put forth by Franks[66] and is shown in **Fig. 4.4b**.

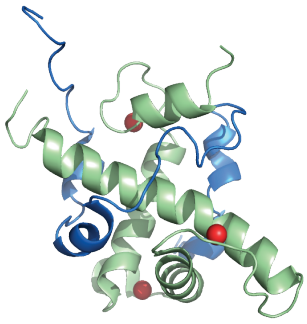

TAZ1:STAT2
PDB: 2ka4

Figure 4.3: Structure of TAZ1:STAT2. PDB 2ka4. TAZ1 in green, STAT2 in blue, coordinated zinc in red.

Using NMR spectroscopy, we mapped the interactions of the BMAL1 TAD switch to the MLL binding site on the KIX domain and the predicted α-helix onto the c-Myb binding site. The *cis* and *trans*-locked BMAL1 TAD had similar binding affinities to the TAD, but displayed divergent thermodynamic profiles for their interaction. Introduction of well characterized point mutations on the c-Myb binding face[19] significantly decreased affinity fo the BMAL1 TAD, as demonstrated by isothermal titration calorimetry (ITC) and NMR, confirming its central role in binding the KIX domain. Our studies have paved the way for future structural and dynamic based studies on the BMAL1 TAD and its interactions with the CBP/p300 KIX and TAZ1 domains.

RESULTS AND DISCUSSION

Dynamic Interactions Of CBP KIX Bound To BMAL1 TAD

Exhibit Multiple Chemical Exchange Regimes

Two distinct motifs of the BMAL1 TAD interact with the KIX domain of CBP, the Φ-X-X-Φ-Φ motif in the alpha helical region (603-IMSLL-607) and the extreme C-terminus.[43] Previous NMR studies in our lab showed that the alpha helical region is the primary interaction site and extreme C-terminus aids in the interaction by increasing the affinity of the TAD to the KIX domain. Based on conserved sequence motifs in these two regions, we hypothesize that these two regions of the BMAL1 TAD interact respectively with the MLL and c-Myb binding sites on the KIX domain. We are interested in mapping these sites to further explore how TAD binding,

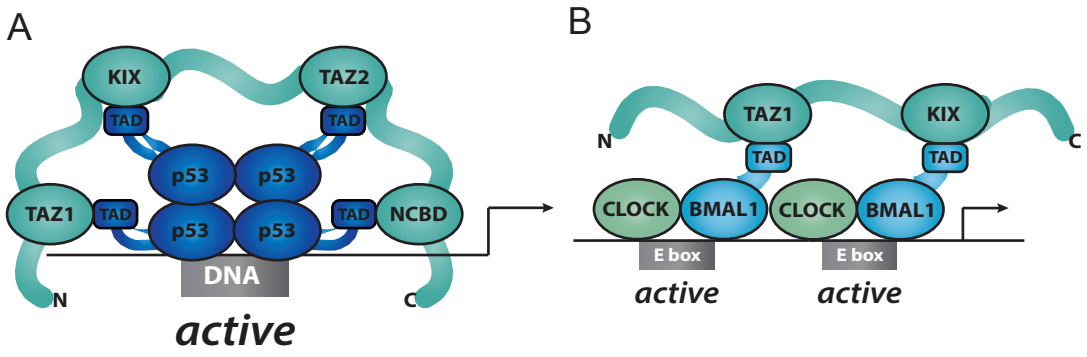

Figure 4.4: Multivariate interactions of transcription factors with CBP KIX. (A) A model of tetrameric p53 binding to four different domains on a signal molecule of CBP. (B) A hypothesized model of tandem CLOCK:BMAL1 heterodimers interacting with the KIX and TAZ1 domains on a single molecule of CBP/p300. Figures reprinted with permission from Kyle Franks 69.

and therefore regulation of CLOCK:BMAL1, might be influenced by the allosteric connection between these two sites.

In order to determine the binding locations of the BMAL1 TAD on the KIX domain, we utilized $^{15}N/^{1}H$ heteronuclear single quantum coherence (HSQC) NMR spectroscopy experiments, allowing us to titrate in binding partners and monitor sequence-specific changes in the local chemical environment that can report on binding. The HSQC spectrum of CBP KIX has previously been assigned.[57] We acquired a standard set of $^{15}N/^{1}H$ HSQC experiments of the ^{15}N labeled CBP KIX domain in the apo state and in the presence of increasing concentrations of BMAL1 TAD (residues 579-626) (**Fig. 4.5a,b**). The changes in resonance frequencies observed in these NMR titration experiments report on both changes in chemical environment upon binding and/or structural dynamics (as shown by perturbations in chemical shift or signal intensity). The readout of all dynamic exchange processes is a function of the difference in chemical environment between the two states, the gyromagnetic ratio of the nuclei (γ) and the strength of the magnetic field (B_0). Equations 4.1 and 4.2 illustrate the relationship that governs the precession frequency of NMR-active nuclei, where Δ is the change in precession frequency of nuclei in a specific chemical environment measured in Hertz and ω is the precession of nuclei in their independent chemical environments measured in radians/sec.

$$w = gB_0 \qquad (4.1)$$

$$\Delta v = \frac{1}{2}\pi \left(w_A - w_B \right) \qquad (4.2)$$

For exchange between two states, the resonance frequency is observed at a location corresponding to the population-weighted average of the two species present in the sample when Δ is greater than the rate of exchange (Δ > k_{ex}; fast exchange). When Δ is significantly less than the rate of exchange (Δ < $k_{ex;}$ slow exchange), then two independent resonances (one for each of the two conformational species) are observed.. In the instance that Δis similar to the rate of exchange, the signal broadens so substantially that the resonances corresponding to mixed species are no longer observed until they become one predominant state again.

Upon titration with BMAL1 TAD, the residues in CBP KIX domain displayed all three types of exchange dynamics (**Fig. 4.5a,b**), rendering it difficult to adequately map the chemical shift changes of CBP KIX when fully bound with BMAL1 TAD. Because the 1:1 complex of ^{15}N KIX:BMAL1 TAD (K_D ~2 μM)[43] displayed less peak broadening than the 1:2 titration point, we

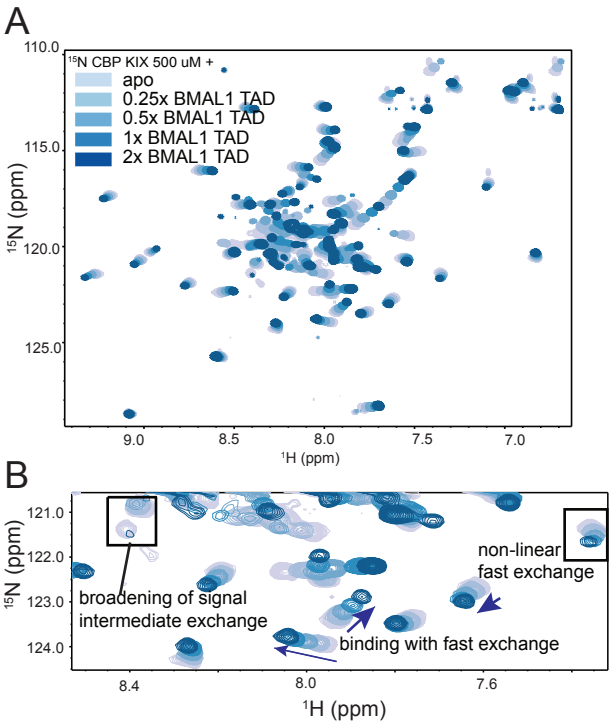

Figure 4.5: Interaction of BMAL1 TAD with ^{15}N CBP KIX occurs in multiple exchange regimes (A) ^{15}N/^{1}H HSQC spectra of CBP KIX with increasing amounts (light to dark) of BMAL1 TAD (residues 579-626) and (B) Region of the ^{15}N/^{1}H HSQC titration shown in A with highlighted examples of fast exchange dynamics, intermediate exchange and non-linear fast exchange.

decided to utilized the 1:1 point for further analyses despite the fact that the KIX domain is not fully bound. To differentiate the relative locations of interactions of the predicated α-helical or the C-terminal switch regions of the BMAL1 TAD, we performed $^{15}N/^{1}H$ HSQC titration experiments with short peptides corresponding to the different regions of the BMAL1 TAD.

Determination Of Appropriate Switch Peptide Construct Length

In order to determine the residues in the C-terminal switch region of the BMAL1 TAD that interacts with the CBP KIX, we synthesized a set of peptides ranging from 622-LPWPL-626 to 618-DFSDLPWPL-626 and used NMR to monitor the interactions between the KIX domain and the switch peptides. Chemical shift perturbations of ^{15}N CBP KIX as a function of switch peptide concentration showed that DLPWPL, SDLPWPL and FSDLPWPL all interacted with CBP KIX in the fast exchange regime (**Fig. 4.6a**). The overall magnitude of chemical shift perturbation and the number of residues affected increased with the longer switch peptides (**Fig. 4.6b**) up through FSDLPWPL. Addition of the longest switch peptide, DFSDLPWPL elicited chemical shift perturbations that were essentially identical to the shorter FSDLPWPL peptide (**Fig. 4.6c**), indicating that the last 8 residues of the BMAL1 TAD are sufficient to interact with the CBP KIX domain.

Mapping BMAL1 TAD Binding Onto CBP KIX

To map how the TAD helix and extreme C-terminus interact with the KIX domain, chemical shift mapping was performed by titrating a truncated Δswitch BMAL1 TAD into ^{15}N CBP KIX (**Fig. 4.7a,b**). The location of chemical shift perturbations were compared to those generated by titrations with the isolated Switch peptide, FSDLPWPL (**Fig. 4.6b** and **Fig. 4.7a,b**). Mapping of the Δδ values greater than 0.05 p.p.m. for both the ΔSwitch BMAL1 TAD and the switch peptide show that binding of both BMAL1 TAD motifs perturb portions of the allosteric network, the switch peptide preferentially perturbs residues near the MLL binding site, while the Δswitch BMAL1 TAD perturbs residues near the c-Myb binding site (**Fig. 4.8a**). Additionally, the binding of Δswitch BMAL1 TAD causes chemical shift perturbations at residues near the “top” of the helical bundle on G1, N-terminal residues of helices α1 and α3 and C-terminal residues of the α2 helix. Intriguingly, some of these residues at the top of the helical bundle are not conserved between CBP and p300 (**Fig. 4.8b,c**), suggesting that these residues could be key to determining the functional differences between CBP/p300 in circadian cycling.

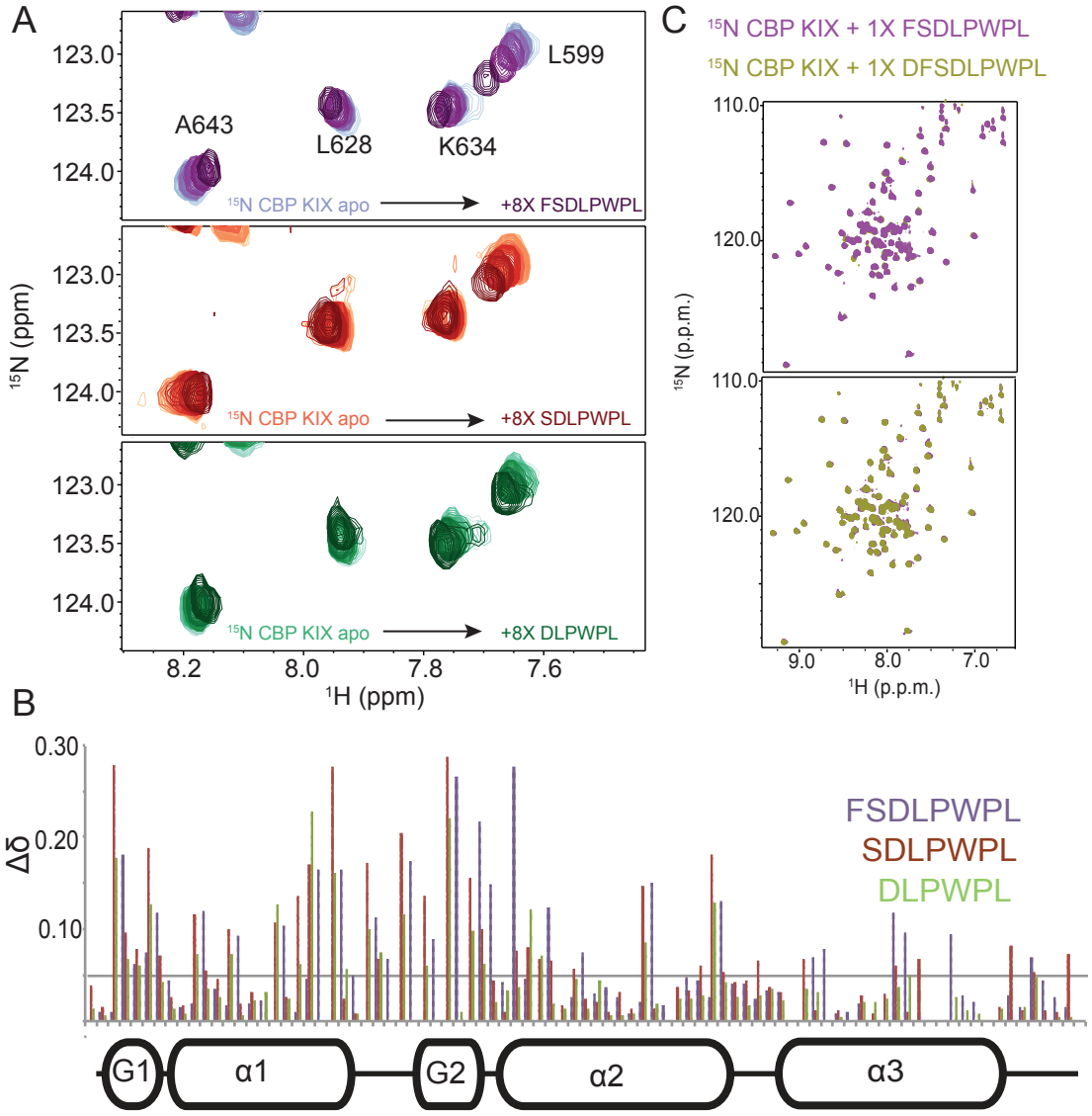

Figure 4.6: Chemical shift perturbations of the KIX domain upon titration of BMAL1 switch peptides. (A) Regions of the overlaid $^{15}N/^{1}H$ HSQC spectra of CBP KIX in the apo state and with increasing amounts of BMAL1 TAD switch peptide FSDLPWPL (top panel), SDLPWPL (middle panel), and DLPWPL (bottom panel). Darker colors indicate increasing concentrations of switch peptides. (B) Plot of chemical shift perturbations (Δδ) of each CBP KIX residue as a function of switch length. Chemical shift perturbations (Δδ in parts per million, p.p.m.) were calculated with 4x stoichiometric excess of switch peptide over CBP KIX. (C) Overlay of $^{15}N/^{1}H$ HSQC spectra of CBP KIX with equimolar FSDLPWPL (purple) and DFSDLPWPL (olive).

Mutations On The C-MYB Binding Face Of CBP Decrease Interaction With BMAL1 TAD

Disruption of the Φ-X-X-Φ-Φ motif in the α-helix with the L606A/L607A point mutations significantly weakens interactions between the TAD and CBP KIX as measured by ITC[43], while deletion of the switch decreases affinity of CBP KIX to the BMAL1 TAD by ~2-fold. By fitting the

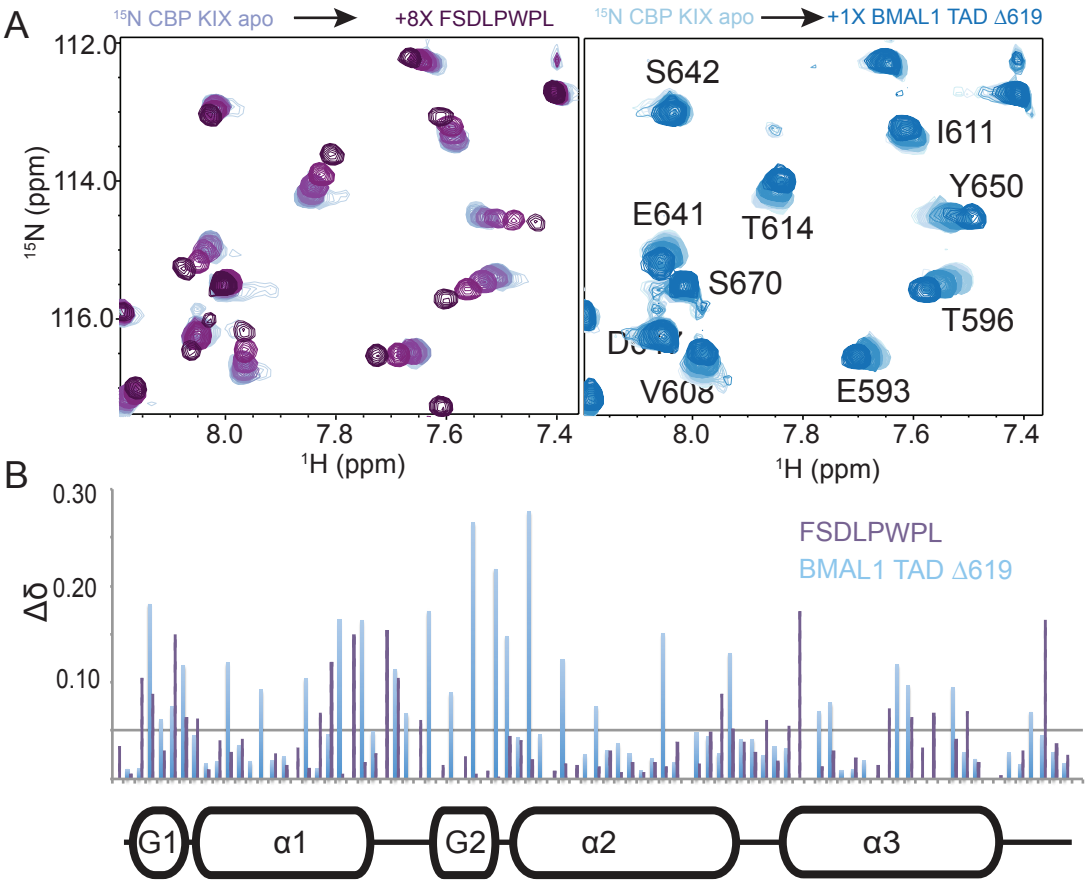

Figure 4.7: Comparison of interactions of CBP KIX with BMAL1 TAD Δswitch and BMAL1 switch peptide. (A) Region of $^{15}N/^{1}H$ HSQC spectrum of CBP KIX with increasing amounts of FSDLPWPL (purple, left panel) and BMAL1 TAD TAD Δswitch (blue, right panel). (B) Plot of chemical shift perturbations (Δδ) of each CBP KIX residue, with 4x of FSDLPWPL (purple) or BMAL1 TAD Δswitch (blue). ch peptides. (B) Plot of chemical shift perturbations (Δδ) of each CBP KIX residue as a function of switch length. Chemical shift perturbations (Δδ in parts per million, p.p.m.) were calculated with 4x stoichiometric excess of switch peptide over CBP KIX. (C) Overlay of $^{15}N/^{1}H$ HSQC spectra of CBP KIX with equimolar FSDLPWPL (purple) and DFSDLPWPL (olive).

titrations of the switch peptide into ^{15}N CBP KIX, we estimated a K_D > 300 μM. Taken together with the studies above, the interaction between the predicted α-helical region of the BMAL1 TAD and the c-Myb site on KIX is the primary driving force of binding, while interactions between the MLL site and the switch are secondary.

To test this prediction, we made three point mutations on the face of the CBP/p300 c-Myb binding site. Although the Y650A, A654Q and Y658A triple mutant (KIX^3) was shown to disrupt haematopoiesis *in vivo*[19], no one has published a biochemical characterization of the mutant

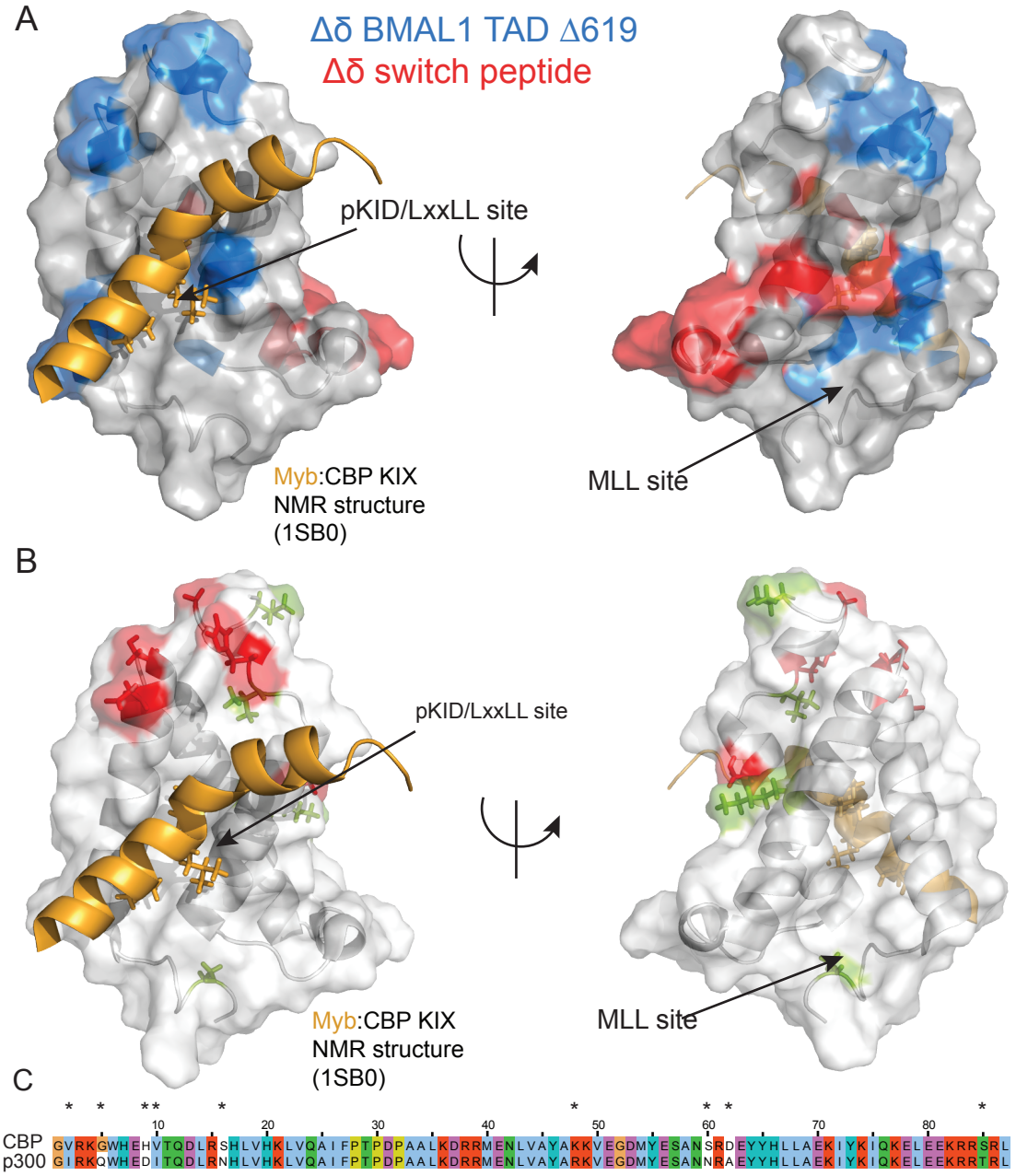

Figure 4.8: Mapping interactions of BMAL1 TAD motifs onto CBP KIX:(A) PDB structure (1SB0) of c-Myb (orange) and CBP KIX (grey) with chemical shift perturbations of ≥ 0.05 p.p.m. with the addition of 4X BMAL1 TAD Δswitch indicated with blue and from the addition of 4X FSDLPWPL in red. (B) Lack of conservation between CBP KIX and p300 KIX is indicated in red (non-conservative residue substitutions G/Q H/D S/N and D/A) and blue (conservative residue substitutions V/I K/R and S/T). (C) Alignment of CBP KIX and p300 KIX amino acid sequence. * indicates differences in sequence.

KIX domain. We found that the KIX^3 mutant (**Fig. 4.9a**) appeared to retain its helical structure, as measured by circular dichroism spectroscopy (**Fig. 4.9b**). Chemical shift perturbations of the BMAL1 TAD upon addition of equimolar CBP KIX^3 occurred at the same residues as with wild type CBP KIX, however the overall magnitude of chemical shifts were decreased nearly 4-fold to suggest significantly weaker affinity of the two proteins (**Fig. 4.9c**). In line with this, no heats were evolved upon isothermal titration of BMAL1 TAD into CBP KIX^3, when run under similar ITC conditions as the wild-type protein (**Fig. 4.9d**). These data indicating that the Y650, A654 and Y658 were responsible for the heat evolved from the wild type interaction or that the interaction between the two peptides was too weak to be detected under these ITC conditions. We fit the NMR titration data with a one site-binding model for selected peaks that displayed fast exchange. Residue 597 displayed near saturation of binding and a K_D of 41 μM was estimated off that single point (data not shown). The other peaks did not display saturation and were therefore not valid reporters of binding affinity.

A number of small molecule regulators of the KIX domain have been developed. Both the c-Myb and MLL binding sites have been targeted; a series of isoxazolidne compounds have been found to be competitive inhibitors of MLL and cJun at the MLL binding site[74] and derivatives of napthol competitively inhibit interactions with ligands at the c-Myb binding site[75-78] Notably, 2-Napthol AS-E phosphate (KG-501) which was identified to inhibit KIX:pKID interactions with an IC50≈90 μM is soluble in aqueous buffer systems and is commercially available.[76] Using NMR, we determined that 2-Napthol AS-E phosphate can decrease the affinity of the CBP KIX to the BMAL1 TAD, but does not disrupt binding altogether (**Fig. 4.9e,f**). Analysis of the ^{1}H/^{15}N HSQC titrations of CBP KIX with 500 μM Napthol AS-E phosphate into ^{15}N BMAL1 TAD show that the chemical shift perturbations follow the same path as titrations of CBP KIX without Napthol AS-E phosphate, but are significantly attenuated. These data indicate that the small molecule competitively inhibits BMAL1 TAD binding to CBP KIX.

Binding Of Mutant Switch Peptides To CBP KIX

In Chapter 2, we used fluorescence polarization to show that affinities of the *cis*- and *trans*-locked isomers of the BMAL1 TAD to CBP KIX are similar. However, CBP KIX is a small bundle of 3-helices[59] and therefore gives only a modest change in the detected rotation of the complex (as measured by milliPolarization value). To determine if the modest, yet reproducible

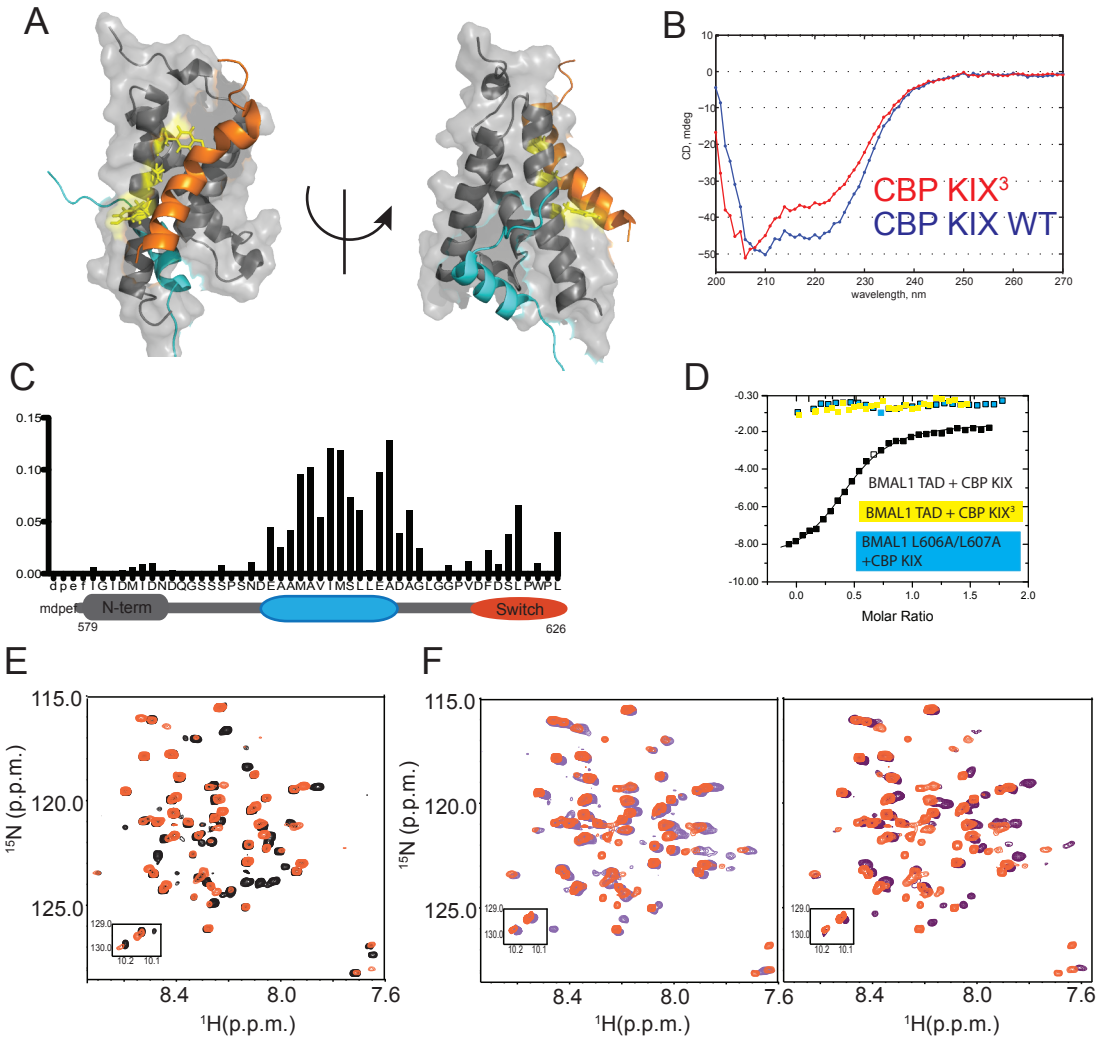

Figure 4.9: Mutation on CBP KIX c-Myb binding face abolishes interactions with BMAL1 TAD (A) PDB structure (2AGH) of c-Myb (orange), CBP KIX (grey) and MLL (cyan) showing the Y650A, A654Q and Y658A mutation sites on the c-Myb binding face in yellow 19. (B) Circular dichroism spectrum of CBP KIX wild type and CBP KIX3 mutant showing that both constructs are helical. (C) Δδ plot showing the chemical shift perturbations of ^{15}N BMAL1 TAD with 1X CBP KIX3 mutant. (D) ITC isotherms of WT BMAL1 TAD with WT CBP KIX (black) or CBP KIX3 (yellow) and L606A/L607A BMAL1 TAD with WT CBP KIX (blue). (E) Overlay of ^{1}H/^{15}N HSQCs of BMAL1 TAD with 500 μM Napthol AS-E phosphate (black) and with 500 μM Napthol AS-E phosphate and 1X CBP KIX (salmon). (F) Overlay of ^{1}H/^{15}N HSQCs of BMAL1 TAD with 1X CBP KIX and 500 μM Napthol AS-E phosphate (salmon) and BMAL1 TAD with 0.5X CBP KIX (light purple) (left panel) and BMAL1 TAD with 1X CBP KIX (dark purple) (right panel).

difference between the *cis*-locked construct and the others was merely an artifact of the experiment; we turned to ITC to validate our results. Intriguingly, the *cis* and *trans*-locked isomers, while possessing equivalent affinities for KIX (**Fig. 4.10a** and **Table 4.4**), deviated significantly in thermodynamic parameters (**Fig. 4.10b**). Enthalpically favorable interactions of KIX with the

Table 4.4: Affinities of CBP KIX for BMAL1 TAD switch isomers.

BMAL1 TAD*	KD (μM)	N
Wild Type	2.78 ±0.18	0.7
P625A	2.64 ±0.49	0.6
$P625dm_P$	2.59 ±0.83	0.7
ΔSwitch	-------	----

*values determined by ITC with n=3 or 4 repeats

trans-locked isomer appear to drive binding, while an increase in entropy is more defined with the *cis*-locked isomer. As would be predicted by its relative isomer equilibrium populations, the WT TAD:KIX interaction profile appears to be more similar to the *trans*-locked than the *cis*-locked TAD.

It is possible that the observed decrease in entropic favorability with the *trans*-locked isomer is a function of the structural characteristics of the two isomers. Parker et. al. [54] suggested that entropic cost of pKID binding to KIX is due to the coupled-folding and binding mechanism of pKID. If this concept is applied to our system, the absolute geometry about the W624-P625 bond may not be a deterministic factor in KIX binding. However, the most thermodynamically favorable secondary structure that the *cis* isomer imparts on the BMAL1 TAD switch region may be more similar to the KIX-bound TAD switch structure than that imparted by the *trans* isomer. The secondary and tertiary structure of a protein is regulated by the orientation of an imide bond [79,80], and in other systems, proper folding of proteins can depend upon the formation of a *cis* isomer.[81] While Ramachandran plots for *cis* and *trans* proline residues show the same regions of available Ψ and ψ and φ angles, the relative distribution of the angles are different (~50:50 α:β regions for $trans_{pro}$, 24:76 α:β cis_{pro}) [82], this could lead to differences in the local structure that could alter the thermodynamics of interaction.

We probed the dynamics and overall chemical environment of BMAL1 TAD bound to CBP KIX for the WT, *trans*-locked and *cis*-locked isomers. Intriguingly, we found that the *cis* and *trans* isomers individually elicited a lesser overall degree of chemical shift perturbation when the locked switch peptides were titrated into ^{15}N CBP KIX (**Fig. 4.10c,d**). This is in direct contrast to what is expected based upon the FP data. Assuming that the P625A and P625dmP mutants are chemically identical to the *trans* and *cis* isomers of the WT TAD respectively, then the

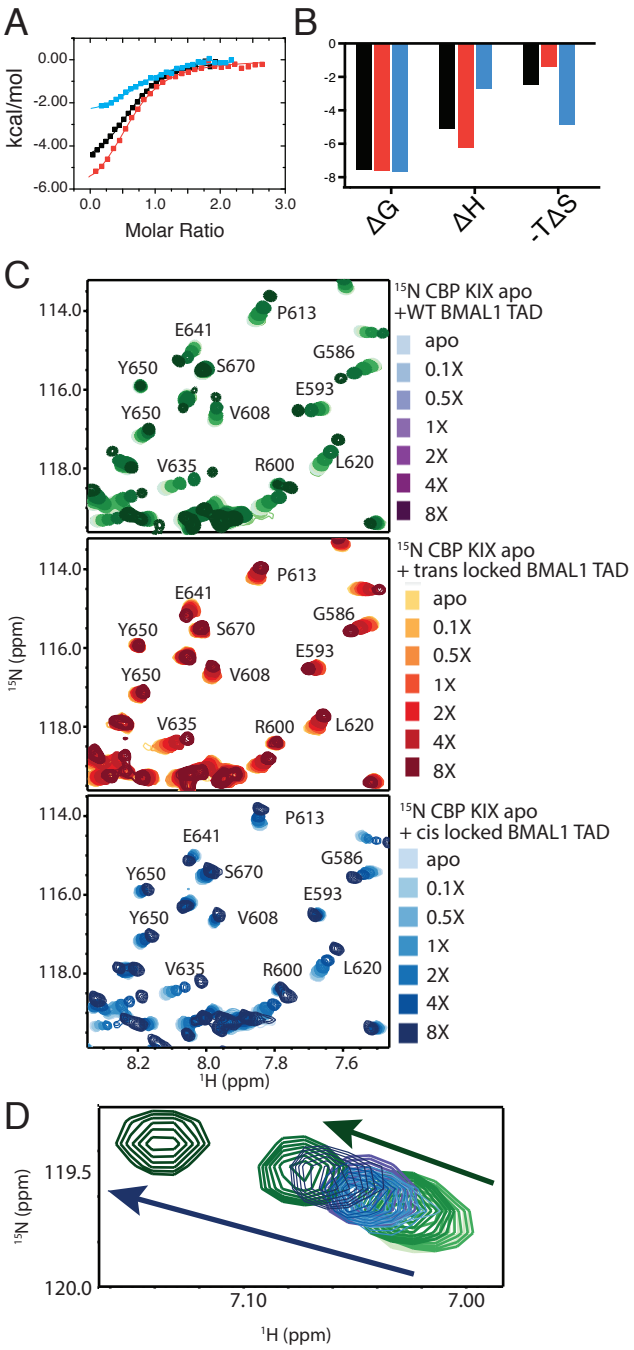

Figure 4.10: Differential interactions of *cis* and *trans* isomers of BMAL1 TAD with CBP KIX. (A) Binding isotherms of BMAL1 short TAD (residues 594-626) wild type (black) P625A (red) and P625dmP (blue) titrated into CBP KIX. (B) Plot of thermodynamic parameters determined from ITC for BMAL1 TAD interactions with CBP KIX (same colors as in A). (C) Regions of $^{1}H/^{15}N$ HSQC spectra from ^{15}N CBP KIX with increasing amounts (light to dark) of wild type (green), P625A (red) and P625dmP (blue) switch peptides. (D) Region of $^{1}H/^{15}N$ HSQC of ^{15}N CBP KIX displaying the chemical shift perturbations caused by equal amounts of wild type switch (green) and *cis*-locked switch (blue to purple)

differences in chemical shift between the apo KIX proteins and the WT- and locked- TAD bound KIX should be identical. The FP data show that the binding affinity for the WT, *cis* locked and *trans* locked peptides are nearly identical. Together these data would suggest the WT, P625A and P625dmp peptides should elicit identical chemical shift perturbations when titrated into ^{15}N CBP KIX. It is possible that deviations from our expected results could be a function of the

structural differences between the native proline residue and its replacement with either alanine or 5,5-dimethylproline; because NMR spectroscopy is a highly sensitive readout of local chemical environment, substitutions at residue 625 could have a significant effect on the chemical shift of interacting residues on the KIX domain. Conversely, it is possible that the process of isomerization actively changes the overall (population weighted average) chemical environment of the nearby residues. However, this hypothesis conflicts with kinetic data presented in chapter 2, showing that the lifetime of the KIX:TAD complex is much shorter than the timescale of isomerization. Only a small fraction of the TAD would undergo isomerization while actively bound to KIX during this experiment, causing these molecules to display a different chemical shift.

W624 *trans*-locked Mutants Can Be Inhibited By CRY1 In Fibroblasts

In chapter 2, we introduced W624 mutants and reported the profound difference in period that the W624A BMAL1 mutant elicited in cycling fibroblasts. In order to further assess the importance of W624 in circadian oscillations, we measured the affinity of the W624 for CBP KIX and assayed the ability of CRY1 to repress W624A BMAL1 mediated transcriptional activation. ITC analysis showed that the BMAL1 W624A, W624Y and W624F mutations did not disrupt interactions with CBP KIX to any appreciable extent (**Fig. 4.11a** and **Table 4.5**). Our earlier NMR mapping[43] showed only modest chemical shift perturbations of W624 upon titration with p300 KIX. Taken together, these data suggest that W624 is not necessary for CBP-mediated transcriptional activation. Our earlier NMR mapping study did demonstrate that W624 was involved the interaction with CRY CC. Due to the low heats evolved in ITC with CRY CC and the high cost involved of purchasing 5,6-TAMRA labeled peptides and production of CRY1 in insect cell systems, we decided not to perform ITC or FP on the W624A mutants and CRY1, and instead turned to a cell-based system to analyze CRY1 mediated transcriptional repression on the W624 mutants.

Table 4.5: Affinities of CBP KIX to the W624 mutants.

BMAL1 TAD*	Kd (μM)	N
N'Y	3.18 ±0.35	0.785
W624A	3.50 ± 0.23	0.408
W624Y	3.32 ±0.29	0.726
W624F	3.38 ± 0.44	0.491

*values determined by ITC with n=1

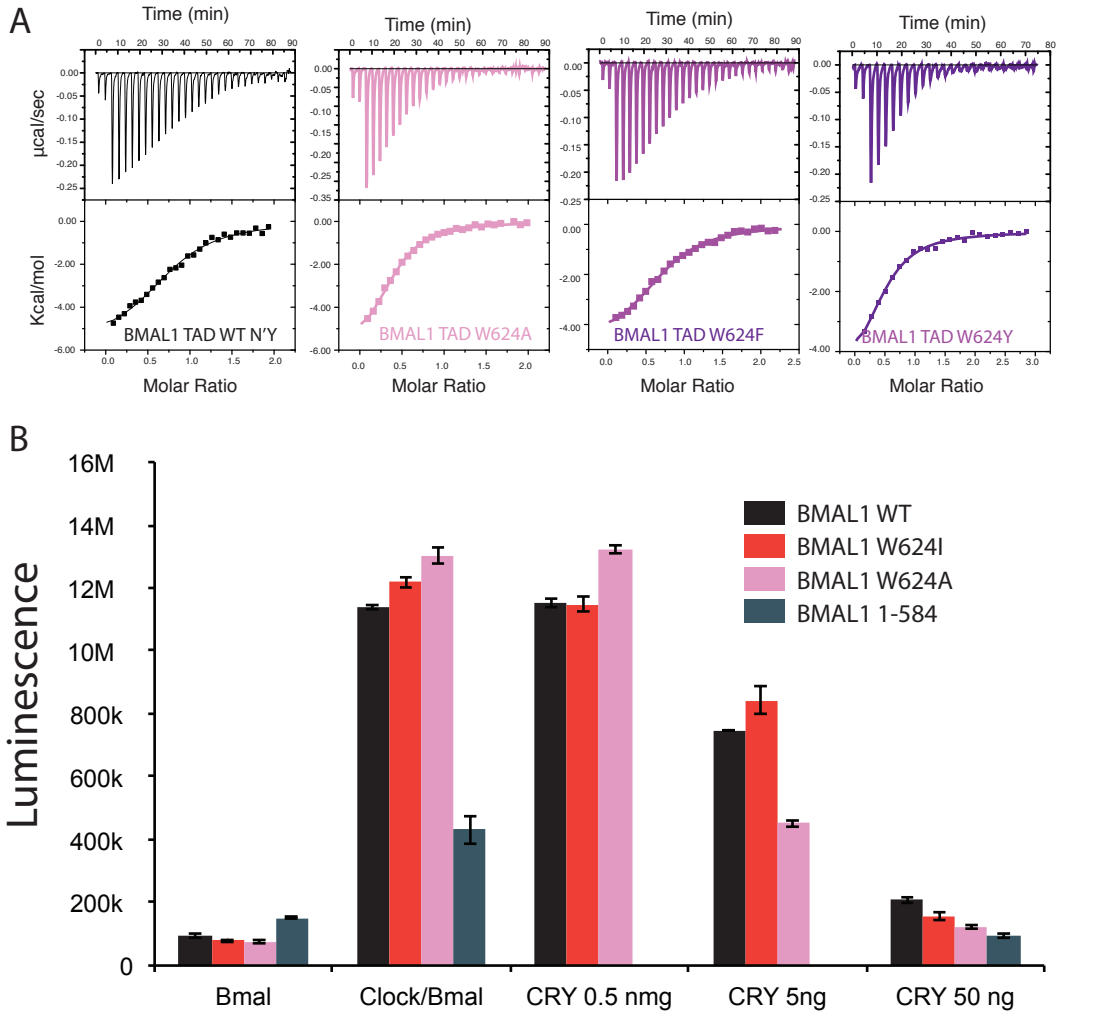

Figure 4.11: Interaction of BMAL1 TAD Trp mutatnts with CBP KIX and CRY1. (A) Isotherms of CBP KIX titrated with short N'Y BMAL1 TAD (594-626) wild type (black, left panel), W624A (pink, second to the left), W624F (plum, third to the left) and W624Y (purple, right panel). (B) *Per1-luc* reporter gene signal from HEK-293T cells as a function of transient transfected BMAL1 mutants (in colors indicated) with varying amounts transfected repressor CRY1

In order to assay the ability of CRY1 to repress BMAL1 harboring the W624A mutation, we used a steady-state luciferase reporter gene assay that contained a *Per1* promoter-driven luciferase reporter (*Per1*^{Luc}) in HEK293T cells.[83] Alongside the W624A mutant, we assayed two other *trans*-locked mutants, W624I and P625A, WT BMAL1 and a ΔTAD BMAL1 (1-584). The Trp and Pro mutants were able to activate transcription at E-box elements to comparable levels as wild type BMAL1 (**Fig. 4.11b**). Upon addition of increasing amounts of CRY1, the activating potential of W624 mutants decreased similarly to wild-type BMAL1. While these data suggest

that the overall magnitude of transcriptional activation and repression is unchanged in the Trp and Pro mutants, small perturbations in K_{on} and K_{off} rates or the lifetime of the complexes could lead to changes in circadian cycling metrics. Slight changes in the dynamics of interactions may not affect the formation of functional complexes, yet they could have profound impacts on the handoff between active and repressive complexes leading to changes in period and amplitude. Previous studies[43] by our lab have resulted in discordant data between steady state and cycling for BMAL1 versus BMAL2; the steady state assay shows that BMAL2 more capable of transcriptional activation than BMAL1, yet is unable to support oscillatory behaviors in cell culture.

In addition to locking the switch into *trans* the Trp mutations elicit a significant change in local chemical environment within the switch; any changes in phenotype or affinity are likely a result of both the alternation of the peptide's chemical properties (lack of a π system) and the locking of the imide bond into its *trans* isomer. Taken together, these data indicate that while W624 mutants of BMAL1 can physically interact with and be inhibited by CRY1, there is a disturbance in the dynamics of the transition between the various active and repressive complexes. These data strengthen the hypothesis that timely handoff between active and repressive states is key to circadian cycling.

Multivalent Interactions With CBP As A Potential Cooperative Mechanism

The majority of CCG promoter regions possess the CLOCK:BMAL1 binding E-box elements in tandem (E1-E2, or EE-elements) [71-73]. Cooperative binding of CLOCK:BMAL1 can occur at these sites to create a tandem heterodimer state (CB2) that is more transcriptionally robust than a singly bound heterodimer (CB1). In other systems, multimeric transcription factors can participate in multivalent interactions with two or more of the four TAD-binding domains of a single molecule of CBP/p300 (**Fig. 4.4a**).[23,24] While previous studies have focused on the KIX containing CH1 region of CBP/p300 as the primary interaction site with BMAL1[28,43], it is possible that additional domains of the co-activator interact with BMAL1 to produce similar multivalent interactions (**Fig. 4.4b**). We decided to focus on the CBP TAZ1 (340-439) domain due to its relative proximity to KIX, and the previous reports which suggest that regions C-terminal to KIX domain do not interact with BMAL1 by yeast two-hybrid.[28]

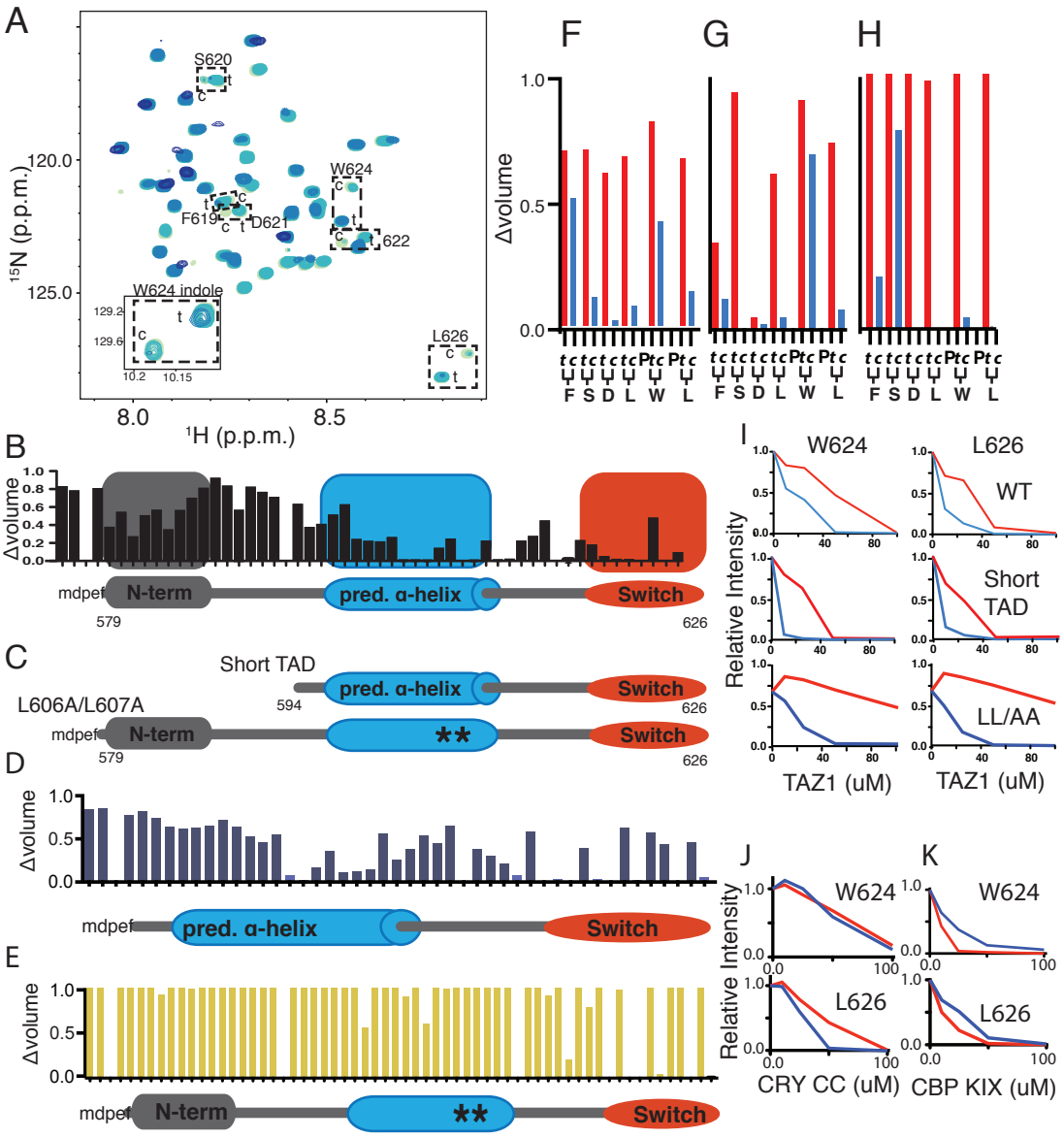

Figure 4.12: Interactions of BMAL1 TAD with TAZ1 domain of CBP. (A) ^{15}N HSQC titration CBP TAZ1 into ^{15}N-labeled BMAL1 TAD (579-626) lightest blue apo-darkest blue 1:1 TAD:TAZ1 (B) Relative volume of apo ^{15}N BMAL1 TAD to ^{15}N BMAL1 Wild Type with 0.5X CBP TAZ1, decreases in intensity are areas in which the BMAL1 TAD changes chemical environment due to CBP TAZ1 interactions. (C) Domain schematics of BMAL1 TAD constructs used to probe the ability for the TAD switch to interact without the N-terminal or alpha helical regions. Region of the relative volume plot of (D) BMAL1 TAD with 0.25X TAZ1 (E) L606A/L607A BMAL1 TAD with 0.5X TAZ1. Region of the relative volume of apo ^{15}N BMAL1 TAD showing differences in volume change for the *trans*-locked isomer (red) and *cis*-locked isomer (blue) from (F)^{15}N BMAL1 TAD WT. (G) ^{15}N BMAL1 TAD short and (H) ^{15}N BMAL1 TAD LL/AA with 0.25X TAZ1. (I) relative intensity of W624A and L626 as a function of CBP TAZ1 concentration for wild type (top panel) short TAD (middle panels) and LL/AA (bottom panels) BMAL1 TAD. (J) Relative intensity of *trans* (red) and *cis* (blue) peaks as a function of CRY1 CC concentration (K) Relative intensity of *trans* (red) and *cis* (blue) peaks as a function of CBP KIX concentration.

In Chapter 2 we reported that the BMAL1 TAD binds to the TAZ1 domain with similar nanomolar affinities for the *cis*, *trans* and WT constructs of the TAD. To further probe the interactions between the BMAL1 TAD and CBP TAZ1, we turned to NMR spectroscopy. Upon addition of CBP TAZ1, ^{15}N BMAL1 TAD displayed chemical shift perturbations in the fast–intermediate exchange timescale for residues in the N-terminus, α-helical region and the TAD switch (**Fig. 4.12a,b**). The location of these shifts is similar to perturbations observed with CRY1 CC and CBP KIX (**Fig. 4.1a**) [43] with the addition of more significant peak loss in the N-terminus indicating an additional interaction motif with TAZ1 (grey panel in **Fig. 4.12b**). We hypothesize that the three motifs on the BMAL1 TAD interact with each of the three independent binding sites on the TAZ1 four-helix bundle.

In order to assess the ability of the switch region to interact with TAZ1, we utilized two TAD mutants, one that lacks the N-terminal motif and one that disrupts the consensus Φ-X-X-Φ-Φ motif in the α-helix with the L606A/L607A (LL/AA) mutations (**Fig. 4.12c**) that disrupt binding at the α-helical region.[43] The ^{15}N short TAD continued to display binding at both the α-helical region and the TAD switch (**Fig. 4.12d**), and the LL/AA mutant eliminated all chemical shifts except at the switch region (**Fig. 4.12e**). Together these data support the hypothesis posited in Xu et. al.[43] that the α-helical region is the primary binding site on the BMAL1 TAD and the switch (and N-terminal region, here) are secondary binding sites.

The *cis* and *trans* isomers display differing dynamics upon interactions with TAZ1 Further analysis of the TAZ1 ^{15}N-HSQC titrations with WT, short TAD and LL/AA constructs revealed a significant difference in changes in peak intensity of the *cis* and *trans* resonances in the TAD switch (**Fig. 4.12a,f**,g,h). While the overall magnitude of the chemical shift changes is equivalent for the two isomers, the two display differing chemical exchange regimes (**Fig. 4.12a,** dashed boxes). The *cis* peaks undergo rapid signal broadening (intermediate exchange) and are mostly broadened by the 0.25X titration point. The *trans* isomer is in fast to intermediate exchange and displays a readable signal out to 0.5X TAZ1. These results are recapitulated in the short TAD BMAL1 (**Fig. 4.12d,f**) and an even more striking discrepancy is visualized in the LL/AA mutant, where at 0.25X TAZ1, the *trans* peaks display nearly no chemical shift or intensity changes, while many of the *cis* peaks are completely broadened (**Fig. 4.12h**). Plots of the relative intensity as a function of TAZ1 concentration highlight this trend throughout the titration experiment

(**Fig. 4.12i**) and suggest that the *cis* and *trans* isomers have differential binding dynamics to TAZ1. This difference is even more striking when the relative peak intensities from the same titrations with CBP KIX and CRY CC show little to no difference (**Fig. 4.12j,k**). We performed ITC to determine the K_D of the BMAL1 TAD for TAZ1. However, no heats were evolved so we could not obtain a binding isotherm (**Fig. 4.13**). Additionally, we purified the TAZ2 domain and determined that it also interacts with the BMAL1 TAD, but with a 15-fold decrease in affinity compared to the TAZ1 domain (**Fig. 4.14**).

Temperature Variations May Allow For Dynamics To Be Captured

Further studies on the interactions of the BMAL1 TAD with CBP KIX will likely require structure elucidation by NMR spectroscopy. In order to obtain a fully bound complex that displays resonances for each non-proline residue, we performed temperature experiments to screen for conditions that might bring residues that displayed signal broadening back into fast exchange. First, we tested the thermal stability of CBP KIX, which maintained its structure up to 50 °C (**Fig. 4.15a**). An overlay of the $^{15}N/^{1}H$ HSQC spectrum at 25 °C before and after a 40 minute incubation at 50 °C displayed a small amount of degradation (**Fig. 4.15b**). A subsequent analysis of a mix of 2:1 BMAL1 TAD:^{15}N CBP KIX by $^{15}N/^{1}H$ HSQC at temperatures ranging from 25 °C to 50 °C showed that the complex was stable up to 45 °C with only slight precipitation (data not shown). At 30 °C, many of the KIX peaks that were broadened at 25 °C moved into fast exchange; however, at 35 °C, a decrease in signal intensity was observed as many other peaks

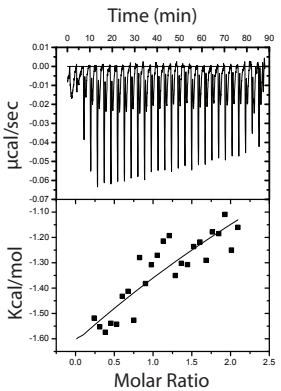

Figure 4.13: ITC analysis of BMAL1 TAD with CBP TAZ1 binding isotherm of BMAL1 titrated into CBP TAZ1.

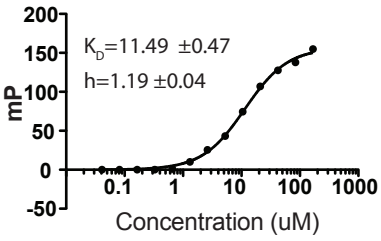

Figure 4.14

Figure 4.14: Interactions of BMAL1 TAD with CBP TAZ2 Fluorescence polarization assay of 5,6-TAMRA BMAL1 TAD WT with varying amounts of CBP TAZ1.

began to broaden (**Fig. 4.16a,b**). These data suggest that the optimum temperature with which to perform subsequent experiments is 30 °C.

Future Directions

Future studies on CBP:BMAL1 TAD interactions should focus on three areas: (1) NMR studies to investigate the dynamics of BMAL1 TAD interactions with both CBP KIX and TAZ1 (2) structural studies of CBP KIX in complex with BMAL1 TAD and (3) expanding the idea of tandem CLOCK:BMAL1 heterodimers using cooperativity to recruit CBP.

Determination of the chemical shifts of the fully TAZ bound BMAL1 TAD would lend insight into the cause of the divergent dynamics of the two isomers. If the timescale of exchange is in the microsecond – millisecond window, it is possible to determine the location of "invisible" resonances in a $^{15}N/^{1}H$ HSQC using CPMG relaxation dispersion experiments. These data would allow for a deeper analysis of the relative *cis* and *trans* chemical shift perturbations.

Dynamics also rule BMAL1 TAD: CBP KIX interactions. Chemical shift perturbations of residues at the top of the CBP helical bundle––one of the only regions that differs from p300 KIX and is not part of the central allosteric region––is intriguing and could lend insight into the differing roles of

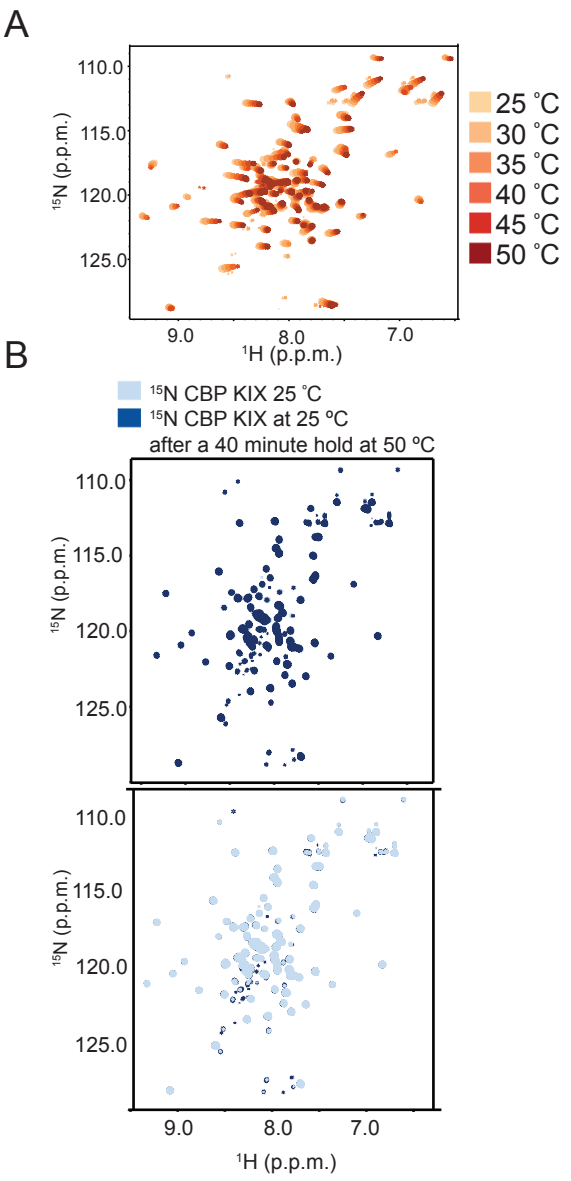

Figure 4.15: Temperature stability of CBP KIX (A) Temperature walk of apo CBP KIX from 25 °C to 50 °C, increasing temperature is denoted by darker color. (B) before (top) and after (bottom) $^{15}N/^{1}H$ HSQCs for a CBP KIX sample stored at 50 °C for 40 minutes.

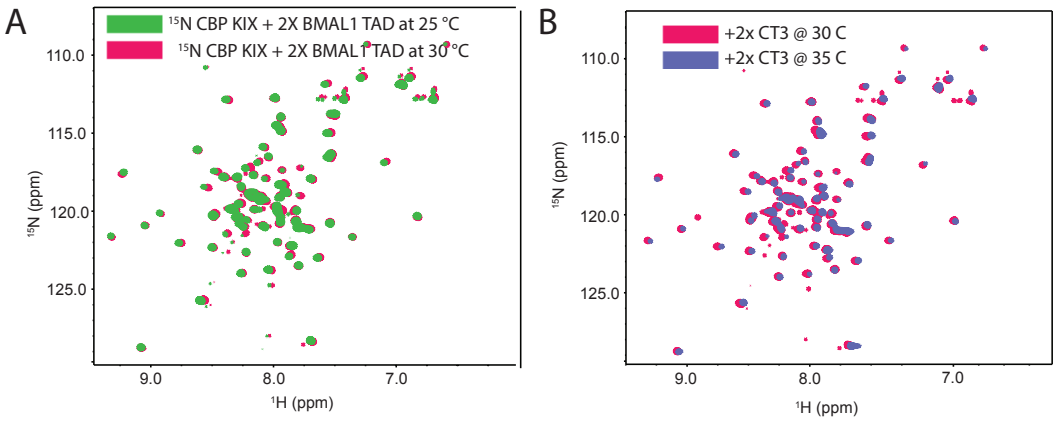

Figure 4.16: Modulation of chemical exchange regime for NMR studies on CBP KIX and BMAL1 TAD (A) Overlay of $^{15}N/^{1}H$ HSQC spectra of ^{15}N CBP KIX with 2X BMAL1 TAD taken at 25 °C (green) or 30 °C (pink). (B) Overlay of $^{15}N/^{1}H$ HSQC spectra of ^{15}N CBP KIX with 2X BMAL1 TAD taken at 35 °C (purple) or 30 °C (pink), showing signal broadening at 25 °C and again at 35 °C.

p300 and CBP in circadian rhythms.[25-27,42] Coupled folding and binding of the BMAL1 TAD could occur through conformational selection, where within a large ensemble of conformations a single lowly-populated state interacts with KIX or a folding-after binding mechanism could occur. Heteronuclear $^{15}N/^{1}H$ NOE experiments can measure fast (sub-nanoscale) motions, while other NMR methods and stopped flow/temperature jump experiments could be used to probe these types of questions. Furthermore, dissection of the thermodynamic driving forces behind the BMAL1 TAD interactions with the TAZ1 and KIX domains may lend some insight into the mechanism of interaction. It is likely that a folding after binding mechanism will have profound effect on the entropy of the system[54] and mutations that alter either the helical content of the BMAL1 TAD or the enthalpic attributes of the interaction could tune the circadian period.

NMR structures have been elucidated for the KIX domain with numerous ligands. To date, a structural analysis of BMAL1 has not been performed, and it would be enlightening to compare the apo and KIX bound BMAL1 TAD to determine if interaction of the KIX domain with the TAD increases helical content. $^{13}C/^{15}N$ NMR experiments should be performed on the complex with alternate labeling of the proteins. Furthermore, a more in-depth study of the KIX^{3} mutant interactions with the BMAL1 TAD is in order. The ITC data suggest a complete attenuation of binding under the conditions assayed with the wild-type KIX, while the NMR data show a 6-fold decrease in chemical shift perturbations. It is possible that the ITC data show no interaction

because the mutations disrupt the enthaplic driving forces of interaction, and it is possible that entropy may drive interactions between KIX[3] and BMAL1 TAD.

One final area of study would include both biophysical studies and cell-based assays. Further biochemical analysis of interactions of BMAL1 TAD with TAZ2 and NCBD may help lead insight into the mechanism of interactions. Cell based studies examining the stoichiometry of transcription factors and co-activators present on tandem E-box elements would test the multivalent interaction hypothesis. Likewise, mutational analysis on one or more of the CBP TAD-interacting domains and subsequence affinity studies and ChiP analysis would identify important regions *in vivo*. These experiments would be coupled with biophysical studies to verify the disruption of binding.

Circadian rhythms consist of many different steps of macromolecular interactions and dissociation. In order to understand the mechanism as a whole, individual steps must be fit together. Enhancing our understanding of the structure and dynamics that underlie the interactions of transcriptional co-activators with CLOCK:BMAL1 is simply one piece of the puzzle. The various conformational ensembles sampled by the BMAL1 TAD and the TAD interacting domains of CBP and p300 are central to the construction and deconstruction of transcriptionally active macromolecule complexes. The kinetics of these fast molecular motions set the timescale of the slower complex formation and dissociation, which in turn drive the circadian clock.

METHODS

Expression And Purification Of Recombinant Proteins

The mouse BMAL1 TAD (residues 579-626) was cloned from full-length mBMAL1 and placed into a pet22b vector backbone[84] (EMD Millpore) under the control of the T7 promoter; the short BMAL1 TAD (residues 594-626) was codon optimized (GeneWiz, South Plainfield, NJ) and cloned into the same vector. Both constructs possessed an N-terminal TEV cleavable His_6-GST tag and ampicillin resistance. The mammalian expression vector for mouse CBP was kindly provided by Andrew Liu (University of Memphis). TAZ1 (residues 340-439) and TAZ2 (residues 1764-1855) domains were amplified and cloned into a pet22b vector backbone devoid of an affinity tag. The plasmid encoding the mouse CBP KIX domain (residues 585-672) was a kind gift from the laboratory of P.E. Wright (The Scripps Research Institute). CBP KIX has native

histidine residues that allow for the purification of the protein using Nickel resin. Mutations were introduced using site directed mutagenesis [85] and confirmed with sequencing.

The Rosetta (DE3) expression stain of *E. coli* containing plasmids with either BMAL1 TAD or CBP KIX, were grown to an OD_{600} of ~0.6-0.9 in the presence of ampicillin (0.1 mg/mL) and chloramphenicol (0.035 mg/mL). Protein expression was induced with 0.5 mM IPTG and allowed to proceed for 16-18 hours at 18 °C in either Luria Broth Medium (for natural abundance proteins) or M9 minimal medium containing 1 g/L $^{15}NH_4Cl$ (for uniformly ^{15}N-labeled proteins).

Cells were collected by centrifugation and lysed in buffer containing 50 mM Tris pH 7.5, 300 mM NaCl and 20 mM imidazole. The soluble fraction of *E. coli* lysates were passed over Ni-NTA resin and the protein of interest eluted using 250 mM imidazole. Eluted protein was buffer exchanged into 20 mM imidazole using a stirred-cell pressure concentrator with 3 KDa MWCO filters from Amicon. Proteolysis was performed with His_6-tagged TEV protease overnight at 4 °C and cleaved protein was retained from the flow-through of a Ni-NTA column. Cleaved proteins were injected onto a Superdex 75 16/60 (GE Life Sciences) size-exclusion column, pre-equilibrated with NMR buffer (10 mM MES pH 6.5 and 50 mM NaCl).

Recombinant expression of TAZ1 and TAZ2 was performed as described above, with the following modifications: 50 μM $ZnSO_4$ was added to the Luria Broth Medium 10 minutes prior to the initiation of a 4 hour 37 °C induction step.

Cells were collected by centrifugation and lysed in a buffer containing 50 mM Tris pH 7.5, 300 mM NaCl, 20 mM DTT, 50 μM $ZnSO_4$. The insoluble fraction of *E. coli* lysates were suspended and washed 2X in the same buffer to remove impurities. The final insoluble pellet was resuspended in 10 mM Tris pH 7.5, 50 μM $ZnSO_4$, 20 mM NaCl, 20 mM DTT, and 6 M urea by sequential sonication and homogenization. Insoluble particulates were removed via centrifugation and the supernatant passed over a 1 mL HiTrap SP XL sepharose cation exchange column. Bound TAZ1 or TAZ2 was washed with 50 mM Tris pH 7.5, 50 μM $ZnSO_4$, 20 mM NaCl and 20 mM DTT and eluted in the same buffer with 50 mM Tris pH 7.5, 50 μM $ZnSO_4$, 1 M NaCl and 20 mM DTT. Eluted protein was quantified and 3 molar equivalent of $ZnSO_4$ titrated into the solution with concurrent pH monitoring. Precipitated DTT•Zn was removed via centrifugation

and the TAZ was further purified on a Superdex 75 16/60 (GE Life Sciences) size-exclusion column, pre-equilibrated with NMR buffer (10 mM MES pH 6.5 and 50 mM NaCl).

Peptide Synthesis And Purification

Switch peptides FSDLPWPL, FSDLPAPL, FSDLPWPL, SDLPWPL, DLPWPL, LPWPL, and PWPL were synthesized using solid phase peptide synthesis on 3-chlorotrityl resin with standard FMOC chemistry, one or two 1:4:4:4:6 molar ratio of resin:HBTU:HOAT:Fmoc-AA-OH:DiPEA coupling reactions were performed in DMF for each amino acid addition. The *cis*-locked switch peptide FSDLPWdmPL was synthesized using solid phase peptide synthesis using standard FMOC chemistry. Coupling of 5,5-dimethylproline (dmP) onto the Leu-Resin was performed using 1:2:2:4 molar ratio of Resin:HATU:Fmoc-DMP-OH:DiPEA, and coupling of the Trp onto the Resin-Leu-DMP was performed using 1:3.8:4:6 molar ratio of Rsin:COMU:Fmoc-Trp-Boc-OH:DiPEA. All other coupling reactions were performed using HBTU/HOAT as described above. All Fmoc-protected amino acids were purchased from Fluka, Nova Biochem, AAPPTec, or Sigma Aldrich. Fmoc-dmP was purchased from PolyPeptide Group (San Diego, California). Peptides were purified by reverse phase C18 HPLC, and their purity and identity were verified by MS/MS on a Waters HPLC-MS/MS system.

BMAL1 TAD P625dmP (NDEAAMAVIMSLLEADAGLGGPVDFSDLPW(dmP)L) and switch peptides FSDLPFPL, FSDLPYPL, FSDLPAPL and FSDLPWAL were purchased from Bio-Synthesis, Inc (Lewisville, Tx). The mouse CRY1 CC peptide (residues 471-503, sequence: MVNHAEASRLNIERMKQIYQQL SRYRGLGLLASV) was synthesized as described previously.[43]

NMR Spectroscopy

NMR experiments were conducted on a Varian INOVA 600-MHz spectrometer equipped with ^{1}H, ^{13}C, ^{15}N triple resonance, Z-axis pulsed filed gradient probe. $^{15}N/^{1}H$ HSQC titrations of BMAL1 TAD with CBP KIX, CRY CC or TAZ1 were performed using 300 µL ^{15}N BMAL1 TAD and 10% D_2O with a stepwise addition of CBP KIX or CC peptide in 10 mM MES pH 6.5, 50 mM NaCl. All NMR data were processed using NMRPipe/NMRDraw.[86] Assignments of mBMAL1 TAD were reported elsewhere.[43] Titration data were analyzed with NMRViewJ using chemical shift perturbations defined by the equation $\Delta\delta_{TOT} = [(\Delta\delta^{1}H)^2 + (\chi(\Delta\delta^{15}N)^2]^{½}$ and normalized with the scaling factor $\chi = 0.5$. All titration data were collected at 25 °C.

Fluorescence Anisotropy Experiments

The BMAL1 TAD WT, P625A P625dmP and Δswitch peptide probes were purchased from Bio-Synthesis, Inc (Lewisville, Tx) with a 5,6-TAMRA fluorescent probe covalently attached to the N-terminus. The C-terminus of the Δswitch peptide was amidated, whereas the others were left as a free carboxyl group to mimic the native C-terminus. Equilibrium binding assays with TAZ2 were performed in 50 mM MES pH 6.5 with 10 mM NaCl in flat-well 384-well black plates. Concentrated stocks of BMAL1 TAD probe peptides were stored at concentrations of 15-200 μM at -70 °C and diluted into assay buffer to 50 nM alone and in the presence of increasing concentrations of TAZ2 protein. Plates were incubated at room temperature for 10-20 minutes prior to analysis. Binding was monitored by changes in fluorescence polarization with a Perkin Elmer En Vision 2103 Multilabel plate reader with excitation at 531 nm and emission at 595 nm. The Hill coefficient, equilibrium dissociation constant and maximum binding capacitiy (Bmax) were calculated by fitting the dose-dependent change in millipolarization (ΔmP) to a one-site specific binding model in GraphPad Prism, with averaged ΔmP values from duplicate or triplicate assays.

Circular Dichroism Spectroscopy

CD spectra were acquired on a JASCO J-1500 CD spectropolarimeter, Four independent spectra were obtained with quartz cells of 1 mm path length with protein samples containing 20-60 μM CBP KIX[3] or TAZ2 domain.

Isothermal Titration Calorimetry (ITC)

Proteins were extensively dialyzed at 4 °C in 10 mM MES pH 6.5, and 50 mM NaCl with 2-kDa molecular-weight- cutoff filter-dialysis tubing (Spectrum Labs) before collection of ITC data. CBP KIX domain was used for analysis of TAD binding by ITC, owing to increased stability over p300 KIX, which was slightly more prone to precipitation under our ITC experimental conditions. ITC was performed on a MicroCal VP-ITC calorimeter at 25 °C with a stir speed of 177 r.p.m., reference power of 10 μcal/s and 10 μL injection sizes. Protein ratios for the cell and syringe for the ITC assays (with two or three independent ITC experiments performed for each complex) are as follows: 207 μM BMAL1 TAD was titrated into 16 uM TAZ1 (stoichiometry of the reaction, N=not determined), 218 μM KIX is titrated into 24 μM BMAL1 TAD (N=0.67), 205 μM CBP KIX into 20 μM BMAL1 TAD (N=0.67), 178 μM CBP KIX into 19.7 μM BMAL1

TAD (N=0.79), 178 μM CBP KIX into 20.7 μM BMAL1 TAD P625A (N=0.65), 205 μM CBP KIX into 19.9 μM BMAL1 TAD P625A (N=0.66), 178 μM CBP KIX into 20.7 μM BMAL1 TAD P625A (N=0.59), 170 μM CBP KIX into 21.9 μM BMAL1 TAD P625dmP (N=0.66), 170 μM CBP KIX into 19.5 μM BMAL1 TAD P625dmp (N=0.67), 240 μM CBP KIX into 16.9 μM BMAL1 TAD P625dmP (N=0.85).

Steady-State Mammalian Two-Hybrid Assays

Transient transfections of BMAL1 and BMAL1 P625A into HEK293T cells were performed in duplicate in 96-well plates and performed 30 hours prior to performing the luciferase reporter assay. In each well, 12.5 mg Per1-Luc reporter, 0.5, 5 or 50 ng pLV156-P(CMV)-mouse Cry1 and 25 ng pLV7P(UBC)-mouse BMAL1 or –mouse BMAL1 W624A or –mouse BMAL1 W624I or –mouse BMAL1 Δ584. When needed, empty vectors were included to make up 115 ng of total plasmid amount. In assays with *Cry1*, indicated amounts of pLV156-P(CMV)-Cry1 were compensated with empty pLV7 destination vector to a total of 50 ng. The reporter assay was performed using DualGlow luciferin reagent (Promega)

REFERENCES

1. Thomas, M. C. & Chiang, C.-M. The general transcription machinery and general cofactors. *Crit. Rev. Biochem. Mol. Biol.* **41,** 105–178 (2006).
2. Zehavi, Y., Kedmi, A., Ideses, D. & Juven-Gershon, T. TRF2: TRansForming the view of general transcription factors. *Transcription* **6,** 1–6 (2015).
3. Czudnochowski, N., Bösken, C. A. & Geyer, M. Serine-7 but not serine-5 phosphorylation primes RNA polymerase II CTD for P-TEFb recognition. *Nature Communications* **3,** 842 (2012).
4. Vo, N. & Goodman, R. H. CREB-binding Protein and p300 in Transcriptional Regulation. *J. Biol. Chem.* **276,** 13505–13508 (2001).
5. Chen, H. *et al.* Nuclear receptor coactivator ACTR is a novel histone acetyltransferase and forms a multimeric activation complex with P/CAF and CBP/p300. *Cell* **90,** 569–580 (1997).
6. Jenster, G. *et al.* Steroid receptor induction of gene transcription: a two-step model. *Proc. Natl. Acad. Sci. U.S.A.* **94,** 7879–7884 (1997).
7. Spencer, T. E. *et al.* Steroid receptor coactivator-1 is a histone acetyltransferase. *Nature* **389,** 194–198 (1997).
8. Wang, Z., Wu, Y., Li, L. & Su, X. D. Intermolecular recognition revealed by the complex structure of human CLOCK-BMAL1 basic helix-loop-helix domains with E-box DNA. *Cell Research* (2013).
9. McManus, K. J. & Hendzel, M. J. CBP, a transcriptional coactivator and acetyltransferase. *Biochem. Cell Biol.* **79,** 253–266 (2001).
10. Borcherds, W. *et al.* Disorder and residual helicity alter p53-Mdm2 binding affinity and signaling in cells. *Nat. Chem. Biol.* **10,** 1000–1002 (2014).

11. Toto, A., Giri, R., Brunori, M. & Gianni, S. The mechanism of binding of the KIX domain to the mixed lineage leukemia protein and its allosteric role in the recognition of c-Myb. *Protein Sci.* **23,** 962–969 (2014).

12. Cook, P. R., Polakowski, N. & Lemasson, I. HTLV-1 HBZ Protein Deregulates Interactions between Cellular Factors and the KIX Domain of p300/CBP. *J. Mol. Biol.* **409,** 384–398 (2011).

13. Korkmaz, E. N., Nussinov, R. & Haliloğlu, T. Conformational Control of the Binding of the Transactivation Domain of the MLL Protein and c-Myb to the KIX Domain of CREB. *PLoS Comput Biol* **8,** e1002420–9 (2012).

14. Arai, M., Dyson, H. J. & Wright, P. E. Leu628 of the KIX domain of CBP is a key residue for the interaction with the MLL transactivation domain. *FEBS Lett.* **584,** 4500–4504 (2010).

15. Lai, Z., Auger, K. R., Manubay, C. M. & Copeland, R. A. Thermodynamics of p53 binding to hdm2(1-126): effects of phosphorylation and p53 peptide length. *ARCHIVES OF BIOCHEMISTRY AND BIOPHYSICS* **381,** 278–284 (2000).

16. Uesugi, M. & Verdine, G. L. The alpha-helical FXXPhiPhi motif in p53: TAF interaction and discrimination by MDM2. *Proc. Natl. Acad. Sci. U.S.A.* **96,** 14801–14806 (1999).

17. Schon, O., Friedler, A., Bycroft, M., Freund, S. M. V. & Fersht, A. R. Molecular Mechanism of the Interaction between MDM2 and p53. *J. Mol. Biol.* **323,** 491–501 (2002).

18. Giles, R. H., Peters, D. J. & Breuning, M. H. Conjunction dysfunction: CBP/p300 in human disease. *Trends Genet.* **14,** 178–183 (1998).

19. Kasper, L. H. *et al.* A transcription-factor-binding surface of coactivator p300 is required for haematopoiesis. *Nature* **419,** 738–743 (2002).

20. Goto, N. K., Zor, T., Martinez-Yamout, M., Dyson, H. J. & Wright, P. E. Cooperativity in Transcription Factor Binding to the Coactivator CREB-binding Protein (CBP). *J. Biol. Chem.* **277,** 43168–43174 (2002).

21. Lee, C. W., Arai, M., Martinez-Yamout, M. A., Dyson, H. J. & Wright, P. E. Mapping the Interactions of the p53 Transactivation Domain with the KIX Domain of CBP †. *Biochemistry* **48,** 2115–2124 (2009).

22. Lee, C. W., Martinez-Yamout, M. A., Dyson, H. J. & Wright, P. E. Structure of the p53 Transactivation Domain in Complex with the Nuclear Receptor Coactivator Binding Domain of CREB Binding Protein. *Biochemistry* **49,** 9964–9971 (2010).

23. Ferreon, J. C. *et al.* Cooperative regulation of p53 by modulation of ternary complex formation with CBP/p300 and HDM2. *Proceedings of the National Academy of Sciences* **106,** 6591–6596 (2009).

24. Teufel, D. P., Freund, S. M., Bycroft, M. & Fersht, A. R. Four domains of p300 each bind tightly to a sequence spanning both transactivation subdomains of p53. *Proc. Natl. Acad. Sci. U.S.A.* **104,** 7009–7014 (2007).

25. Hosoda, H. *et al.* CBP/p300 is a cell type-specific modulator of CLOCK/BMAL1-mediated transcription. *Mol Brain* **2,** 34 (2009).

26. Lee, Y. *et al.* Coactivation of the CLOCK-BMAL1 complex by CBP mediates resetting of the circadian clock. *J. Cell. Sci.* **123,** 3547–3557 (2010).

27. Koike, N. *et al.* Transcriptional architecture and chromatin landscape of the core circadian clock in mammals. *Science* **338,** 349–354 (2012).

28. Takahata, S. *et al.* Transactivation mechanisms of mouse clock transcription factors, mClock and mArnt3. *Genes to Cells* **5,** 739–747 (2000).

29. Goodman, R. H. & Smolik, S. CBP/p300 in cell growth, transformation, and development. *Genes & Development* (2000). doi:10.1101/gad.14.13.1553

30. Kee, B. L., Arias, J. & Montminy, M. R. Adaptor-mediated recruitment of RNA polymerase II to a signal-dependent activator. *J. Biol. Chem.* **271,** 2373–2375 (1996).

31. Nakajima, T. *et al.* RNA helicase A mediates association of CBP with RNA polymerase II. *Cell* **90,** 1107–1112 (1997).

32. Cho, H. *et al.* A human RNA polymerase II complex containing factors that modify chromatin structure. *Molecular and Cellular Biology* **18,** 5355–5363 (1998).

33. Wang, N. & Mapp, A. K. KINETIC AND CONFORMATIONAL CHARACTERIZATION OF TRANSCRIPTIONAL ACTIVATOR- COACTIVATOR INTERACTIONS. 1–178 (2013).

34. Ogryzko, V. V., Schiltz, R. L., Russanova, V., Howard, B. H. & Nakatani, Y. The transcriptional coactivators p300 and CBP are histone acetyltransferases. *Cell* **87,** 953–959 (1996).

35. Kalkhoven, E. CBP and p300: HATs for different occasions. *Biochemical Pharmacology* **68,** 1145–1155 (2004).

36. Waltzer, L. & Bienz, M. Drosophila CBP represses the transcription factor TCF to antagonize Wingless signalling. *Nature* **395,** 521–525 (1998).

37. Chen, W. *et al.* Distinct Roles for CBP and p300 on the RA-Mediated Expression of the Meiosis Commitment Gene Stra8 in Mouse Embryonic Stem Cells. *PLoS ONE* **8,** e66076–8 (2013).

38. Yao, T. P. *et al.* Gene dosage-dependent embryonic development and proliferation defects in mice lacking the transcriptional integrator p300. *Cell* **93,** 361–372 (1998).

39. Kawasaki, H. *et al.* Distinct roles of the co-activators p300 and CBP in retinoic-acid-induced F9-cell differentiation. *Nature* **393,** 284–289 (1998).

40. Yuan, Z. M. *et al.* Function for p300 and not CBP in the apoptotic response to DNA damage. *Oncogene* **18,** 5714–5717 (1999).

41. Etchegaray, J.-P., Lee, C., Wade, P. A. & Reppert, S. M. Rhythmic histone acetylation underlies transcription in the mammalian circadian clock. *Nature* **421,** 177–182 (2003).

42. Curtis, A. M. *et al.* Histone acetyltransferase-dependent chromatin remodeling and the vascular clock. *J. Biol. Chem.* **279,** 7091–7097 (2004).

43. Xu, H. *et al.* Cryptochrome 1 regulates the circadian clock through dynamic interactions with the BMAL1 C terminus. *Nat. Struct. Mol. Biol.* **22,** 476–484 (2015).

44. De Guzman, R. N., Wojciak, J. M., Martinez-Yamout, M. A., Dyson, H. J. & Wright, P. E. CBP/p300 TAZ1 domain forms a structured scaffold for ligand binding. *Biochemistry* **44,** 490–497 (2005).

45. Palazzesi, F., Barducci, A. & Tollinger, M. The allosteric communication pathways in KIX domain of CBP. in (2013). doi:10.1073/pnas.1313548110/-/DCSupplemental

46. Brüschweiler, S., Konrat, R. & Tollinger, M. Allosteric Communication in the KIX Domain Proceeds through Dynamic Repacking of the Hydrophobic Core. *ACS Chem. Biol.* **8,** 1600–1610 (2013).

47. Law, S. M., Gagnon, J. K., Mapp, A. K. & Brooks, C. L. Prepaying the entropic cost for allosteric regulation in KIX. *Proc. Natl. Acad. Sci. U.S.A.* **111,** 12067–12072 (2014).

48. Brüschweiler, S. *et al.* Direct Observation of the Dynamic Process Underlying Allosteric Signal Transmission. *J. Am. Chem. Soc.* **131,** 3063–3068 (2009).

49. Gianni, S., Morrone, A., Giri, R. & Brunori, M. A folding-after-binding mechanism describes the recognition between the transactivation domain of c-Myb and the KIX domain of the CREB-binding protein. *Biochemical and Biophysical Research Communications* **428,** 205–209 (2012).

50. Shammas, S. L., Travis, A. J. & Clarke, J. Remarkably Fast Coupled Folding and Binding of the Intrinsically Disordered Transactivation Domain of cMyb to CBP KIX. *J. Phys. Chem. B* **117,** 13346–13356 (2013).

51. Wright, P. E. & Dyson, H. J. Linking folding and binding. *Curr. Opin. Struct. Biol.* **19,** 31–38 (2009).

52. Dogan, J., Gianni, S. & Jemth, P. The binding mechanisms of intrinsically disordered proteins. *Phys. Chem. Chem. Phys.* **16,** 6323–6331 (2014).

53. Gianni, S., Dogan, J. & Jemth, P. Coupled binding and folding of intrinsically disordered proteins: what can we learn from kinetics? *Curr. Opin. Struct. Biol.* (2016). doi:10.1016/j.sbi.2015.11.012

54. Parker, D. *et al.* Role of secondary structure in discrimination between constitutive and inducible activators. *Molecular and Cellular Biology* **19,** 5601–5607 (1999).

55. Wang, N. *et al.* Ordering a Dynamic Protein Via a Small-Molecule Stabilizer. *J. Am. Chem. Soc.* **135,** 3363–3366 (2013).

56. Denis, C. M. *et al.* Functional redundancy between the transcriptional activation domains of E2A is mediated by binding to the KIX domain of CBP/p300. *Nucleic Acids Research* **42,** 7370–7382 (2014).

57. Zor, T., De Guzman, R. N., Dyson, H. J. & Wright, P. E. Solution Structure of the KIX Domain of CBP Bound to the Transactivation Domain of c-Myb. *J. Mol. Biol.* **337,** 521–534 (2004).

58. Wang, F., Marshall, C. B. & Yamamoto, K. Structures of KIX domain of CBP in complex with two FOXO3a transactivation domains reveal promiscuity and plasticity in coactivator recruitment. in (2012). doi:10.1073/pnas.1119073109/-/DCSupplemental

59. Radhakrishnan, I. *et al.* Solution Structure of the KIX Domain of CBP Bound to the Transactivation Domain of CREB: A Model for Activator:Coactivator Interactions. *Cell* **91,** 741–752 (1997).

60. Wang, F., Marshall, C. B. & Ikura, M. Transcriptional/epigenetic regulator CBP/p300 in tumorigenesis: structural and functional versatility in target recognition. *Cell. Mol. Life Sci.* **70,** 3989–4008 (2013).

61. Krois, A. S., Ferreon, J. C., Martinez-Yamout, M. A., Dyson, H. J. & Wright, P. E. Recognition of the disordered p53 transactivation domain by the transcriptional adapter zinc finger domains of CREB-binding protein. *Proc. Natl. Acad. Sci. U.S.A.* **113,** E1853–E1862 (2016).

62. Wojciak, J. M., Martinez-Yamout, M. A., Dyson, H. J. & Wright, P. E. Structural basis for recruitment of CBP/p300 coactivators by STAT1 and STAT2 transactivation domains. *EMBO J.* **28,** 948–958 (2009).

63. Mukherjee, S. P. *et al.* Analysis of the RelA:CBP/p300 Interaction Reveals Its Involvement in NF-κB-Driven Transcription. *Plos Biol* **11,** e1001647–20 (2013).

64. Miller Jenkins, L. M. *et al.* Characterization of the p300 Taz2–p53 TAD2 Complex and Comparison with the p300 Taz2–p53 TAD1 Complex. *Biochemistry* **54,** 2001–2010 (2015).

65. Miller, M., Dauter, Z., Cherry, S., Tropea, J. E. & Wlodawer, A. Structure of the Taz2 domain of p300: insights into ligand binding. *Acta Cryst (2009). D65, 1301-1308 [doi:10.1107/S0907444909040153]* 1–8 (2009). doi:10.1107/S0907444909040153

66. Franks, K. M. Clockwork: exploring activation mechanisms of the circadian transcription factor CLOCK:BMAL1. 1–27 (2016).

67. De Guzman, R. N., Martinez-Yamout, M. A., Dyson, H. J. & Wright, P. E. Interaction of the TAZ1 domain of the CREB-binding protein with the activation domain of CITED2: regulation by competition between intrinsically unstructured ligands for non-identical binding sites. *J. Biol. Chem.* **279,** 3042–3049 (2004).

68. De Guzman, R. N., Liu, H. Y., Martinez-Yamout, M., Dyson, H. J. & Wright, P. E. Solution structure of the TAZ2 (CH3) domain of the transcriptional adaptor protein CBP. *J. Mol. Biol.* **303,** 243–253 (2000).

69. De Guzman, R. N., Goto, N. K., Dyson, H. J. & Wright, P. E. Structural Basis for Cooperative Transcription Factor Binding to the CBP Coactivator. *J. Mol. Biol.* **355,** 1005–1013 (2006).

70. Hung, H.-C., Maurer, C., Kay, S. A. & Weber, F. Circadian transcription depends on limiting amounts of the transcription co-activator nejire/CBP. *J. Biol. Chem.* **282,** 31349–31357 (2007).

71. Rey, G. *et al.* Genome-Wide and Phase-Specific DNA-Binding Rhythms of BMAL1 Control Circadian Output Functions in Mouse Liver. *Plos Biol* **9,** e1000595–18 (2011).

72. Shimomura, K. *et al.* Usf1, a suppressor of the circadian Clock mutant, reveals the nature of the DNA-binding of the CLOCK:BMAL1 complex in mice. *Elife* **2,** e00426 (2013).

73. Nakahata, Y. *et al.* A direct repeat of E-box-like elements is required for cell-autonomous circadian rhythm of clock genes. *BMC Mol. Biol.* **9,** 1 (2008).

74. Bates, C. A., Pomerantz, W. C. & Mapp, A. K. Transcriptional tools: Small molecules for modulating CBP KIX-dependent transcriptional activators. *Biopolymers* **95,** 17–23 (2010).

75. Li, B. X., Yamanaka, K. & Xiao, X. Structure–activity relationship studies of naphthol AS-E and its derivatives as anticancer agents by inhibiting CREB-mediated gene transcription. *Bioorganic & Medicinal Chemistry* **20,** 6811–6820 (2012).

76. Best, J. L. *et al.* Identification of small-molecule antagonists that inhibit an activator: coactivator interaction. *Proc. Natl. Acad. Sci. U.S.A.* **101,** 17622–17627 (2004).

77. Li, B. X. & Xiao, X. Discovery of a Small-Molecule Inhibitor of the KIX–KID Interaction. *ChemBioChem* **10,** 2721–2724 (2009).

78. Gee, C. T., Koleski, E. J. & Pomerantz, W. C. K. Fragment Screening and Druggability Assessment for the CBP/p300 KIX Domain through Protein-Observed 19F NMR Spectroscopy. *Angew. Chem. Int. Ed.* **54,** 3735–3739 (2015).

79. Sarkar, P., Reichman, C., Saleh, T., Birge, R. B. & Kalodimos, C. G. Proline *cis-trans* Isomerization Controls Autoinhibition of a Signaling Protein. *Mol. Cell* **25,** 413–426 (2007).

80. Guan, R.-J. *et al.* Structural Mechanism Governing *Cis* and *Trans* Isomeric States and an Intramolecular Switch for *Cis*/*Trans* Isomerization of a Non-proline Peptide Bond Observed in Crystal Structures of Scorpion Toxins. *J. Mol. Biol.* **341,** 1189–1204 (2004).

81. Schmid, F. X. Prolyl isomerase: enzymatic catalysis of slow protein-folding reactions. *Annu Rev Biophys Biomol Struct* **22,** 123–142 (1993).

82. MacArthur, M. W. & Thornton, J. M. Influence of proline residues on protein conformation. *J. Mol. Biol.* **218,** 397–412 (1991).

83. Gekakis, N. *et al.* Role of the CLOCK protein in the mammalian circadian mechanism. *Science* **280,** 1564–1569 (1998).

84. Sheffield, P., Garrard, S. & Derewenda, Z. Overcoming expression and purification problems of RhoGDI using a family of ‘parallel’ expression vectors. *Protein Expr. Purif.* **15,** 34–39 (1999).

85. Liu, H. & Naismith, J. H. An efficient one-step site-directed deletion, insertion, single and multiple-site plasmid mutagenesis protocol. *BMC Biotechnol* **8,** 91 (2008).

86. Delaglio, F. *et al.* NMRPipe: a multidimensional spectral processing system based on UNIX pipes. *J. Biomol. NMR* **6,** 277–293 (1995).

CHAPTER 5

CONCLUSIONS AND FUTURE DIRECTIONS

EVOLUTIONALLY TUNED CIRCADIAN OSCILLATIONS REGULATE PHYSIOLOGY

The daily rotation of the earth about its axis is arguably one of the oldest and most fundamental environmental processes that impacts the fitness of terrestrial organisms. The evolution of internal timekeeping mechanisms confers a selective advantage to our prehistoric predecessors by synchronizing physiology and behaviors with the solar day. The conservation of this trait in nearly all present-day organisms[1-3] is clear evidence that these internal clocks are crucial to biological fitness[4-10]. The central timekeeping mechanism in mammals is driven by finely tuned interactions between the transcription factor CLOCK:BMAL1 and cognate transcriptional regulators.[11-13] Auxiliary transcription-based loops and a host of accessory proteins contribute to the extraordinarily specific system that allow for robust, yet adaptable daily oscillations.

Cycling metrics such as period, damping and amplitude are reflections of the biochemical processes that maintain dynamic homeostasis in oscillating cells. The period, or frequency, of cycling reflects the time it takes to complete one round of transcriptional activation and repression by CLOCK:BMAL1. The amplitude of independently oscillating cells is a measure of the robustness of the molecular oscillations. However, the most commonly performed cycling studies record amplitude as a function of the synchrony of many cellular oscillators in culture.[14] The slow decrease in amplitude of cycling in synchronized cell cultures *in vitro* does not represent a loss of circadian rhythmicity in individual cells, but in most instances, likely reflects a desynchronization of individual oscillators in the collective culture[15-17]. This process of signal damping is attenuated in the SCN, where the highly coupled neuronal network allows for intercellular communication.[16,18]

At an organismal level, the SCN confers robustness to daily oscillations, while peripheral clocks present at the level of each organ have lower amplitude clocks that allow a level of plasticity to the timing of physiological processes .[8-20] The phase of peripheral oscillators can be reprogramed independent of SCN signaling through metabolic cues[21-23]. Uncoupling of the SCN and peripheral clocks allows organisms to respond to unanticipated environmental stressors.

The ability to flexibly reprogram cellular clocks is a function of the vast network of biochemical pathways (auxiliary loops and accessory proteins) that converge on CLOCK:BMAL1 [24-26].

The mechanism by which the molecular clock confers both robustness and plasticity to circadian cycling has be highly tuned through selective advantage. While some of these processes have been identified, the circadian system has yet to be fully elucidated. Throughout this dissertation, I have identified and characterized the role of the dynamic BMAL1 TAD in the regulation of circadian cycling. In this chapter, I consider the role of the BMAL1 TAD in the greater context of a cycling cell and explore the fundamental physical properties that underlie molecular motions in the BMAL1 TAD.

MOTIONS OF DISORDERED REGIONS DEFINE TIMESCALE OF BIOLOGICAL PROCESSES

The distillation of biochemistry down to its fundamental principles unveils the important role of thermodynamics and kinetics in biological pathways.[27] These basic physical properties govern the equilibrium populations (thermodynamics) and free energy barrier (kinetics) between conformational ensembles of proteins. When these physical processes are considered in the context of time, the field of protein dynamics emerges as a crucial element in mechanistic biology. Originally only applied to protein folding, the concept of free energy landscape of proteins can be applied to folded proteins and intrinsically disordered proteins alike; as a molecule reaches bottom of the folding funnel it encounters a rugged landscape of free energy wells dictated by the relative competition for the most entropically and enthalpically favorable conformations of individual amino acids (**Fig. 5.1a**).

Even most stable, globular proteins are anything but static; fast timescale (picosecond-nanosecond) motions such as bond vibrations and side chain rotations drive slower (microsecond to seconds), more biologically relevant motions[27-29]. The conformational ensemble of favorable structures that persist at the bottom of a folding well convert on a timescale relative to the free energy of activation ($\Delta G^{\neq}$) (**Fig. 5.1a**); tier1 and tier2 motions are those with a small $\Delta G^{\neq}$, and tier 0 motions are slower motions with high activation energy (**Fig. 5.1b**). Conformational dynamics of all timescales are the driving force behind binding[27,30] and dissociation[31] of ligands in biological systems spanning a wide spectrum of structural order.

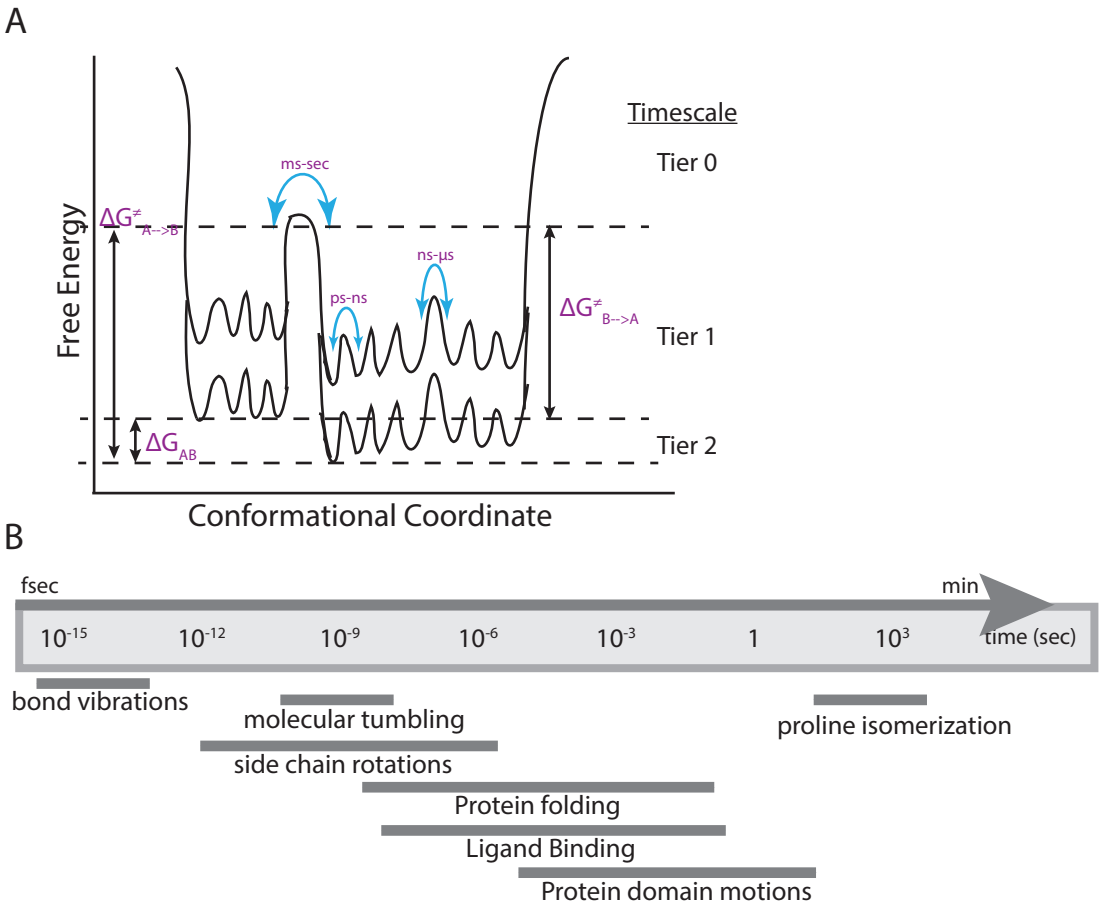

Figure 5.1: The multidimensional energy landscape dictates the timescale of molecular motions. (A) The multi-dimensional landscape of a protein motions when at equilibrium (at the bottom of a folding funnel). The equilibrium populations of each state are a function of the Boltzmann distributions of the free energy of each state. Tier 0 processes are slow timescale due to the large difference in free energy barrier between states, while tier 1 and tier 2 processes are faster timescale motions. (B) Timescale of various dynamic processes in proteins based upon the experimental data from computational modeling and biophysical experimental techniques.

Many well-folded proteins possess regions of disorder; dubbed intrinsically disordered regions (IDRs), these dynamic domains can function as linkers between functional domains, modulate protein activity through conformational changes[32,33], and can act as protein and ligand-interacting domains themselves.[30] Intrinsic plasticity allows for promiscuity in binding partners and specific tailoring of binding affinity. Flexible binding modes allow many types of interaction such as IDPs that wrap around their binding partners to interact with multiple regions and/or facilitate allosteric interactions.[34-38]

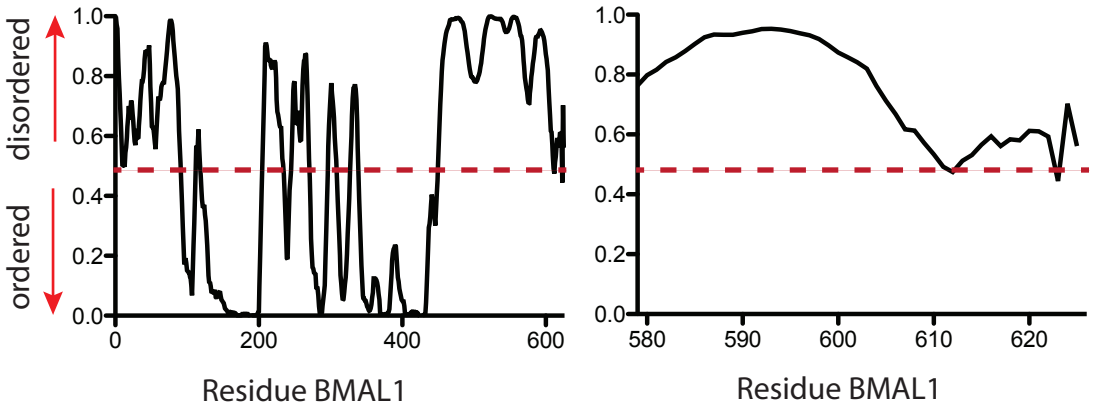

Figure 5.2: The BMAL1 TAD is an intrinsically disordered region (A) PONDR® plot of full length BMAL1 (left) and the BMAL1 TAD (right). Curves below the dashed line are predicted to be ordered and those above are predicted to be disordered. Intrinsically disordered regions (IDRs) are defined as those longer than 30 amino acids in length.

MOLECULAR MOTIONS OF THE BMAL1 TAD

Transcription factors are more likely to possess regions of disorder compared to other proteins.[34] For example, the transcription factors p53, GCN4, HMGA and CRCA1 all possess intrinsically disordered regions that interact with numerous binding partners. In the circadian clock, both BMAL1 and CLOCK possess intrinsically disordered regions that are imperative for normal circadian cycling[39] (and unpublished data). Analysis of the BMAL1 primary sequence by the predictors of natural disordered regions (PONDR®) (**Fig. 5.2** left panel) [40] shows that the C-terminus is disordered, with the exception of two short regions that correspond to the α-helical region and a short region in the TAD switch (**Fig. 5.2** right panel).

Analysis of the Cα and Cβ secondary chemical shifts (**Supplemental Fig. 2.4d**) of the BMAL1 TAD by the torsion angle likelihood obtains from shift and sequence similarity (TALOS) prediction software suggests that a short helix from 598-603 is the only structural feature (**Fig. 5.3a**). However the difference between TAD and random coil ^{13}C shifts barely exceeded cutoffs for helical prediction in this region.[41,42] These data are supported by heteronuclear nuclear overhauser effect (HETNOEs) experiments of the BMAL1 TAD (**Fig. 5.3b**), in which negative values are indicative of large amplitude motions on the sub-nanosecond timescale and thus disorder. These data suggest that the a-helix initiates at Asp596 and continues through Met604, after which the TAD takes on an extended conformation until residue Ala609. A gly-cine-rich linker following this core allows the C-terminal seven residues (in red) to sample many

conformations, not stabilized by any apparent contacts between the C-terminus and the helix (**Fig. 5.3c**).

In this dissertation, I have shown that the intrinsically disordered BMAL1 TAD interacts with the CBP KIX and TAZ1 domains and the CC helix of CRY1 with differing affinities. Additional work in our lab has shown that the BMAL1 TAD also interacts with the newly identified protein CHRONO (computationally highlighted repressor of the network oscillator) [43-46], which acts as a transcriptional repressor. The BMAL1 TAD possesses three independent motifs with which it binds its partners, a short hydrophobic motif in the N-terminus, the central α-helical region, and the extreme C-terminus that harbors the slow conformational switch. Based on chemical shift perturbations due to binding CBP KIX, TAZ1 or CRY1 CC on ^{15}N BMAL1 TAD, we find that the chemical environment of the hydrophobic N-terminal motif of the TAD is more perturbed in its interactions with TAZ1 than with KIX and CRY1 CC (**Figs. 2.4a,b** and **4.12b**). While the three transcriptional regulators interact at overlapping regions with the TAD, we do observe differences in specific resides. For example, W624 appears to be more important in the interactions with the CRY1 CC helix than with KIX. These data indicate that the BMAL1 TAD, like other IDRs, is capable of interacting with its partners in a variety of orientations.

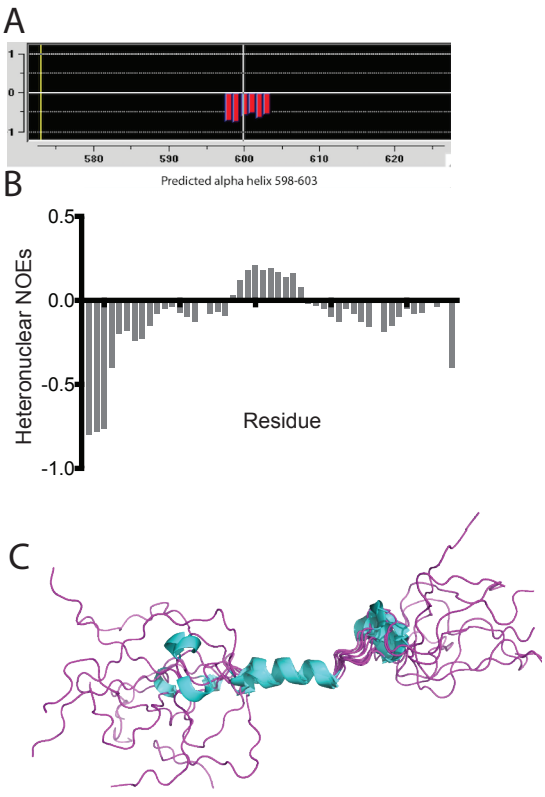

Figure 5.3: Fast timescale motions of the BMAL1 TAD (A) TALOS prediction of secondary structure of the BMAL1 TAD based secondary chemical shifts for Cα and Cβ chemical shifts (B) heteronuclear nuclear overhauser effect (HETNOE) data of the BMAL1 TAD as a function of residue number and the (C) associated structure of the BMAL1 TAD derived from the HETNOE data.

Furthermore, by mapping the interactions of BMAL1 TAD motifs onto ^{15}N CBP KIX, we show that the α-helical region and the C-terminal switch region likely interact with two different sites. These data suggest an important role of the flexible linker (608-618)

between these two motifs, which allows the TAD to wrap around the KIX domain to make both interactions. The paramagnetic relaxation enhancement studies in chapter 2 confirm the importance of the linker region as the C-terminus rearranges upon binding CRY CC to come closer to the α-helix (**Fig. 2.4d,e,f**). A small decrease of NMR signal at the α-helix region upon titration with CBP KIX, indicates a similar rearrangement, but the loss of signal is significantly less than with CRY CC. We posit that the difference in peak broadening from the paramagnetic-induced relaxation enhancement is due to a larger distance between the c-Myb and MLL binding sites on CBP KIX compared to the linear CC helical peptide. These data allow us to propose a structural model of the interactions of the TAD with KIX and CRY CC as shown in **Fig. 5.4**.

The various conformational ensembles adopted by the BMAL1 TAD mostly likely allows for this variability in binding modes. The backbone and side chain motions that the BMAL1 TAD undergo are in the fast timescale regime (**Supplemental Fig. 2.4d** and **Fig. 5.3**); these motions have an impact on the conformational ensembles sampled by the central α-helix and TAD switch [27-29]. Helix formation occurs on the timescale of microseconds, the fastest of all the classified Tier 0 (slow exchange) processes. The concept of conformational selection suggests that a substrate binds a disordered ligand only when the ligand samples the *preformed bound-like* conformation; the concept of coupled folding and binding is diametrically opposed to this, where interactions between substrate and ligand induce the 'proper' folding of the disordered ligand[47-51]. Studies by Parker et. al.[52] suggested that the thermodynamic profiles of complex formation between KIX and its ligands is a function of the stability of the *preformed bound-like* conformation of a TAD prior to binding. If this holds true for the BMAL1 TAD,

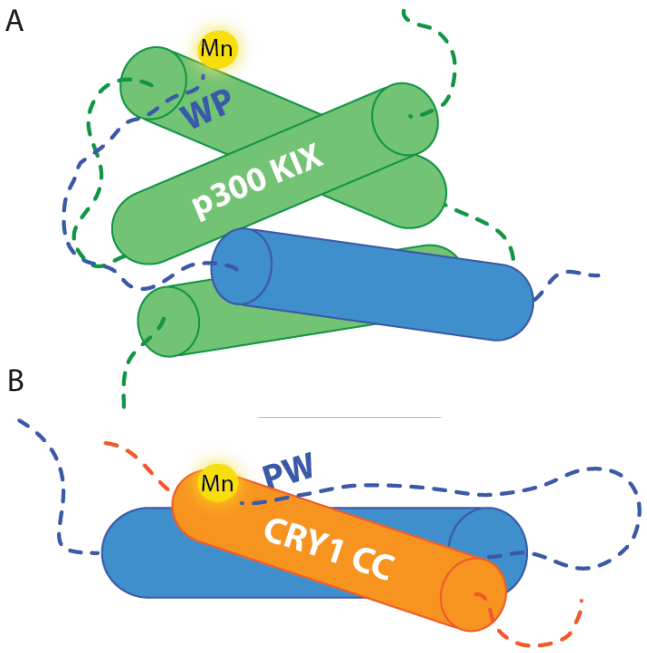

Figure 5.4: The BMAL1 TAD undergoes structural rearrangements upon binding. Model of BMAL1 TAD binding (A) CBP KIX and (B) CRY CC based upon PRE data shown in Chapter 1.

then the favorable entropy observed upon titration of BMAL1 TAD into CBP KIX suggests that a conformational selection process is occurring and that BMAL1 TAD samples its preformed state prior to binding. It is equally as likely, however, that the solvation of water molecules around the apo BMAL1 TAD is significantly more ordered than that around the TAD:KIX complex.

In addition to the fast stochastic motions and the intermediate timescale of α-helix formation, the BMAL1 TAD undergoes a unique slow conformational exchange: a *cis/trans* isomerization about the W624-P625 bond (chapter 3 in this dissertation). Notably, we were able to show that locking the isomerizing switch into *trans* using a proline to alanine mutation in cycling fibroblasts causes a one-hour shortening of the circadian period. Kinetic analysis of the switch shows that it takes approximately 6.3 minutes to transition from *trans* to *cis* and 3.6 minutes to transition from *cis* to *trans* at room temperature. The lifetimes ($1/k_{off}$) of the BMAL1 TAD:CRY CC and BMAL1 TAD:KIX complexes can be estimated from the rate equilibrium dissociation constants reported in chapter 2 and Xu et al.[39], assuming a k_{on} of $1x10^7$ $M^{-1}s^{-1}$. Comparing these values with the experimentally measured timescales of isomerization shows that the difference in timescale is over 3 orders of magnitude. Even more extreme differences in timescales emerge when comparing the sub-nanosecond motions suggested by the HETNOE data (**Fig. 5.3b,c**) and the TAD switch. These analyses suggest that the range in timescale of motions that regulate circadian cycling is enormous. Data presented in chapter 2 and Xu et. al.[39] showed that point mutations in the isolated BMAL1 TAD that cause small shifts in the affinity of CRY CC and CBP KIX can elicit large changes in cycling phenotypes, on the order of a ~5 hour shift in period. Considered alongside one another, these two sets of data illustrate how small perturbations in the timescales of both fast and slow conformational exchange are poised to have profound biological ramifications for circadian cycling.

It is important to note that kinetics are highly dependent on environmental conditions, competition, subcellular compartmentalization and reactant concentration. The cellular milieu is far more complex and viscous than laboratory buffer conditions and the absolute magnitude of the *in vivo* timescales may be different than those derived from our *in vitro* studies. Furthermore, the presence of additional interacting proteins could significantly alter the timescale of these motions. For example, we have shown that peptidyl prolyl isomerases (PPIases) have the

capacity to regulate the *cis/trans* isomerization *in vitro*; some of these PPIases are localized in the nucleus and could act on the TAD to change kinetics of switch isomerization in the cell.

DIFFERENTIAL INTERACTION OF *CIS* AND *TRANS* ISOMERS

Our data show that the *cis* and *trans* isomers have similar affinity for CBP KIX and TAZ domains, as well as CRY1, yet further analysis by NMR reveals differences in their binding modes. Binding of the *trans* isomer to the CBP KIX is enthalpically driven, and binding of the *cis* isomer is entropy driven. While this could be a result of the side chain replacements that we made to lock the TAD into *cis* or *trans*, these differences could be a true indication of differing binding mechanisms between the two isomers. It is possible that while the absolute configuration about the W624-P625 bond does not affect binding, it could affect the greater structural attributes of the switch region; in other systems, *cis* and *trans* imide bonds support differing local secondary structures.[53] If the conformational ensemble of one of the isomers is more closely related to the KIX-bound state, the binding mode could be significantly altered. Applying the argument of Parker et. al. [52] to this scenario could suggest that the *cis* isomer undergoes fewer structural rearrangements than the *trans* isomer; this would indicate a more *conformational selection* type mechanism that forgoes the initial thermodynamically driven attraction in favor of less entropic *cost associated* with conformational change. The *trans* isomer, in this case would undergo a more *coupled folding and binding-type* mechanism, where the initial attraction results in a more thermodynamically favorable interaction and an entropic folding cost.

As discussed in chapter 4, the differing dynamics that *cis* and *trans* isomers display upon interaction with the TAZ1 domain could also indicate differential binding modes. The lack of ITC data for this interaction does not allow us to draw parallels between thermodynamic profiles for complex formation and the dynamics of binding by NMR. While lacking some mechanistic details, these data demonstrate that dynamics within the BMAL1 TAD are an important part of establishing timing within the mammalian circadian clock. Further studies to characterize the structures of the apo and KIX, TAZ1 and CRY1 bound BMAL1 TAD would lend insight into this intriguing set of data. Placing these data into the context of computational and mathematical models of oscillatory behaviors may help to provide further perspective for the notable role that small molecular changes can have on a larger system.

DYNAMIC TRANSITIONS AT THE HEART OF THE MOLECULAR OSCILLATOR

As described in chapter 1 of this dissertation, there are three (known) distinct phases of circadian cycling, the active phase where CBP/p300 recruit transcriptional machinery to the CLOCK:BMAL1-bound E-box elements, an early repressive phase characterized by a megadalton compilation of transcriptional repressors including PER and CRY proteins, and the late repressive phase, where CRY1 interacts with CLOCK:BMAL1 to hold off activation (**Fig. 1.2c**). The biochemical processes that impart the delay in negative feedback predicted by the Goodwin oscillator are key determinates of circadian cycling. The stepwise post-translational modification of PER and CRY that have been extensively studied are an essential component to slowing down nuclear entry and activity of the repressors. Computational modeling studies have suggested that residence time and stoichiometry of transcriptional repressors at CLOCK:BMAL1:E-box elements defines the period and robustness of cycling.[54-56] Yet, I believe that our model of circadian cycling regulation is not yet complete. In order for circadian cycling to occur, punctuated transitions between regulatory species at the promoter must occur quickly.[57] Therefore, the dynamic processes of binding, dissociation, competition and structural rearrangements at the central node of the pacemaker, the CLOCK:BMAL1:E-box complex needs to be included in mechanistic models. In this dissertation, I have expanded on previous studies that suggest that the BMAL1 TAD is an important element in the chronometric recruitment of transcriptional regulators and thus a central regulator of circadian cycling metrics.[58,59]

FUTURE DIRECTIONS

A greater understanding of the dynamics that underlie the hand off between coactivators and repressor to the BMAL1 TAD will help us develop a more complete picture of the molecular basis of circadian cycling. Studies that focus on the structure and dynamics of the BMAL1 TAD and its interactions with CBP KIX, CBP TAZ1, and CRY1 will further this goal. Structural elucidation using NMR or X-ray crystallography will lend insight into the key residues involved in recruitment of transcriptional regulators. Relaxation dispersion studies could help determine the dynamics of bound and unbound BMAL1 TAD to KIX, TAZ1 and CRY. These data could be used to determine if the TAD binds to its partners through a coupled folding and binding mechanism or conformational selection.

Investigations into the differential roles of CBP and p300 could lend insight into the possibility antagonistic roles of these two co-activators. Further analysis of the triple mutant at the c-Myb site on KIX (KIX^3) may lend insight into the thermodynamic driving force for the interaction. The NCBD domain of CBP and p300 is also a TAD-interacting domain and should be analyzed for possible interactions with the BMAL1 TAD. Mutational analysis and *in vivo* studies with different constructs of CBP could highlight the important role of cooperative binding of CBP to tandem CLOCK:BMAL1 heterodimers.

We propose further investigations into the biological role of the BMAL1 TAD switch. These would include measurements of relative amounts of *cis* and *trans* isomers at various circadian times in both the cytoplasm and nucleus of cycling cells, determining the role of PPIases in regulating the switch and determining the mechanism by which the switch controls the period of circadian cycling. Identification of PPIases that act on the TAD switch *in vivo* could lead to the development of small molecule modifiers of the clock and lead to improvements to current therapeutics.[60-62]

REFERENCES

1. Friedrich, M. Biological Clocks and Visual Systems in Cave-Adapted Animals at the Dawn of Speleogenomics. *Integrative and Comparative Biology* **53,** 50–67 (2013).
2. Gehring, W. & Rosbash, M. The Coevolution of Blue-Light Photoreception and Circadian Rhythms. *Journal of Molecular Evolution* **57,** S286–S289 (2003).
3. Moran, D., Softley, R. & Warrant, E. J. Eyeless Mexican Cavefish Save Energy by Eliminating the Circadian Rhythm in Metabolism. *PLoS ONE* **9,** e107877–8 (2014).
4. Hurd, M. W. & Ralph, M. R. The significance of circadian organization for longevity in the golden hamster. *Journal of Biological Rhythms* **13,** 430–436 (1998).
5. Daan, S. *et al.* Lab Mice in the Field: Unorthodox Daily Activity and Effects of a Dysfunctional Circadian Clock Allele. *Journal of Biological Rhythms* **26,** 118–129 (2011).
6. DeCoursey, P. J., Walker, J. K. & Smith, S. A. A circadian pacemaker in free-living chipmunks: essential for survival? *J. Comp. Physiol. A* **186,** 169–180 (2000).
7. Nikhil, K. L., Ratna, K. & Sharma, V. K. Life-history traits of Drosophila melanogaster populations exhibiting early and late eclosion chronotypes. *BMC Evolutionary Biology* 1–14 (2016). doi:10.1186/s12862-016-0622-3
8. Woelfle, M. A., Ouyang, Y., Phanvijhitsiri, K. & Johnson, C. H. The Adaptive Value of Circadian Clocks. *Current Biology* **14,** 1481–1486 (2004).
9. Green, R. M. Circadian Rhythms Confer a Higher Level of Fitness to Arabidopsis Plants. *PLANT PHYSIOLOGY* **129,** 576–584 (2002).
10. Vaze, K. M. & Sharma, V. K. On the Adaptive Significance of Circadian Clocks for Their Owners. *Chronobiol Int* **30,** 413–433 (2013).
11. Egli, M. & Johnson, C. H. Biochemistry That Times the Day. *Biochemistry* **54,** 104–109 (2015).
12. Gustafson, C. L. & Partch, C. L. Emerging models for the molecular basis of mammalian circadian timing. *Biochemistry* **54,** 134–149 (2015).

13. Merbitz-Zahradnik, T. & Wolf, E. How is the inner circadian clock controlled by interactive clock proteins?: Structural analysis of clock proteins elucidates their physiological role. *FEBS Lett.* **589,** 1–14 (2015).

14. Izumo, M., Sato, T. R., Straume, M. & Johnson, C. H. Quantitative analyses of circadian gene expression in mammalian cell cultures. *PLoS Comput Biol* **2,** e136 (2006).

15. Welsh, D. K., Imaizumi, T. & Kay, S. A. Real-time reporting of circadian-regulated gene expression by luciferase imaging in plants and mammalian cells. *Meth. Enzymol.* **393,** 269–288 (2005).

16. Welsh, D. K., Yoo, S.-H., Liu, A. C., Takahashi, J. S. & Kay, S. A. Bioluminescence imaging of individual fibroblasts reveals persistent, independently phased circadian rhythms of clock gene expression. *Curr. Biol.* **14,** 2289–2295 (2004).

17. Nagoshi, E., Brown, S. A., Dibner, C., Kornmann, B. & Schibler, U. Circadian gene expression in cultured cells. *Meth. Enzymol.* **393,** 543–557 (2005).

18. Ko, C. H. *et al.* Emergence of Noise-Induced Oscillations in the Central Circadian Pacemaker. *Plos Biol* **8,** e1000513–19 (2010).

19. DeWoskin, D., Geng, W., Stinchcombe, A. R. & Forger, D. B. It is not the parts, but how they interact that determines the behaviour of circadian rhythms across scales and organisms. *Interface Focus* **4,** 20130076–20130076 (2014).

20. Schibler, U., Ripperger, J. & Brown, S. A. Peripheral circadian oscillators in mammals: time and food. *Journal of Biological Rhythms* **18,** 250–260 (2003).

21. Damiola, F. *et al.* Restricted feeding uncouples circadian oscillators in peripheral tissues from the central pacemaker in the suprachiasmatic nucleus. *Genes & Development* **14,** 2950–2961 (2000).

22. Takahashi, J. S., Hong, H.-K., Ko, C. H. & McDearmon, E. L. The genetics of mammalian circadian order and disorder: implications for physiology and disease. *Nat Rev Genet* **9,** 764–775 (2008).

23. Eckel-Mahan, K. & Sassone-Corsi, P. Metabolism and the Circadian Clock Converge. *Physiol. Rev.* **93,** 107–135 (2013).

24. Patel, V. R., Eckel-Mahan, K., Sassone-Corsi, P. & Baldi, P. How pervasive are circadian oscillations? *Trends in Cell Biology* **24,** 329–331 (2014).

25. Patel, V. R. *et al.* The pervasiveness and plasticity of circadian oscillations: the coupled circadian-oscillators framework. *Bioinformatics* **31,** 3181–3188 (2015).

26. Roenneberg, T., Daan, S. & Merrow, M. The art of entrainment. *Journal of Biological Rhythms* (2003). doi:10.1177/0748730403253393

27. Henzler-Wildman, K. & Kern, D. Dynamic personalities of proteins. *Nature* **450,** 964–972 (2007).

28. DuBay, K. H., Bowman, G. R. & Geissler, P. L. Fluctuations within Folded Proteins: Implications for Thermodynamic and Allosteric Regulation. *Acc. Chem. Res.* **48,** 1098–1105 (2015).

29. Yang, L.-Q. *et al.* Protein dynamics and motions in relation to their functions: several case studies and the underlying mechanisms. *Journal of Biomolecular Structure and Dynamics* **32,** 372–393 (2013).

30. Mittag, T., Kay, L. E. & Forman-Kay, J. D. Protein dynamics and conformational disorder in molecular recognition. *J. Mol. Recognit.* n/a–n/a (2009). doi:10.1002/jmr.961

31. Seo, M.-H., Park, J., Kim, E., Hohng, S. & Kim, H.-S. Protein conformational dynamics dictate the binding affinity for a ligand. *Nature Communications* **5,** 3724 (2014).

32. Sarkar, P., Reichman, C., Saleh, T., Birge, R. B. & Kalodimos, C. G. Proline *cis-trans* Isomerization Controls Autoinhibition of a Signaling Protein. *Mol. Cell* **25,** 413–426 (2007).

33. Sarkar, P., Saleh, T., Tzeng, S.-R., Birge, R. B. & Kalodimos, C. G. Structural basis for regulation of the Crk signaling protein by a proline switch. *Nat. Chem. Biol.* **7,** 51–57 (2010).

34. Liu, J. *et al.* Intrinsic Disorder in Transcription Factors †. *Biochemistry* **45,** 6873–6888 (2006).

35. Gianni, S., Dogan, J. & Jemth, P. Coupled binding and folding of intrinsically disordered proteins: what can we learn from kinetics? *Curr. Opin. Struct. Biol.* (2016). doi:10.1016/j.sbi.2015.11.012

36. Gianni, S., Morrone, A., Giri, R. & Brunori, M. A folding-after-binding mechanism describes the recognition between the transactivation domain of c-Myb and the KIX domain of the CREB-binding protein. *Biochemical and Biophysical Research Communications* **428,** 205–209 (2012).

37. Korkmaz, E. N., Nussinov, R. & Haliloğlu, T. Conformational Control of the Binding of the Transactivation Domain of the MLL Protein and c-Myb to the KIX Domain of CREB. *PLoS Comput Biol* **8,** e1002420–9 (2012).

38. Thakur, J. K., Yadav, A. & Yadav, G. Molecular recognition by the KIX domain and its role in gene regulation. *Nucleic Acids Research* **42,** 2112–2125 (2014).

39. Xu, H. *et al.* Cryptochrome 1 regulates the circadian clock through dynamic interactions with the BMAL1 C terminus. *Nat. Struct. Mol. Biol.* **22,** 476–484 (2015).

40. Romero, D. P., Obradovic, Z. & Dunker, A. K. Natively Disordered Proteins. *Appl-Bioinformatics* **3,** 105–113 (2004).

41. Wang, Y. & Jardetzky, O. Probability-based protein secondary structure identification using combined NMR chemical-shift data. *Protein Sci.* **11,** 852–861 (2002).

42. Wishart, D. S. & Sykes, B. D. The 13C chemical-shift index: a simple method for the identification of protein secondary structure using 13C chemical-shift data. *J. Biomol. NMR* **4,** 171–180 (1994).

43. Goularte, N. F. Investigating the molecular mechanism of CHRONO: a novel repressor of the circadian clock. 1–25 (2015).

44. Anafi, R. C. *et al.* Machine learning helps identify CHRONO as a circadian clock component. *Plos Biol* **12,** e1001840 (2014).

45. Annayev, Y. *et al.* Gene Model 129 (Gm129) Encodes a Novel Transcriptional Repressor That Modulates Circadian Gene Expression. *Journal of Biological Chemistry* **289,** 5013–5024 (2014).

46. Goriki, A. *et al.* A Novel Protein, CHRONO, Functions as a Core Component of the Mammalian Circadian Clock. *Plos Biol* **12,** e1001839–15 (2014).

47. Dyson, H. J. & Wright, P. E. Coupling of folding and binding for unstructured proteins. *Curr. Opin. Struct. Biol.* **12,** 54–60 (2002).

48. Wright, P. E. & Dyson, H. J. Linking folding and binding. *Curr. Opin. Struct. Biol.* **19,** 31–38 (2009).

49. Fuxreiter, M. *et al.* Disordered Proteinaceous Machines. *Chem. Rev.* **114,** 6806–6843 (2014).

50. Dogan, J., Gianni, S. & Jemth, P. The binding mechanisms of intrinsically disordered proteins. *Phys. Chem. Chem. Phys.* **16,** 6323–6331 (2014).

51. Pancsa, R. & Fuxreiter, M. Interactions via intrinsically disordered regions: What kind of motifs? *IUBMB Life* **64,** 513–520 (2012).

52. Parker, D. *et al.* Role of secondary structure in discrimination between constitutive and inducible activators. *Molecular and Cellular Biology* **19,** 5601–5607 (1999).

53. MacArthur, M. W. & Thornton, J. M. Influence of proline residues on protein conformation. *J. Mol. Biol.* **218,** 397–412 (1991).

54. Kim, J. K. & Forger, D. B. A mechanism for robust circadian timekeeping via stoichiometric balance. *Mol. Syst. Biol.* **8,** 630 (2012).

55. Sato, T. K. *et al.* Feedback repression is required for mammalian circadian clock function. *Nat. Genet.* **38,** 312–319 (2006).

56. Lee, C., Etchegaray, J. P., Cagampang, F. R., Loudon, A. S. & Reppert, S. M. Posttranslational mechanisms regulate the mammalian circadian clock. *Cell* **107,** 855–867 (2001).

57. Forger, D. B. & Peskin, C. S. Stochastic simulation of the mammalian circadian clock. *Proc. Natl. Acad. Sci. U.S.A.* **102,** 321–324 (2005).

58. Takahata, S. *et al.* Transactivation mechanisms of mouse clock transcription factors, mClock and mArnt3. *Genes to Cells* **5,** 739–747 (2000).

59. Czarna, A. *et al.* Quantitative analyses of cryptochrome-mBMAL1 interactions: mechanistic insights into the transcriptional regulation of the mammalian circadian clock. *Journal of Biological Chemistry* **286,** 22414–22425 (2011).

60. Kim, J. K. *et al.* Modeling and Validating Chronic Pharmacological Manipulation of Circadian Rhythms. *CPT: pharmacomet. syst. pharmacol.* **2,** e57–11 (2013).

61. Librodo, P., Buckley, M., Luk, M. & Bisso, A. Chronotherapeutic Drug Delivery. *Journal of Infusion Nursing* **35,** 329–334 (2012).

62. Skelton, R. L., Kornhauser, J. M. & Tate, B. A. Personalized medicine for pathological circadian dysfunctions. *Frontiers in pharmacology* (2015). doi:10.3389/fphar.2015.00125